Structural and functional characterisation of the Alzheimer's disease risk factor TREM2



Aleksandra Szykowska

Nuffield Department of Medicine and Linacre College

University of Oxford

Trinity term 2021

Thesis submitted for the degree of Doctor of Philosophy in Clinical Medicine

Declaration

I declare that no parts of this thesis or its research herein have been reproduced or accepted for another award or degree or diploma at any other university or learning institution. This thesis contains no other person's work except where stated in text. Chapter 4, Chapter 5 and parts of Chapter 2 are based on the publication:

Aleksandra Szykowska, Yu Chen, Thomas B. Smith, Charlotta Preger, Jingjing Yang, Dongming Qian, Shubhashish M. Mukhopadhyay, Edvard Wigren, Stephen J. Neame, Susanne Gräslund, Helena Persson, Peter J. Atkinson, Elena Di Daniel, Emma Mead, John Wang, John B. Davis, Nicola A. Burgess-Brown, Alex N. Bullock,

Selection and structural characterization of anti-TREM2 scFvs that reduce levels of shed ectodomain, Structure, 2021, https://doi.org/10.1016/j.str.2021.06.010.

Acknowledgements

I would like to thank a number of people for their support in allowing the work described here to be realised. Firstly, I would like to thank my academic supervisors: Dr Nicola Burgess-Brown for always believing in me; John Davis, who brought Eisai and Oxford University together and with whom conversations always resulted in exciting questions; Alexander Bullock, who provided a wealth of advice and challenged many of my ideas and Elena Di Daniel who introduced me to cell biology. I would like to thank Eisai inc. not only for the funding of this project but also for providing me with many excellent colleagues. In particular, I would like to thank Peter Atkinson, who is also my industrial supervisor and Stephen Neame and Andy Takle who contributed their advice. Special thanks are owed to John Wang and Julie Chen, who supervised Weihua Li, Jieru Li, Dongming Qian, and Jingjing Yang, who produced some of the reagents and data included in this thesis. I want to thank my colleagues in Karolinska Institutet: Charlotta Preger, Edvard Wigren, Susanne Gräslund and Helena Persson for work in generating scFv by phage display. A number of people contributed to this work by sharing reagents: The pHTBV1.1 BacMam vector was kindly provided by Professor Frederick Boyce, Harvard; The HEK293-TREM2-DAP12 cell line was a kind gift from Professor Peter St-George Hyslop. Additionally, I would like to thank my colleagues in UK-Oxford Drug Discovery Institute (ODDI): Thomas Smith, Juliane Obst and Emma Mead, for help and advice and early work in developing assays used in Chapter 6. I would also like to thank my friends in Oxford who became my second family and colleagues at the SGC, but particularly Alejandra Cid-Fernandes and Tina Bohstedt, who supported me through many difficult times.I would like to thank my sister, Ada, who believed in me from the beginning until the end. Her faith in me is humbling.

My final but most important thanks are dedicated to my grandmother Mariana Makselon, whose disease inspired me to pursue this degree.

Structural and functional characterisation of the Alzheimer's disease risk factor TREM2

Aleksandra Szykowska, Linacre College, Nuffield Department of Medicine and Linacre College, University of Oxford, Trinity term 2021

Abstract

Single point mutations in TREM2, a receptor expressed by microglia in the brain, are associated with an increased risk of neurodegeneration, including Alzheimer's disease. Numerous studies support a role for TREM2 in sensing damaging stimuli and triggering signalling cascades necessary for neuroprotection. TREM2 contains an immunoglobulin-like domain followed by a flexible stalk region, a transmembrane domain and a cytoplasmic tail. Despite its significant role, ligands and regulators of TREM2 activation, and the mechanisms governing TREM2-dependent responses and its cleavage from the membrane, remain poorly characterised. Here, I characterise phage display generated single-chain variable antibody fragments (scFvs) to human TREM2 ectodomain. The highest published affinity to human TREM2 was measured for one of the produced antibodies. Co-crystal structures revealed the binding of two scFvs to an epitope on the TREM2 Ig-like domain distal to the putative ligand-binding site. Functional activity was observed for oligomeric scFv species, which inhibited the accumulation of soluble TREM2 shed by transfected HEK293 or THP-1 cells. Treatment of HEK293 cells with fluorochrome-conjugated scFvs and quantification of surface TREM2 revealed scFv-induced receptor endocytosis as the likely mechanism of action in these cells. Furthermore, the multivalent scFv led to the activation of a TREM2 signalling cascade measured by phosphorylation of spleen tyrosine kinase in human iPSC-derived macrophages (iMac) and THP-1 cells. Similar activation in iMac cells was achieved upon conversion to monoclonal antibodies, with agonist values exceeding those in the literature. Further studies in combination with physiological ligands, such as apoptotic neurons, need to be performed to probe the overall effect on the TREM2 pathway and microglial activity in models of AD. The detailed characterisation of the epitopes and properties of these antibodies should facilitate the use of these renewable binders as structural and functional biology tools for TREM2 research.

Table of content

Declaration ii
Acknowledgements iii
Abstract v
Table of content vi
Abbreviations xi
Chapter 1 Introduction 15
1.1 Alzheimer's disease 15
1.1.1 Epidemiology of AD and environmental risk factors 16
1.1.2 Familial AD risk factors 17
1.1.3 Late-onset AD and GWAS risk loci 22
1.2 Neuroinflammation, microglia and TREM2 25
1.2.1 Neuroinflammation 25
1.2.2 Microglia 27
1.2.3 TREM2 28
TREM2 structure 28
TREM2 mutations 32
TREM2 in animal models of AD 34
TREM2 in disease-associated microglia (DAM) 36
TREM2 signalling pathways 38
TREM2 ligands 41
1.3 Aims of thesis
Chapter 2 Materials and methods 47
2.1 Bacterial strains 47
2.2 Vectors 48
2.3 Media composition 50
2.4 Cloning 50
2.4.1 Construct design 50
2.4.2 Ligation independent cloning (LIC) 51
2.4.3 Mutagenesis 54
2.4.4 Competent cell preparation 55
2.4.5 Transformation of *E. coli* 55
2.5 Protein purification methods 56
2.5.1 IMAC 56
2.5.2 SEC 56

2.5.3 Protein A 57
2.6 Small scale *E. coli* test expression 58
2.6.1 Buffers 58
2.6.2 Test expression 58
2.6.3 Test purification of soluble proteins 59
2.6.4 Test purification of secreted proteins 59
2.6.5 Large scale *E. coli* expression and purification of deglycosylation enzymes 60
2.7 Baculovirus-*Sf9* protein production 62
2.7.1 Production of recombinant baculoviruses 62
2.7.2 Transfection of *Sf9* with bacmid DNA 63
2.7.3 Test expression 64
2.7.4 Large scale Purification 64
Antigen TREM2 and TREM2 N79A mutants 64
ScFvs…… 65
TREM2-scFv co-expression 66
2.7.5 *In vitro* biotinylation for antigen generation 66
2.7.6 Deglycosylation attempts of TREM2 66
2.8 Mammalian Expi293F™ protein expression 67
2.8.1 Viral transduction of mammalian cells for test expression 67
2.8.2 Mammalian test purification 67
2.8.3 DNA production and transient transfection of Expi293F™ 67
2.8.4 Large scale purification of TREM2 in Expi293F 69
2.9 LPS quantification and purification 70
2.10 Phage display and antibody validation 71
2.11 Mass spectrometry 72
2.11.1 Intact mass spectrometry 72
2.11.2 Tryptic digest LC-MS/MS 72
2.12 Differential scanning fluorimetry (DLS) 73
2.13 X-ray crystallography 75
2.13.1 Alexa fluor 555 and 488 staining 75
2.13.2 Sitting drop vapour diffusion Crystallisation 75
2.13.3 Crystal growth optimisation 76
2.13.4 Complex formation and crystallisation77
scFv-4 PDB: 6YMQ 77
scFv-4 PDB: 6Y6C 77
scFv-2 PDB: 6YYE 78
2.13.5 Data collection and structure determination 78

2.14 Measuring scFvs affinity to TREM2 79
2.14.1 BLI 79
2.14.2 SPR 80
2.15 Multi-angle light scattering of scFvs 80
2.16 Cell maintenance and differentiation 81
2.16.1 HEK293 81
2.16.2 THP-1 82
2.16.3 iMac 82
2.17 TREM2 detection by western blot 82
2.18 Shedding assay 84
2.18.1 HEK293 and THP-1 84
2.18.2 iMac 84
2.19 sTREM2 ELISA 84
2.19.1 ELISA validation 85
2.19.2 Normalisation to cell number 85
2.20 Surface TREM2 ELISA 86
2.21 Immunocytochemistry 87
2.21.1 Alexa fluor 647 conjugation and HEK293 treatment 87
2.21.2 Lysosomes, endosomes and TREM2 staining 87
2.22 TREM2 activation assay 88
2.22.1 Antibody and antibody fragment stimulation 88
2.22.2 Apoptotic SH-SY5Y stimulation 88
2.22.3 HTRF 89
2.23 Software and statistical analyses 90
Chapter 3 Production of TREM2 protein for crystallography and antigen generation 91
3.1 Introduction 91
3.2 Initial TREM2 construct design 96
3.3 High-throughput cloning and small scale expression testing of TREM2 constructs for further studies 99
3.4 Generation of TREM2 antigen 101
3.5 Optimisation of insect cell TREM2 for crystallisation 103
3.5.1 Optimisation of TREM2 deglycosylation for crystallisation 103
3.5.2 Characterisation of insect cell produced TREM2 glycosylation 106
3.5.3 MS/MS fingerprinting of glycosylation sites 107
3.5.4 Site-directed mutagenesis of the Asn79 glycosylation site 109
3.5.5 Large scale purification of TREM2 glycosylation mutant for crystallisation 110
3.6 Production of TREM2 in mammalian cells for crystallisation 112

3.6.1 Cloning, expression and purification of TREM2 in mammalian Expi293F™ 112
3.7 Discussion 115
Chapter 4 Production and characterisation of single-chain variable antibody fragments 119
4.1 Introduction 119
4.2 Selection and validation of scFvs binding to TREM2 123
4.3 Optimisation of scFvs production in *E. coli* 127
4.4 Optimisation of scFv production in *Sf9* cells 129
4.4.1 Optimisation of protein stability – differential scanning fluorimetry (DSF) 129
4.4.2 Analysis of oligomeric state by SEC and SEC-MALS 131
4.4.3 ScFvs monomer-dimer equilibrium 133
4.4.4 Confirmation of binding to TREM2 134
4.5 Development and validation of antibody IgG1 and Fab conversions 136
4.6 Discussion 139
Chapter 5 Structure and epitope determination of TREM2-scFv complexes 143
5.1 Introduction 143
5.2 Structure of TREM2 (a.a.19-131) and scFv-2 146
5.2.1 Optimisation of complex formation and initial screening 146
5.2.2 Optimisation of crystallisation of TREM2-scFv-2 complex 148
5.2.3 Optimisation of the solubility of TREM2-scFv complexes 153
5.2.4 Structure of TREM2 with scFv-2 154
5.3 Structure of TREM2 (a.a.19-131) and (a.a.19-174) with scFv-4 157
5.3.1 Optimisation of complex formation and initial screening 157
5.3.2 Structure of TREM2 with scFv-4 160
5.4 Comparison of TREM2 structures and biological assembly prediction 163
5.5 Mapping of scFv-3 and TREM2 epitope with use of mAb conversions 169
5.6 Discussion 170
Chapter 6 Functional impact of scFvs and mAb antibodies on cells expressing TREM2 and DAP12 175
6.1 Introduction 175
6.2 Expression levels of TREM2 in THP-1, HEK-TREM2/DAP12 and iPSC-derived macrophages 179
6.3 Impact of scFvs on soluble TREM2 and internalisation 182
6.3.1 Reduction of sTREM2 accumulation in HEK293 conditioned medium by scFv-3 and scFv-4 184
6.3.2 Dimers of scFv-3 and scFv-4 lead to TREM2 internalisation 188

6.4 ScFv dimers are modest agonists of TREM2 in iPSC-macrophages. 195
6.4.1 ScFvs do not cause lasting TREM2 internalisation in iMac cells... 196
6.4.2 ScFvs induce shedding reduction and SYK signalling in differentiated THP-1 cells..... 198
6.5 Activity of monoclonal antibody conversions in iMac cells..... 200
6.6 Validation of a physiological iMac ligand for further studies of the functional properties of derivative mAbs 202
6.7 Discussion 204
6.7.1 Comparison of scFvs with published mAb molecules 207
Chapter 7 Conclusions and future plans 212
Appendix …….....
Bibliography……. ..... ……..225

Abbreviations

ADAM	Disintegrin and metalloproteinase
ADC	Antibody-drug conjugate
APOA1	Apolipoprotein A1
APOE4	Apolipoprotein E ε4
APOE	Apolipoprotein E
Aβ	Amyloid-β
BACE1	β-secretase 1
BCR	B-cell antigen receptor
BLI	Bio-layer interferometry
BMM	Bone marrow-derived macrophages
CDR	Complementarity determining regions
Cryo-EM	Cryogenic electron microscopy
CSF-1	colony-stimulating factor-1
CNS	Central nervous system
CSF	Cerebrospinal fluid
CV	Column volumes
DAP12	DNAX-activation protein 12
DOPS	1,2-dioleoyl-sn-glycero-3-phospho-L-serine
DPBS	Dulbecco's PBS
Dsb	Disulfide bond formation proteins
E. coli	Escherichia coli

EC50	Half maximal effective concentration
EGFR	Epidermal growth factor receptor
ELISA	Enzyme-linked immunosorbent assay
Endo F1	Endoglycosidase F1
Endo H	Endoglycosidase H
ER	Endoplasmic reticulum
Fab	Antigen-binding fragment
FAD	Familiar Alzheimer’s disease
FBS	Fetal bovine albumin
Fc	Fragment crystallisable
Fv	Variable fragment
GAGs	Sulfated glycosaminoglycans
GlcNAc	N-acetylglucosamine
GntI	N-Acetylglucosaminyltransferase-I
GPCR	G-protein-coupled receptors
GWAS	Genome wide association studies
HDL	High-density lipoprotein
HSPGs	Heparan sulfate proteoglycans
HTP	High-throughput
HTRF	Homogeneous Time Resolved Fluorescence
iMac	Human iPSC-derived macrophages
Ig	Immunoglobulin

IgSF	Immunoglobulin superfamily
IL-1	Interleukin-1
IMAC	Immobilised metal affinity chromatography
KO	Knockout
LC-MS/MS	Liquid chromatography with tandem mass spectrometry
LDLR	LDL-receptor
LIC	Ligation independent cloning
LOAD	Late-onset Alzheimer’s disease
mAb	Monoclonal antibodies
MALS	Multi-angle light scattering
MBP	Maltose-binding protein
MCI	Mild cognitive impairment
MDM	Monocyte-derived macrophages
MS	Mass spectroscopy
mTOR	Mammalian target of rapamycin
NMR	Nuclear magnetic resonance
NF-κB	Nuclear factor kappa B
NFAT	Nuclear factor of activated T-cells
NHD	Nasu-Hakola disease
OmpA	Outer-membrane protein
PDB	Protein Data Bank
PEI	Polyethylenimine

PNgase F	N-glycosidase F
PMA	Phorbol-12-myristate-13-acetate
P-SYK	SYK phosphorylated at Tyr525/526
RTPPmu	Receptor-type tyrosine-protein phosphatase mu
sAPPβ	Soluble amyloid precursor protein-β
scFvs	Single-chain variable fragments
SEC	Size exclusion chromatography
Sf9	Spodoptera frugiperda
SHIP-1	SH2 Domain-Containing Inositol Phosphatase 1
SNP	Single nucleotide polymorphisms
SP	Signal peptide
SPR	Surface Plasmon Resonance
sTREM2	Soluble TREM2
SYK	Spleen tyrosine kinase
TEV	Tobacco Etch Virus
TOF	Time of flight
TREM2	Triggering receptor expressed on myeloid cells 2
TSA	Thermal shift assay
TYROBP	Protein tyrosine kinase binding protein
VH	Variable heavy
VL	Variable light
WT	Wild-ty

Chapter 1

Introduction

1.1 Alzheimer's disease

A single case of the disease first described over a hundred years ago by Alois Alzheimer has since become a global healthcare issue, with up to 121 million cases projected by 2050 (Patterson C, 2018). The first patient, Auguste D, had symptoms including memory loss, paranoia, sleep disturbances, and disorientation (Alzheimer, 1906; Alzheimer et al., 1995). A post-mortem examination of the brain revealed the hallmarks of the disease known today as Alzheimer's disease (AD): decreased brain volume, Amyloid Beta plaques, and Tau neurofibrillary tangles.

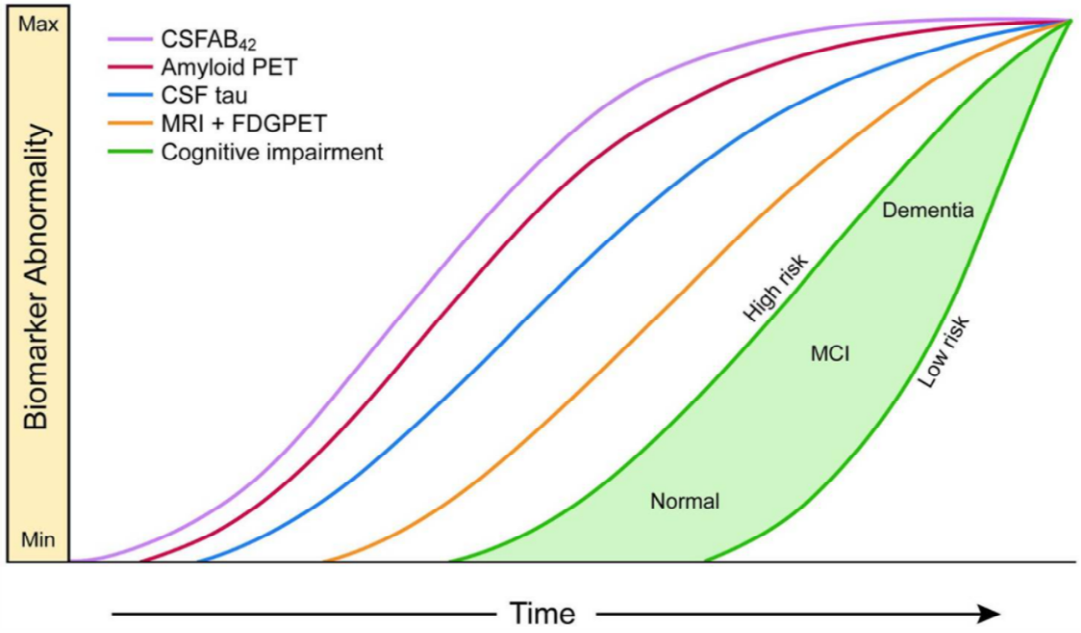
Alzheimer's disease is a type of neurodegenerative disorder with dementia as a major symptom. Dementia is characterised as progressive cognitive decline in patients suffering from various diseases of the central nervous system (CNS), which can also include vascular dementia, dementia with Lewy bodies and frontotemporal dementia (FTLD) (Prado et al., 2019). Early symptoms of dementia can be confused with normal ageing but will lead to more severe deterioration in memory, cognition, and practical abilities, and AD patients will eventually require specialist care.

1.1.1 Epidemiology of AD and environmental risk factors

A report from 2018 estimates that by 2050 there will be 152 million people worldwide suffering from dementia and that 50-75% will be caused by Alzheimer's disease (Patterson, 2018). The driving force behind the staggering numbers is caused by increased life expectancy, especially in developing countries. In 2018, dementia and AD became the leading cause of death in England and Wales (Office for National Statistics, 2018). The cost of dementia to the economy, which includes but is not limited to the economic price of "informal" caregivers, reached 1 trillion US dollars in 2018 (Patterson, 2018). The social and psychological cost and impact on individuals and their families are much more challenging to estimate. The estimated economic burden in the UK alone is estimated at £26 billion per annum (Lewis et al., 2014).

The chances of developing late onset Alzheimer's disease (LOAD), the most common form of dementia, increase with age with the probability doubling every five years (Hebert et al., 2013). In the US, the AD risk rises from 3% at the age of 65-74 to 17% at 75-85 and 32% above 85 (Hebert et al., 2013). What makes AD unique is the extended 15-20 year pre-clinical stage and a shorter 7-10 year-long clinical stage when patients develop symptoms and are diagnosed (**Figure 1.1**).The length of the pre-clinical stage is one of the most challenging features of AD with negative implications for diagnosis, clinical trial enrolment and the potential length of necessary treatment. A significant effort has been undertaken to identify AD biomarkers that would allow diagnosis of patients at risk before symptom onset (Jack et al., 2013; Selkoe and Hardy, 2016). In 2020, the lancet published a report to assess environmental risks of AD, which identified poor education, hypertension, obesity, hearing loss, traumatic brain injury, alcohol misuse, smoking, depression, physical inactivity, social isolation, diabetes, and

air pollution (Livingston et al., 2020). These 12 factors are predicted to account for 40% of cases of LOAD worldwide.



(Figure from Jack et al., 2012)

Figure 1.1. A hypothetical temporal model of amyloid hypothesis including AD biomarkers in pre-clinical stage. *The white area of the graph represents the pre-clinical stage where the levels of tau and amyloid deposition increase from the minimum to maximum. The Green area is the clinical stage where cognitive impairment can be diagnosed, and the age of onset will vary according to each individual. The biomarkers, which increase with time in the clinical and pre-clinical stage, are: Aβ42 peptide in the cerebrospinal fluid (CSF) or later amyloid PET – purple and red lines respectively, tau in CSF-blue line, and lastly neurodegeneration be measured by fluorodeoxyglucose (FDG)-PET or MRI. The disease progression is expressed as time. Patients at high risk have a cognitive impairment curve shifted to the left on the time axis and patients who are protected have it shifted to the right. This reflects the highly individual response to pathology which is increasing with age in low and high risk groups (Jack et al.,2013, permission for publication in the thesis were obtained from Elsevier).*

1.1.2 Familial AD risk factors

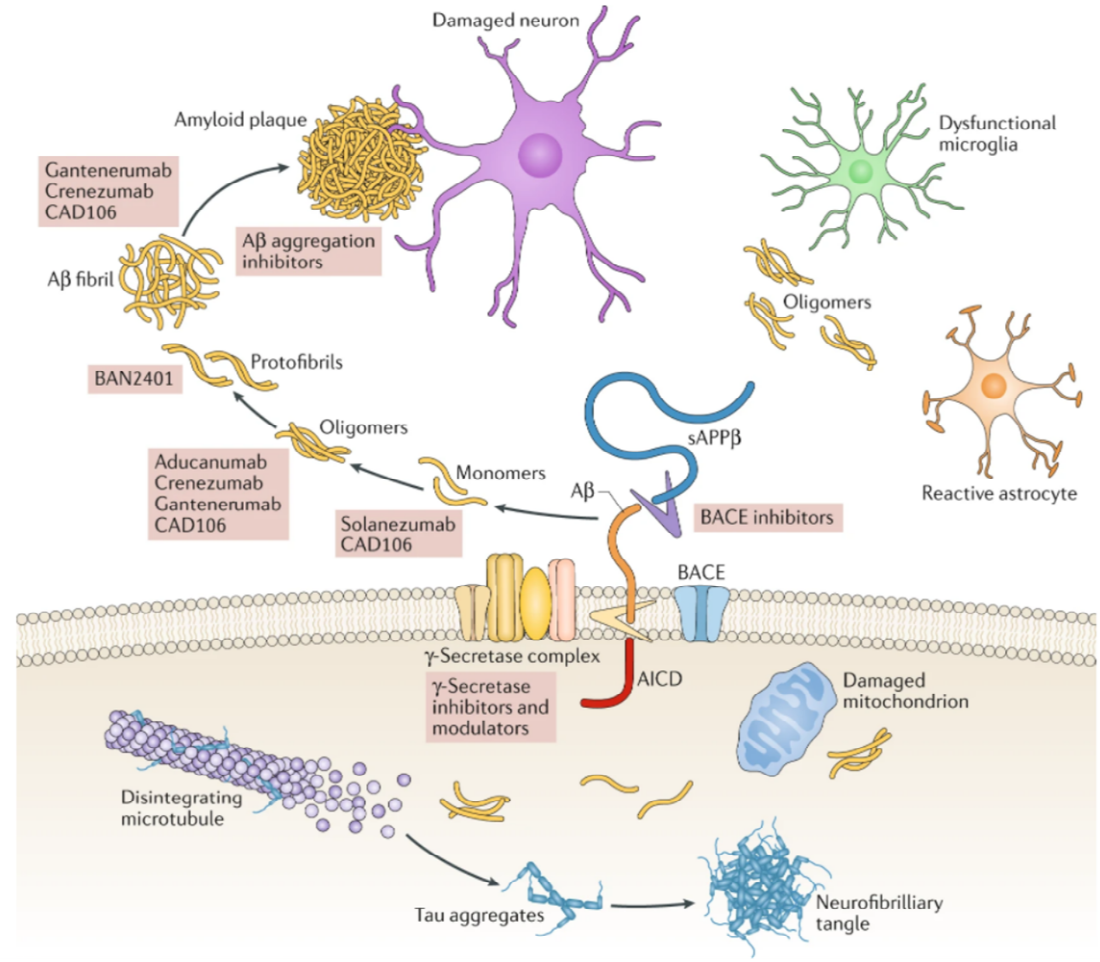
Familial AD (FAD) is a heritable autosomal dominant disorder defined by transparent genetic background and earlier onset of symptoms than LOAD. Despite the low prevalence of FAD (less than 1% of total AD cases), the solid genetic links

profoundly impacted our understanding of AD pathology and led to the development of the first treatments following the amyloid hypothesis (Campion et al., 1999). The amyloid hypothesis posits that peptide called Amyloid β-42 (Aβ-42) lead to the formation of oligomers and β-amyloid aggregates, which trigger the events leading to hyperphosphorylation of TAU and neurodegeneration. Mutations in genes of the Aβ production pathway: presenilin 1 (*PSEN1*) and presenilin 2 (*PSEN2*), and amyloid precursor (*APP*) are characterised by high penetration and always lead to the development of symptoms by the age of 65 in a small fraction of AD cases while the majority of genes causing AD remains unknown (Cacace et al., 2016; Campion et al., 1999; Scheuner et al., 1996; Wingo et al., 2012)

Neuropathology: β-amyloid

The component of senile plaques is a short 42 amino acid-long peptide called Aβ-42, which is a product of proteolytic cleavage of APP by β and γ gamma secretases (**Figure 1.2**). APP is a transmembrane protein of not well-defined function mutated in some FAD patients (Guo et al., 2021; Kang et al., 1987; Taylor et al., 2008). These mutations disrupt the physiological processing of APP and its sequential trimming to short and potentially beneficial Aβ-40 peptide and lead to an increase in less soluble Aβ-42 peptide instead (Kim et al., 2007; Scheuner et al., 1996). With time, Aβ-42 secreted to the extracellular matrix of neurons will start accumulating into oligomers and fibrils of β -sheet and ultimately create large aggregates called plaques. Not surprisingly, the active centre of γ secretase enzyme, which catalyses the cleavage of APP, consists of presenilin 1 or 2, which are mutated in FAD (Scheuner et al., 1996). These mutations lead to a change in the enzyme activity and a subsequent increase in Aβ-42 production (Citron et al., 1997). The discovery of *APP A673T*, a protective allele that was shown to decrease the generation of amyloidogenic species of Aβ *in vitro,*

further validated the therapeutic potential of anti-amyloid approaches (**Figure 1.3**)(Jonsson et al., 2012).



(Figure from Panza et al., 2019)

Figure 1.2. Hallmarks of AD pathology and drugs in phase III clinical trials. *APP is cleaved by γ-secretase complex, which includes presenilin which is coded by PSEN1 or PSEN2, and later by β-secretase 1 (BACE1) releasing Aβ peptide and sAPPβ (sAPPβ). γ-secretase also releases amyloid intracellular domain (AICD). In AD, Aβ-42 production is increased, which leads to oligomerisation and plaque formation. Tau pathology is characterised by the formation of neurofibrillary tangles (NFT) of hyperphosphorylated tau, which cannot bind and stabilise microtubules. The disease is also characterised by reactive astrogliosis and microgliosis. Drugs targeting proteolytic cleavage of APP and aggregation events are currently in clinical trials (Panza et al., 2019, permission to publish the figure was obtained from Elsevier).*

Despite all the gathered evidence, it remains unclear which species: monomers, oligomers, fibrils or aggregates are responsible for downstream cytotoxicity (De et al., 2019; Selkoe, 2008; Wang et al., 2017). Since amyloid aggregates are found in the brains of patients without dementia, it was proposed that FAD and LOAD mutations lead to an acceleration of normally occurring Aβ accumulation or that soluble forms of Aβ are responsible for neuron loss (Haass and Selkoe, 2007). In agreement with the former, loss of function mutations in several genes involved in protein clearance or age-related decrease in removal efficiency has been identified as a relevant factor in neurodegenerative diseases (Ciryam et al., 2016; Hardy, 2019; Mawuenyega et al., 2010).

Neuropathology: TAU

Another hallmark of AD is intracellular neurofibrillary tangles (NFT) of abnormally phosphorylated microtubule-associated protein TAU (*MAPT* gene) present in neurons and glial cells in the CNS (Buée et al., 2000). TAU has a vital role in stabilising microtubules, and mutations in *MAPT* either increase the aggregation rate of TAU or decrease its ability to bind microtubules. As in the case of Aβ-42, the subsequent increase in soluble TAU leads to a supersaturated state leading to the formation of β-sheet containing tangles (**Figure 1.2**). TAU aggregates are present in several neurodegenerative disorders collectively named primary tauopathies when observed in the absence of amyloid pathology (Buée et al., 2000).

Due to asymmetrical and extended shape, neurons require a well-functioning cytoskeleton and efficient transport of signalling molecules to the synapses. These requirements create a particular vulnerability to dysregulation of TAU physiological functions and result in the appearance of dystrophic neurites close to amyloid deposits

(Jin et al., 2011; Roy et al., 2005). Dystrophic neurites are swollen neuronal processes containing aggregated proteins and various organelles, including lysosomes and autophagosomes, which contribute to synaptic loss and are often accompanied by activated microglia and astrocytes (Condello et al., 2015; Sharoar et al., 2019).

Clinical trials targeting amyloid and TAU

Despite the overwhelming evidence that various Aβ-42 forms can lead to cytotoxicity, therapeutics directed at the amyloid production pathway did not produce positive phase III clinical outcomes yet (Huang et al., 2020; Panza et al., 2019). The therapeutic approaches focused primarily on the inhibition of β-secretase or γ-secretase or reduction of Aβ deposits by monoclonal antibodies. While the adverse side-effects caused by inhibition for secretases could be predicted, anti-Aβ antibodies did not produce positive outcomes in trials of solanezumab, gantenerumab, ponezumab or bapineuzumab (**Figure 1.2**) (Makin, 2018; Mullard, 2021a; Panza et al., 2019). The recent controversy surrounding the U.S. Food and Drug Administration (FDA) decision to approve aducanumab, an antibody is targeting Aβ plaques, which did not provide satisfactory cognitive improvement in patients, highlights growing desperation to find treatment for AD (Mullard, 2021a). One of the most common arguments used to explain these failures is too late intervention in patients with already established plaque burden or wrong Aβ species targeted by the therapeutics.

Contrary to amyloid, NFT TAU levels correlate positively with neuronal loss and AD progression, which is consistent with reports of dependency of amyloid toxicity on TAU expression in mice (Braak and Braak, 1991; Gómez-Isla et al., 1997; Jin et al., 2011; Roberson et al., 2011; Spillantini et al., 1998). As a result, many researchers hypothesise that developing anti-TAU agents can be a better strategy in slowing down

neuronal loss and cognitive decline. While most drugs targeting TAU posttranslational modifications or anti-TAU vaccines are still undergoing clinical trials, semorinemab that targets N-terminal sequence of TAU has failed the recent phase III studies (Mullard, 2021b). As in the case of amyloid, too late intervention or the wrong subtype of TAU target were suggested as reasons behind the drug failure. More drugs targeting TAU-aggregation or TAU expression are also currently in development. For years AD research focused on pinpointing a single culprit, but after three decades of failed trials, it is clear that disease aetiology is much more complex, with many factors contributing to neuronal death and cognitive dysfunction.

1.1.3 Late-onset AD and GWAS risk loci

Patients with LOAD develop the same hallmarks of neurodegeneration as FAD patients but with later onset and without a clear mechanism leading to an increase in Aβ-42 production. In addition to environmental factors, the significant risks for LOAD are age and genetic susceptibility caused by single nucleotide polymorphisms (SNP). The heritability of LOAD can be as high as 75%, as demonstrated by the study of twins (Gatz et al., 2006). However, genetic aetiology is described as oligo- or polygenic, where products of many SNPs result in the onset of disease (Escott-Price et al., 2015; Zhang et al., 2020). Since LOAD is the leading cause of dementia worldwide, an increased effort to identify these genetic factors by genome-wide association studies (GWAS) has been made in the last 20 years. It resulted in the discovery of 44 gene loci associated with increased risk of AD with selected genes implicated in Aβ production pathway, immune functions, lipid and cholesterol metabolism, endocytosis and angiogenesis (**Figure 1.3**) (Jansen et al., 2019; Jun et al., 2016; Kunkle et al., 2019; Lambert et al., 2013; de Rojas et al., 2021; Sims et al., 2017; Zhang et al., 2020).

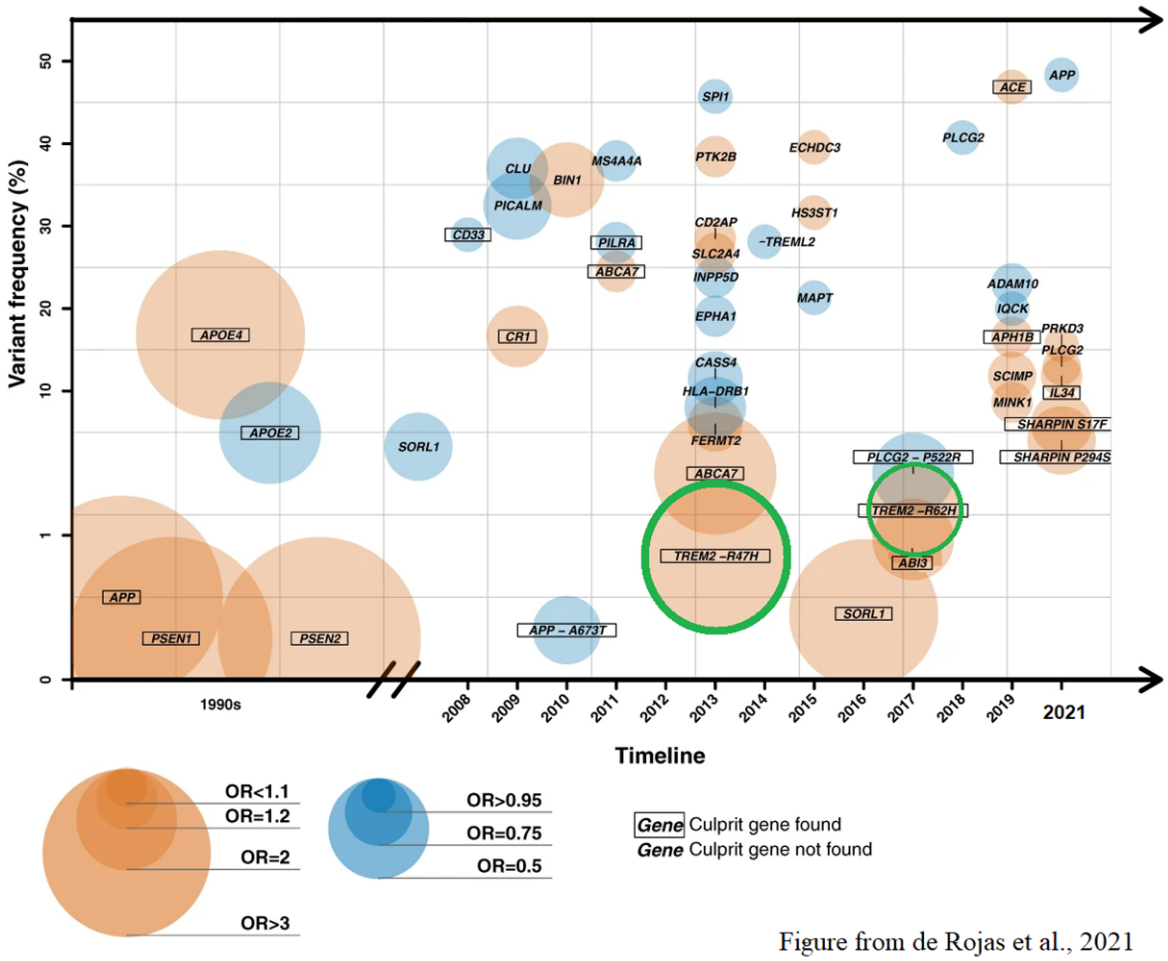


Figure from de Rojas et al., 2021

***Figure 1.3. History of genetic risk factors for AD**. The timeline of discovery is plotted against variant frequency in the population. For common variants, only signals firmly replicated in large meta-GWAS were shown; for rare variants, only variants widely replicated without conflicting reports are shown (Jansen et al., 2019; Jun et al., 2016; Kunkle et al., 2019; Lambert et al., 2013; de Rojas et al., 2021; Sims et al., 2017). The GWAS risk alleles associated with AD are shown in orange circles, while protective alleles are shown in blue. Odds ratio (OR) is shown by increasing the size of the circle, TREM2 rare variants are shown in the green circle (de Rojas et al., 2021, the permission to include the figure in this thesis was obtained under conditions described in Creative Commons CC-BY licence).*

Apolipoprotein E

Apolipoprotein E (*APOE*) is exceptional among LOAD risk genes since the isoform ε4 (*APOE4*) confers the highest genetic risk for LOAD. One or two copies of ε4 increase the chances of developing AD by 3 and 12-fold with a shift of the disease

onset by up to 9 years per single copy (**Figure 1.3**) (Corder et al., 1993; Raber et al., 2004). In contrast, the ε3 allele is the most common and neutral in terms of the risk, and the ε2 allele is protective, strengthening the significance of *APOE* in AD (**Figure 1.3**) (Corder et al., 1993). APOE is the most abundant brain apolipoprotein secreted by astrocytes and microglia and is lipidated to form lipoprotein particles containing cholesterol and lipids and, as a consequence, is a major lipid-transporter in the CNS (Pitas et al., 1987; Yamazaki et al., 2016, 2019).

Naturally, the direct link between *APOE* isoforms and Aβ deposition has been investigated in depth over the last twenty years. A number of studies confirmed increased amyloid seeding and subsequent amyloid deposition in *APOE4* carriers compared to *APOE3* (Castellano et al., 2011; Huynh et al., 2017; Liu et al., 2017; Schmechel et al., 1993). The early hypothesis proposed that APOE is an Aβ-42-clearance chaperone, and a number of changes in the way isoforms interact with various ligands and receptors were demonstrated (Castellano et al., 2011; Yamazaki et al., 2016, 2019). The latter hypothesis contrasts with results of a study showing that Aβ-42 is removed independently of APOE by low-density lipoprotein receptor-related protein 1 (LRP1) receptor in astrocytes in physiological conditions, and *APOE* isoforms compete differentially with Aβ for receptor binding, resulting in a decrease of Aβ removal (Verghese et al., 2013).

Interestingly, the protective variants of *APOE* are classified as loss of function mutants. Similarly to *APOE2*, a Christchurch *APOE3* mutation (*APOE3CH*) was shown to reduce interaction with heparan sulfate proteoglycans (HSPGs) and LDLR receptors (**Figure 1.3**) (Arboleda-Velasquez et al., 2019; Mahley et al., 1999). The loss of function of these isoforms has a positive effect on AD, as shown by a single case of *PSEN1* carrier homozygous for *APOE3CH*. Despite significant amyloid load, the

patient did not develop TAU pathology or dementia symptoms, albeit more cases are necessary to confirm the protective effects of this variant (Arboleda-Velasquez et al., 2019). Consistent with an independent role for APOE4, the murine *ApoE4* isoform was found to mediate neurodegeneration even in the absence of amyloid pathology, as shown by increased microglia activation and neuron loss in P301S Tau model (Shi et al., 2017). Furthermore, mutations in lipid metabolism genes such as *ABCA7*, together with immune genes, have been identified as significant AD risk factors by GWAS studies which is consistent with studies on the relationship between lipids and inflammatory signalling (**Figure 1.3**) (Jones et al., 2010; Varshney et al., 2016; Yamazaki et al., 2016) Interestingly, roles for lipids and immune cells feature strongly in other age-related diseases such as cardiovascular disease (Varshney et al., 2016).

1.2 Neuroinflammation, microglia and TREM2

1.2.1 Neuroinflammation

A growing number of AD risk genes identified by GWAS are found to cluster with immune system functions (Jones et al., 2010; Karch and Goate, 2015). Among them are genes involved in complement activation (Complement receptor type 1, *CR1*), immune cell activation and signalling (Phospholipase C gamma 2, *PLCG2* ; Sialic acid-binding Ig-like lectin 3, *CD33*; membrane-spanning 4-domains subfamily gene cluster, *MS4A*; Inositol Polyphosphate-5-Phosphatase D, *INPP5D/SHIP-1*) and actin cytoskeleton (*ABI3*, Abelson interactor 3) (**Figure 1.3**) (Efthymiou and Goate, 2017; Jones et al., 2010; Karch and Goate, 2015; Lambert et al., 2013; de Rojas et al., 2021). These findings were consistent with the early observation of increased numbers of activated microglia and astrocytes by Alzheimer and were later validated by the

presence of high concentrations of pro-inflammatory cytokines such as interleukin-1 (IL-1) in AD patient brain samples (Griffin et al., 1989, Alzheimer et al., 1995). Even in the absence of AD mutations, traumatic brain injury, one of the environmental risks factors of neurodegeneration, triggers neuroinflammation, which can persist years after the accident (Livingston et al., 2020; Shitaka et al., 2011; Smith et al., 1997).

The inflammatory responses are considered to be a secondary process triggered by other factors such as amyloid or tau deposits but are thought to fuel the processes leading to further pro-inflammatory signals. As an example, early *in vitro* studies uncovered a mechanism of upregulation of APP expression and processing in response to IL-1 release suggesting an additional role in amplifying AD pathology (Dash and Moore, 1995; Donnelly et al., 1990). Hence, despite this potentially causative relationship, chronic inflammation may be responsible for the significant neuron loss by complement activation, upregulation of cytokine and chemokine production, nitric oxide, and reactive oxygen release (Gomez-Nicola et al., 2013; Holmes and Butchart, 2011).

Consistently, an early observation that long-term users of nonsteroidal anti-inflammatory drugs (NSAID) have a lower incidence of AD led to several attempts trialling NSAID use for prevention of AD, which did not meet clinical endpoints (Miguel-Álvarez et al., 2015). These disappointing results may indicate a much more complex relationship between inflammation and neurotoxicity or inappropriately late timing of therapeutic intervention in AD, which has plagued early clinical trials (Hoozemans et al., 2011).

1.2.2 Microglia

Microglia are the primary cell type producing pro-inflammatory cytokines and modulating the inflammatory response in the central nervous system (CNS). These brain resident macrophages separated from other myeloid precursors early during embryo development by the blood-brain barrier (Ajami et al., 2007; Bruttger et al., 2015; Ginhoux et al., 2010). As phagocytic cells, they survey the environment similarly to macrophages but also play a role in brain neurogenesis and development (Cunningham et al., 2013; Gomez-Nicola and Perry, 2015; Nimmerjahn et al., 2005; Paolicelli et al., 2011; Schafer et al., 2012). The latter involves synapse pruning by activation of the complement cascade and autophagy, a process thought to be dysregulated in neurological disorders such as schizophrenia, autism and AD (Kim et al., 2017, 2013; Schafer et al., 2012; Sellgren et al., 2019). Consequently, microglia depletion was shown to be beneficial in some animal models of neurodegenerative diseases (Mancuso et al., 2019; Obst et al., 2020a).

Microglia appeared to be the first cells responding to damage in the CNS and were shown to be attracted to the damage by recognising molecular patterns associated with cell death as shown by accumulation in the proximity of amyloid deposits (Condello et al., 2015; Davalos et al., 2005; Duan et al., 2009; Gehrmann et al., 1993; Yuan et al., 2016). Because of that, microglia are highly adaptive and can switch from surveillance mode to a more proliferative state with altered gene expression and cell morphology (Davalos et al., 2005; Nimmerjahn et al., 2005). A rapid increase in microglia numbers termed microgliosis was already noted by Alzheimer and is found in many CNS disorders (Ajami et al., 2007; Gomez-Nicola et al., 2013; Graeber et al., 1988). Historically, different states of microglia were termed as either anti-inflammatory M1 or pro-inflammatory M2, a view that is now considered overly

simplistic as microglia exist in a dynamic range of states (Gomez-Nicola and Perry, 2015; Ransohoff, 2016). The latter was established thanks to the rise of single-cell and single-nuclei RNA sequencing (scRNA-seq, snRNA-seq) technology, which demonstrated the existence of different microglia populations, including murine disease-associated microglia (DAM), which are found in many CNS diseases (Deczkowska et al., 2018; Keren-Shaul et al., 2017; Olah et al., 2020).

1.2.3 TREM2

Among the genes upregulated in DAM is the Triggering receptor expressed on myeloid cells 2 (*TREM2*), previously identified by GWAS as a prominent AD risk factor (**Figure 1.3**) (Guerreiro et al., 2013; Jonsson et al., 2013; Robinson et al., 2017). The *TREM2 R47H* rare variant confers a four-fold increase in AD risk, second after *APOE4* but with significantly lower frequency in the population (**Figure 1.3**) (Guerreiro et al., 2013; Jonsson et al., 2013).

TREM2 structure

TREM2 is a type 1 single transmembrane receptor expressed on the surface of some myeloid cells, including tissue-resident macrophages such as osteoclasts in the bone and microglia in the brain (Lee et al., 2021a). Consequently, homozygous mutations in TREM2 cause aggressive early-onset dementia with bone fractures called Nasu-Hakola disease (NHD) (Hakola, 1972; Paloneva et al., 2003). The disease is caused by missense mutations leading to a lack of TREM2 or DNAX-activation protein 12 (DAP12) expression (Paloneva et al., 2002, 2003). The latter, also known as protein tyrosine kinase binding protein (TYROBP), is a common adaptor protein in immune

activation cascades that interacts with receptors to transduce the signal into the cells (Hamerman et al., 2006).

TREM2 belongs to the immunoglobulin (Ig) superfamily and consist of a single Ig V-type domain, stalk sequence and transmembrane domain followed by a short cytoplasmic tail of unknown function (**Figure 1.4a**). The crystal structure of TREM2 extracellular domain (a.a.19-131) confirmed the presence of the classical β-sandwich fold consisting of two sheets of antiparallel β-strands named A, B, C, C', C'', D, E, F, G (**Figure 1.4b**). (Kober et al., 2016; Sudom et al., 2018). The structure of the stalk is unknown; however, the His157 was shown to be the site for disintegrin and metalloproteinase 10/17 (ADAM10/17) protease cleavage resulting in the release of soluble TREM2 (sTREM2) into the extracellular matrix (Thornton et al., 2017) (**Figure 1.5**).

In single Ig domain-containing proteins, three flexible loops termed complementarity determining regions (CDR) are predicted to be involved in ligand recognition (**Figure 1.4c**). Regrettably, the structural data confirming the nature of TREM2 ligands and their interactions with these CDRs remains scarce. In 2018, a hexameric structure of TREM2 Ig-domains with phosphatidylserine soaked in the already formed crystals provided initial evidence for the involvement of CDR2 in phosphatidylserine binding but remains a subject of discussion (PDB:6B8O Sudom *et al.*, 2018). Furthermore, the R47H ligand-recognition mutant X-ray crystal structure did not produce electron density in the CDR2 region, which could be the result of a significant remodelling event leading to structural disorder or experimental conditions (PDB:5UD8 Sudom *et al.*, 2018). Byrne et al. noted that all TREM2 structures deposited previously in the PDB contain crystal-packing interactions between CDR2 of two neighbouring TREM2 molecules with resulting in crystallisation induced

conformational changes and negative impact on TREM2-ligand structural studies (PDB:6XDS) (Byrne et al., 2021).

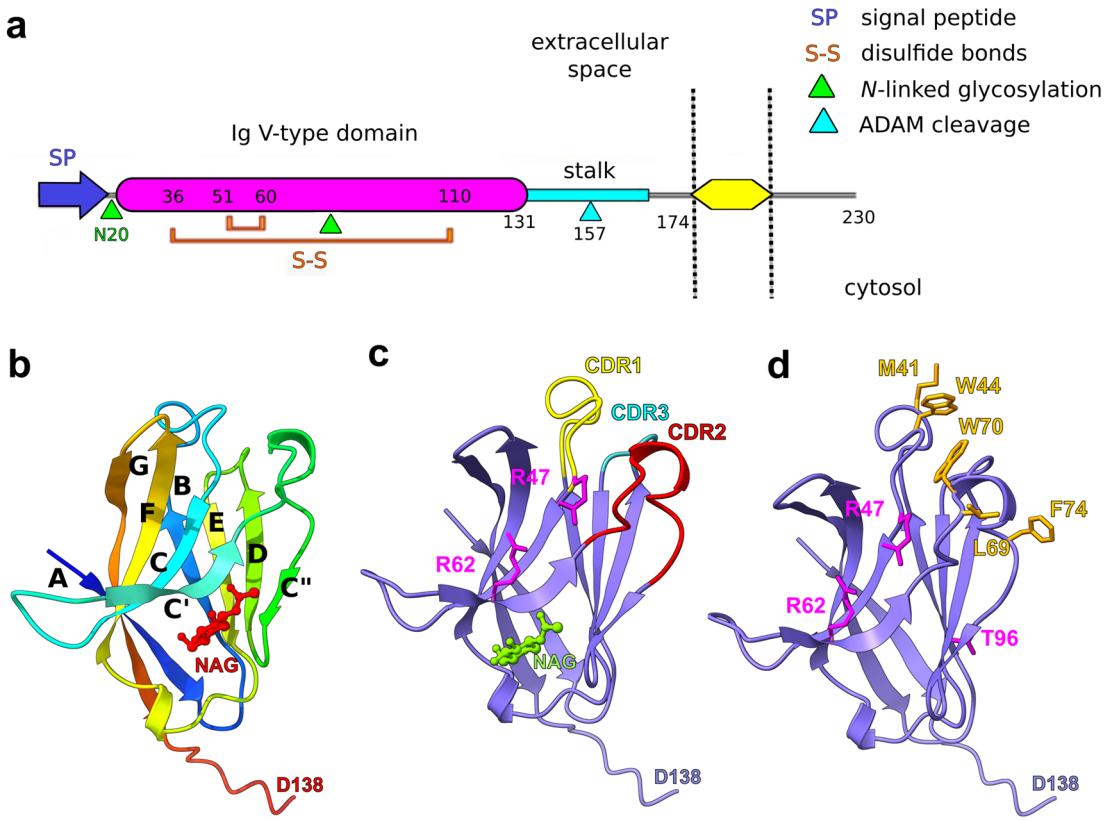


Figure 1.4. TREM2 domains and structure. *(a) Catoon representation of TREM2 domains. TREM2 consists of signal peptide (a.a.1-18), Ig V-type domain (a.a.19-131), stalk (a.a.132-174), transmembrane domain (a.a.175-197) and cytoplasmic tail (a.a.198-230). The signal peptide (SP) is absent in mature protein and the TREM2 Ig domain has two glycosylation sites (shown as green triangles) and two disulphide bridges (S-S). Amino acids important to domain booundaries and the ADAM cleavage site within the stalk are numbered.TM- transmembrane domain. (b-d) Crystal structure of TREM2A (a.a.19-174, 6Y6C) showing (a) β-strand organisation and glycosylation in red; (b) CDR1-3 shown in red, yellow and cyan with R47 and R62 sidechains shown in pink, (c) hydrophobic patch aminoacids M41, W44, L69, W70, F74 identified by Kober et al. shown in gold with AD mutants in pink (Kober et al.,2021).*

More recently, a hydrophobic patch amino acids Met41, Trp44, Leu69, Trp70, Phe74 acids were shown to be crucial for interactions with purified APOE *in vitro* (**Figure 1.4c**) (Kober et al.2021). Despite this progress, there are no reliable structures

of TREM2 with binders and the mechanisms of ligand recognition and subsequent conformational changes leading to signal transduction remain unknown.

The transmembrane domain (TM) of TREM2 contains a motif with positively charged lysine residue (Lys186) responsible for interaction with two negatively charged aspartic acid residues (Asp50) in DAP12 dimer, which is a conserved mode of interaction in immuno-receptors and provides an explanation for Nasu-Hakola disease aetiology (Call, 2010; Feng et al., 2005; Knobich, 2015; Lanier et al., 1998) (**Figure 1.5**). The nuclear magnetic resonance (NMR) experiments revealed the presence of a kinked α-helix in TREM2 TM, which undergoes a conformational change into continuous helix and stabilisation upon interaction with DAP12 (Steiner et al., 2020). The transmembrane C-terminal fragment of TREM2 (CTF) which remains after ADAM cleavage, is further cleaved by γ-secretase, after which interaction between DAP12 and TREM2 terminates (Steiner et al., 2020, Wunderlich et al., 2013) (**Figure 1.5**).

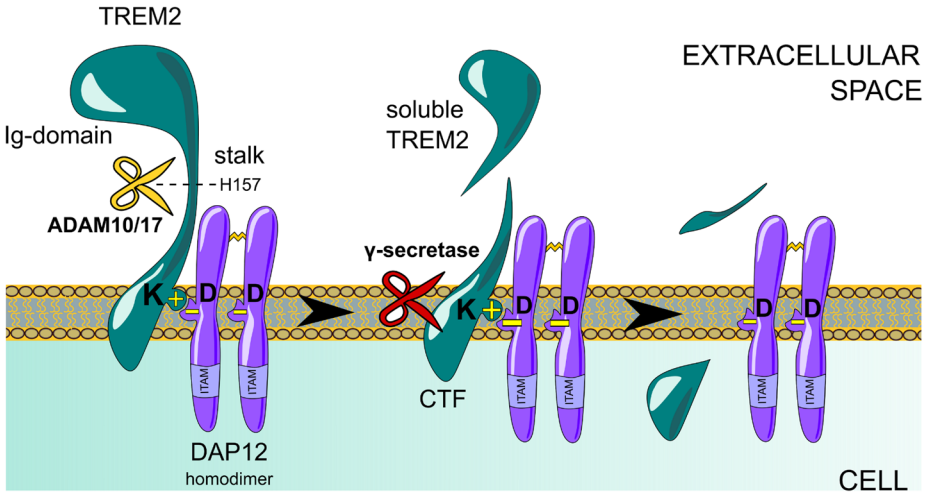


Figure 1.5. Sequential proteolytic cleavage of TREM2-DAP12 complex. *TREM2 is shed by ADAM sheddase followed by cleavage by γ-secretase. Cleavage by γ-secretase is thought to*

terminate any signalling. CTF-C-terminal fragment of TREM2, H157- ADAM10/17 cleavage site in TREM2 stalk, D-aspartic acid, L-lysine.

TREM2 mutations

Single point mutations of TREM2 mutations have been implicated in many neurodegenerative disorders (Jay et al., 2017a; Yeh et al., 2016) (**Figure 1.6**). Many of these mutations result in the expression of an incorrectly folded protein which has reduced surface expression (Kleinberger et al., 2014; Kober et al., 2016; Thornton et al., 2017; Yeh et al., 2016). The other mutations are located in the Ig-like domain and decrease TREM2 interactions with its ligands (Yeh et al., 2016). Of particular interest are mutations causing AD: R47H and R62H in the proximity of TREM2 CDRs but also H157Y, a mutant of the shedding site (Guerreiro et al., 2013; Jiang et al., 2016; Jin et al., 2014; Jonsson et al., 2013; Sims et al., 2017; Song et al., 2017; Thornton et al., 2017).

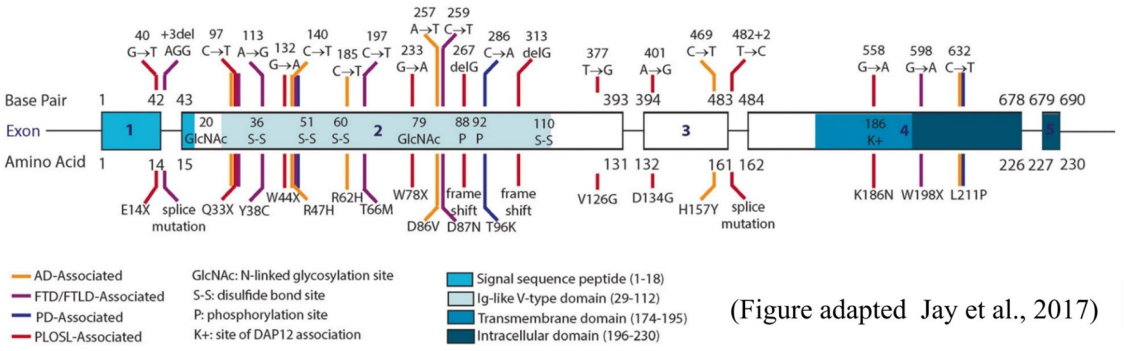


Figure 1.6 TREM2 variants are associated with neurodegenerative disorders. *TREM2 mutations and locations in DNA and protein sequence are shown. TREM2 has been implicated in Nasu-Hakola disease (NHD/PLOSL), Alzheimer's disease (AD), frontotemporal dementia (FTD), frontotemporal lobar dementia (FTLD) and Parkinson's disease (PD). The majority of the mutations are located in the Ig domain in exon 2 (Part of the figure used from Jay et al., 2017, Permission to publish figure was obtained under conditions described in Creative Commons CC-BY licence).*

TREM2 R47H was discovered first as a prominent factor for AD by GWAS studies (Guerreiro et al., 2013; Jonsson et al., 2013; Robinson et al., 2017). TREM2 R47H substitution is located between CDR1 and CDR2 TREM2 loop and is well established as a ligand-binding mutant after studies demonstrating decreased ability to bind lipoproteins, lipids and Aβ and phagocytic defects (Atagi et al., 2015; Nugent et al., 2019; Wang et al., 2015b; Yeh et al., 2016) (**Figure 1.4b**). Although crystal structures of TREM2 R47H has been solved, the region of interest is missing from the final X-ray model and authors concluded R47H leads to destabilisation of CDR loops and resulting structural disorder (Sudom et al., 2018). More recently, another mutation located in the same region, R62H, was shown to increase the risk of AD and cause reduction in Aβ binding (Sims et al., 2017; Song et al., 2017). Kober et al. proposed that the TREM2 region consisting of Arg62, Arg47 but also Asn68, Arg76, Arg77 creates a functional basic patch on the TREM2 surface which is essential to ligand binding and is reduced by the mentioned mutations (Kober et al., 2016). However, work by Dean et al. suggested that TREM2 mutations instead lead to the destabilisation of CDR loops of Arg47 and Arg62 is not fully understood.

The H157Y mutation leads to increased cleavage of TREM2 by ADAM proteases and potential decrease of active TREM2 on the surface of microglia (Schlepckow et al., 2017; Thornton et al., 2017). As a result, H157Y mutant had decreased activation in response to ligands and a phagocytosis defect similarly to ligand binding mutants (Schlepckow et al., 2017; Song et al., 2017). Thus, the discovery of the shedding site mutant revealed a new potential for therapeutic interventions at the TREM2 stalk sequence.

TREM2 in animal models of AD

The association between *TREM2* variants and an increased risk of AD sparked a significant body of work using *Trem2* knockout (KO) animal models. Early work modelling of TREM2 deficiency in AD animal models was primarily focused on the direct impact on the levels of amyloid due to the importance of the amyloid hypothesis. Studies of TREM2 depletion in 5xFAD and APP/PS1 mice led to conflicting results regarding TREM2 effect on Aβ at different stages in AD pathology (Jay et al., 2015, 2017b; Meilandt et al., 2020; Wang et al., 2015b, 2016). However, a beneficial impact on amyloid accumulation, neurite dystrophy and cognitive functions was supported by a study where human TREM2 was over-expressed in 5xFAD mice (Lee et al., 2018a). On the other hand, the acute attempts to decrease murine TREM2 expression at different stages resulted in a dramatic decrease of plaque load and microglia accumulation but only when TREM2 expression was inhibited in mice with already established Aβ pathology (Schoch et al., 2021). These results can partially be explained by differences in expression levels of human transgenes containing FAD mutations, mice age, genetic background, pathology accumulation rates or the highly dynamic and complex regulation of TREM2 and microglia processes during AD pathology.

While the impact of TREM2 on amyloid deposition remains unclear, TREM2 was consistently shown to change amyloid plaque compaction. *Trem2*$^{-/-}$ or T*rem2*^{R47H} microglia are deficient in microglia barrier formation, raising the proportion of diffuse and more toxic plaques in AD brains, which correlated with increased phosphorylation of TAU and neuronal dystrophy (Meilandt et al., 2020; Wang et al., 2016; Yuan et al., 2016). Recent studies indicate that microglia may actually promote the formation of dense plaques by exclusive phagocytosis of soluble Aβ species by TAM phagocytic receptors, which expression can be regulated by TREM2 (Huang et al., 2021).

Furthermore, the ability of TREM2 to promote the formation of the barrier was shown to decline with age, which reduces the ability of microglia to contain the spread of neuritic dystrophy *in vivo* (Condello et al., 2015; Yuan et al., 2016).

Since most murine AD models do not present both amyloid and TAU pathology, several studies investigated the role of TREM2 in pure tauopathy models. In two studies, TREM2 activated stress kinases and TAU phosphorylation, resulting in brain atrophy and increased neuroinflammation in PS19 and hTau mouse models expressing human TAU (Bemiller et al., 2017; Leyns et al., 2017). A convincing proof for beneficial TREM2 impact comes from TauPS2APP mouse model, which displays both amyloid and TAU tangles characteristic of human AD. In this model, deletion of *Trem2* led to a drastic increase in dystrophic neurites and brain atrophy (Lee et al., 2021b). The damage was also shown to be dependent on the amyloid pathology, suggesting that TREM2 and microglia may be limiting the transition of amyloid pathology to TAU pathology and further toxicity.

Soluble TREM2 resulting from full-length receptor cleavage by ADAM protease has been shown to have pro-inflammatory and pro-survival impact on microglia cells in mice *in vivo* (Zhong et al., 2017, 2019). Furthermore, the injection of recombinant sTREM2 into the mouse brain increased Aβ phagocytosis and reduced amyloid plaque (Zhong et al., 2017). Soluble TREM2 was also found to be increased in cerebrospinal fluid (CSF) of AD patients, possibly due to microglia activation occurring during neuroinflammation (Piccio et al., 2008; Suárez-Calvet et al., 2016). The significance of sTREM2 as a human AD biomarker has also been recently demonstrated by finding that an increased ratio of sTREM2 to phosphorylated TAU was associated with slower brain atrophy and cognitive decline (Ewers et al., 2019).

TREM2 in disease-associated microglia (DAM)

Microglia under conditions of stress such as neurodegeneration, are particularly sensitive to loss of TREM2. Wang et al. have first demonstrated that the changes in TREM2-deficient microglia are also dependent on the presence of pathology in mice (Wang et al., 2015b). Wild-type (*WT*) microglia and *Trem2 KO* cells isolated from mice without any AD genetic background were shown to have a similar transcriptional signature. However, the transcriptional profile of microglia in 5xFAD mice is drastically different to wild type microglia. Upon additional *Trem2* deletion, this unique signature is absent, and microglia resemble *WT* population again (Wang et al., 2015b). These early results implied that microglia deficient in TREM2 are not able to detect CNS damage.

Further studies indicated that TREM2 is necessary to modify the transcriptional program leading to the transition from homeostatic to disease-associated microglia (DAM) (Keren-Shaul et al., 2017; Lee et al., 2021b; Nugent et al., 2019; Ulland et al., 2017; Wang et al., 2015b). DAM transition was shown to trigger a change in the regulation of lipid metabolism and transport, processes necessary for the effective removal of damaged myelin in mice *in vivo* (Gouna et al., 2021; Keren-Shaul et al., 2017; Lee et al., 2021b; Nugent et al., 2019; Ulland et al., 2017). Consequently, pathways upregulated in DAM microglia involved also phagocytosis and lysosomal degradation (Keren-Shaul et al., 2017; Nugent et al., 2019). As a result, TREM2-deficient microglia are defective in the storage and removal of toxic myelin components such as cholesterol esters (CE), which were also shown to induce toxic phosphorylation of TAU in human iPSC-neurons (Gouna et al., 2021; van der Kant et al., 2019; Nugent et al., 2019).

Strikingly, APOE, which is mainly produced by astrocytes, was shown to be up-regulated up to 25 times in DAM than in homeostatic microglia (Keren-Shaul et al., 2017; Krasemann et al., 2017; Nugent et al., 2019). Deletion of *ApoE* led to a very similar phenotype to *Trem2 -/-* mice with observed changes in plaque morphology, decreased microgliosis and increased neuronal dystrophy, implying the existence of an APOE-TREM2 pathway (Keren-Shaul et al., 2017; Krasemann et al., 2017; Nugent et al., 2019). According to Lewcock, APOE expression upregulated by TREM2 activation during DAM transition is required under stress conditions to transport degraded and toxic lipid metabolites from the cell and re-establish homeostasis in the process (Lewcock et al., 2020). The fact that DAM numbers were found to increase with age in the absence of pathology can be attributed to TREM2 response to damaged neurons and myelin phagocytosis during natural ageing (Cignarella et al., 2020; Kleinberger et al., 2017; Nugent et al., 2019).

There are many concerns regarding attempts to model AD in mice. The most significant is the lack of prolonged ageing process during a human lifespan, and that related damage cannot be modelled appropriately in mice. Secondly, despite confirmation of DAM transcriptional profile in human tissue microglia, the signature is more nuanced and spread over few microglia populations (Alsema et al., 2020; Olah et al., 2020). These factors could mean that TREM2 effects on human microglia during AD can be less significant. Additionally, multiple studies imply that depletion of microglia may be beneficial during neurodegeneration despite the proposed beneficial role for TREM2, stressing the potential for negative pro-inflammatory impact of these cells in murine models (Mancuso et al., 2019; Obst et al., 2020a). Finally, because TREM2 regulates highly dynamic processes in microglia, which are challenging to model by animal knockout models where the temporal relationship between AD

pathology and microglia response is lost, TREM2 agonist and antagonist molecules need to be developed to evaluate their therapeutic potential. The latter has been addressed recently by industrial and academic collaborations with the overwhelming evidence suggesting a beneficial TREM2 role in mice models of AD (Cheng et al., 2018; Cignarella et al., 2020; Ellwanger et al., 2021; Fassler et al., 2021; Ibach et al., 2021; Price et al., 2020; Schlepckow et al., 2020; Wang et al., 2020).

TREM2 signalling pathways

TREM2 and DAP12 signalling is part of tightly controlled and conserved signalling cascades, which control immune cells proliferation, survival, activation and inflammatory responses (Billadeau and Leibson, 2002; Ben Mkaddem et al., 2019). The ITAM cascades are considered to be cell-activating elements that lead to increased cell response of immune cells through activation of phosphoinositide 3-kinase (PI3K), protein kinase C (PKC), and calcium mobilisation (**Figure 1.7**) (Ben Mkaddem et al., 2019). The activating elements are balanced with the activation of receptors containing tyrosine-based inhibition motifs (ITIM) and subsequent cross-interplay between the pathways resulting in an elaborate functional immune response (Billadeau and Leibson, 2002; Ben Mkaddem et al., 2019).

The current model of TREM2 activation proposes that DAP12 interacts with TREM2 upon ligand recognition and is necessary to transduce the signal from TREM2. (**Figure 1.7**). The intracellular part of DAP12 contains ITAM motifs, which can be phosphorylated by proto-oncogene tyrosine-protein kinases (SRC) family of kinases at two sites and lead to the recruitment of spleen tyrosine kinase (SYK) and downstream signalling (Lowell, 2011; Peng et al., 2010). In the case of TREM2, many processes such as phagocytosis or lipid metabolism were found to be mediated by PLCγ2, which

generates secondary signalling molecules: inositol 1,4,5-trisphosphate (IP3) and diacylglycerol (DAG) in human iPSC microglia (Andreone et al., 2020). Consequently, *PLCG2 -P522R* variant was recently shown to be protective in AD (**Figure 1.3**, **Figure 1.7**) (Andreone et al., 2020; Takalo et al., 2020). In osteoclasts, TREM2 activation by synthetic mAb allowed to validate the transient nature of SYK signalling cascade that is immediately deactivated by INPP5D/SHIP-1, which is proposed to be part of a large signalling complex at the plasma membrane (Peng et al., 2010)(**Figure 1.7**). SHIP-1 was also found to regulate microglia biology in human iPSC cells (Obst et al., 2020b). Its crucial role is highlighted by the discovery of the protective AD variant by GWAS (**Figure 1.3**) (Lambert et al., 2013).

TREM2 effects on cell survival and proliferation are dependent on Wnt/β-catenin signalling pathway and inhibition of apoptotic AKT/GSK3β pathway in primary mouse microglia (**Figure 1.7**) (Zheng et al., 2017). Furthermore, both SYK and SRC are also components of the colony-stimulating factor-1 receptor (CSF-1R) pathway, which works in synergy with TREM2 β-catenin pathway (Otero et al., 2009; Zou et al., 2008). As a result, TREM2 was shown to be crucial to sustaining microglia viability in the absence of optimal levels of colony-stimulating factor-1 (CSF-1), which is hypothesised to occur during rapid microglia expansion (Otero et al., 2012; Wang et al., 2015b).

TREM2 signalling pathways are implicated in microglia metabolism. Mice lacking TREM2 had disrupted mammalian target of the rapamycin (mTOR) signalling, which regulates ATP levels and biosynthetic pathways (**Figure 1.7**) (Held, 2018; Ulland et al., 2017). More importantly, the relevance of this finding to human CNS disease was confirmed by similar autophagosome accumulation defects in the brains of *R47H* and *R62H* carriers (Ulland et al., 2017). These findings are consistent with the proven role

of TREM2 in the regulation of lipid and cholesterol metabolism during DAM transition (Nugent et al., 2019).

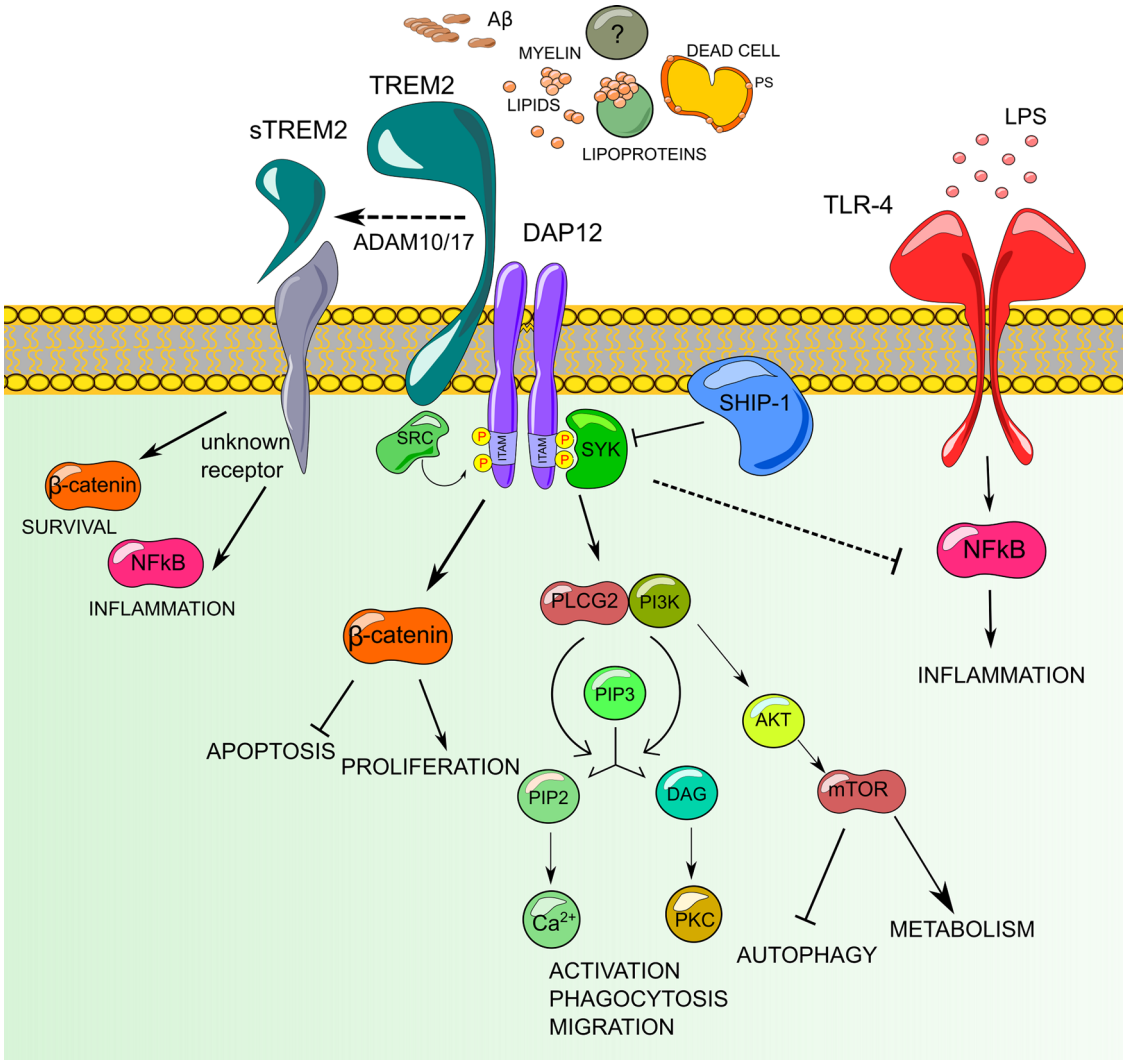


Figure 1.7. TREM2 signalling pathways in microglial. *Upon lipid, lipoprotein or other ligand recognition TREM2/DAP12 membrane complex is phosphorylated by SRC and SYK is recruited to the activation complexes. Phosphorylation of SYK mediates survival, migration, phagocytosis, metabolism and regulated autophagy. In human microglia, many of these functions are mediated by PLCG2. The neuroprotection is achieved by inhibition of the proinflammatory TLR-4 pathway. Soluble TREM2 is cleaved by ADAM10/17 proteases and was shown to stimulate macrophage survival and inflammation independently of the full-length receptor, implying the existence of an unknown sTREM2 TREM2 receptor.*

One of the crucial and beneficial roles of TREM2 during AD is the dampening of excessive immune response resulting in a reduction in neuroinflammation. Consistently with complex regulation of ITAM/ITIM signalling pathways, this neuroprotective role was shown to depend on inhibition of toll-like receptor (TLR) and Fc-receptor (FcR)-mediated production of inflammatory TNF or NF-κB activation, which lead to the production of pro-inflammatory cytokines (Andreone et al., 2020; Hamerman et al., 2006; Ulrich and Holtzman, 2016) (**Figure 1.7**) However, a negative feedback loop in response to LPS was also found to down-regulate TREM2 expression highlighting the many levels of regulation involved in the immune response (Liu et al., 2020).

The outcomes of TREM2 activation can be additionally regulated by ectodomain shedding. The anti-inflammatory activity of TREM2 was shown to persist after the TREM2 shedding, conversely to phagocytosis, which required the presence of intact receptors in the transfected HEK293 cells (Yao et al., 2019). Soluble TREM2 (sTREM2) was also shown to have pro-inflammatory properties and promote survival through AKT–GSK3β–β-catenin pathway and increased phagocytosis independently of full-length receptor in mice *in vivo* (Zhong et al., 2017, 2019). Overall, these *in vitro* studies validate the significance of TREM2 mediated signalling in regulating brain homeostasis and controlling microglia response to changes in CNS.

TREM2 ligands

TREM2 is proposed to interact with ligands by the CDR loops located within its globular ectodomain (Sudom et al., 2018; Kober et al., 2021). In 2015 and 2016, the study by Yeh and Wang et al., identified isolated and purified phospholipids, lipoproteins and lipoprotein particles as TREM2 ligands by biolayer interferometry

(BLI) and NFAT reporter cell activity sensitive to calcium release (Wang et al., 2015b; Yeh et al., 2016). Before that, TREM2 was known as a pattern recognition receptor interacting with bacterial cells and, more recently, mammalian apoptotic cells (Daws et al., 2003; Hsieh et al., 2009; Kober and Brett, 2017; Shirotani et al., 2019).

Initially, the lipids identified to stimulate TREM2 activation included phosphatidylcholine, sphingomyelin, phosphatidylinositol, phosphatidylserine and sulfatides, which are common components of the plasma membrane and neuronal myelin (Nugent et al., 2019; Sudom et al., 2018; Wang et al., 2015b). While the impact of phosphatidylserine, the "eat me" signal which flips to the outer side of the plasma membrane in the apoptotic cells and promotes phagocytosis, has been well documented in the literature, the other interactions remain more challenging to replicate (Bailey et al., 2015; Nagata et al., 2016; Poliani et al., 2015; Scott-Hewitt et al., 2020; Shirotani et al., 2019; Wang et al., 2015b). Importantly, sphingomyelin and phosphatidylserine are the only ligands that were shown to lead to phosphorylation of SYK in human induced pluripotent stem cell (iPSC) macrophages *in vitro* (Nugent et al., 2019).

Interactions of TREM2 with apolipoproteins (APOE, APOJ, APOA and APOB), have been of special interest due to APOE genetic variants and TREM2 involvement in lipid metabolism (Atagi et al., 2015; Keren-Shaul et al., 2017; Krasemann et al., 2017; Lessard et al., 2018; Nugent et al., 2019; Yao et al., 2019). The previous studies on TREM2 interactions questioned whether lipid rather than protein component mediates these interactions. While Atagi et al. have shown that the interaction of TREM2 with APOE does not depend on lipidation, others have reported an increase in affinity when APOE is lipidated (Atagi et al., 2015; Kober et al., 2021). Furthermore, differential binding of TREM2 to APOE isoforms has been investigated with the conclusion that affinity remains similar, suggesting that *APOE4* impact on AD cannot be explained by

changes in the ability to interact with TREM2 (Atagi et al., 2015; Jendresen et al., 2017; Kober et al., 2021). As a consequence, recent findings demonstrated that APOE2, APOE3 and APOE4 lipid complexes are composed of different phospholipids. Consequently, APOE4 complexes led to a decrease in microglia migration, phagocytosis of Aβ and decreased cognition, further implicating lipids as crucial components regulating microglia responses (Fitz et al., 2021).

The structure of TREM2 with APOE complex remains unknown and it is unclear whether additional physical interactions are mediated by different molecules. Kober et al. recently identified lipidated APOE binding sites in a hydrophobic patch of TREM2 CDRs by mutagenesis and surface plasmon resonance (Kober et al., 2021)(**Figure 1.4d**). Interestingly, no TREM2 and APOE interaction was identified in another study, while TREM2 was found to interact with isolated Cyclophilin A with high affinity. Cyclophilin was crucially shown to stimulate SYK signalling and induce cytokine production in mouse macrophages *in vitro* (Ji et al., 2021). The latter is unusual since the residue identified to be responsible for the interaction: Proline 144 is located within the TREM2 stalk domain, and TREM2-signalling pathways are known for their anti-inflammatory impact. The authors hypothesise that high-affinity ligand such as Cyclophilin A will lead to different functional responses than low-affinity ligand such as ApoE, which has been shown for other ITAM signalling cascades (Billadeau and Leibson, 2002; Ji et al., 2021; Ben Mkaddem et al., 2019).

Direct interaction of TREM2 with Aβ peptide has long been disputed, particularly in the context of Aβ phagocytosis. Previously, TREM2 was shown to facilitate uptake of Aβ only in an lipoprotein-mediated manner, but more recent studies demonstrated independent interactions with isolated Aβ *in vitro* (Kober et al., 2021; Lessard et al., 2018; Yeh et al., 2016; Zhao et al., 2018). Kober group has also shown that TREM2

and sTREM2 inhibit polymerisation of monomeric Aβ-42, hinting at its protective function during Aβ deposition (Kober et al., 2021). It remains unclear whether TREM2 primary role is the upregulation of pathways involved in Aβ removal or a more direct role in the Aβ phagocytosis.

More potential TREM2 ligands such as hsp60, which can be exposed by apoptotic cells or galactin-3, which was found to promote Aβ toxicity, were proposed; albeit these results have not been replicated thus far (Boza-Serrano et al., 2019; Stefano, 2009). Others have also suggested that TREM2 interacts with other components on the surface of cells, namely proteoglycans containing highly sulfated glycosaminoglycans (GAGs) such as heparin sulfate, which is also a ligand for APOE (Ji et al., 1994; Kober et al., 2016; Libeu et al., 2001; Park et al., 2000).

The wealth of published interactions paints an image of a promiscuous receptor *in vitro* whose interactions *in vivo* must be carefully regulated by other microglia pathways, cell surface expression, ligand type, its affinity, avidity and concentration (Kober and Brett, 2017). Additionally, a number of contradictory results can be attributed to many studies performed in non-physiological cell systems such as HEK293 or transfected T-cells over-expressing TREM2 and DAP12 (Poliani et al., 2015; Shirotani et al., 2019; Sudom et al., 2018; Yao et al., 2019; Yeh et al., 2016). While this solution has the advantage of isolating interactions that otherwise would be masked by redundant pathways in microglia, it may result in conclusions not relevant to human microglia in the CNS.

The heterogeneous nature of commercial TREM2 ligands, especially lipid particles, can result in unknown composition and difficulties in measurements of affinity *in vitro* or the analysis of the ligand-binding site by structural biology. In 2016, only reliable TREM2 agonists reported in the literature had been proprietary antibodies

or the commercial AF1828 (R&D Systems) (Cheng et al., 2018). After this project commenced, a number of TREM2-activating antibodies were developed; however, TREM2 epitopes and structural information for these interactions are largely absent (Ellwanger et al., 2021; Ibach et al., 2021; Schlepckow et al., 2020; Wang et al., 2020). As a consequence, the molecular mechanism of how ligand-induced conformational change in TREM2 propagates signals through the membrane to DAP12 and its intracellular components is not fully understood. Despite the fact that TREM2 research is a rapidly evolving field with the potential to offer insight into novel therapeutic strategies, the lack of reliable data supported by structural information on TREM2 ligand interactions hampers the development of small molecule TREM2 agonists and antagonists. The novel antibody molecules modulating TREM2 signalling can validate this therapeutic strategy for AD treatment and provide starting points for future drug candidates.

1.3 Aims of the thesis

This thesis is based on the hypothesis that TREM2-targeting antibodies can modulate TREM2-signalling pathways and change the microglia response these pathways regulate. Furthermore, antibodies should be perfectly poised to impact TREM2 signalling and sTREM2 shedding due to TREM2 localisation on the cell surface. In the future, the produced antibodies can be used both as free tools in TREM2 research as well as molecular probes, which can reveal the impact of TREM2 modulation on AD progression.

The thesis aims to achieve the following goals:

1) To successfully produce human TREM2 (**Chapter 3**):
    i) In order to raise antibodies against TREM2 antigen in the form of biotinylated TREM2 antigen
    ii) In order to validate epitope by X-ray crystallography in the form of de-glycosylated TREM2
2) To identify novel antibody ligands binding to the TREM2 Ig domain in the form of single-chain variable fragments (scFvs) in collaboration with colleagues at the Karolanska Institutet (**Chapter 4**):
    i) To establish production protocol for these scFv and perform characterisation experiments
    ii) To characterise their affinity towards TREM2 in collaboration with Eisai
3) To characterise TREM2 epitope in detail by X-ray crystallography of scFv-TREM2 complexes (**Chapter 5**).
    i) To identify conditions in which the complexes are created
    ii) To identify conditions in which both components can be crystallised
4) To validate the impact of produced TREM2 antibodies on TREM2 shedding and activation in cellular assays (**Chapter 6**):
    i) By the use of HEK293 system where TREM2 is over-expressed for sTREM2 detection
    ii) By the use of novel human iPSC technology in the cellular assays to investigate microglia-specific SYK activation

Chapter 2

Materials and methods

2.1 Bacterial strains

MACH1	T1 phage-resistant strain for the preparation of DNA for transformation and transfection of mammalian cells.
BL21(DE3)-R3-pRARE2	*E. coli* for heterogenous expression of genes utilising T7 polymerase expression system. Adapted from BL21(DE3) and Rosetta2 to produce a phage-resistant BL21(DE3)-R3. Chloramphenicol resisant plasmid pRARE2 (isolated from Rosetta2 cells), which carries seven rare-codon tRNA genes for expression of human proteins.
T7 shuffle	*E. coli* K12 which expresses a chromosomal copy of the disulfide bond isomerase DsbC facilitating formation of disulfide bonds in the cytoplasm. Uses T7 polymerase expression system.
DH10Bac	Used for recombination of plasmid DNA into bacmid DNA for baculovirus expression system. Contains a baculovirus shuttle vector (bMON14272, kanamycin) and a helper plasmid with transposase (pMON7142, tetracycline).

Table 2.1. Bacterial strains

2.2 Vectors

pNIC-BASY	*E. coli* pET expression vector with OmpY (a.a.1-353) and His_6 tag N-terminal fusion peptide, with TEV protease cleavage site. Includes sites for LIC cloning, and a "stuffer" fragment that includes the SacB gene, allowing negative selection on 5% sucrose. Resistant to kanamycin.
pNIC-BASF	*E. coli* pET expression vector with OmpF (a.a.1-201) and His_6 tag N-terminal fusion peptide, with TEV protease cleavage site. Includes sites for LIC cloning, SacB gene, kanamycin resistance gene.
pHAT6	Initial vector for production of scFvs in *E. coli*. Contains MBP signal sequence and Hisx6 followed by FLAG-tag at the C-termini. Kanamycin resistant.
pNIC-MBP2-LIC	*E. coli* pET expression vector with MBP-His_6 tag in N-terminal fusion peptide, with TEV protease cleavage site. Includes LIC sites, sacB and kanamycin resistance gene.
pFB-Sec-NH	Baculovirus transfer vector with gp64 signal sequence and His_6 tag in 44-aa N-terminal fusion peptide, with TEV protease cleavage site. Includes LIC sites, sacB and ampicillin resistance gene.
pFB-Sec-Bio	Baculovirus transfer vector with gp64 signal sequence and His6 tag in 44-aa N-terminal fusion peptide, with TEV protease cleavage site, and C-terminal biotin attachment site. The vector also includes a secreted version of birA under the control of the p10 promoter for *in vivo* Biotinylation. Includes LIC sites, sacB and ampicillin resistance gene.
pFB-CT10HF-LIC	Baculovirus transfer vector with C-terminal His_{10} tag and FLAG tag, preceded by a TEV protease cleavage site. Includes LIC sites, sacB and ampicillin resistance gene.

pFB-LIC-Bse	Baculovirus transfer vector with His_6 tag in 22-aa N-terminal fusion peptide, with TEV protease cleavage site. Includes LIC sites, sacB and ampicillin resistance gene.
pHTBV1.1-CT10H-SIII-LIC	Baculovirus transfer vector for expression of proteins in mammalian cells, with C-terminal His_{10} tag and SIII tag, preceded by a TEV protease cleavage site. Includes LIC sites, sacB and ampicillin resistance gene, and full length VSVG for more efficient transduction
pHTBV1.1-SecNH-Bio	Baculovirus transfer vector for secretion of proteins in mammalian cells, with an N-terminal RPTPmu signal peptide and TEV-Cleavable His_6 tag and a C-terminal biotinylation sequence Includes LIC sites, sacB, VSVG and ampicillin resistance gene.
pTT5	Vector for mammalian transient expression. Contains signal peptide at the N-termini for secretion to the medium and C-terminal TEV recognition site followed by His-tag. Ampicilin resistant.

Table 2.2. List of E. coli, baculovirus and mammalian expression vectors.

2.3 Media composition

SOB medium	0.5% (w/v) yeast extract (Merck), 2% (w/v) tryptone (Merck), 10 mM NaCl, 2.5 mM KCl, 20 mM $MgSO_4$
SOC medium	SOB medium containing 20% filtered glucose
Luria broth (LB)	2.5% LB powder (Merck), 5% of LB powder is used for 2x LB
Home-made terrific broth (TB)	1.2% tryptone (Merck), 2.4% yeast extract (Merck), 0.5% glycerol. After autoclaving 0.17 M KH_2PO_4 and 0.72 M K_2HPO_4 are added.
TB +	5% Terrific broth (Merck), 2% glycerol. After autoclaving the following are added: 1 mL of 1000x trace metals, 1 mM of 1 M magnesium sulphate (autoclaved), 10 mM ammonium sulphate (autoclaved), 0.5% glucose (autoclaved).
1000x trace metal solution	50 mM $FeCl_3$ 20 mM $CaCl_2$ 10 mM $MnCl_2$ 10 mM $ZnSO_4$ 2 mM $CoCl_2$ 2 mM $CuCl_2$ 2 mM $NiCl_2$ 2 mM Na_2MoO_4 2 mM Na_2SeO_3 2 mM H_3BO_3, 60 mM HCl

Table 2.3. E.coli media composition

2.4 Cloning

2.4.1 Construct design

The first TREM2 cloning campaign aimed to produce TREM2 suitable for crystallisation. The TREM2 DNA was sourced from the Mammalian Genomic consortium (MGC: BC032362.1) collection and encompassed the soluble ectodomain (a.a.1-174). C-terminal truncation series were based on PsiPred prediction (see links for software at the end of this section (Jones, 1999; Orlandi et al., 1989). The constructs were made using independent ligation cloning (LIC). The list of constructs and primers

can be found in (**Appendix Table 1, Appendix Table 2**). ScFvs re-cloning to *E. coli* and *Sf9* vectors was also performed by LIC.

2.4.2 Ligation independent cloning (LIC)

To achieve simultaneous cloning of 96 constructs of TREM2, high-throughput (HTS) protocols were employed (Savitsky et al., 2010). Cloning by LIC allows simultaneous amplification of DNA inserts into vectors of choice (Strain-Damerell et al., 2014). The method is based on the 3 to 5' exonuclease activity of T4 polymerase, which generates sticky DNA ends in the absence of nucleotides. For this purpose, a 5' DNA overhangs are added to PCR primers which are identical to terminal sequences of linearised LIC-adapted vector. After T4 polymerase treatment of vector and inserts, both DNA fragments were mixed and annealed before transformation to the *E. coli*. The LIC-protocols were performed as previously described in Strain-Damerell et al., 2014 (**Figure 2.1**).

PCR was performed with Herculase Fusion II DNA polymerase (Agilent, 600675). The final PCR reaction consisted of HercII buffer (Agilent), 0.3 mM dNTP mix (Invitrogen), 1% of Herculase polymerase, 0.3 µM of each primer and 0.25 ng/mL template DNA in nuclease-free water (Ambion). The PCR plate was covered with an adhesive film and placed in a Bio-Rad C100 Touch thermocycler (Bio-Rad). Inserts were amplified by touch down PCR (Korbie and Mattick, 2008):

95°C, 10 min

(95°C, 30 sec; 68°C, 30 sec; 68°C, 1-3 min*) x5 cycles

(95°C, 30 sec; 60°C, 30 sec; 68°C, 1-3 min*) x5 cycles

(95°C, 30 sec; 55°C, 30 sec; 68°C, 1-3 min*) x5 cycles

(95°C, 30 sec; 50°C, 30 sec; 68°C, 1-3 min*) x10 cycles

68°C, 10 min

15°C hold

*1-3 min elongation temperature was adjusted to the longest DNA insert in each PCR plate.

The PCR products were visualised by electrophoresis on 1.5% agarose gel containing SybrGreen (Invitrogen). The appropriate amount of agarose was dissolved in 1 TAE (40 mM Tris-acetate, 1 mM EDTA, pH 8.3). Small and large gels were run at 120 V or 150 V for 30 or 60 min, respectively. A 1 kb plus ladder (Invitrogen) was used to validate the size of the fragments

In cases when the DNA template had the same antibiotic resistance as the vector, the inserts were treated with Dpn1 according to a standard protocol to remove template DNA and avoid carry-over. If the PCR product had the appropriate size, the components were cleaned by clean up plate (MSNU03050, Milipore) on a vacuum manifold (Milipore).

Vectors were linearized by appropriate restriction enzyme according to manufacturer instruction (NEB) (**Table 2.2**) (Strain-Damerell et al., 2014). T4 polymerase was added to vectors in the presence of 25 mM dCTP or dGTP (vector-dependent). Conversely, T4 polymerase treatment of PCR products was performed in the presence of the complementary dNTP (**Figure 2.1**). The reactions were incubated for 30 minutes at room temperature (RT) following heat inactivation at 75ºC for 20 minutes in a thermocycler. For annealing, 2 μL DNA insert was mixed with 1 μL of vector DNA and incubated at RT for 30min, followed by transformation into MACHI. For transformation, annealed DNA was incubated with cells for 30 min following heat-

shock at 42ºC for 45 s. Transformed cells were plated out onto LB-Agar with appropriate antibiotics containing 5% sucrose for SacB selection. The correct clones were confirmed directly by screening each colony and PCR followed by gel electrophoresis (Strain-Damerell et al., 2014).

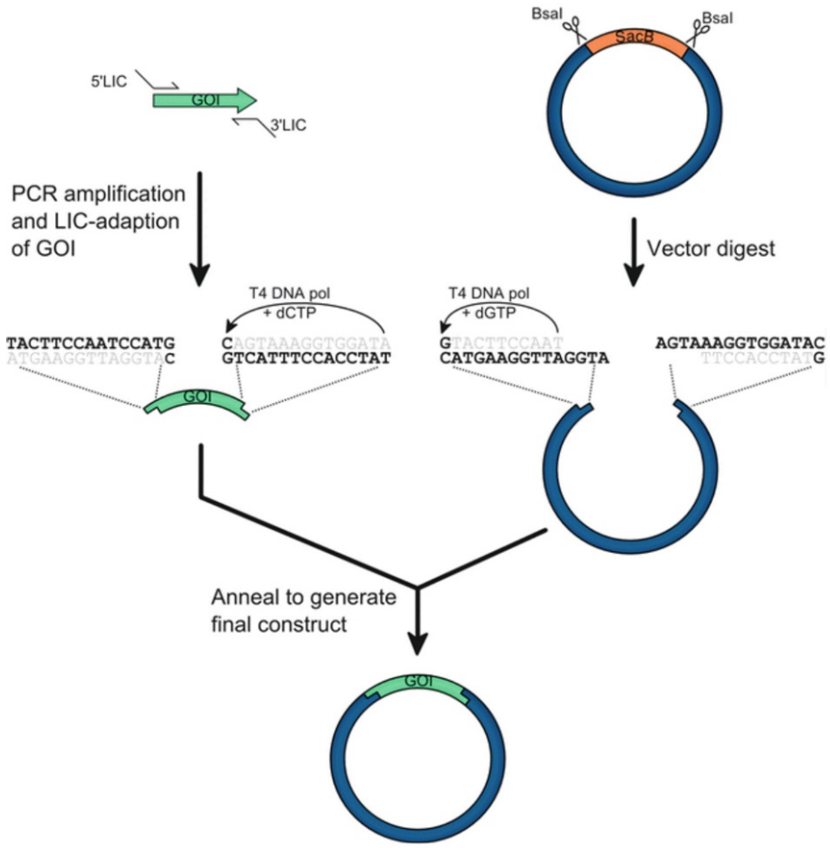


Figure from Strain-Damerell et al., 2014

Figure 2.1. Schematic representation of LIC-cloning. *The protocol is shown in the example of BsaI cleaved vector. SacB gene is interrupted by the correct insertion of DNA into the vector. This excludes the majority of vector-only false positives since SacB product, Levansucrase, is toxic to bacteria in the presence of sucrose. The vector containing clones are identified by antibiotic resistance (Strain-Damerell et al., 2014, rights to publish this image were obtained from Springer).*

2.4.3 Mutagenesis

The point mutation is incorporated into the middle of 20-30 bp long MutR and MutF primers. Each one of them, drives amplification into two different directions.

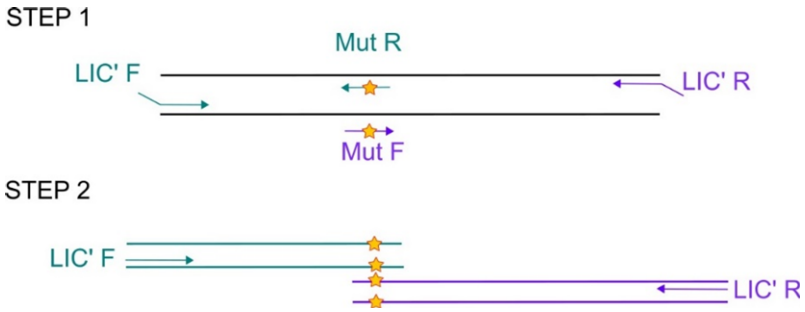


Figure 2.2. Two-step PCR mutagenesis.

Mutagenesis was performed in two steps (**Figure 2.2**). The first two PCR products were amplified separately by PCR reactions containing MutF and LIC-R primers and the second reaction with LIC-F and MutR primers. LIC primers correspond to the end of DNA insert and contain standard LIC sites for vector annealing. The first PCR reaction resulted in the production of two separate products, which was later used together as a template for the second round of amplification with LIC-F and LIC-R primers. The product of step one was treated with Dnp1 and cleaned up. Thanks to the long overlap in DNA sequences close to the mutated site, the templates can anneal together during the PCR.

The PCR composition is as previously described with a double concentration of primers. The PCR for steps 1 and 2 is performed as follows:

95°C, 10 min

(95°C, 30 sec; 62°C, 30 sec; 68°C, 1-3 min*) x15 cycles

68°C, 5 min

15°C hold

The resulting product is analysed for size and treated as DNA insert for further LIC-cloning into amplification vector.

2.4.4 Competent cell preparation

TFB1 buffer was prepared by mixing 30 mM potassium acetate, 100 mM RbCl, 10 mM $CaCl_2$ x $2H_2O$, 15% glycerol, at pH 5.85 adjusted with 1M acetic acid. Afterwards, 50mM $MnCl_2x4H_2O$ is added and solution is filter sterilised. TFB2 was prepared by mixing 10mM MOPS free acid, 75 mM $CaCl_2$ x $2H_2O$, 10 mM RbCl, 15% glycerol, adjusted to pH 6.5 with 1M KOH and filter sterilised.

Competent cells were obtained with the calcium method (Dagert and Ehrlich, 1979). MACH1, BL21(DE3)-pRARE-R3 or T7 Shuffle were streaked on plates containing appropriate antibiotics. A couple of colonies were streaked and used to inoculate starter culture of 2 x 5 mL SOB (37°C, 700 RPM). The overnight culture was used to inoculate 1 L of SOB and was grown until OD600 reached 0.5 (37°C, 180 RPM). Cells were harvested by centrifugation at 1,800 x *g* for 10 min at 4°C in pots kept on ice. The pellets were gently resuspended in ice-cold TFB1. After removal of the solution by centrifugation, cells were resuspended in 80 mL of ice-cold TFB2 and immediately frozen in liquid nitrogen in pre-chilled Eppendorf tubes.

2.4.5 Transformation of *E. coli*

An aliquot of competent cells was thawed on ice, and 30-50 µL was added to a sterile eppendorf tube containing DNA solution followed by 30 min incubation. Cells were heat-shocked for 45 sec at 42°C and placed back on ice. 100 uL of SOB with glucose and without antibiotics was added, and cells were grown for 1-2 hours at 37°C

with 350 rpm shaking. After incubation, 100 uL of cells were plated on LB-agar with antibiotics and incubated overnight at 37℃. The resulting colonies were either used for the preparation of DNA (MACH1) by Monarch miniprep DNA kit (NEB) or inoculation of expression cultures (Rosetta).

2.5 Protein purification methods

2.5.1 IMAC

IMAC (Immobilized Metal Ion Affinity Chromatography) is based on the high affinity of tandem histidine tags (His6 or His10) to metal ions immobilised on a matrix. In this study Ni-NTA (nickel-nitrilotriacetic acid) columns that contain Ni-NTA immobilised to agarose resin bed. Proteins bound to the resin can be released by increasing the concentration of Imidazole, which has a higher affinity to the resin. The method is one of the most cost-effective ways to purify large amounts of medium though Ni-NTA columns (Qiagen) connected to fast protein liquid chromatography (FLPC) machines such as AKTA. The disadvantage is medium purity and potential for purification of aggregates.

2.5.2 SEC

SEC (Size exclusion chromatography), also known as gel filtration, is the most common polishing step in protein chromatography. The column filled with the stationary phase (such as dextrans) with pores of various sizes is filled by the liquid phase (buffer). A sample containing proteins to be separated injected slowly at the top of the resin. Separation occurs when larger particles are excluded from travelling

through small pores in the resin and are eluted at earlier times (retention volumes) than small particles.

The practical advantage is the simultaneous ability to evaluate sample quality (correct folding), size, oligomeric state and confirm complex formation between proteins. The disadvantage is potential non-specific interactions with resin bed and the requirement for globular proteins (elongated proteins will travel differently to commercially available protein standards). It can be used both as an analytical and preparative step in protein purifications. In this study, Superdex 200 (Cytiva) was used, which is suitable for resolving proteins in 10,000 - 600,000 Da range.

2.5.3 Protein A

Protein A from *Staphylococcus aureus* is a protein of 42000 Da, which binds most classes of human IgG antibodies. Although the general assumption is that Protein A can be used only for the purification of Fc-containing antibody fragments, the same protein can also bind a VH domain-containing proteins (such as small scFvs) through a different binding site (Graille et al., 2000). Protein A FF (Cytiva) columns used in this study contain molecules of these proteins cross-linked to Sepharose resin. The elution of proteins is based on the temporary weakening of protein-protein interactions by elution at pH 3, followed by immediate neutralisation. The advantage is a very high purity and purification of correctly folded proteins containing VH domain.

2.6 Small scale *E. coli* test expression

2.6.1 Buffers

Binding buffer: 50 mM HEPES pH 7.5, 500 mM NaCl, 5% glycerol, 20 mM Imidazole, protease inhibitors (1:1000 v/v), 1 mM TCEP

Wash buffer: 50 mM HEPES pH 7.5, 500 mM NaCl, 5% glycerol, 40 mM Imidazole, 1 mM TCEP

Elution buffer: 50 mM HEPES pH 7.5, 500 mM NaCl, 5% glycerol, 300 mM Imidazole, 1 mM TCEP

2.6.2 Test expression

E. coli constructs were tested for expression at 1 mL scale. Expression plasmids were used to transform *E. coli* BL21 (DE3)-R3-pRARE2 or *E. coli* T7 shuffle competent cells by a heat shock. Couple of colonies were inoculated into 1 mL of 2 x LB medium containing 50 µg/mL kanamycin or 200 µg/mL and 34 µg/mL chloramphenicol or in a 96-deep well block. The cultures were grown in a Glas-Col shaker at 37°C, with shaking at 700 rpm overnight. The following morning, 20 µL of the culture was used to inoculate 1 mL of homemade Terrific Broth (TB) medium containing salts and 50 µg/mL kanamycin (or 200 µg/mL ampicillin) in two 96-deep-well blocks. One block was used for determining the optical density (OD) measured by absorbance at 600 nm. The second was used for protein purification. Cultures were incubated OD was 2-3, after which they were placed at room temperature for 30 min while the incubator cooled to 18°C. Expression was induced by adding 0.1 mM IPTG to each well. For test expression containing pGroEL/ES plasmid, the expression was first induced with 5 mM L-Arabinose for an hour at 18°C. The blocks were then

returned to the incubator and bacteria cultured overnight at 18°C, with shaking at 700 rpm. Cells or medium were harvested at 3,000 x *g* for 20 min and re-suspended in 200 µl of binding buffer (cells).

2.6.3 Test purification of soluble proteins

The OmpY and F fusion proteins should be secreted to the periplasm or medium, but the whole-cell extracts were tested for the presence of protein. The lysis buffer contained 0.1% DDM and 0.5 mg/mL lysozyme, which improved protein lysis. The cells were freeze-thawed at -80°C for 20 min to aid further lysis. Debris was removed by centrifugation at 2,600 x *g* for 20 min, and the supernatant containing soluble proteins was incubated with 50 µl of 50% (v/v) Nickel Sepharose 6 FF (Cytiva) at 18°C for 60 min with shaking at 400 rpm. A vacuum manifold was used to facilitate the removal of the flow-through, and subsequent three 200 µl washes with wash buffer. The plate was incubated with 40 µL of elution buffer for 20 min at RT, shaking at 400 rpm. Bound protein was eluted by centrifugation at 300 x *g* for 3 min. Eluates were analysed by SDS-PAGE to ascertain solubility.

2.6.4 Test purification of secreted proteins

For secreted proteins, the medium is harvested after spinning at 3,000 x *g* for 20 min, and 50 µL of 50% (v/v) Nickel Sepharose 6 FF is added to the block for 1 hour at 18°C with shaking at 400 rpm. After incubation, the medium with resin is transferred to a 96-well filter block, and flow-through is removed by centrifugation at 300 x *g* for 2min. Resin is washed three times in binding buffer followed by a single wash with 40 mM imidazole. Elution is performed as above.

2.6.5 Large scale *E. coli* expression and purification of deglycosylation enzymes

Endo F1 (Endoglycosidase F1) clone in pGEX-X3 vector containing N-terminal GST-tag was a gift from Jo Nettleship. DNA was transformed freshly into Rosetta cells and plated on 100 mg/mL Ampicillin and 25 mg/mL kanamycin LB-agar. 10 colonies were inoculated into overnight starter culture containing the same antibiotics. Next day each expression culture was inoculated with 2% (v/v) of LB with antibiotics. Cultures were grown at 37°C, 200 rpm until OD reached 0.8 and expression was and induced with 0.2mM IPTG. Growth was continued for 4 h, and cells were collected by centrifugation for 10 min at 30,000 x *g* at 4°C. Pellets were resuspended in 20 mM Tris-HCl pH 8.5, 500 mM NaCl and 5% glycerol with protease inhibitors III (Sigma) frozen until purification. Cells were thawed in warm water and sonicated 15 min 3s on, 8 s off at 35% amplitude in 50 mL aliquots (Q500, Qsonica). Lysates were clarified by 45 min centrifugation at 30,000 x *g* and 4ºC. The supernatant was collected and diluted 5 times with 50mM Tris-HCl pH 8 in order to reduce the salt concentration to 100 mM. Proteins were purified on a gravity column containing 20 mL of equilibrated GST beads (Cytiva), beads were washed 5 times the column volume (CV) using the Tris-HCl, pH 8 and 100 mM NaCl solution. Finally, proteins were eluted using freshly made 20 mM Tris-HCl pH 8.5, 100 mM NaCl, 20 mM reduced glutathione (Cytiva). Fractions were polled, desalted on PD10 to 25 mM Tris-HCl pH 7.5, 150 mM NaCl, 20% glycerol and frozen in liquid nitrogen.

Endo H (Endoglycosidase H), truncated version (a.a.10-281) was cloned into pNIC-LIC-Bsa4. Cells were grown in kanamycin-containing plates and expression was performed as above, but after IPTG induction, cells were grown at 18°C until the next day. Cells were collected, and pellets were resuspended in 50 mM HEPES pH 7.5, 150

mM NaCl and 5% glycerol, 1mM TCEP with protease inhibitors III (sigma) frozen until purification. Cells were broken in C3 homogeniser by passing 3 times at 15 kPsi. The lysate was clarified by spinning for 30,000 x *g* at 4ºC. 4mL of equilibrated Ni-Sepharose 6 FF (Cytiva) was added to the clarified lysate, incubated with rotation for 1h at 4ºC. Afterwards, the resin was spun at 500 x g for 10min, and the supernatant was removed. The resin was transferred to the gravity column and washed with 20 CV of lysis buffer, followed by a wash with buffer containing 10 mM imidazole and elution with 250 mM NaCl and 500 mM NaCl. Buffer was exchanged to 50 mM HEPES pH 7.5, 150 mM NaCl and 5% glycerol, 0.5mM TCEP on PD10 column and samples were frozen after concentration.

PNGase (Peptide-N-Glycosidase F) The expression plasmid was received from Liz Carpenter. His-tagged full-length PNGase in pOPH6 plasmid is secreted to the periplasm by OmpA leader sequence and purified by osmotic shock and IMAC. Transformed BL21 strain was used to inoculate starter culture. 2% of the starter culture was inoculated into 2xYT broth medium containing 100 mg/mL ampicillin and cells were grown at 37℃ at 180 rpm until OD 600 nm reached 1.1. The incubator was cooled down to 18℃ for an hour, and protein expression was induced with 0.3 mM IPTG, and cells were grown until the next day.

Cells were harvested by centrifugation and dissolved in sucrose buffer containing 30% sucrose, 20 mM Tris-HCl pH 7.5, 2.5 mM EDTA and 20 mg/L lysozyme. The cell suspension was mixed gently at RT for 45 min, and osmotic shock was induced by the addition of an excess of ice-cold 5 mM $MgCl_2$ solution containing protease inhibitor set III (Sigma). The solution was incubated at 4℃ for 45-60min with gentle mixing. The solution was centrifuged at 15,000 x g for 20min and supernatant was incubated with

Ni-Sepharose resin for 1 h with gentle rotation at 4℃ after the addition of 50 mM HEPES and 250 mM NaCl and benzonase. The resin was spun at 400 x *g* and resuspended in 20 CV of 50 mM HEPES pH 7.4, 500 mM NaCl and 5% glycerol. The beads were transferred next to the gravity column and washed with buffers containing 20 mM, 40 mM and 70 mM imidazole and elution was performed with 250 mM imidazole. The last fraction was pooled and frozen in liquid nitrogen before SEC on Superdex 200 16/60 in 20 mM HEPES pH 7.4, 150 mM NaCl, 5% glycerol. The monomeric peak was pooled, and glycerol was adjusted to 20% before aliquoting and freezing in liquid nitrogen.

2.7 Baculovirus-*Sf9* protein production

2.7.1 Production of recombinant baculoviruses

The positively verified clones for expression in *Sf9* insect cells were transposed by transformation to DH10Bac *E. coli*. The pFB/pHTBV1.1 are transfer vectors based on technology that allows for recombination with bacmid DNA present in DH10Bac. The bacmid DNA and transfer vectors utilise Tn7 transposon elements. The enzyme transposase is additionally expressed from helper plasmid in Dh10Bac (Mahajan et al., 2021).

The successful transposition disrupts the *lacZ* gene within the Tn7 sites of the bacmid, which in turn results in lack of β-galatosidase expression. The enzyme catalyses the conversion of 5-bromo-4-chloro-3-indoyl-β-d-galactopyranoside, known as X-Gal (Glycosynth), to a blue product when both are present in the medium. That property allows for the selection of successfully transposed bacmids by picking only white colonies. Apart from 100 μg/mL X-gal, the LB-agar plates contain also a number of

additives that additionally facilitate selection: 40 μg/mL IPTG (to induce expression of *LacZ*), 10 μg/mL tetracycline (helper plasmid), 50 μg/mL kanamycin (bacmid) and 7 μg/mL gentamycin (for pFB insert). All reagents purchased from Apollo Scientific Ltd.

After Dh10Bac transformation, the plates were incubated at 37℃ for 3 days to allow high expression of *lacZ*. The white colonies were picked, and 2xLB containing antibiotics was inoculated with a single colony. The medium contains identical antibiotics as selection plates, but gentamycin concentration is reduced to 1 μg/mL. The bacmid DNA was purified from 1 mL of culture by DNA production kit (Milipore).

2.7.2 Transfection of *Sf9* with bacmid DNA

Sf9 cells were initially transfected to produce amplified viruses that were later used for infection of large scales of insect cells or transduction of small and large scale of Expi293F^{TM} for mammalian expression (2.8.1)

1 mL ($2x10^5$ cells) of *Sf9* cells at the exponential-growth stage were used per each transfection. The 24-well plates containing cells were incubated for 1 hour at 27℃ to allow cell attachment. The transfection solution consists of 2 uL of jetPRIME (Polyplus) in 50 uL of jetPRIME buffer per each transfection. 50 μL of the solution was aliquoted into a sterile 96-well microtitre plate where 5 μL of bacmid DNA at concentration >0.5 μg/μL was dispensed. The solutions were gently mixed by tapping the plate and incubated for 30 min at RT. Then, 50 μL of the transfection solution was added to the cells and incubated for 4 h at 27 ℃. Positive controls expressing proteins and cells with jetPRIME only were included as controls. After 4 h, 0.8 mL of Sf-900 II serum-free medium (SFM) (Life Technologies) containing 2% (v/v) fetal bovine serum (FBS) (Life Technologies) and antibiotics Pen/Strep 0.1% (v/v) (Gibco) were added to each well. Cells were incubated at 27℃ for 6 days in a container protecting from evaporation. The

resulting solution contains P0 virus. After centrifugation at 1,500 x *g* for 20 min at room temperature, the solution was transferred to a new sterile 96-well block and stored at 4°C. The further amplification rounds generate P1 virus and P2 virus. Firstly, 3 mL of *Sf9* cells in 900-II SFM medium containing 2% (v/v) FBS at $2x10^6$ were infected with 120 µL of P0. Cells were incubated at 450 rpm at 27°C for 72 hours. Secondly, 50 mL of cells are infected with 120 µL of P1 to generate P2. For test expression of secreted proteins, a replica of P1 amplification was prepared, and after 72 hours and incubation at 27°C with 200 rpm shaking, the cells are cleared away by 1,500 x g centrifugation, and medium is used directly for test expression.

2.7.3 Test expression

Test expression of proteins expressed for 72 hours in *Sf9* cells was performed as previously described for *E. coli* (**2.6.2**). The buffer composition was as follows: binding buffer contained 50 mM HEPES pH 7.5, 300 mM NaCl, 5% glycerol, 5 mM imidazole, 1 mM TCEP, while imidazole concentration was increased to 30 mM in the wash and 300 mM in the elution buffers. The initial spinning is performed at 1500 x g to reduce cell lysis.

2.7.4 Large scale Purification

Antigen TREM2 and TREM2 N79A mutants

The secreted proteins were purified by IMAC and SEC. The clarified supernatants were loaded onto 5 mL of Ni-NTA (Qiagen) per each 750-1000 mL of culture at 10 mL/min on AktaXpress (Cytiva). The resin was washed with 20 column volumes (CV) of 50 mM HEPES pH 7.4 and 300 mM NaCl, 5% glycerol, 5 mM

imidazole followed by 10 CV of 10 mM imidazole and 600 mM NaCl containing buffer. Proteins were eluted with a buffer containing 500 mM imidazole. Proteins were purified further by size exclusion chromatography (Superdex 200, 16/60) in 20 mM HEPES pH7.4, 300 mM NaCl and 5% glycerol. Monodisperse peaks were concentrated, frozen in liquid nitrogen and stored at -80°C.

ScFvs

ScFvs were expressed for 72 hours after infection with 7 mL of P2 virus. IMAC was performed as in the case of TREM2, except for a change to pH 6.8 in all buffers used, which decreased precipitation for all scFvs. Eluted proteins were diluted and cleaved with TEV protease overnight (O/N) at 4°C followed by loading onto a 1 mL Protein A FF (Cytiva) column at 3 mL/min. The resin was washed with 20 CV of base buffer (BB: 25 mM HEPES pH 7.5, 150 mM NaCl) followed by a wash with 10 CV of BB containing 0.05% Triton-X. Proteins were eluted with 0.1 M acetic acid pH 3 at 0.5 mL/min, neutralised to pH 7 with 1M Tris-HCl, pH 9 and immediately buffer exchanged on PD10 columns. For crystallisation protein buffers were as follows: scFv-1 120 mM Citrate pH 7, 50 mM L-arginine, 50 mM L-glutamic acid, scFv-2: 100 mM HEPES pH 7.2, 25 mM NaCl, 100 mM L-arginine, 100 mM L-glutamic acid, scFv-3: 100 mM Tricine pH 8, scFv-4: 100 mM Tricine pH 8.

For cell biology, scFv-2, scFv-3 and scFv-4 oligomers were further separated by double SEC on Superdex 200 16/60 conjugated to EndoTrapHD (Lionex) in LPS-free DPBS (Gibco). Proteins were concentrated to 1-2 mg/mL, clarified by centrifugation at 30,000 x g and immediately frozen in liquid nitrogen and used for the assay within a week. Other scFvs were buffer exchanged to PBS on NAP5 or PD10 columns (Cytiva).

Proteins were clarified by centrifugation at 30,000 x *g* and immediately frozen in liquid nitrogen and used for the assay within a week.

TREM2-scFv co-expression

The co-expression protocols were performed as above by co-infecting *Sf9* cells with two viruses. The concentration of P2 viruses was reduced to 3.5 mL of each P2 per 1 L of insect cells.

2.7.5 *In vitro* biotinylation for antigen generation

Frozen TREM2 (a.a.19-131) containing Avi-tag purified in *Sf9* was thawed and *in vitro* biotinylated using recombinant BirA enzyme by Edvard Wigren (Karolinska Institutet). BirA was used at the enzyme to substrate ratio of 1:50, w/w. The reaction was performed in a buffer containing 10 mM Tris-HCl, 50 mM NaCl and 10 mM MgOAc, pH 8.0 for 14 h, at 4°C in the presence of 0.1 mM biotin in the presence of 10 mM ATP. Subsequently, the buffer was exchanged by dialysis to 20 mM HEPES, 300 mM NaCl, 5% glycerol and 0.5 mM TCEP pH 7.5.

2.7.6 Deglycosylation attempts of TREM2

PNGase (purified in house) was used only for analytical purposes and was incubated with denatured proteins for 15-30 min at 37°C or o/n at 4°C.

Endo F1 or Endo H (purified in house) were used for attempts to remove glycosylation. Initial trials were performed by incubation of TREM2 with increasing concentrations of enzymes at pH 6 or 7 overnight at 4°C or 20°C.

2.8 Mammalian Expi293F™ protein expression

2.8.1 Viral transduction of mammalian cells for test expression

The initial TREM2 screening campaign included BacMam expression constructs in pHTBV1.1 utilising baculovirus transduction. P2 virus generated in *Sf9* cells was concentrated by mixing with 20% PEG 10,000 (Fluka) solution containing 200 mM NaCl. Per each infection, 300 µL of P1 virus was mixed with 75 µL of PEG solution and mixed in 24-well block and shaken for 5 min at 18°C, 300rpm and incubated at 4°C o/n. The next day the plate was shaken again for 30min and centrifuged at 3,000 x *g* for 45 min. The supernatant was aspirated, and 3 mL of Expi293F™ cells at 2x 10^6 were added directly to the pelleted virus. Cells were incubated at 37°C with 8% CO2 and shaking set at 200 rpm for 72 h. For secreted protein expression, cells were removed by centrifugation at 1,500 x *g*, and the medium was used directly for test expression.

2.8.2 Mammalian test purification

Test expression of proteins expressed by transient expression or bacmid transduction in Expi293F™ cells was performed as previously described for *Sf9* cells for IMAC purifications (2.7.3).

2.8.3 DNA production and transient transfection of Expi293F™

The alternative to the use of baculovirus for transduction of mammalian cells is a transient expression with plasmid DNA. Transient expression allows for direct use of plasmids generated in MACH1 and omission of time-consuming Dh10Bac recombination and transfection of *Sf9* cells with bacmids.

For transient expression, DNA was produced in *E. coli* and prepared by maxiprep kit (Sigma). The 2xLB medium containing the appropriate antibiotic was inoculated with glycerol stock and incubated at 37℃ with 350rpm shaking o/n. The next day 0.1% was used to inoculate each litre of 2xLB medium, and cells were grown at 200 rpm shaking until OD 600 nm reached 4-5. The amount of culture needed per each maxiprep column was calculated according to the manufacturer instruction. The columns were first regenerated in 1M HCl for 24 hours and washed with 5 column volumes (CV) of nuclease-free water. DNA after lysis and purification was precipitated with 70% (v/v) of ethanol and 0.3M sodium acetate pH 5.2 overnight at 4℃. The next day DNA was centrifuged 15,000 x *g* for 20 min at 4℃, and the pellet was washed with 2 mL of 70% ethanol before another centrifugation step. The DNA pellet was allowed to air dry in a sterile fume hood followed by resuspension in 1 mL of TAE and storage at 4℃.

For expression, 1 mg of DNA is required per litre of Expi293F^{TM} culture at 2x10^{6}. Linear Polyethylenimine (PEI) 25,000 (Polysciences) was used at a ratio 3 to 1 (PEI to DNA) (ratio 1:6 was used by purifications performed by Eisai) and was optimised for each PEI preparation. PEI was prepared by dissolving it in miliQ water pH 2 and mixing for 2 hours before re-adjusting pH to 6.8 with NaOH. DNA and PEI were mixed in Opti-mem (Gibco) separately at 5% volume of final expression culture. After that, both solutions were merged inverted six times before incubation for 15 min and dropwise addition to the Expi293F^{TM} cells. Cells were incubated for 72 hours in 2 L roller bottles at 120 RPM (Greiner Bio-one) or 24-well blocks for test expression at 200 RPM. For small test expression, 5mM sodium butyrate was added at the time of transfection to facilitate chromatin access during expression. Large scale expressions were performed in a maximum of 750 mL per flask in the presence of 2 mM VPA (Sigma). 4.3 uM

kifunensine (Carbosynth) was added to inhibit glycosylation at the time of transfection. Alternatively, Expi293F^{TM}GnT- (Thermofisher Scientific) cell line was used.

2.8.4 Large scale purification of TREM2 in Expi293F

pTT5:TREM2 (a.a.19-131) was purified by Dongming Qian (Eisai). Culture supernatants were collected, and TREM2 was purified by affinity chromatography (Ni-NTA, Qiagen) in buffers containing 20 mM Tris-HCl pH 8, 500 mM NaCl, 5% glycerol followed by size exclusion chromatography (Superdex 75 10/30GL, Cytiva). The purified protein was deglycosylated with EndoH (PE019, Novoprotein) in 50 mM sodium citrate pH 5.5 overnight at 4°C, at the ratio of 1 mg protein: 2000 U EndoH. EndoH was removed using a second Ni-NTA affinity column, and the purified protein was stored in buffer containing 50 mM Tris-HCl pH 8.5, 200 mM NaCl, and 5% glycerol at 10 mg/mL concentration.

TREM2-avi (a.a.19-138 and 19-174) for crystallisation were expressed and purified similarly, but transfection was performed with DNA to L-PEI ratio at 1:3 and cells were grown in 2 L roller bottles (Greiner Bio-one). IMAC was performed in base buffer containing 20 mM HEPES 7.4, 300 mM NaCl, 5% glycerol. Secreted proteins from each 0.75-1 litre volume of culture were clarified and loaded on 5 mL HisTrap columns (Cytiva). The column was washed with 30 CV of base buffer and washed with 10 CV of 30 mM imidazole-containing buffer. Proteins were eluted in 300 mM imidazole and either purified by SEC or de-glycosylated.

Endo H large scale deglycosylation of Expi293F^{TM} (with 1mg/L kifunensine) or Expi293F^{TM}GnTI- produced TREM2 was performed after IMAC. Sodium Citrate pH 5 was added to the solution until the pH reached 6-6.5, and deglycosylation with 1:40

molar ratio of Endo H was performed overnight at 4°C. For this, a sample was diluted to approximately 1 mg/mL to avoid aggregation. The next day pH was raised to 7 with 1M HEPES pH 8, and protein was gently concentrated at 3 000 x *g* on Vivaspin 10MWCO (Cytiva) concentrator before size exclusion on Superdex 200 16/60 (Cytiva). Alternatively, SEC has also been performed also before de-glycosylation.

2.9 LPS quantification and purification

ScFv-2, ScFv-3 and scFv-4 for assay were purified on Superdex200 16/60 in LPS-free DPBS buffer (Gibco) connected to EndoTrapHD column containing resin conjugated to Polymixin B, which binds endotoxin.

LPS endotoxin levels were quantified by ToxiSensor LAL Endotoxin Assay Kit (GeneScript) according to the manufacturer's instruction. Lyophilized Amebocyte Lysate (LAL) reagent is made from horseshoe crab and is very sensitive to endotoxin leading to clotting reaction. The endotoxin contamination was measured at tresholds: 0.05, 0.1 and 0.2 Endotoxin Unit (EU)/mL. ScFvs were diluted in endotoxin-free water to 10 µg/mL, and the 200 µL solution was assayed against particular endotoxin sensitivity. Two repeats were used per sample, and endotoxin contamination was validated by the formation of a solid clot after incubation for 1 hour at 37°C with LAL reagent. A sample containing both endotoxin standard and scFv was included to exclude inhibition of LAL assay. Only samples with contamination below 0.1 EU/mL measured at a protein concentration of 10 µg/mL were used to treat iMac cells.

2.10 Phage display and antibody validation

The phage display was performed by Charlotte Preger, and Edvard Vigren purified proteins from TOP10 for these experiments. Antibody generation through phage display selection was performed as described previously, using the *in vitro* biotinylated TREM2 (19-131) from *Sf9* cells as antigen and a human synthetic single-chain fragment variable (scFv) library (Preger et al., 2020). Briefly, four rounds of selections were performed using streptavidin beads (Dynabeads M-280 streptavidin, Invitrogen) to immobilise the biotinylated TREM2 antigen. In the first two rounds, phages were incubated with immobilised antigen after a pre-selection on naked beads. In rounds 3 and 4, phage and antigen were incubated in solution before capturing on beads. The antigen-phage incubation time was decreased from 3 h in the first round to 1.5 h in rounds 2, 3, and 4. Furthermore, the selection pressure was augmented by increasing the number of washing steps and decreasing the amount of antigen added (200, 100, 50 and 10 pmol, respectively) between the different rounds. The enriched phages were recovered using trypsin digestion and amplified overnight by infection of *E. coli* XL1-blue. Amplification in round 1 was done using agar plates and in rounds 2, 3 and 4 in solution. Amplified phages were precipitated using PEG/NaCl and used for the next round of selection. Phagemid DNA from rounds 3 and 4 were purified and the scFv genes were transferred to an expression vector as described previously (Preger et al., 2020).

Following selections, cloning and transformation, a total of 188 colonies were picked from rounds 3 and 4 and analysed further. ELISA revealed 8 colonies as potential binders, of which 5 were identified as unique clones after DNA sequencing. These five were considered suitable for further validation, which was performed as previously described, including ELISA, HTRF, Luminex, and SPR (Preger et al., 2020). Based on

these results four scFv candidates, scFv-1, scFv-2, scFv-3, scFv-4, were selected to be produced in large-scale and tested in additional binding kinetics and co-crystallisation trials.

2.11 Mass spectrometry

2.11.1 Intact mass spectrometry

To evaluate the glycosylation or biotinylation state of each purified protein, denaturing intact electrospray mass spectrometry (ESI-MS) was performed on LC-QTOF (Agilent). 1 µg of protein sample resuspended in 0.1% formic acid was injected onto Zorbax 5um 300SB-C3 columns where they were desalted by elution off a C3 column in a gradient of 5-95% isopropanol in 0.1% formic buffer. Desalted proteins were ionized by an electrospray and accelerated by an electric field. The m/z ratio was determined by the ionisation quadrupole time-of-flight mass spectrometer. Spectra were analysed and de-convoluted using the MassHunter software (Agilent).

2.11.2 Tryptic digest LC-MS/MS

Experiments were performed by Oxtawia Borkowska (University of Oxford). To perform glycosylation state analysis, samples were separated on SDS-PAGE and protein bands were excised from SDS-PAGE gels and stored in 10% MeOH at 4℃. Prior to digestion, the methanol solution was removed and replaced with 100% acetonitrile for 2-5 minutes. The solution was then removed and replaced with 100mM NH4HCO3 pH 8.0. Dithiothreitol was added and incubated at 56℃ for 40 min followed by iodoacetamide addition at RT for 10min in the dark. Samples were digested by trypsin (sequencing grade, Sigma) at 37℃ for 16 hours. LC-MS/MS was performed

using a Dionex U3000 nano HPLC coupled to a Bruker Esquire HCT ion trap mass spectrometer. 1-5 μL of tryptic digest was loaded onto a 200 μm ID x 5 cm PS-DVB monolith column (Pepswift, Dionex Corp). Compound extraction and peptide deconvolution was performed using the DA data analysis (Bruker Daltonik), and database searching was performed using the Mascot 2.2.04 search algorithm (MatrixScience, parameters: charge states +2, +3; MS tolerance 1.5Da; MSMS tolerance 0.5 Da; UniProt_SwissProt database without taxonomic restrictions) (Perkins et al., 1999).

2.12 Differential scanning fluorimetry (DLS)

Thermal shift assay, also called differential scanning fluorimetry or thermofluor, is an inexpensive method to monitor conformational changes of macromolecules during thermal denaturation in different conditions (Chari et al., 2015). Sypro orange dye binds hydrophobic patches in proteins which are usually found protected within the protein structure. The water molecules, on the other hand, quench the fluorescence emitted by the dye, so usually, protein binding is associated with an increase in the signal. As temperature increases, hydrophobic residues become exposed, and an increase in fluorescence is observed, after denaturation protein aggregation leads to a decrease in recorded fluorescence again (**Figure 2.3**).

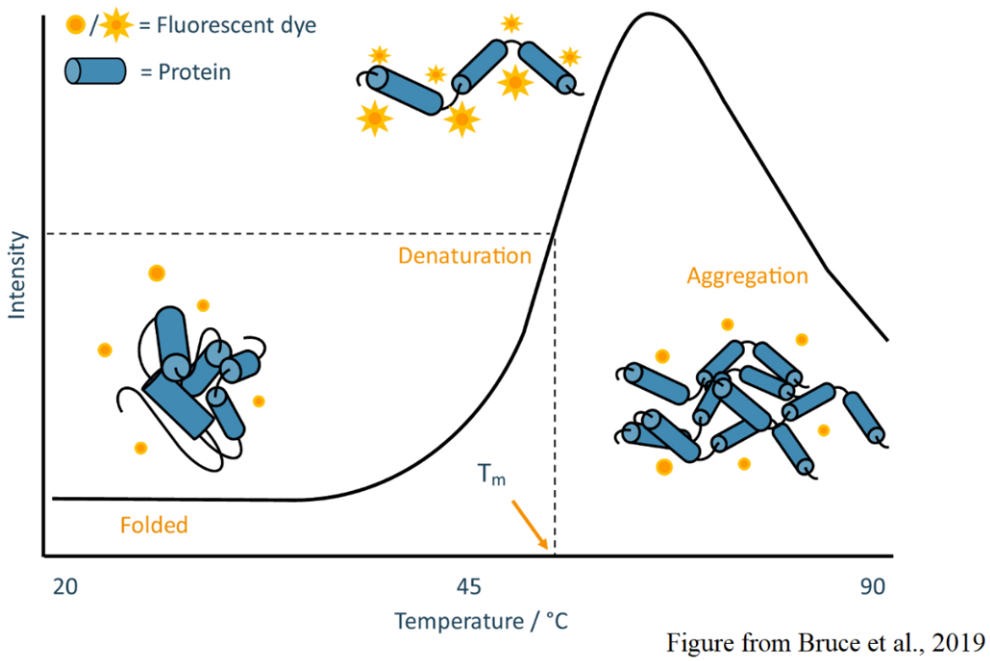


Figure 2.3. Profile of thermal denaturation and emitted fluorescence during DSF *(Bruce et al., 2019, Permission to publish figure in the thesis has been obtained from JoVE).*

RUBIC buffer screen (Molecular dimensions) solution is mixed with 10% of scFvs (v/v) purified on Protein A (3-5 mg/mL) and 10% of Sypro orange diluted 1:1000 (Thermofisher Scientific) in a white 96-well plate and (MLL9651, Biorad). Plates are incubated in the dark MxPro instrument (Agilent). To achieve denaturation, the temperature was raised every 0.5 min until 90°C was reached. Fluorescence data was initially extracted using a tool developed by Radek Nowak, and the resulting data were fitted according to the ProtePlex method (Chari et al., 2015).

2.13 X-ray crystallography

2.13.1 Alexa fluor 555 and 488 staining

The initial crystallisation of TREM2 complexes with scFv-2 and scFv-4 was performed with components stained separately with Alexa fluor 488 or 555 (Thermofisher Scientific). Only 1 in 1000 lysines present in protein sequence is stained with NHS-reactive ester by incubation for 30min at 4°C. The conjugation allows for the detection of highly concentrated protein deposits such as a protein crystal but does not impact the crystallisation process. After staining at low protein concentration, complexes are mixed, and L-arginine and L-glutamic acid is added to quench the reaction. For the follow-up, proteins were crystallised without the Alexa fluorochromes.

2.13.2 Sitting drop vapour diffusion Crystallisation

Vapour diffusion crystallisation is based on the change in concentration of a reservoir precipitant solution and experimental drop where protein sample is mixed with the precipitant solution. Initial protein sample of known concentration is mixed with a precipitant solution, and concentration of protein increases with time as water and volatile components are exchanged between the drop and. The increase in protein concentration leads to supersaturation state and nucleation events resulting in crystal formation when appropriate conditions are met. The requirements for protein crystallisation are notoriously difficult to identify and require a large number of precipitant types and concentrations to be screened.

For each of these experiments, a sitting drop experiment was set up where drop consisted of 150 nL of solution and contained three different ratios of precipitant to

protein solution: 1 to 1, 1 to 2 and 2 to 1 aliquoted into sub wells of Swissci3 plates (Hampton Research), next to reservoir sub well.

To sample the chemical matrix, three different coarse screens were used with 96 conditions available in each screen: Joint Centre for Structural Genomics (JCSG) (Molecular Dimensions), Hampton crystal screen (HCS) and Hampton Index screen (HIN) (Hampton Research). The protein and precipitant solutions were aliquoted using Mosquito liquid handler (TTP Lab Tech), and crystal growth was monitored for 60 days at 4 and 20°C in formulatrix crystallisation imager (Formulatrix).

2.13.3 Crystal growth optimisation

The early crystallisation hits from the coarse screens often require improvement in size and morphology to achieve good resolution. These optimisations are usually achieved by a fine screen designed around a single or couple of the initial conditions. Each component would vary in concentration across 96 conditions resulting in the formation of a grid screen. Occasionally different protein concentrations can be tested, or crystals can be frozen with different cryo-preservants for mounting. Dehydration attempts of scFv-2-TREM2 crystals were performed by adding a reservoir solution to the experimental drop, which contained a 10-15% higher precipitant concentration. Drops were exposed to air for 3 min before vitrification.

Matrix seeding was used if the previous attempts failed to produce better-diffracting crystals and are employed in optimisations of scFv-2-TREM2. Crystals or crystalline matter are crushed in 50 µL of reservoir solution by vortexing and seeding into the original course screens. This occasionally can produce new crystal hits and improve the morphology of crystals previously not suitable for diffraction experiments.

Additive screen SilverBullet (Hampton Research) contains 96 conditions with 1-20 small molecule additives in each well which can improve crystallisation. The screen is used usually in combination with buffer identified initially to produce crystals and was used in optimisations of scFv-2-TREM2.

2.13.4 Complex formation and crystallisation

scFv-4 PDB: 6YMQ

After Protein A purification, scFv-4 in 100 mM Tricine, pH 8 and pTT5:TREM2 (a.a.1-131) were mixed at molar ratio 1:1.1 and after dilution in 50 mM Tris-HCl 8.5, 200 mM L-Arg/L-Glu pH 8, 150 mM NaCl. For crystallisation, buffer was exchanged into 20 mM Tricine pH 8, 200 mM NaCl, 200 mM L-arginine, 200 mM L-glutamic acid. The complex was concentrated to 14 mg/mL, and crystals were grown by sitting drop vapour diffusion in a solution containing 39% MPD, 0.2 M ammonium acetate, 0.1 M citrate pH 5.5 at 20°C. Crystals were mounted directly from the drop and vitrified in liquid nitrogen.

scFv-4 PDB: 6Y6C

Antibody scFv-4 was buffer exchanged into 25 mM HEPES, 300 mM NaCl and 5% glycerol was mixed with TREM2-avi (a.a.1-174) at molar ratio 1:1.1 after dilution in the same buffer. The complex was concentrated to 12.5 mg/mL, and crystal plates were set up after 32,000 x *g* spin for 20 min. Protein crystals appeared after 1 day in a solution containing 0.2 M potassium chloride, 35% pentaerythritol propoxylate 5/4, 0.1 M HEPES pH 7.5 at 20°C. Crystals were cryo-protected after adding a reservoir solution containing 20% ethylene glycol and vitrified in liquid nitrogen.

scFv-2 PDB: 6YYE

Protein A purified antibody scFv-2 in 100 mM citrate buffer pH 6 and 250 mM L-arginine and 50 mM L-glutamic acid was desalted to 100 mM HEPES pH 7 following staining with Alexa 488.: TREM2 (a.a 19-131) in Tris-HCl -based buffer had to be desalted to 100 mM HEPES and 100 mM NaCl before staining with Alexa 555. Both components were mixed together at a molar ratio 1.3:1 before the addition of 200 mM NaCl and 100 mM L-arginine, 100 mM L-glutamic acid. The complex was concentrated to 10 mg/mL, and precipitation was removed by centrifugation. Crystals were grown in 15 mM nickel chloride, 0.1 M Tris-HCl pH 8.5, 2.2 M ammonium acetate at 20°C. Crystals were cryo-protected with a reservoir containing 20% ethylene glycol before vitrification.

2.13.5 Data collection and structure determination

For scFv-4 structures (6YMQ, 6Y6C), data were collected on Beamline I24 at the Diamond Light Source using the X-ray wavelength of 0.9688Å and processed using Xia2 package and DIALS (G. Winter 2010; 2018).

For the lower resolution scFv-2 dataset (6YYE), data were collected on beamline I03 at the Diamond Light Source using the X-ray wavelength 0.9763 Å. The initial model was built using PhenixRefine and coot modelling using Xia and DIALS dataset. Later the model was used to refine against AutoProc processed dataset with ellipsoidal truncation by Staraniso (Evans, 2006; Kabsch et al., 2010; Vonrhein et al., 2011, 2018). The model was finished by refinement in Buster v.2.10.3 (Bricogne et al., 2016) and final rounds of Phenix refine (Liebschner et al., 2019).

The first dataset of scFv-2 (6YYE) was phased using the structure of another scFv (PDB: 6G8R) generated from the same library and solved previously (Fairhead et al.,

2019). TREM2 was phased using PDB 5UD7 (Sudom et al., 2018). The resulting scFv-2 co-structure (PDB 6YYE) was used for the phasing of PDB 6YMQ. Phenix molecular replacement was used to phase the data and coot to build a model (Emsley et al., 2010; Liebschner et al., 2019). Models were improved by iterative cycles of Phenix Refine and coot rebuilding.

2.14 Measuring scFvs affinity to TREM2

2.14.1 BLI

Bio-Layer Interferometry (BLI) is an optical technique used to measure label-free interactions between molecules. The binding of scFvs produced in Stockholm to mammalian deglycosylated TREM2 (19-131) was estimated by BLI. Biotinylated TREM2 at 20 µg/mL was immobilised on Streptavidin sensors (Pall). A serial dilution of scFvs from 1.25 uM to 0.6 nM in 100 mM NaCl, 0.1% BSA, 25 mM HEPES, 0.05% Tween20 buffer were analysed by injecting blank buffer, followed by the lowest to the highest concentration of the analyte. The sensors were washed with buffer (30 s), incubated with scFvs (association 150s) and washed with buffer again (dissociation 1000s) for 13 cycles. Only one sensor was used to analyse all concentrations since only an estimate of the binding was required. A reference sensor without TREM2 was analysed alongside to estimate non-specific binding. Reference signal was subtracted from the ligand sensor data.

The approximate K_D was calculated by ForteBio Data Analysis 11 software using Langmuirian 1:1 model and the relationship between k_{on} and k_{off}. ScFv-3 binding required the use of a bivalent analyte model to estimate binding and most likely was caused by fast dissociation constants. Later, the analysis binding between mammalian

pTT5:TREM2 (a.a.19-174) and new scFvs optimised produced in Sf9 cells was performed in more detail. The same concentrations were used, but a single sensor Super-Streptavidin (Pall), was used for each concentration of the analyte and as a reference sensor. ScFv-1 binding was not analysed due to low initial binding validated by SPR and BLI.

2.14.2 SPR

The work was performed by Jingjing Yang (Eisai). ScFv-1 was determined to be a weaker binder of TREM2 and thus was not analysed in detail. Approximate binding kinetics of Protein A purified ScFv-2, scFv-3 and scFv-4 and Fab and IgG conversions were determined by SPR performed on a Biacore 8K instrument. Biotinylated and glycosylated TREM2 (a.a.19-174) produced in Expi293F^{TM} human cells was immobilised on a streptavidin-coated chip supplied in the Biotin CAPture kit (28-9202-34, Cytiva) at 0.5 μg/mL concentration. Antibodies were diluted in 10 mM HEPES, 150 mM NaCl, 0.05% P-20, and injected at a flow rate of 30 μL/min for 60 seconds followed by dissociation for 120 seconds (unless specified otherwise). The binding response was calculated after subtracting the signal coming from a blank flow cell and the buffer. Langmuirian 1:1 model or bivalent analyte was used to calculate the binding kinetics. For scFv-3 and scFv-4, avidity contributed to obtained values. ScFv-4 showed some non-specific interaction with the reference sensor, and so calculated values are used as approximation only.

2.15 Multi-angle light scattering of scFvs

Multi-angle light scattering (MALS) detectors provide an opportunity to measure the accurate molecular weight of components. The method is based on measuring the

proportion of light scattered by different sizes of analytes into multiple angles relative to the incident of the detector laser beam. When combined with SEC it allows separation of different species according to size first. The molecular weight is derived from the first principles calculations performed by the software.

The experiments were performed in the Molecular biochemistry suite Laboratory, Department of Biochemistry, Oxford University by David Stadon. The scattering of molecules was performed during size exclusion chromatography on an analytical Superdex 200 10/300 GL column (Cytiva) equilibrated with DPBS (Gibco). 150-200 µg of scFv-3 or scFv-4 were injected onto the column. Elution was monitored via online static light-scattering (DAWN HELEOS 8+, Wyatt Technology), differential refractive index (Optilab T- rEX, Wyatt Technology) and UV (SPD-20A, Shimadzu) detectors. Proteins had previously been purified by size-exclusion chromatography. Data were analysed using the ASTRA software package (Wyatt Technology).

2.16 Cell maintenance and differentiation

2.16.1 HEK293

The HEK293 TREM2-DAP12 cell line was a kind gift from Professor Peter St-George Hyslop and generated as described previously (Thornton et al., 2017). HEK293 wild type cell line was purchased from ATCC (CRL1573).

WT HEK293 and HEK293 cells stably expressing WT hTREM2 and hDAP12 were cultured in T-175 flasks (Greiner Bio-one) in DMEM (Gibco) with 10% heat-inactivated foetal bovine serum (FBS) (Gibco) at 37°C, 5% CO_2. The cell culture medium for the HEK293 TREM2-DAP12 cells was supplemented with 1.8 mM puromycin hydrochloride (Cayman Chemical).

2.16.2 THP-1

THP-1 (ATCC,TIB-202) cells were maintained in solution in T175 flasks in RPMI (Gibco), 10% FBS, 2% Glutamax, 0.05 µM Beta Mercaptoethanol 37°C, 5% CO_2. Three days before the assay, cells are harvested and counted and differentiated in a medium containing 100 ng/uL PMA (Sigma).

2.16.3 iMac

Maintenance and differentiation of factories was performed by Juliane Obst as previously described (Hall-Roberts et al., 2020; Wilgenburg et al., 2013). Shortly, the protocol used is as follows: $4x10^6$ iPSC cells were seeded into an Aggrewell-800 plate well (STEMCELL Technologies) to form embryoid bodies in mTeSR™1 media (STEMCELL Technologies). Cells were fed daily with a medium containing 50 ng/mL BMP4 (Peprotech), 50 ng/mL VEGF (Peprotech), and 20 ng/mL SCF (Miltenyi Biotec) growth factors. The embryoid bodies were cultured for 5–6 days in growth factors, but after the first 2 days, they were transferred into low-adherence 6-well plates. Embryoid bodies were further differentiated in T175 flasks (150 per flask), known as factories. iPSC-macrophage precursors, emerging into the supernatant after approximately 3-4 weeks, were harvested weekly and plated into desire assay format before differentiation for 6–10 days to iMac at 37°C/5% CO2, in X-VIVO15 with 100 ng/mL M-CSF, 2mM Glutamax, 100 U/mL pen-strep. Because iMac are harvested and used only once a week, generation of three biological replicates therefore requires at least three weeks.

2.17 TREM2 detection by western blot

Rabbit monoclonal TREM2 (Abcam, ab209814) 1: 750

Rabbit polyclonal GAPDH (Sigma, 9545) 1: 2000

Goat anti-rabbit IgG-HRP (Life technologies, 656120) 1: 5000

Table 2.4. Table of antibodies and dilutions used for western-blot of TREM2.

IPSC-derived macrophages were differentiated for 1 or 8 days by seeding 1 x 106 cells per well (Corning Costar, 3516). THP-1 cells were plated at 1 x 10^6 in a medium containing PMA. HEK-TREM2 cells were plated at 0.5 x 10^6 24 hours before. Cells were washed with 1 mL of DPBS followed by incubation in the appropriate medium for 17 hours. The medium was harvested, and cells were lysed in 120 µL Pierce IP buffer containing complete protease inhibitors (Roche). Samples were stored at -80℃ and defrosted when needed. Protein concentration in samples was adjusted using Bradford assay (Thermofisher Scientific). 30 µg of the sample was separated by SDS-PAGE in SDS-glycine buffer and transferred to nitrocellulose membrane by semi-dry transfer (Bio-rad). Membranes were blocked for 1 hour in 5% BSA (Sigma) in PBS containing 0.05% Tween (PBS-T), separated and incubated with primary antibodies in blocking buffer at 40C o/n. The next day the membranes were washed with TBS-T, incubated with secondary antibody for 2 h at RT and bands were visualised by addition of SuperSignal West Dura (Thermofisher Scientific) followed by imaging in LAS 4000 (FujuFilm). Membranes were subsequently stripped for 30 minutes using restore buffer (Thermofisher Scientific) and probed with GAPDH antibody using the same protocol.

2.18 Shedding assay

2.18.1 HEK293 and THP-1

HEK293 transfected with TREM2-DAP12 were plated in 96-well PDL-coated plates (Corning Biocoat, 354640) at $30x10^3$ cells per well, grown for 24 h, washed with culture medium and treated with antibodies for 5 h. THP-1 cells were seeded at $50x10^3$ counted, and 100 ng/uL PMA was added to the culture medium for 72 hours before the assay. Cells were washed before the assay. After antibody incubation, the medium was collected and transferred into a new plate, centrifuged at 1,000 x *g* followed by supernatant transfer into a fresh plate that was stored at -80°C. Cells were fixed in 4% PFA for 10-15 min at RT and stored in PBS until nuclei counting or used for PrestoBlue HS assay.

2.18.2 iMac

iMac cells differentiated for at least 7 days and seeded at $30x10^5$ in 96-well CellCarrier Ultra plates (PerkinElmer). Cells were washed with differentiation medium ant antibodies diluted in the same medium were added for 5 our 17 hours. The medium was harvested, clarified by centrifugation and stored at -80°C. Cells were fixed in 4% PFA for 10-15 min at RT and stored in PBS until nuclei counting.

2.19 sTREM2 ELISA

TREM2 ELISA was performed by coating high bind 96-well plates (Sigma, M4436-040EA) with 8 µg/mL TREM2 antibody (Abcam, ab209814) overnight at 4°C followed by blocking in PBS with 1% BSA (Sigma) for one hour. 100 µL of the defrosted cell supernatants were added at the appropriate dilution in DMEM containing

1% BSA alongside a standard curve with TREM2 peptide a.a.19-174 (Sino Biologicals, 11084-H08H) and incubated for 2 h, at RT. 25 µL of the biotinylated detection antibody (R&D, BAF1828) at 1.5 µg/mL was added for an hour, followed by the addition of HRP conjugated streptavidin diluted to 1:30,000 in PBS (ThermoFisher Scientific, 34028). 100 µl TMB ELISA substrate (ThermoFisher Scientific) was added for 20 min followed by reaction quenching by the addition of 100 µl of 2 M sulphuric acid (Immuno Chemistry technologies). Optical density (OD) at 450 nm was measured using a plate reader (SpectraMax M2). OD measurements in the linear range (0.8-1.9) were chosen for analysis, and TREM2 concentration was interpolated from the TREM2 standard curve.

2.19.1 ELISA validation

To ensure that scFv binding to TREM2 did not interfere with the ELISA capture and detection antibodies, the medium conditioned in HEK293 cells for 5 h was harvested from HEK293 cells and spiked with scFvs, and ELISA was performed in comparison to the non-spiked samples.

In order to estimate TREM2 epitope recognition by the ELISA antibodies, TREM2 proteins (a.a.19-138 and 19-174) purified from *sf9* cells were diluted to 2441 pg/mL in DMEM containing 1% BSA using five-fold serial dilutions and analysed using the protocol described above.

2.19.2 Normalisation to cell number

The results of sTREM2 ELISA were normalised to the density measured after plate fixation and staining with Hoechst 33342 followed by Opera Phenix imaging at

20 x magnification. The nuclei were either calculated with nuclei counting protocols (low density) or by Hoechst 33342 signal area (high density, sticky cells).

In the absence of OperaPhenix availability during 2020, PrestoBlue HS (Thermofosher) was used to measure cell viability. 40 uL of conditioned medium was kept in the wells, and 5 uL of PrestoBlue and 5 uL fresh medium were added to the cells for 1 hour at 37℃. The viability was measured by fluorescence according to the manufacturer's instructions. The cell counting or PrestoBlue were kept consistent between the biological repeats of each experiment.

2.20 Surface TREM2 ELISA

For detection of TREM2 on fixed HEK293 cells, the cells in 96-well plates were prepared as described above and later were treated with scFv for 5 hours. After the medium was removed, cells were washed with PBS and fixed with 4% PFA for 10 min. To prevent unspecific staining with antibodies, cells were blocked in 50 µL of PBS with 5% normal donkey serum containing 5% BSA for 1 hour at RT. After optimisations, BAF1828 (R&D systems) at a concentration of 0.9 µg/mL was incubated with cells in a blocking buffer for one hour. Cells were washed three times with 0.1% Triton-X100 for 10 min with gentle rocking. HRP conjugated streptavidin diluted at 1:120,000 (ThermoFisher Scientific, 34028) in PBS was added for an hour. After washing, TMB ELISA substrate and quenching solution were added. The standard curves for this experiment cannot be generated and raw OD was used to visualise data.

2.21 Immunocytochemistry

2.21.1 Alexa fluor 647 conjugation and HEK293 treatment

Purified scFv-2, scFv-3 and scFv-4 oligomers and control non-TREM2 scFvs were incubated with Protein A and Alexa Fluor 647 NHS ester (Thermofisher Scientific) at 1:10 molar ratio for 17 h, at 4°C and excess dye was removed by NAP5 columns (Cytiva). The staining efficiency was assessed by measuring the concentration of fluorochrome and protein by nanodrop. For all of the proteins tested except for scFv-2 the efficiency was between 3-4 moles of dye per scFv monomer.

HEK293 and HEK293 transfected with TREM2-DAP12 were prepared for the ELISA in 96-well PDL-coated plated and treated with scFv-4 for 5 h at 10 µg/mL. Cells were fixed in 4% paraformaldehyde in PBS (Santa Cruz Biotechnology) for 15 min and kept at 4°C until imaging. Nuclei were stained with Hoechst 33342 for 30 min in the dark, and cells were imaged using an OperaPhenix confocal microscope with 40 x magnification or 64 x when specified.

To inhibit endocytosis, the same experiment was performed at 4℃ or in the presence of 80 µM Dynasore. Control cells and Dynasore (Biotechne) treated cells were incubated in FBS-free medium Opti-Mem (Gibco) with or without inhibitor for 60 minutes. Then conjugated scFv were diluted in Opti-Mem with or without inhibitor and incubated for 4 hours unless specified otherise.

2.21.2 Lysosomes, endosomes and TREM2 staining

anti-TREM2 AF1828 (R&D Systems), 1:30 dilution
anti-goat IgG-Alexa Fluor 488 (Thermofisher Scientific, A11055), dilution 1: 1000
anti LAMP1 (CST,9091), 1: 200
anti-RAB9A (CST, 5118), 1:100

anti-Rabbit Alexa Fluor 568 1:1000 (Thermofisher Scientific, A10042), 1: 1000

Table 2.5. List of antibodies and dilutions used for immunocytochemistry

Fixed HEK293 cells were permeabilised with PBS containing 0.1% Triton-X100 for 20 min at RT. Cells were blocked in 100 µL of PBS with 0.05% Triton-X100 including 10% normal donkey serum and 5% BSA overnight. The primary antibody combinations were prepared in blocking solution and incubated with cells for 2 hours at RT with gentle shaking. The antibodies were removed by three washes in PBS containing 0.3% Triton for 15 minutes. The secondary antibodies were diluted in blocking buffer and incubated for 1 hour at RT. Afterwards, plates with cells were stained for nuclei and imaged by confocal microscope Opera Phenix.

2.22 TREM2 activation assay

2.22.1 Antibody and antibody fragment stimulation

iMac or THP-1 cells in 96-well plates after differentiation were treated with antibody solutions for 4 min 30 seconds. The solution was removed, and 50 µL of HTRF buffer containing Complete protease inhibitors (Roche) and PhosphoSTOP phosphatase inhibitors (Roche) was added to each well and incubated for 30min at RT before freezing at -80 ℃. The goat polyclonal TREM2 antibody (AF1828, R&D Systems) was used as a positive control at a concentration of 3.3 µg/mL.

2.22.2 Apoptotic SH-SY5Y stimulation

SH-SY5Y Human Neuroblastoma Cell Line (ECACC #94030304) were cultured in were 1:1 mixture Eagle’s Minimum Essential Medium (Sigma, M2279) and Ham’s

F12 Nutrient Mixture (Sigma, N4888) containing 15% Foetal Bovine Serum (FBS), 1% Non-essential amino acids (Sigma, M7145), 2 mM Glutamax (Gibco) and 1% (v/v) Penicillin-Streptomycin (Gibco) in T75 or T175 flasks. Cells were detached by TrypLE treatment for 2-3 minutes at 37°C. Cells were resuspended in PBS and centrifuged at 400 x *g* for 5. Cells were re-suspended in 2 mL of PBS, and 2 mL of 4% paraformaldehyde was added. Apoptosis was induced for 10 min at RT with occasional gentle agitation. Another 15 mL of PBS was added, and cells were centrifuged at 1200 x *g* for 7 minutes and resuspend in a low amount macrophage medium (or THP-1 medium) before counting.

50 µL of neurons at appropriate density was added to each 96-well of iMac or THP-1 cells and incubated at 4°C for 60 min to allow the neurons to settle to the bottom of the plate. Next, the plates were moved to 37°C for an hour, after which medium was removed, and 50 µL of HTRF buffer was added.

2.22.3 HTRF

HTRF (Homogeneous Time-Resolved Fluorescence) is based on FRET (fluorescence resonance energy transfer) technology when energy is transmitted from donor to acceptor molecule while they are in proximity (10-100 Å). Excitation of the donor by an energy source such as a flash lamp triggers an energy transfer towards the acceptor, which results in the emission of fluorescence at a given wavelength. In the case of TREM2, two antibodies conjugated to fluorochromes (cryptate or d2 molecules) bind either phospho-SYK or SYK epitopes are used.

P-SYK (Tyr525/526) and Total SYK (Perkin Elmer) assays were performed according to the instructions for adherent cells, and 4 µL of antibody mix was added to 16 µL of samples in the microplate (PerkinElmer, ProxiPlate Plus) followed by

incubation overnight at RT. Plates were read using standard HTRF flash lamp protocol in Pherastar FSX (300 flashes per second). P-SYK results were obtained after dividing the 650 nm signal by donor background emission at 620 nm and multiplying by 10,000. Results were normalised after subtracting background and dividing P-SYK results by T-SYK. The final results were multiplied by 10,000.

2.23 Software and statistical analyses

PISA software, https://www.ebi.ac.uk/pdbe/pisa/(Krissinel and Henrick, 2007).

Unimod, https://www.unimod.org/modifications_list.php

Matthews coefficient calculations, http://www.ruppweb.org/mattprob/

Glycosylation prediction http://www.cbs.dtu.dk/services/NetNGlyc/

Molecular graphics and analyses were performed with UCSF ChimeraX, developed by the Resource for Biocomputing, Visualization, and Informatics at the University of California, San Francisco, with support from National Institutes of Health R01-GM129325 and the Office of Cyber Infrastructure and Computational Biology, National Institute of Allergy and Infectious Diseases (Goddard et al., 2018). Crystal lattice images were generated using PyMOL (Schrödinger, LLC.).

Chapter 3

Production of TREM2 protein for crystallography and antigen generation

3.1 Introduction

Structural and functional studies are important to understand the mechanisms of TREM2 in microglial function, especially during AD progression. No TREM2 structures were known when this project was initiated, and TREM2 had never been shown to form a stable complex with any of its proposed ligands. We hypothesised that heterologous expression of human TREM2 could lead to the generation of folded protein which will be suitable to use as an antigen in antibody production. Furthermore, the same protein of high homogeneity could be used to validate TREM2 epitopes for these antibodies by X-ray crystallography. We decided to test one prokaryotic and two eukaryotic expression systems for the ability to produce soluble and high purity TREM2 ectodomain fragments.

The closest homolog of TREM2 with a known three-dimensional structure is TREM1. The TREM1 ectodomain structure has been solved as a monomer or a dimer in biological assembly by two different groups (PDB:1Q8M and 1SMO) (Radaev *et al.*,

2003; Kelker *et al.*, 2004). The two proteins share only 30% homology in the ectodomain sequence but contain a similar V-type Ig-like domain. This is consistent with a low sequence identity but a general shared fold of proteins belonging to the immunoglobulin superfamily (IgSF) (Halaby and Mornon, 1998).

TREM2 presents a challenging target for biochemical and structural studies due to the presence of posttranslational modifications and the transmembrane domain. Since the majority of point mutations associated with neurodegeneration are located in the ectodomain, our and other efforts to produce heterogeneously expressed protein for the purpose of X-ray crystallography have been focused on this region. This 156 amino acid long Ig-like domain is considered complex for its size, with two disulphide bonds and two glycosylation sites. Not surprisingly, early attempts to refold it from inclusion bodies expressed in *Escherichia coli (E. coli*) were unsuccessful (Kober et al., 2014). The same group also reported the purification and crystallisation of TREM2 from mammalian cells treated with glycosylation inhibitor- kifunensine to block complex glycosylation, but the protein structure was not published nor deposited in protein data bank until late 2016 (PDB) (Kober et al., 2014, 2016). This chapter describes strategies to express and purify TREM2 in bacterial, insect and mammalian cells for the purpose of X-ray crystallography and antigen generation for scFv phage display, both of which require correctly folded protein.

The prokaryotic expression system is significantly less costly and time-consuming than any other expression platform, in addition to lacking the complexity of protein glycosylation. The eukaryotic expression systems, including *Spodoptera frugiperda* (*Sf*9) insect cells and mammalian Expi293^{TM} cells, can modify polypeptides by adding disulphide bonds and sugar groups, although the latter differs significantly in its complexity.

The TREM2 sequence is predicted to contain two *N*-linked glycosylation sites at asparagine 20 and 79, located within the consensus sequon of Asn-X-Ser/Thr (where X is any amino acid except for proline) (Bause, 1983). It is well established that the large size and complexity of glycans can increase surface entropy, heterogeneity and flexibility, which is disadvantageous to the crystallisation process (Chang et al., 2007; Davis and Crispin, 2010). Thus, the successful production of correctly folded TREM2 in bacterial cells could benefit protein production for X-ray crystallography purposes. I have chosen a different strategy of fusing TREM2 to bacterial outer-membrane protein F (OmpF) or osmotically inducible protein Y (OmpY) for secretion to the medium (Kotzsch et al., 2011). For these proteins to be secreted to the outer membrane, they are first transported through a periplasmic environment where the formation of disulphide bonds is catalysed by Dsb (disulphide bond formation) proteins (Sevier and Kaiser, 2002). The method is based on the underexplored ability of laboratory bacterial strains to secrete proteins and the resulting secretion of target proteins fused to these carriers (Zhang et al., 2006).

Contrary to mammalian *O*-linked glycosylation, which also occurs in bacterial cells, *N*-linked glycosylation is a co-translational process that significantly impacts protein folding and stability and can be performed by eukaryotic cells only (Parodi, 2000). Although a lack of *N*-linked glycosylation machinery in bacteria could benefit the formation of TREM2 crystals, it can also be deleterious to protein folding and even disrupt potential crystal contacts formed by sugar groups (Mesters and Hilgenfeld, 2007). Consequently, TREM2 constructs for expression in insect cells, which are perfectly poised to produce functionally active glycoproteins, were generated. *N*-linked glycosylation in these cells results in paucimannose core α1−6-fucosylated Man3GlcNAc2 glycans, relatively compact high mannose sugars suitable for direct

crystallisation (Garcia et al., 1996; Petrescu et al., 2004). Additionally, *in vitro* treatment by endoglycosidases such as Endo H or Endo F 1, 2, 3 can result in glycans trimmed to a single *N*-acetylglucosamine (GlcNAc), preserving protein solubility and homogeneity. A practical advantage, also, was the wealth of experience and the vector database for expression in *Sf9* that the Structural Genomics Consortium (SGC) has accumulated thus far.

Finally, mammalian cells generate the most complex glycosylation pattern with highly heterogeneous sugar groups, which reflect human expression most accurately but are an obstacle to crystallisation. Such glycans are resistant to endoglycosidases and thus require removal of the entire sugar molecule by *N*-glycosidase F (PNGase F), transforming the original asparagine into aspartic acid (**Figure 3.1a**). Although the enzyme can be used against both insect and mammalian proteins, its action may be restricted by poor substrate accessibility or leads to a dramatic change in protein solubility. Thus, current methods commonly focus on targeting the glycosylation pathway during protein translation in the endoplasmic reticulum (ER) (**Figure 3.1b**). (Chang et al., 2007). A compound called kifunensine, isolated initially from *Kitasatosporia kifunense,* inhibits α-mannosidase I, which catalyses the removal of mannose groups required to form complex glycans and has been successfully used in the production of TREM2 (Kober et al., 2014, 2016; Sudom et al., 2018). Furthermore, HEK293S and Expi293F^{TM}GnTI- (Thermofisher Scientific) cell lines lacking acetylglucosaminyltransferase I (GnTI) were recently generated (**Figure 3.1b**). (Reeves et al., 2002). GnTI acts downstream of mannosidase I and catalyses the addition of *N*-acetylglucosamine (GlcNAc), resulting in the first step in complex glycan formation. Both approaches result in the generation of compact oligo mannose glycans, which,

similarly to sugars produced in insect cells, can be cleaved with endoglycosidases (Chang et al., 2007; Nettleslip, 2012).

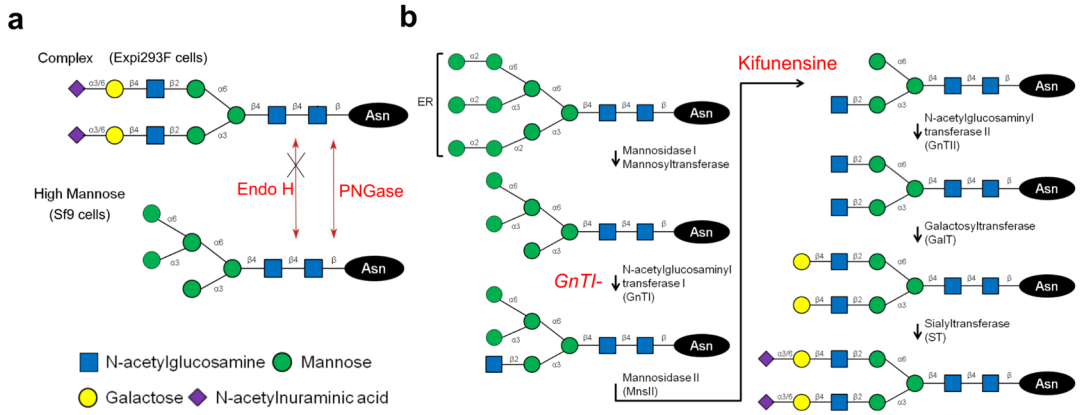


Figure adapted from Nettleship, 2012

Figure 3.1. Types of glycosylation produced in eukaryotic cells. *(a) Complex and high mannose sugar groups are produced by mammalian and insect cells, respectively. Endoglycosidase H/ F1 (Endoglycosidase) and PNGase (Peptide-N-Glycosidase F) cleavage sites are marked. (b) Glycosylation pathway in mammalian cells with enzymes involved in the pathway. GnT1- mutant site is marked in red, intervention site of compound kifunensine is also shown (Figure adapted from Nettleship, 2012, Permission to publish figure was obtained under conditions described in Creative Commons CC-BY licence).*

As a transmembrane type I protein, the TREM2 sequence contains an N-terminal signal peptide (a.a.1-18), which targets the protein to the ER where posttranslational modifications such as glycosylation and disulphide formation occur (Hegde and Bernstein, 2006; Martoglio and Dobberstein, 1998). Successful clearance of the ER secretory pathway is often considered a quality control step leading to the expression of correctly folded proteins, which can be exploited for heterogeneous protein over-expression (Ellgaard, 1999). Therefore, correct recognition of the signal peptide by the signal recognition particle (SRP) and its particular sequence is crucial in deciding the protein's quality and fate (Hegde and Bernstein, 2006; Martoglio and Dobberstein,

1998). Thus, special attention was paid to the presence and sequence of the signal peptide attached to the N-terminus of TREM2.

This chapter describes the cloning and expression of TREM2 ectodomain variants into nine different vectors across three different expression systems. Firstly, TREM2 was successfully purified in *Sf9*, a well-established system for the production of human glycoproteins. The soluble and correctly folded Ig-domain TREM2 (a.a.19-131) produced in *Sf9* was used as an antigen for the generation of antibody fragments. Production of TREM2 for crystallography required additional construct design and mammalian Expi293^{TM} system and was established later, resulting in a large amount of homogenous TREM2.

3.2 Initial TREM2 construct design

Different truncations of the TREM2 ectodomain were prepared after the initial screening campaign involving the design of constructs in seven different expression vectors (**Table 2.2**). Because the structure of TREM2 was unknown at the time, in silico domain prediction was used to design boundaries of TREM2 constructs. The beginning and end of Ig domain boundary was determined using psiPRED, a tool for secondary structure prediction (http://bioinf.cs.ucl.ac.uk/psipred, Buchan and Jones, 2019). PsiPRED identified nine β-strands in the TREM2 sequence in agreement with the expected Ig domain V-type fold (Halaby and Mornon, 1998). **Figure 3.2** also shows the position of only one predicted α-helix at a.a.175-197.

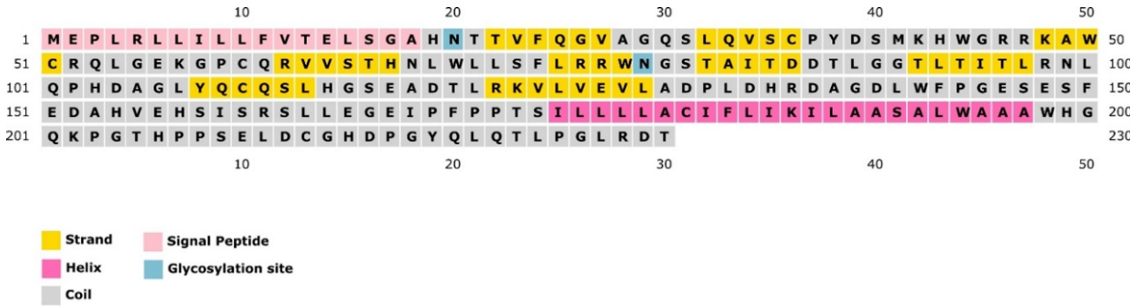


Figure 3.2. TREM2 secondary structure prediction. TREM2 secondary structure content was analysed by PsiPRED server*. TM α-helix is presented in magenta, β-strands in yellow and coil in grey colour. Signal peptide (light pink) and glycosylation site (blue) locations were extracted from UniProt (accession: Q9NZC2).*

The variation in construct design at the N-terminus was limited due to potentially immediate start of the Ig-like domain at Threonine 22 **(Figure 3.2**). Thus, the main variation were introduced by truncating the TREM2 sequence at the C-terminus. I designed a three TREM2 constructs terminating after the last β-strand of the ectodomain at Asp131, Ala138, or Gly146, all lacking the stalk sequence and three constructs spanning the stalk and ADAM cleavage site (Arg161, Gly165, Ser174) (**Figure 3.3a**). The longest TREM2 construct (a.a.19-174) terminated just before the transmembrane domain. TREM2 signal peptide was included, omitted, or replaced by the sequence in the expression vector (**Figure 3.3a**). All vectors contained a polyhistidine tag (His_6 or His_{10}) with an associated Tobacco Etch Virus (TEV) cleavage sequence for tag removal when required. Additionally, the location of the tag was restricted to the C-terminus if the native signal peptide was present.

Apart from cloning TREM2 into bacterial LIC-adapted pBAS-Y and pBAS-F for secretion to the medium, TREM2 was cloned into four vectors for the baculovirus *Sf9* system and one mammalian expression vector (**Figure 3.3b**). First, TREM2 was cloned into the baculoviral transfer vector pFB-Sec-NH, which contains a gp64 signal peptide

to direct proteins for secretion into the medium (Wang et al., 2015c). In parallel, the ability of the native signal peptide to efficiently target TREM2 for secretion was tested by including it with the mature peptide sequence in the non-secretion vector pFB-LIC-Bse.

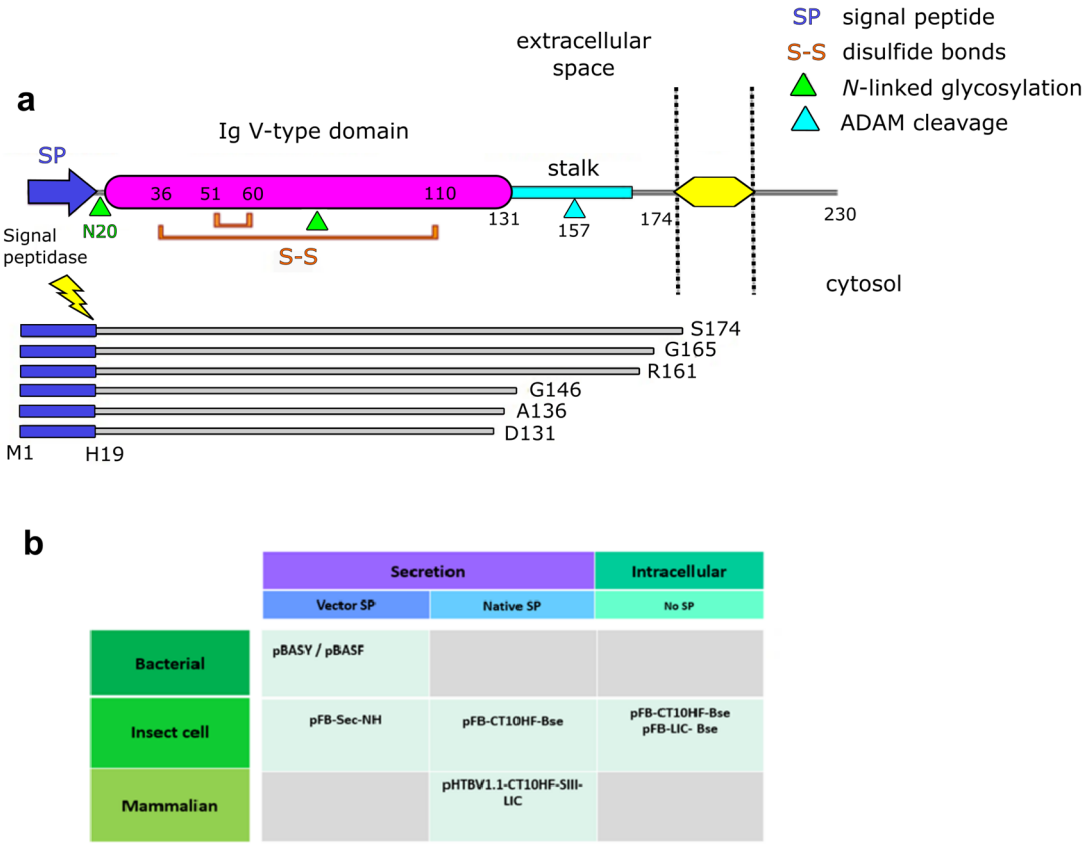


Figure 3.3. Design of TREM2 ectodomain constructs. *(a) TREM2 construct boundaries are marked by amino acid single letter residue symbol followed by the number according to the Uniprot Q9NZC2 sequence. The start and end of signal peptide and peptidase cleavage site are marked by a blue box. (b) Table illustrated strategy of TREM2 signal peptide (SP) choice in respect to expected localisation of the product and vector and expression system used.*

Intracellular expression for constructs without any signal peptide was tested by generating constructs with both N- and C-terminal histidine tags in pFB-LIC-Bse and pFB-CT10HF-LIC, respectively. Due to the lack of an available mammalian secretion vector at the time, TREM2 was cloned with its native signal peptide into the mammalian

expression vector pHTBV1.1-CT10H-SIII-LIC, which provides C-terminal His_{10} and Strep-II tags.

3.3 High-throughput cloning and small scale expression testing of TREM2 constructs for further studies

High-throughput (HTP) protocols generated in the SGC were used to clone, express and purify TREM2. All inserts were successfully generated by PCR and LIC cloned into *E. coli* expression or baculovirus transfer vectors. Plasmids for bacterial expression were transformed into BL21(DE3)-R3-pRARE2, a phage-resistant bacterial strain that carries the pRARE2 plasmid coding for seven tRNA genes that are not common in bacterial proteins. Plasmids for eukaryotic expression were transformed into the DH10Bac strain for transposition into bacmid DNA and subsequent production of viruses for eukaryotic cell protein production. All proteins were tested for recombinant expression on a 1 or 3 mL scale and initially purified by immobilised metal affinity chromatography (IMAC).

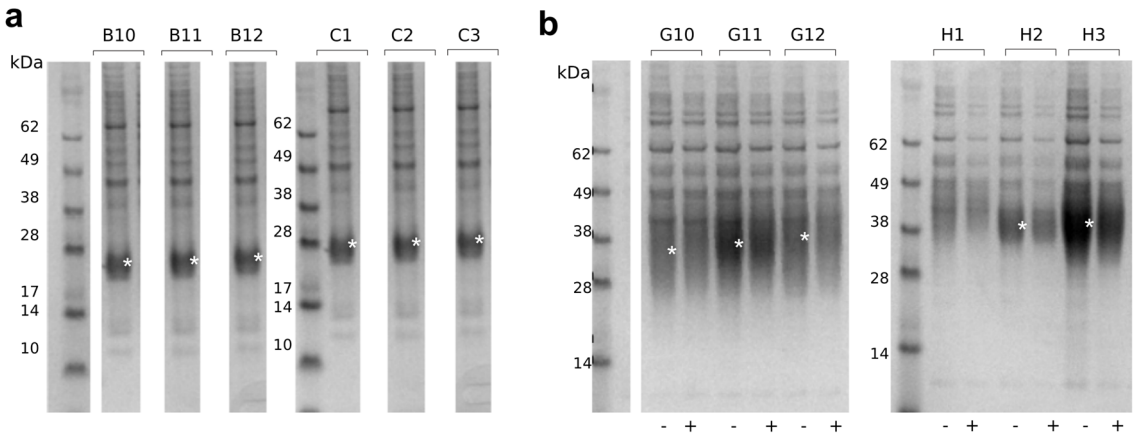


Figure 3.4. Results of eukaryotic TREM2 small-scale expression. *(a) SDS-PAGE images of 3 mL test expression in Sf9 insect cells. Proteins secreted to the medium were purified by IMAC and elutions were analysed by SDS-PAGE. pFB-sec-NH construct boundaries are B10 (H19-D131), B11 (H19-A138), B12 (H19-G146), C1 (H19-R161), C2 (H19-G165), C3 (H19-S174)*

(b) SDS-PAGE images of 3 mL test expression in mammalian Expi293F™ cells. Proteins secreted to the medium were purified StreptactinXT with (+) or without (-) addition of 50 mM HEPES pH 7.5 and 200 mM NaCl, and elutions were analysed. pHTBV1.1-CT10H-SIII-LIC construct boundaries are G10 (H19-D131), G11 (H19-A138), G12 (H19-G146), H1 (H19-R161), H2 (H19-G165), H3 (H19-S174). Bands positively identified as TREM2 by MS/MS analysis are shown by asterisks.

Initial results of expression allowed to establish successful combinations of the signal peptide, construct boundaries and expression system to generate particular TREM2 proteins required for antigen generation or crystallography experiments. Bacterial TREM2 expression from both vectors did not result in the significant production of soluble protein. In eukaryotic expression, only the proteins secreted to the medium were purified successfully (**Figure 3.4**). In *Sf*9 cells, constructs containing the native signal peptide of TREM2 failed to produce protein, and only insect cell native gp64 leader sequence in pFB-Sec-NH produced well-secreted proteins (**Figure 3.4a**). In mammalian Expi293F™ cells, on the other hand, native TREM2 signal peptide led to efficient secretion (**Figure 3.4b**). As expected, the expressed proteins were glycosylated, appearing as smeary (non-resolved) bands on coomassie stained SDS-PAGE and migrated differently to the expected molecular weight. Figure 3.4b confirms significantly more heterogeneous TREM2 glycosylation in Expi293™ than in *Sf9* cells. Different C-terminal truncations of TREM2 were generated to increase the success rate of obtaining soluble protein, but the choice of vector and signal peptide had a much higher impact on the success rate in TREM2 production.

3.4 Generation of TREM2 antigen

During phage display, the target antigen is immobilised on magnetic streptavidin beads for phage presentation and selection (Preger et al., 2020). So the next step in antigen generation was to produce biotinylated TREM2 that can bind streptavidin. In order to generate antigen with Ig-domain only or Ig-domain plus the entire stalk sequence, I selected the short, medium, and long TREM2 sequences (a.a.19-131; a.a.19-136; a.a.19-174) to be cloned into pFB-Sec-Bio5 containing the 15 amino acid Avi-tag at the C-termini. Proteins produced from this vector are secreted to the medium in the same manner as from pFB-Sec-NH and contain a lysine within the Avi-tag, which can be recognised by biotin ligase (BirA). The vector also encodes the *E.coli biotin ligase* (BirA) enzyme itself for *in cellulo* biotinylation. This time, to constructs: Ig- only TREM2 (a.a.19-131) and one stalk-containing TREM2 (a.a.19-174) construct were selected for immediate scale-up (**Figure 3.5a a,b**).

TREM2 proteins secreted to the medium from *Sf9* cells are correctly folded as shown by SEC (**Figure 3.5a,b**). Proteins secreted to the medium from *Sf9* cells for three days were purified by IMAC on a large scale. This revealed degradation of the longer TREM2 (a.a.19-174) construct as evidenced by lower molecular weight products (**Figure 3.5a b, multiple asterisks**), but good stability of the shorter TREM2 (a.a.19-131) construct (**Figure 3.5a a**).

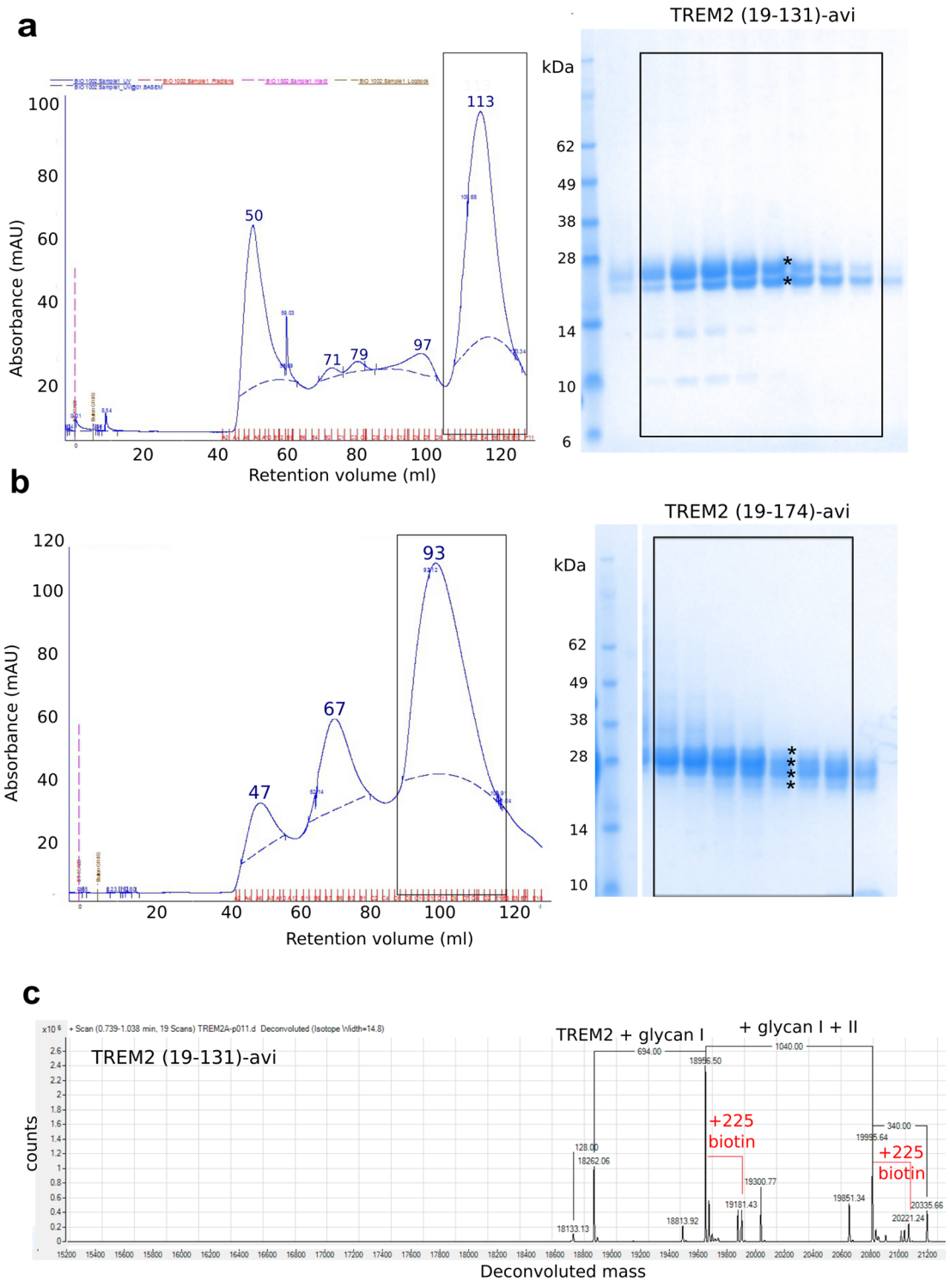


Figure 3.5. Selection and purification of TREM2 for antigen selection. *(a) Purification results of in cellulo biotinylated TREM2 (19-131). Protein was purified by IMAC and size exclusion chromatography. SEC chromatogram and SDS-PAGE of fractions 113 mL (bracket) are shown on the left and right. Bands identified by MS/MS tryptic digest as TREM2 are marked by asterisks. (b) Purification results of in cellulo biotinylated TREM2 (19-174) were performed*

similarly to (a) but with TEV cleavage and TEV removal step before SEC. Fractions of peak at 93 mL are shown in SDS-PAGE in brackets. (c) Intact Mass Time of flight (TOF) analysis of short construct TREM2 (19-131) showing multiple peaks for glycosylation and small fraction of biotinylated protein with shift of 225 Da. Glycosylation was identified by matching mass increase to unimod.org database and single glycosylated state is marked as TREM2 + glycan I (TREM2 I) and double glycosylated state as TREM2 + glycan I+II (TREM2 I+II).

Mass Spectrometry analysis confirmed that the double band appearing during SDS-PAGE of TREM2 (a.a.19-131) was due to glycosylation rather than degradation or contamination (**Figure 3.5a,c, Figure 3.7**). Due to correct better stability, TREM2 Ig domain (a.a.19-131) was selected as an antigen for phage display. A 225 Da shift during the time of flight mass spectrometry (MS TOF) determined that the sample partially was biotinylated (**Figure 3.5c**). Since more efficient biotinylation is required for appropriate antigen concentration during phage display, the purified protein was further biotinylated *in vitro* at the Karolinska Institute.

3.5 Optimisation of insect cell TREM2 for crystallisation

3.5.1 Optimisation of TREM2 deglycosylation for crystallisation

For crystallisation purposes, optimisation began with *Sf9*-produced proteins since these cells produce oligo-mannose sugars, which could be easily removed by Endo F or Endo H after initial purification. A number of constructs were scaled up, and generally, *Sf9* cells produced good yields of folded TREM2 secreted to the medium. One of the best-behaved constructs was TREM2 (a.a.19-161), containing Ig-domain and the majority of the stalk sequence shown to be homogenous by SEC analysis (**Figure 3.6a**).

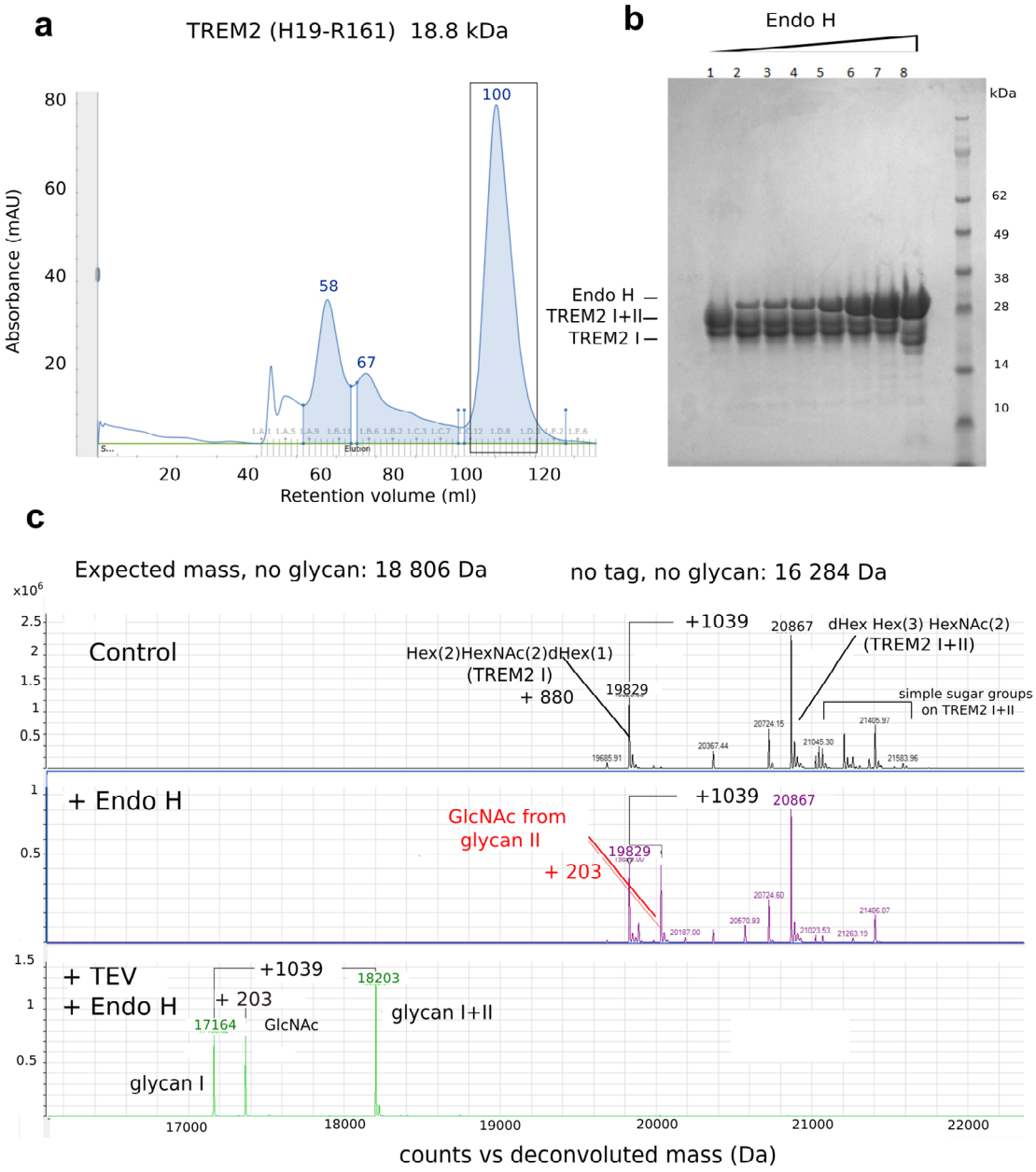


Figure 3.6 Endo H treatment of TREM2. *(a) SEC of TREM2 (a.a.19-161) on Superdex 200 16/60. TREM2 monodisperse fractions used for de-glycosylation are shown in a box. (b) TREM2 was treated with an increasing concentration of Endo H at pH 6.5, and cleavage was monitored by SDS-PAGE. The last sample (8) was also cleaved with TEV. A small decrease in density of top band (TREM2 I+II) can be observed after treatment. (b) De-glycosylation was controlled by MS analysis on QTOF instrument after addition of Endo H. Hex(2)HexNAc(2)dHex(1) (glycan I) and second dHex(1)Hex (3)HexNAc(2) (glycan I+II) were detected with additional masses indicating small sugar groups in control and deglycosylated*

sample (top panel). The last sample shown in the bottom panel was treated with Endo H and TEV.

However, the *N*-linked glycosylation pattern turned out to be more heterogeneous than expected. As previously, TREM2 separated during SDS-PAGE into two species according to their glycosylation state (**Figure 3.6b**). The molecular weight change caused by the presence or absence of a single glycan is enough to cause a shift during electrophoresis. Still, relatively little smearing suggested compact glycosylation. In agreement, MS TOF analysis revealed two main peaks consisting of single, glycosylated species (TREM2 I) and double glycosylated species (TREM2 I+II) without the presence of non-glycosylated protein (**Figure 3.6c, top panel**).

Since *Sf9*-produced TREM2 consisted of two distinct protein populations, further enzymatic removal of *N*-linked glycans was necessary to maximise successful crystallisation. As described before, PNGase F can be used to remove all glycosylation from the polypeptide, but unfortunately, it led to TREM2 deglycosylation only under protein-denaturing conditions. On the other hand, Endo F1 and Endo H enzymes leave a single N-acetylglucosamine (GlcNAc) residue attached to the asparagine, resulting in more limited glycan trimming.

Various TREM2 constructs and different pH conditions were tested, but none of these enzymes showed robust activity. Purified proteins were also tested for the presence of the fucosyl group, which produces glycans resistant to Endo F1 treatment by simultaneous treatment with Fucosylase (NEB) and Endo F1 with no improvement. Only minimal improvement in the double glycosylation site was observed after Endo H treatment (**Figure 3.6a**). MS confirmed the appearance of single GlcNAc residue after the treatment, which indicates trimming of the core oligo mannose sugar, but the

efficiency was very low (**Figure 3.6b, top and middle panels**). Because data interpretation of glycosylation patterns is very challenging due to the complexity of glycans, possible degradation, and variable signal peptide cleavage, TEV was used to remove signal peptide for analytical purposes in the bottom panel (**Figure 3.6**). Despite unsuccessful deglycosylation, the protein was biochemically stable and monodisperse, so crystallisation trials were undertaken without positive outcomes (**5.2.1**).

3.5.2 Characterisation of insect cell produced TREM2 glycosylation

Since TREM2 could not be deglycosylated using standard methods, glycosylation was analysed further. First, TREM2 *N*- or *O*-linked glycosylation type had to be confirmed since any enzymatic treatment does not work against the latter. Treatment with PNGase F resulted in complete deglycosylation observed as a significant shift on SDS-PAGE, confirming the presence of *N*-linked glycans **(Figure 3.7a, glycan 0).** Unfolding of the TREM2 substrate and exceptional stability of the enzyme under denaturing conditions allowed PNGase F to be used for quality control purposes after denaturation.

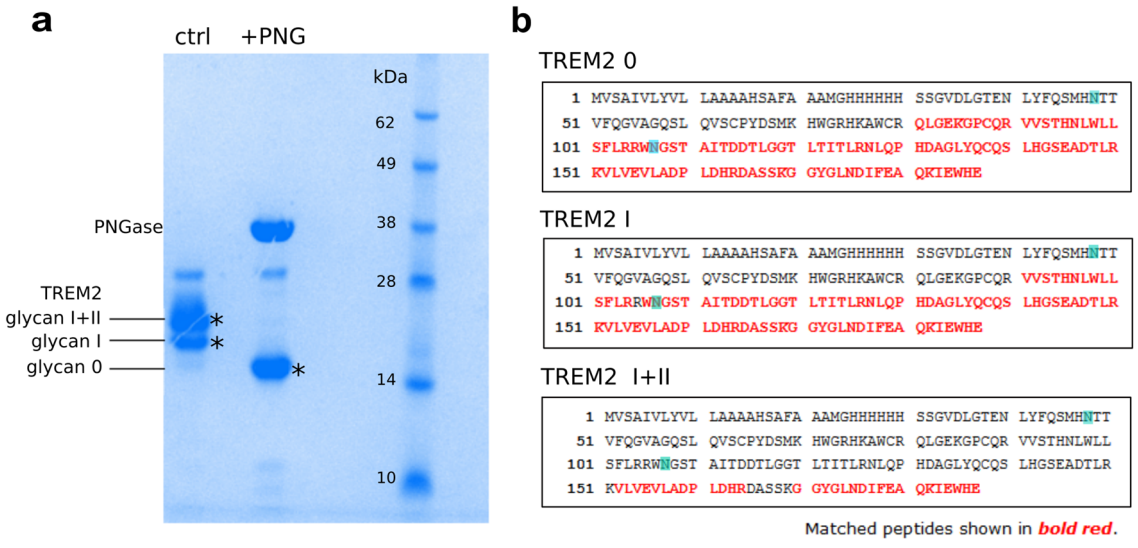


Figure 3.7. Glycosylation site analysis of proteins expressed in Sf9 cells*. (a) TREM2 (a.a.19-131) was incubated for 5 minutes with PNGase F at 100°C in SDS-PAGE denaturing buffer followed by 30 minutes incubation at RT. Bands submitted for MS/MS tryptic digest are marked by an asterisk. Expected glycosylation states on TREM2 are labelled as 0, I and I+II. (b) Mascott server analysis of peptides detected by LC-MS/MS from bands submitted for trypsin digest from panel a. TREM2 sequence is shown for each band with glycosylation sites marked in green. Detected and matched peptides are shown in red. Expected glycosylation states on TREM2 are labelled as 0, I and I+II. The sequence numbering corresponds to TREM2 containing pFB-NH-sec vector signal peptide and His-tag followed by TEV eg. Asn47 is Asn20 in TREM2 sequence.*

3.5.3 MS/MS fingerprinting of glycosylation sites

The fact that TREM2 produced in insect cells produced a single-glycosylated species meant that the second site is not necessary for the protein folding and can be removed to increase monodispersity. However, the position of the non-obligatory glycan had to be first identified. To reveal which of the two glycosylation sites, Asn20 or Asn79 is not essential to TREM2 integrity, trypsin digestion followed by LC-MS/MS was performed (Liquid chromatography with tandem mass spectrometry). A similar methodology to the previously published method was used, but my approach required that two glycosylated species are separated during SDS-PAGE (**Figure 3.7a**) (Nettleship et al., 2007). Protein samples excised from SDS-PAGE are digested by trypsin, which fragments each species into small peptides. Peptides are separated and detected during ESI LC-MS/MS. Later, the detected masses are matched to Mascot database which performs in-silico digestion of all proteins included in the database and contains theoretical ion mass all tryptic peptides. (Perkins et al., 1999).

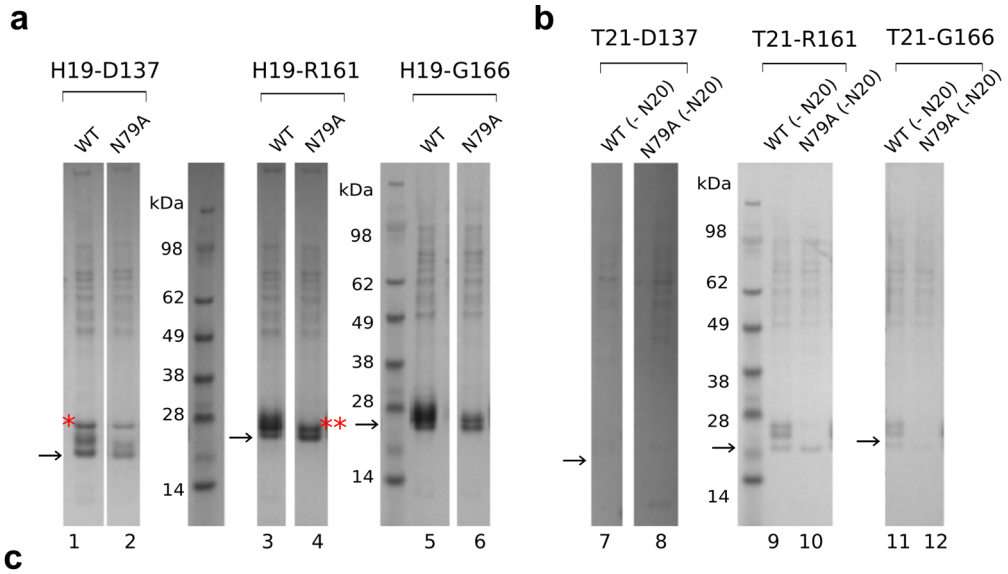
Good quality data is indicated by multiple peptides of exact molecular weight, which match and cover a large portion of the sequence. The precise molecular weight

(MW) of large sugar groups attached to the peptide containing glycosylated asparagine is unknown, which means the peptides cannot be identified only by their expected MW. That indicates the presence of glycosylation. However, the lack of detection cannot be considered absolute evidence since many technical aspects can cause it. Thus, the interpretation of the results was based on the positive identification of the peptide, which is not glycosylated in the single glycosylated state (TREM I). Additionally, a control sample that is fully deglycosylated is required to assess which peptides can be generated and detected in control conditions. For example, in TREM2, the lack of detection of peptide-containing Asn20 in the control sample meant that this peptide and its glycosylation could not be analysed by this method (**Figure 3.7b**, **TREM2 0**). Figure 3.7b demonstrates the expected decrease in the number of detected peptides when analysing samples from fully deglycosylated to single and double glycosylated states.

The peptide containing Asn79, was detected only in the single glycosylated band (TREM2 I) and not a double glycosylated band (TREM2 I+II) (**Figure 3.7b, TREM2 I**). As expected, it was also positively identified in the control sample, which was fully deglycosylated (**Figure 3.7b, TREM2 0**). Since the single glycosylated (TREM I) sample is glycosylated at one position only based on SDS-PAGE migration pattern, the lack of sugar groups at Asn79 indicates that glycosylation is present only at Asn20. As expected, the same Asn79 peptide was not detected when TREM2 I+II band was analysed, indicating it could have undergone glycosylation (**Figure 3.7b, TREM2 I+II**). Furthermore, this is in agreement with the preferential glycosylation of Asn20 detected by NetNGlyc server analysis (http://www.cbs.dtu.dk/services/NetNGlyc/). The analysis results indicate that the obligatory glycosylated residue in TREM2 preparations from insect cells is Asn20, and therefore mutagenesis of Asn79 site may be less likely to impact protein folding negatively.

3.5.4 Site-directed mutagenesis of the Asn79 glycosylation site

TREM2 remains soluble after the removal of glycosylation at Asn79. I generated a DNA template with asparagine 79 mutated to alanine (N79A) based on previous results. New constructs were cloned, and a test expression was performed as previously described. All tested boundaries of TREM2 (a.a.19-136), (a.a.19-161) and (a.a.19-166) yielded stable protein secreted to the medium. Mutation of Asn79 resulted in successfully decreased glycan density compared to wild-type (WT) TREM2 on SDS-PAGE (**Figure 3.8a, lanes 2-6**).



c

	Swissprot sequences: number of peptides of detected target, OS=organism	
1 *	127	Apolipoprotein A-I OS=Bos taurus
	50	Chaperone protein HscA homolog OS=Haemophilus influenzae (strain PittEE)
	44	Apolipoprotein N-acyltransferase OS=Gloeobacter violaceus (strain PCC 7421)
	44	DNA translocase FtsK 1 OS=Ralstonia solanacearum (strain GMI1000)
	43	Accession: PYRG_CALS4
4 **	116	Apolipoprotein A-I OS=Bos taurus
	103	Triggering receptor expressed on myeloid cells 2 OS=Homo sapiens
	51	Genome polyprotein OS=Hepatitis C virus genotype 1b (isolate HC-J1)
	49	Accession: AGAS_STRCO
	48	Accession: DPO1_CALBD

***Figure 3.8. Test expression of constructs based on WT mutant glycosylated DNA template at N79A and APOA1 identification**. The expected size of TREM2 ae shown by arrows. (a) SDS-PAGE analysis of IMAC elutions of constructs H19-161, H19-166 and H19-166 in pFB-sec-NH. Proteins were purified by IMAC from 3 mL of insect cell medium. (b) IMAC elutions of constructs without the first glycosylation site at N20: T21-161, T21-166 and T21-166 in pFB-sec-NH. (c) LC MS/MS detection of trypsin digested samples. SDS-PAGE bands marked by*

asterisk were analysed. The results of mascot search in Swiss Prot database are shown on the right including the number of peptides detected per target protein and the protein species. TREM2 (human) and/or APOA1 (bovine) were detected as top the most abundant proteins.

In addition, I tested whether the obligatory glycosylation site can be removed by construct design. New constructs with the N-terminus starting at Thr21, which excludes the early glycan site at Asn20, were designed and test expressed. Not surprisingly, the truncation resulted in a drastic decrease in yields, indicating the importance of the sequence to protein folding or/and secretion (**Figure 3.8b, lanes 7, 9, 11**). Additional mutation of Asn79 abolished expression further (**Figure 3.8b, lanes 8, 10, 12**).

APOA1 contamination was partially responsible for multiple band appearance. The top band, which can be observed prominently in the case of TREM2 (a.a.19-137) (**Figure 3.8a, lane 2**) was later identified as bovine apolipoprotein A1 (APOA1) by tryptic digest LC ESI-MS in some of the samples (**Figure 3.8c**).

3.5.5 Large scale purification of TREM2 glycosylation mutant for crystallisation

To generate homogenous TREM2 for crystallisation experiments, TREM2 (a.a.19-161, N79A), which expressed better than the other mutants, was produced (**Figure 3.8a, lane 4**). Large-scale purification revealed correctly folded protein at the retention volume (rt) of 97 mL during SEC. An increased proportion of aggregates at earlier retention was detected when compared to TREM2 (**Figure 3.9a compared with Figure 3.6a**). SDS-PAGE and MS analysis of monomeric fractions confirmed a more homogenous glycosylation pattern and qualified the protein for crystallisation trials (**Figure 3.9b,d**). Next, I attempted to remove the remaining glycosylation to increase homogeneity further, but consistently with previous results, Endo H treatment was unsuccessful (**Figure 3.9c,d**).

Mutation of glycosylation site decreased protein expression and increased aggregation. Unfortunately, the resulting protein was prone to precipitation during purification and could not be effectively concentrated above 1 mg/mL, with the yield severely affected by the mutation. Regrettably, X-ray crystallography requires significant amounts of purified proteins at high concentrations. So despite the successful increase in homogeneity, the resulting TREM2 was unsuitable for my aim of obtaining multiple co-crystal structures of TREM2 and scFv ligands.

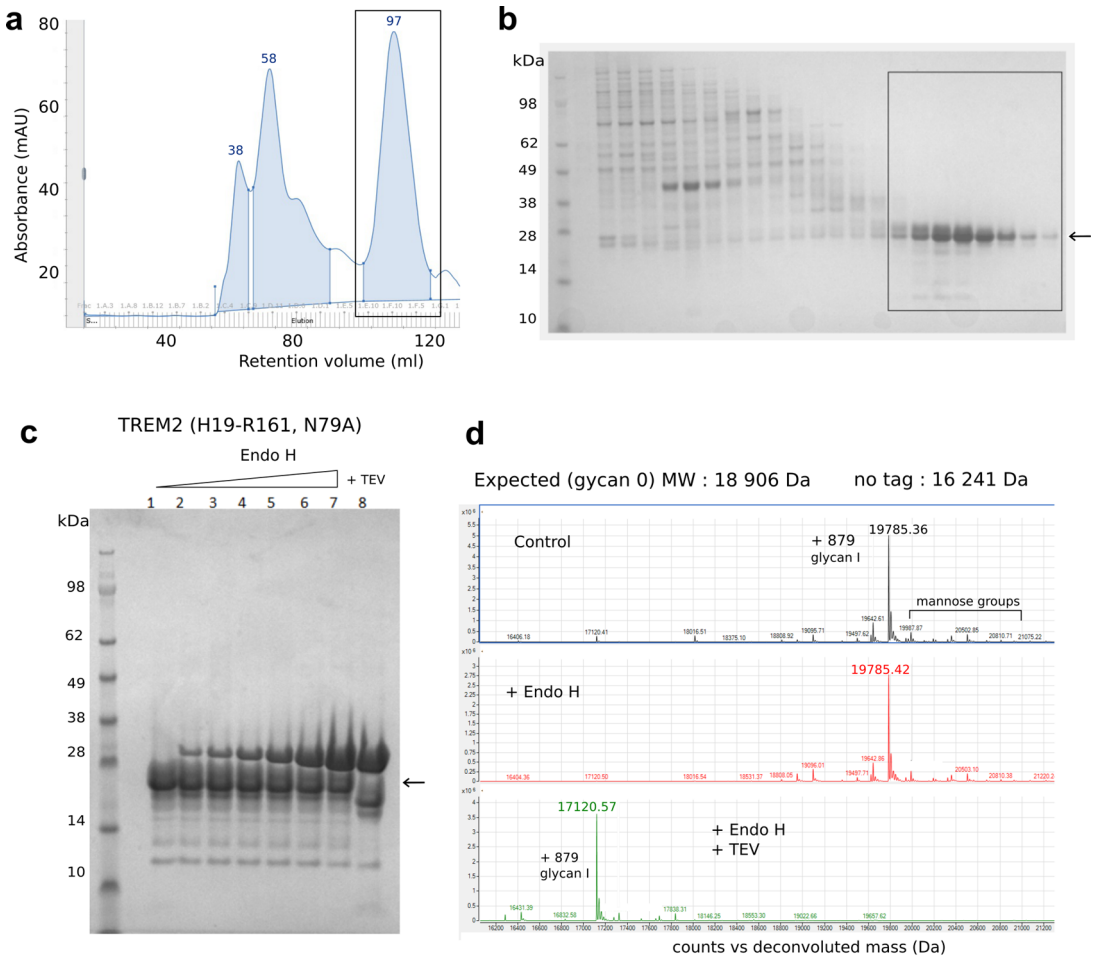


Figure 3.9. Large scale purification of glycosylation mutant of TREM2*. (a) SEC chromatogram of TREM2 mutant N79A (aa.19-161) purified on Superdex 200 16/60. Soluble aggregates and contaminants elute at 38mL and 58mL, whereas TREM2 monomer elutes at 97mL and is marked by a box. (b) SDS-PAGE analysis performed on SEC fractions from panel a. Expected migration this TREM2 construct is marked by an arrow. (c) Endo H treatment performed o/n at 20°C at pH 6.5 with increasing concentrations of enzyme (1-7). Sample 8 was*

additionally digested with TEV protease. (d) Intact MS analysis of samples 1, 7 and 8. Addition on Endo H does not lead to changes in protein composition. Molecular weight of tagged (18 kDa) and untagged TREM2 (16 kDa) is increased by 879 Da due to glycosylation (unimod database: Hex(2)HexNAc(2)dHex(1)). Additional simple sugar mannose groups on the glycan are detected.

3.6 Production of TREM2 in mammalian cells for crystallisation

3.6.1 Cloning, expression and purification of TREM2 in mammalian Expi293F™

Following difficulties in producing homogenous TREM2 in insect cells and successful deposition of a TREM2 structure produced in mammalian cells and solved by the Kober group, a new similar TREM2 ectodomain construct was generated, which additionally contained GTK linker between TREM2 and C-terminal His-tag and no TEV cleavage site (Kober et al., 2016). The latter changes were introduced based on success in TREM2 production by Eisai scientists. I cloned, expressed and purified pHL-sec:TREM2 (a.a.19-131) from Expi293™ conditioned-medium, but the resulting protein did not express well and aggregated during concentration. In the meantime, scFvs antibodies were selected, and optimisations of antibody purification could be commenced (**4.4**). So an Ig TREM2 protein similar to that solved by the Kober group was provided by scientists at Eisai to start crystallisation trials with already selected antibodies (cloning and purification performed Eisai and Viva Biotech Ltd). This protein could be concentrated effectively but did not behave well in the presence of purified scFvs (**5.2.1**). All of these TREM2 constructs contained C-terminal rather than N-terminal His-tag. In my previous experiments, N-terminally His_6-tagged TREM2 expressed well in *Sf9*, so I cloned TREM2 into a similar mammalian vector pHTBV1.1-SecNH-Bio that incorporates N-terminal RTPPmu signal peptide (receptor-type

tyrosine-protein phosphatase mu) optimised for mammalian expression followed by N-terminal His_6 and C-terminal Avi-tag (**Figure 3.4**). Additionally, the Ig-only construct of TREM2 was extended to Asp138 to improve Ig-domain folding.

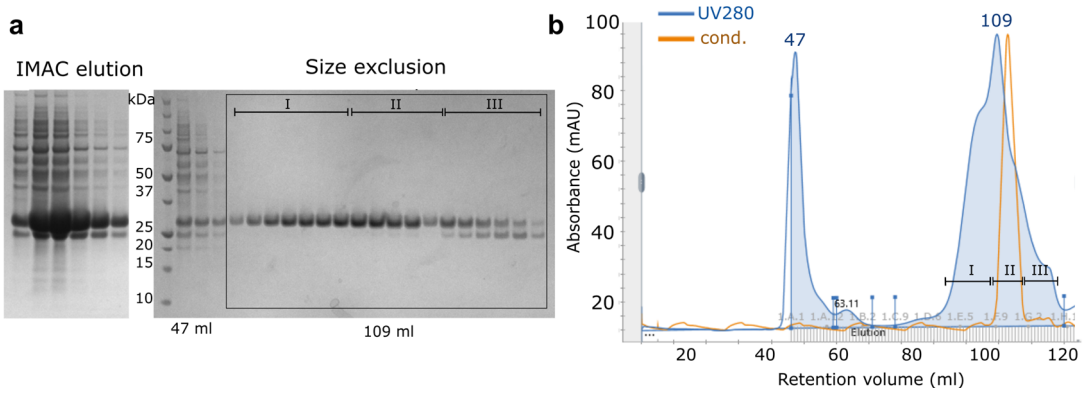


Figure 3.10. Purification of TREM2 Ig-domain (a.a.19-138) expressed in Expi293™ cells in the presence of kifunensine. *(a) Purification steps of TREM2 shown by SDS-PAGE. Protein is first captured by nickel affinity chromatography as shown by fractions eluted by high imidazole concentrations (IMAC elution) followed by polishing by SEC as shown by image on the right. SEC fractions representing fractions of 47 mL and 109 mL (bracketed, I-III) are shown. (b) Results of SEC on Superdex 200 16/60 column. The main UV280 absorbance signal (blue) at a retention peak of 109 mL can be divided into I, II, III fractions which are also indicated on the SEC gel in panel a. Change in conductometry level is shown by the orange line and can be used to explain the change in retention behaviour of I and II fractions.*

Transient expression of TREM2 constructs in Expi293™ cells leads to high yields of biochemically stable TREM2 proteins. The pHTBV1.1-SecNH-Bio vector can generate baculoviruses for transduction of mammalian cells; however, transient transfection allows faster screening for positive outcomes. Proteins were also expressed in the presence of complex glycosylation inhibitor, kifunensine, which allows for later glycan trimming with Endo H. Expression of TREM2 (a.a.19-138) and TREM2 (a.a.19-174) resulted in the highest expression of TREM2 in all the conditions tested so far (**Figure 3.10a, Figure 3.11a**). The quality of TREM2 (a.a.19-138) was validated by SEC and indicated polydispersity in the monomeric peak at the retention of 109 mL

(**Figure 3.10b**). The width of the peak indicated non-specific interaction with dextran, which is consistent with some TREM2 interactions reported in the literature (Byrne et al., 2021; Daws et al., 2003). The peak can be subdivided into three fractions, I, II and III, with the latter containing a lower molecular mass species visible on SDS-PAGE, which was identified as TREM2 by LC-MS/MS (**Figure 3.10b**, data not shown). SEC fractions of peak I and II did not contain any other protein species. Instead, an increase in ionic strength indicated by the conductance reading (orange line) likely weakened the non-specific interactions with the column media (**Figure 3.10a, b**). TREM2 protein in peak I and II was frozen in liquid nitrogen and later used for co-crystallisation experiments following deglycosylation.

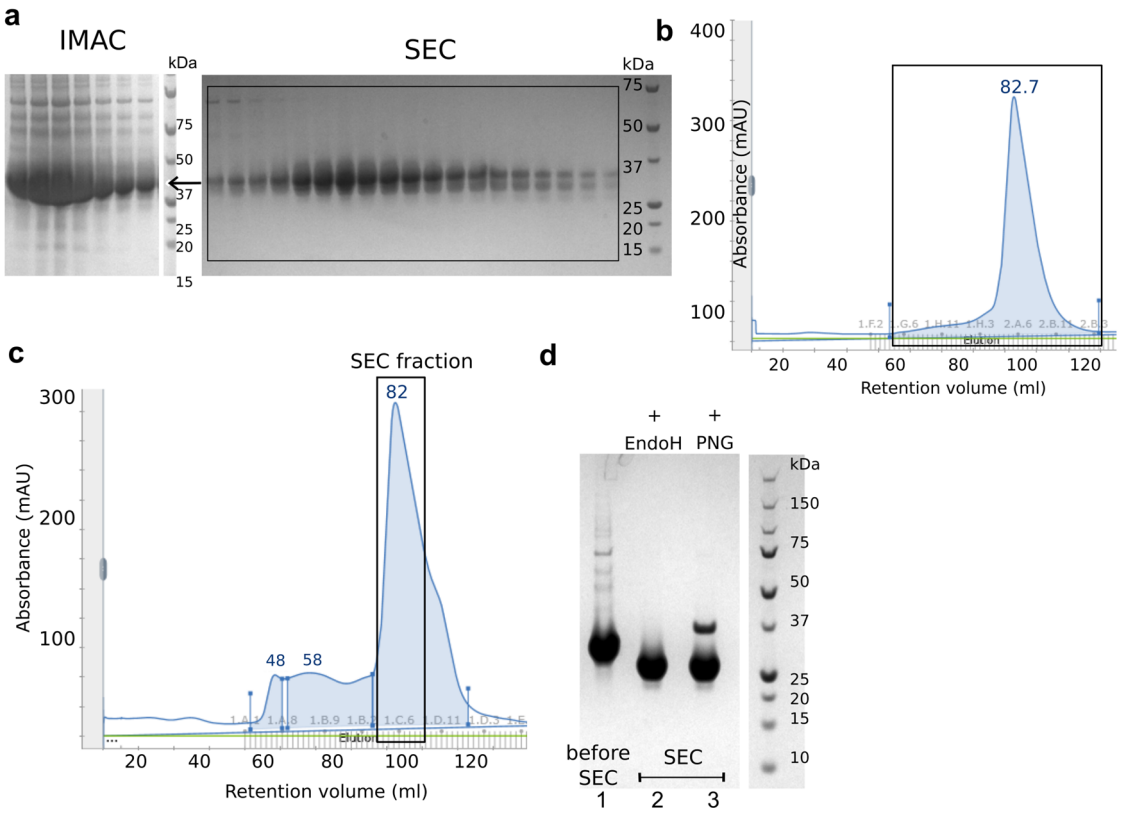


Figure 3.11. Purification of TREM2 ectodomain (a.a.19-174) from Expi293F™ GnTI- cells. *(a) Purification steps of TREM2 shown by SDS-PAGE. Protein is first captured by IMAC as shown by high elution fractions (IMAC) followed by a polishing SEC step. The expected size of deglycosylated TREM2 is shown by an arrow. All SEC fractions from b are analysed by SDS-*

PAGE (boxed fractions). (b) Results of SEC on a Superdex 200 16/60 column. Thus obtained sample was deglycosylated o/n with Endo H. (c) SEC Assessment of TREM2 folding after Endo H deglycosylation. Fractions past boxed fractions contain Endo H enzyme and thus are excluded from the pooling. (d) Efficient protein deglycosylation was confirmed by SDS-PAGE after comparison of control sample before SEC and without Endo H (lane 1) and digested sample (lane 2). PNGase F treatment was used to confirm complete glycan removal (lane 3).

The emerging significance of the TREM2 stalk sequence for ectodomain shedding demonstrated the potential value of solving the structure of a longer TREM2 (a.a.19-174) construct. The kifunensine requirement was bypassed by the use of the new cell line Expi293F^{TM} GnTI-. The longer protein produced by this method produced even higher yields (**Figure 3.11a**). A simultaneous improvement in homogeneity was achieved, as demonstrated by the monodisperse single peak at 82 mL during SEC (**Figure 3.11b**). The latter revealed low aggregation as indicated by the absence of a 49 mL retention peak and an overall decrease in non-specific interaction with the resin (**Figure 3.11b**). TREM2 remained correctly folded after deglycosylation with Endo H as suggested by a second SEC purification step (**Figure 3.11b**). A peak shoulder is visible due to the remaining Endo H and was avoided during sample freezing. Full deglycosylation was confirmed by comparing Endo H treatment with PNGase (**Figure 3.11d**). This protein was later used to generate our highest resolution data set in a complex with scFvs by X-ray crystallography.

3.7 Discussion

This chapter describes the successful development of protocols for the purification of TREM2 for antigen generation and X-ray crystallography from insect and mammalian cells. Despite previously reported successes in production of other

human proteins TREM2 could not be expressed as a soluble protein in *E. coli* by fusions with OmpF and OmpY targeting proteins to the periplasm (Kotzsch et al., 2011). Such periplasmic environment can yield properly formed disulphide bonds, but *N*-linked co-translational glycosylation is absent in prokaryotic cells and appears to be required for correct TREM2 folding and expression. However, others have successfully purified and crystallised the TREM2 R47H mutant by refolding from *E. coli* inclusion bodies (Sudom et al., 2018). In the resulting crystal structure, a large region containing R47H and N79 underwent remodelling with a significant disorder and loss of electron density. Despite successful expression, the lack of glycosylation might therefore have had a deleterious impact on the local protein structure in addition to the effects of R47H. This success may be somewhat specific to the R47H mutation since previously described attempts to purify WT protein from inclusion bodies did not produce folded protein (Kober et al., 2014).

The insect cell- produced TREM2 unexpectedly displayed a variable occupancy of one of the N-linked glycosylation sites. The resulting heterogeneity did not interfere with antigen preparation, however, it was undesirable for crystallisation due to increased heterogeneity. Contrary to our assumptions based on the literature, the glycans could not be removed by standard enzymes (Nettleslip, 2012). A steric hindrance between the enzyme and the longer than expected mannose chains could result in decreased digestion efficacy. Consistent with this, additional simple sugar moieties beyond the 1038 Da core glycan I or II were consistently detected by intact MS (**Figure 3.6b, Figure 3.9d**).

To increase TREM2 homogeneity for crystallisation, the non-essential glycan in the TREM2 sequence was identified and later removed it by mutagenesis. While Asn79 glycosylation may not be an absolute requirement for TREM2 protein folding, the

stability and biochemical properties of the mutant were negatively altered in agreement with the significant impact of glycans on protein folding and stability (Mitra et al., 2006; Shental-Bechor and Levy, 2008).

Interestingly, TREM2 occasionally was contaminated with APOA1. Sf9 test expression protocol uses 2% fetal bovine serum (FBS), which contains many components, including APOA1 (Zheng et al., 2006). This is consistent with TREM2 and lipoprotein interactions reported in the literature, including APOA1 (Yeh et al., 2016). However, these results were not consistent and require further validation work.

The first attempts to produce Ig-domain TREM2 in mammalian cells by a protocol similar to Kober et al. did not result in large quantities of soluble protein (Kober et al., 2016). The lowered expression could be caused by reduced transfection efficiency caused by the use of linear polyethylenimine 25k (L-PEI25) rather than trimethylene carbonate modified L-PEI25 transfection reagent. Decreased expression or capture could also be caused by different C-termini containing three amino acid linker between TREM2 and histidine tag instead of TEV recognition sequence. These changes were introduced after discussions with Eisai scientists based on successful use in pTT5:TREM2 production but could be inappropriate for pHL-Sec vector used by Kober group (see Chapter 2).

Despite good expression, pTT5:TREM2 (a.a.19-131) had a tendency to precipitate in the presence of scFv. Consequently, I generated novel pHTBV1.1-avi TREM2 (a.a.19-138) and TREM2 (a.a.19-174) constructs with His-tag at the opposite end and additional C-terminal Avi-tag. This time, TREM2 was not only expressed at high levels but also exhibited superior biochemical behaviour at high concentrations. This was consistent with the similar behaviour of N-terminally His-tagged TREM2 produced previously in *Sf9* cells but could also be attributed to the presence of Avi-tag

at the C-termini. As a result, these mammalian proteins exhibited preferable biochemical properties during the formation of scFvs complexes (described in Chapter 5).

Overall, my trials led to the successful purification of human TREM2 ectodomain for antigen production and crystallography. Antigen generation for phage display generally has lower protein requirements than X-ray crystallography but required biotinylation. Because of that, biotinylated *Sf*9-produced TREM2 was developed earlier and was used for antigen generation to allow for efficient time management during this project. This strategy proved successful and allowed for simultaneous optimisation of Expi293^{TM}-produced TREM2 and scFv already obtained from phage display (Chapter 4, Chapter 5).

Chapter 4

Production and characterisation of single-chain variable antibody fragments

Parts of this chapter are based on the publication: *Selection and structural characterization of anti-TREM2 scFvs that reduce levels of shed ectodomain*, Structure, 2021, https://doi.org/10.1016/j.str.2021.06.010. Permission to publish relevant figures was obtained under conditions described in the Creative Commons CC-BY licence.

4.1 Introduction

Immunoglobulins are highly specific molecules used by the immune system as a defence against pathogens and toxins. The specificity of antigen-antibody interaction has been harnessed and exploited in diagnostics and research and, more recently, in therapeutics. Due to TREM2 surface expression, antibodies are valuable reagents to probe the functional properties of the TREM2 signalling pathway. We hypothesised that scFv antibody fragments binding at different sites on TREM2 might differentially affect

receptor signalling, internalisation or cleavage and be a valuable tool for the scientific community. Upon successful TREM2 antigen generation, we tested whether scFv can be developed against glycosylated TREM2 Ig-domain in collaboration with Karolinska Institute. The goal was to confirm binding to TREM2 by SPR and to optimise the purification so obtained scFv can be used to generate both X-ray crystallography and functional studies in cell assays.

At the start of this project, there were few anti-TREM2 antibodies available, and these were poorly validated. For example, the majority of these have been found to work poorly in immunocytochemistry experiments, suggesting that they are not active against correctly folded TREM2 and few have functional effects (personal communication, Hazel Hall-Roberts). One of the most widely used and robust functional antibodies, AF1828 (R&D Systems), is a polyclonal antibody with an unknown epitope and finite source. Therefore, we set out to develop renewable binders against TREM2 through a collaboration with the phage display laboratory of Drs Helena Persson and Susanne Gräslund.

Antibodies and antibody fragments can be described based on the presence and size of heavy and light chains and their antigen binding regions. The most prevalent antibody format is the full-length IgG molecule, a Y-shaped antibody with two antigen-binding fragments (Fab) and one crystallisable fragment (Fc) domain (**Figure 4.1a**) (Hentrich et al., 2018). IgG molecules are naturally occurring bivalent immunoglobulins, which means they can increase their affinity to the target by having two antigen-binding sites, an effect termed avidity. Within the IgG molecule, both the heavy and light chain consist of constant and variable parts; the latter is the source of variation between different antibodies resulting in their ability to capture different ligands (**Figure 4.1a**). Human immunoglobulins are commonly engineered into

monovalent (Fab, scFv) or bivalent antibody fragments (Fab′2, dimeric scFv, scFv-Fc fragments) (**Figure 4.1b**). Additionally, camelids produce antibodies that consist only of a single variable domain called nanobodies. Each antibody format has advantages and disadvantages regarding costs, production, selection and biophysical properties.

Single-chain variable fragments (scFvs) are small and can be easily produced by phage display. The smallest functionally active part of the antibody is the variable fragment (Fv) which consists of variable heavy (VH) and variable light (VL) domains from the heavy and light chains, respectively. Each domain contains three hypervariable regions known as complementarity determining regions (CDRs). In scFvs, the light and heavy chain domains need to be connected by an engineered polypeptide linker due to a lack of stabilising elements present in the rest of the immunoglobulin structure (**Figure 4.1b**). The length of VH-VL linker can have an impact on higher oligomer formation with a linker longer than 12 amino acids predicted to form monomers (Kortt et al., 2001). They are small (~25 kDa) and comparably rigid as monomers compared to other antibodies. Because the likelihood of successful crystallisation decreases with size and flexibility, scFvs were optimised for that purpose. They can be expressed and purified from *E. coli* and quickly converted into other formats using standard molecular biology methods.

Due to their successful expression in *E. coli*, scFvs can be developed using phage display. In contrast, IgG production requires expensive and time-consuming hybridoma platforms which utilise the immunisation of animals (Köhler and Milstein, 1975). Furthermore, the latter means that the success is dependent on immune response and some antigens can often lead to the death of immunized animal when the antigen is toxic. In 1989, the immunoglobulin genes were cloned for the first time, which led to the development of methods based on recombinant DNA libraries (Orlandi et al., 1989).

The display technology allows for the production of clonally selected antibody fragments with homogenous paratopes (epitope-interacting residues in the antibody) and thus can be used to probe protein structure-function relationships. A number of display protocols exist, including ribosome, yeast and phage display. The latter is the most widespread thanks to flexibility, speed and simple methodology (**Figure 4.1c**). CDR sequences produced in this manner can be easily converted to Fab and IgG fragments.

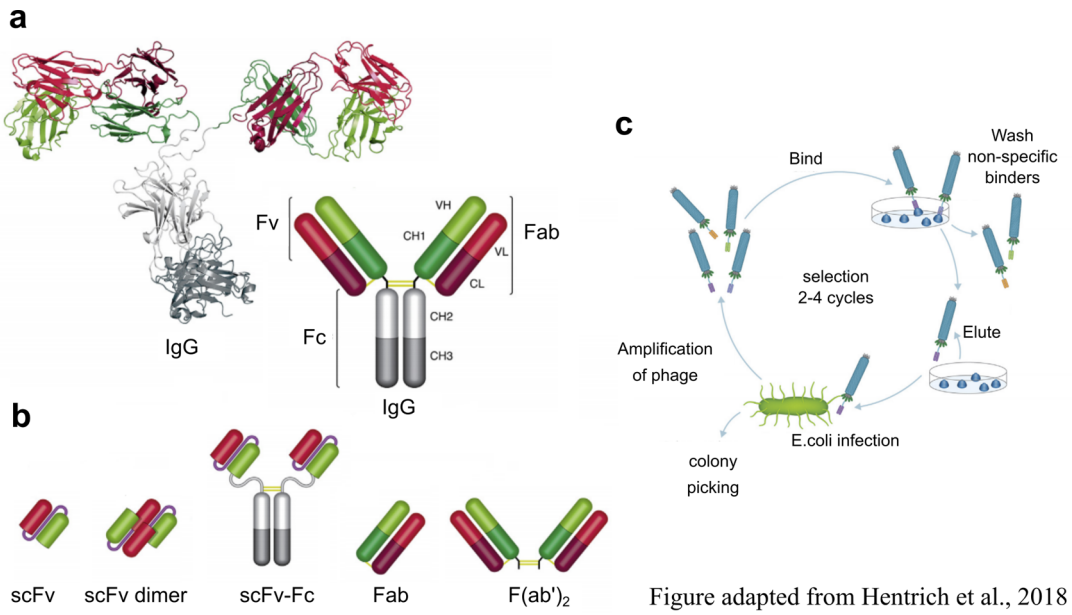


Figure adapted from Hentrich et al., 2018

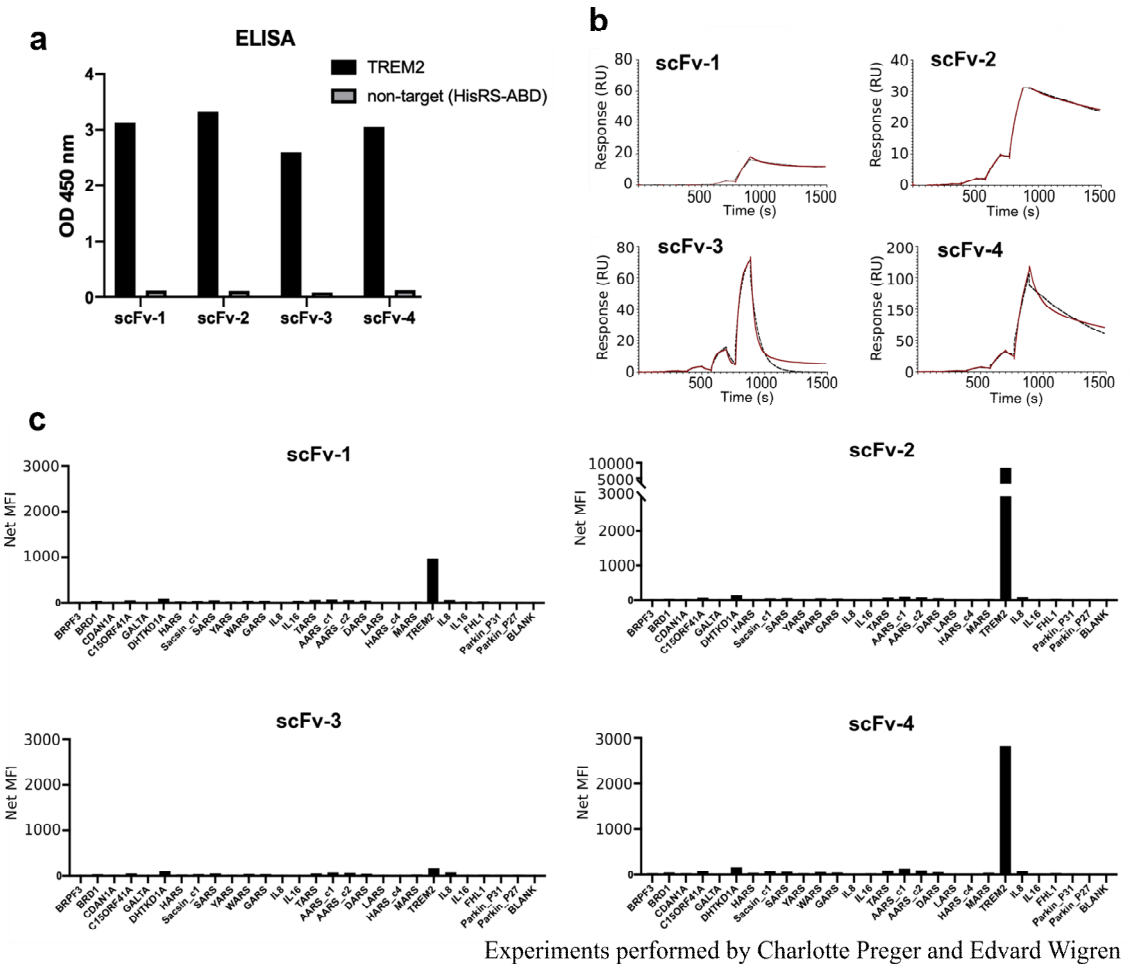
Figure 4.1. Human antibody and antibody fragments and phage display overview. *(a) Crystal structure of a full-length IgG antibody (PDB 1IGT) and its schematic representation. Disulphide bonds are shown in yellow. (b) Some of the recombinant antibody types. ScFv dimer consists of two covalently or non-covalently bound monomers, scFv-Fc are two scFvs connected by the Fc domain. Two Fabs can also be joined by disulphides naturally occurring in IgG as in F(ab')2. The constant element is divided into CH1, CH2, and CH3 domains in the heavy chain and one CL domain in the light chain. The variable domain (Fv) consists of only variable light (VL) and variable heavy (VH) domains. All domains are coloured as in panel a. (c) During phage display, a phage library is incubated with the antigen, and phages that did not bind to the antigen are washed away. The bound phages are eluted and amplified by the infection of E. coli. New phages are selected in E. coli and produced for the next round of selections (Hentrich et al., 2018, permission to publish the figure was obtained from Elsevier).*

This chapter briefly describes the work performed by our phage display collaborators at the Karolinska Institutet, who selected scFvs against TREM2 antigen for which protein production was described in the previous chapter, and also the cloning, expression, purification and characterisation of the oligomeric state of scFvs purified in the *Sf9* baculovirus expression system, that I have conducted. My collaborators at Eisai additionally prepared antibody conversions, including Fab and IgG1, which revealed improved biochemical properties and were shown to work well as tools capturing TREM2 by standard methods. The scFvs and their stable conversions were prepared for crystallisation experiments and screening of their functional properties as described in Chapters 5 and 6.

4.2 Selection and validation of scFvs binding to TREM2

To facilitate the development of renewable antibody binders against TREM2, Charlotte Preger (SciLifeLab) performed phage display selections using the SciLifeLab synthetic library of human scFvs constructed and designed as previously reported (Preger et al., 2020; Säll et al., 2016). A TREM2 antigen comprising the ectodomain of human TREM2 (a.a.19-131) was expressed recombinantly in *Sf9* insect cells, *in vitro* biotinylated and immobilised on streptavidin-coated magnetic beads. Following four rounds of phage selections and binding analyses, scFv-1, 2, 3 and 4 were selected for further characterisation. The initial selections were based on results from Surface Plasmon Resonance (SPR), Enzyme-linked immunosorbent assay (ELISA), homogenous time-resolved FRET (HTRF) described in Preger et al., 2020 (**Figure 4.2**). Luminex experiments were also performed to assess non-specific binding of selected scFv by analysing binding to antigen compared to a set of randomly selected proteins (**Figure**

4.2c). ScFv-1 and scFv-3 performed worse in the SPR and Luminex validations but due to an unusually small number of positive hits, all four scFvs were sent to Oxford for further validation.



Experiments performed by Charlotte Preger and Edvard Wigren

Figure 4.2. Initial validation of scFvs against TREM2. *(a) Validation of scFvs binding to TREM2 by ELISA. The same purified antigen TREM2 (black bars) or a non-target protein (HisRS-ABD, grey bars) was added to a streptavidin-coated plate, followed by the addition of bacterial lysate containing scFvs. Bound scFv were detected using anti-FLAG M2 HRP-conjugated antibody and TMB substrate. (b) Initial SPR Single Cycle Kinetic measurements of scFvs purified from E. coli using Biacore T200 (Cytiva). An anti-FLAG M2 antibody was immobilised on a CM5 sensor chip and FLAG-tagged scFv was captured on the surface. Antigen TREM2 (a.a.19-131) purified from insect cells was injected with increasing concentrations (0.16, 0.8, 4, 20 and 100 nM). Response was measured in resonance units (RU) over time (s). Red lines represent the measured data values, and dashed black lines represent the fit of the curve based on a 1:1 Langmuir binding model. (c) Luminex binding of scFvs to a*

panel of 27 proteins including TREM2. Proteins were added to neutravidin coupled magnetic color-coded beads before the addition of scFv (bacteria supernatant). Binding was detected using an RPE-conjugated anti-FLAG M2 antibody and analysed using FLEXMAP 3D (Luminex corp.) recording median fluorescence intensity (MFI). (Permission to publish the figure was obtained from the collaborator: Dr Charlotte Preger).

Initially, scFvs obtained from phage display were cloned into the bacterial expression vector pHAT-6, which provides an Outer membrane protein A (OmpA, aa 1-21) signal sequence followed by a C-terminal $Hisx_6$-FLAG-tag, and expressed in bacteria (work performed by Edvard Wigren, Karolinska Institute) (**Figure 4.2b**). The initial binding of these preparations to the *Sf9* antigen was confirmed by SPR (data not shown, Charlotte Preger). TREM2 proteins produced in *Sf9* and mammalian Expi293F^{TM} cells are expected to share epitopes necessary for scFv binding but differ in their glycosylation. I, therefore, validated the binding of the scFvs to glycosylated TREM2 (a.a.19-174) expressed in Expi293F^{TM} cells by Bio-layer interferometry (BLI). The resulting dissociation constant (K_D) values were estimated from kinetic data fitted to Langmuirian 1:1 binding mode. Preliminary measurements revealed that all antibody fragments showed strong binding to TREM2 except for scFv-1, which proved to be a weak binder with a K_D in the micromolar range (**Figure 4.3c**).

The measured affinities for the Expi293F^{TM}-produced TREM2 were scFv-2 K_D = 7 ± 4 nM, scFv-3 K_D = 180 ± 4 nM, scFv-4 K_D = 8 ± 15 nM (**Figure 4.3c**), in agreement with preliminary SPR studies performed at the Karolinska Institute with my *Sf9*-produced TREM2. The binding kinetics of scFv-3 displayed a moderate affinity with fast dissociation rates (k_{off}) and could be only be analysed after fitting data to the bivalent analyte model. It is desirable to achieve an equilibrium state observed as signal plateau during association steps of SPR or BLI so more reliable analysis required further

optimisations. Despite the former, the initial analysis revealed that scFv-2, scFv-3 and scFv-4 bind similarly to both *Sf9* and Expi293F^{TM}-produced TREM2.

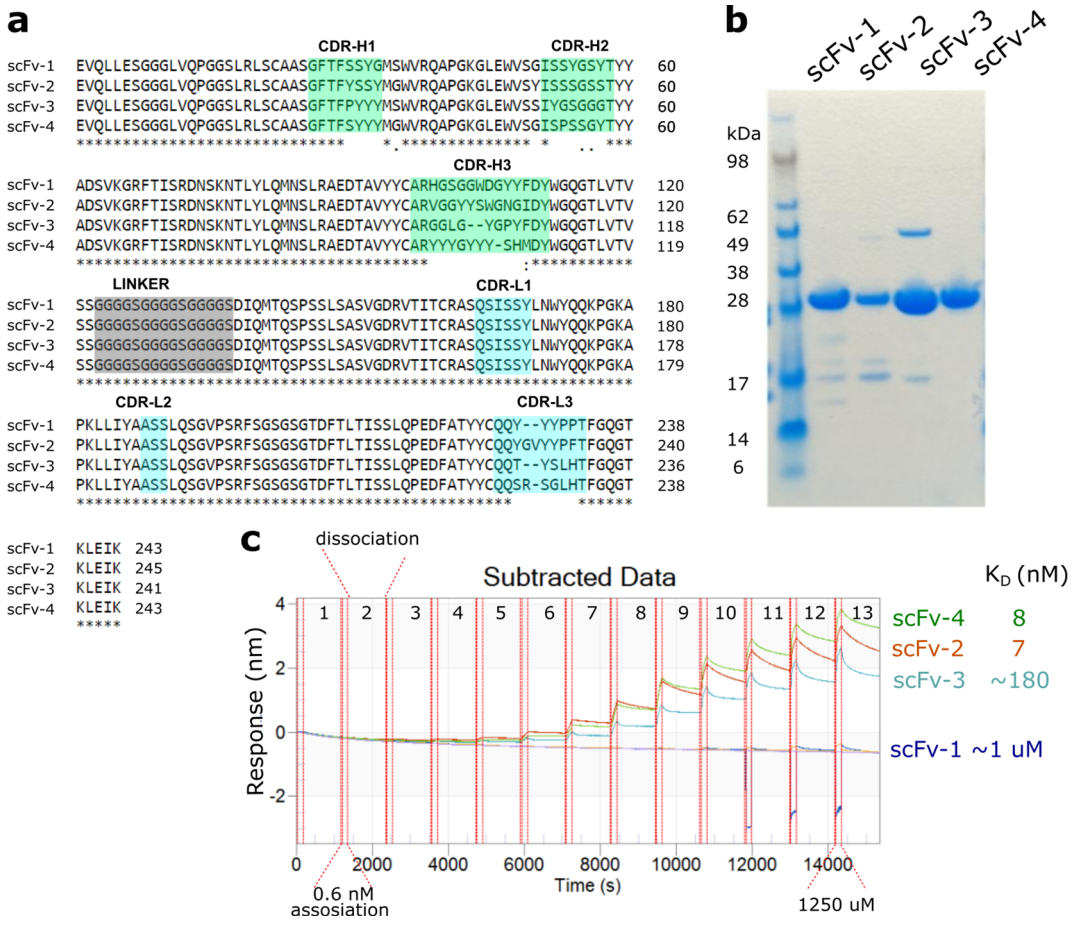


Figure 4.3. Production and validation of scFvs. *(a) ScFv sequences aligned by Clustal O with the three heavy chains CDR H1-3 highlighted in green and light chains CDRL1-3 in blue, 15 a.a.linker in grey. Boundaries for CDRs are as defined by the IMGT nomenclature (Lefranc et al., 2003). The scFvs originate from the SciLifeLab library, in which sequence diversity was introduced into four of the six CDRs: CDR-H1, CDR-H2, CDR-H3 and CDR-L3. (b) Test expression of scFvs in TOP10 E. coli performed by Edvard Wigren. Whole-cell E. coli extracts were purified on Protein A resin and eluted with low pH. (c) BLI experiment testing scFv binding to glycosylated TREM2 (a.a.19-174). Eisai provided biotinylated and fully glycosylated TREM2 produced in mammalian Expi293F^{TM} cells. TREM2 was immobilised on a sensor, and 13 cycles of washing, association and dissociation were performed with increasing concentrations of scFvs (shown by dotted red lines). The signal detected by the reference sensor*

without the TREM2 ligand was subtracted before analysis. The BLI response was measured in nm against time in seconds. Apparent K_D measurement results are shown.

4.3 Optimisation of scFvs production in *E. coli*

As in the case of TREM2, good yields of the heterogeneously expressed protein is required for crystallography, so a better expression and purification method had to be established in Oxford. Since scFvs 2-4 appeared to retain binding to mammalian TREM2, scale-up of their expression for crystallisation and cell biology experiments was performed. ScFv-1 was used as a negative control in all the experiments. Firstly, I attempted to optimise the expression yields beyond those obtained in the *E. coli* TOP10 cell line used by my collaborators at the Karolinska Institute. Because the standard expression methods of these constructs in *E. coli* Rosetta did not produce any soluble protein, so scFvs were fused to maltose-binding protein (MBP) and His_6-tag in pNIC-MBP2-LIC vector and tested for protein expression in *E. coli* T7 Shuffle cells (NEB). MBP fusions can increase solubility, while the Shuffle cells are engineered to catalyse the formation of disulphide bonds in the cytoplasm by DsbC enzymes (Raran-Kurussi and Waugh, 2012). These cells were also transformed with the plasmid pGro7 (TaKara) encoding for the GroEL/GroES chaperone shown to increase correct folding of MBP-fusions (Raran-Kurussi and Waugh, 2012). Additionally, a set of constructs with the Avi and FLAG-tag at the C-termini from the pHAT-6 vector was generated to increase variability. ScFv-1, scFv-3 and scFv-4 showed expression in standard terrific broth (TB) medium (**Figure 4.4a**) as well as in TB+ media containing additives that increase *E. coli* biomass (**Figure 4.4b)**. GroEL/GroES co-expression did not have a significant effect (**Figure 4.4b).** Despite the positive expression and identification of TREM2 by LC-MS/MS (marked as asterisks), the resulting yields were still insufficient for crystallisation studies.

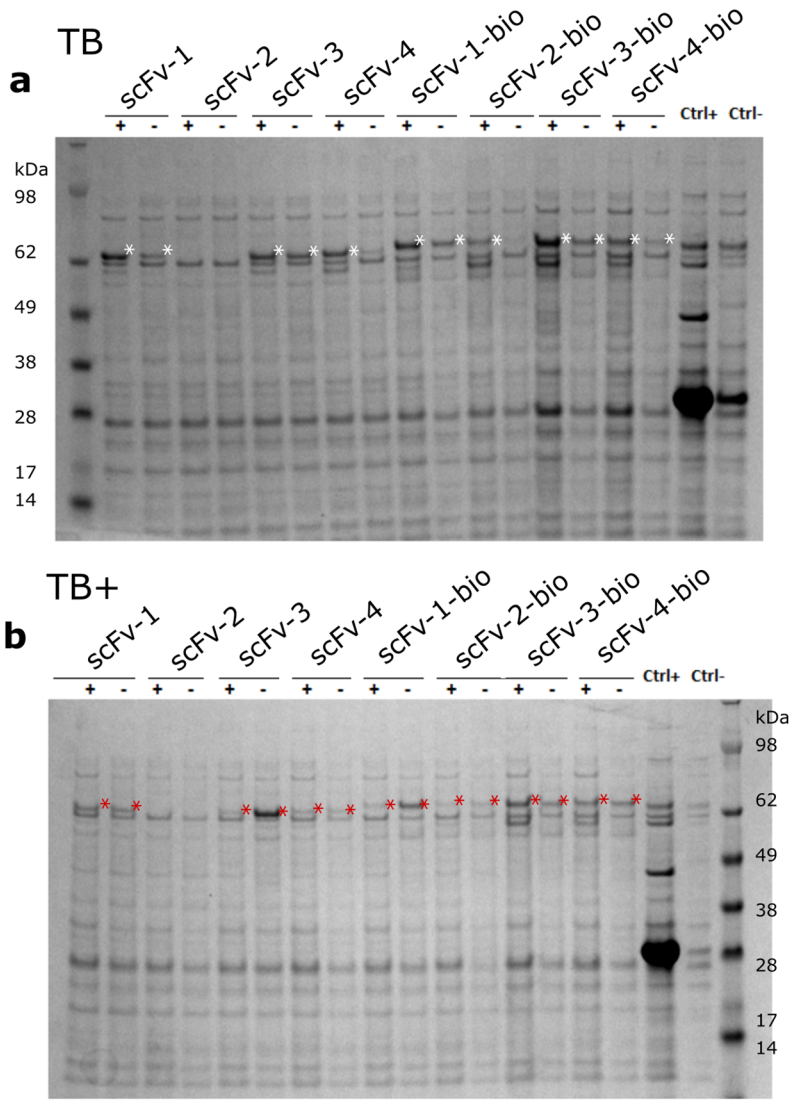


Figure 4.4 Test results of co-expression of scFvs-MBP with GroEL/GroES chaperone in E. coli T7 Shuffle*. Proteins were test expressed from 1 mL and purified by IMAC, final elution samples are shown. Test expression was performed o/n at 18°C for scFvs and scFvs containing the original Flag and His-tag from pHAT-6 vector (labelled as scFv-bio). Expression of GroEL/ES (+) was induced with 5 mM L-arabinose for an hour before induction of scFvs expression with 0.1 mM IPTG. (a) TB medium was tested alongside enriched version (b) TB+ containing additives. The MBP-scFv fusions have a molecular mass of approximately 70 kDa, and positive bands are marked with a white or red asterisk. E. coli transformed with an expression plasmid for TEV protease was used as a negative control (Ctrl-) or positive control when the expression was induced with IPTG (Ctrl+).*

4.4 Optimisation of scFv production in *Sf9* cells

ScFvs can be expressed robustly by secretion from *Sf9* insect cells. After a failure in obtaining well expressed scFvs in *E. coli,* I cloned the antibody fragments into the same vector, pFB-sec-NH, which was previously successfully used to express TREM2 containing disulphides in the structure. Initially, this led to a modest improvement in expression levels of 5-fold compared to *E. coli* TOP10. By increasing the concentration of the baculovirus used for large scale protein production, the yields could be improved by up to 40-fold (**Figure 4.5a,b**). The additional advantage was lower initial contamination with Lipopolysaccharide (LPS, also called endotoxin), which is derived from *E.coli* cell wall and is therefore abundant in *E. coli* preparations. Endotoxin stimulates inflammatory responses in mammalian cells and represents challenge in cell biology experiments on human macrophages (Schwarz et al., 2014).

4.4.1 Optimisation of protein stability – differential scanning fluorimetry (DSF)

The stability of scFvs at low concentrations is high, but aggregation can be observed at high protein concentrations. The main challenge in scFv preparation was achieving high protein concentrations, which were particularly important to crystallisation and efficient purification procedures. Extensive efforts were made to increase protein solubility, especially during protein concentration before SEC analysis. Initially, protein concentration methods led to protein aggregation, as judged by attempts to analyse oligomeric states by SEC analysis. However, protein A purification is based on a native protein-protein interaction and led to an enrichment of natively folded scFvs (**Methods 2.5.3**). That meant that initial crystallisation trials and cell biology experiments could be performed (**Chapters 5 and 6**).

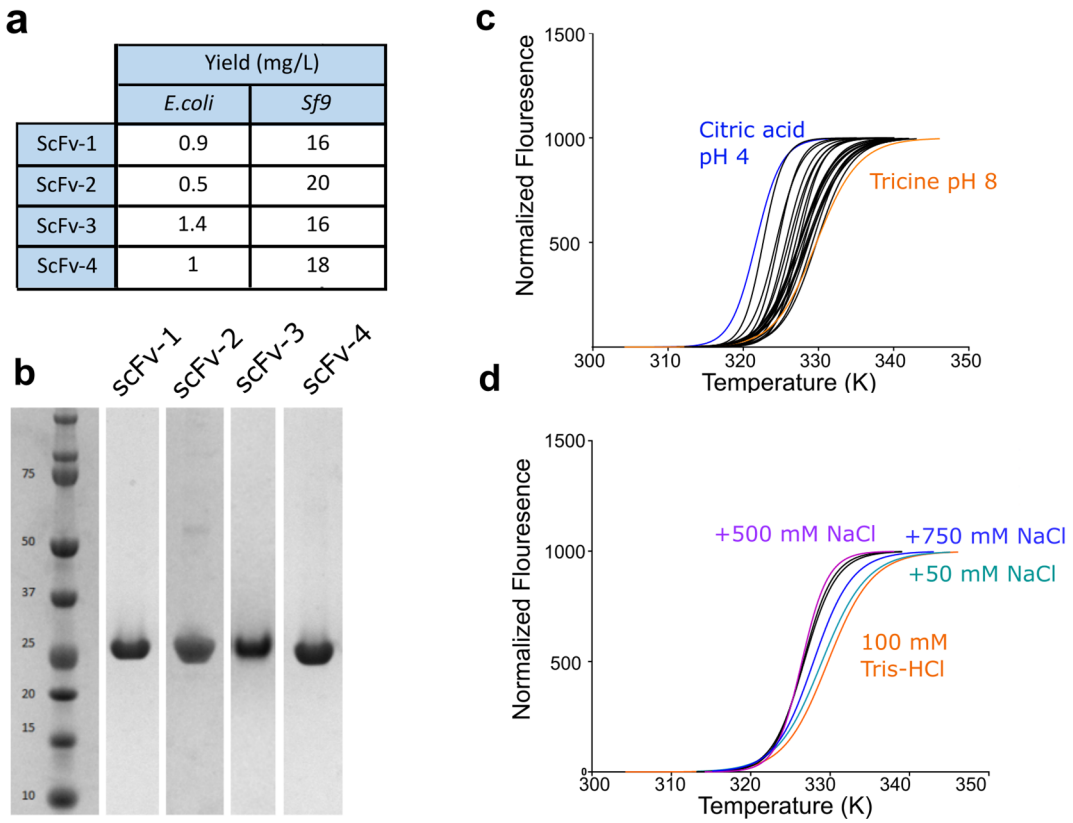


Figure 4.5 Optimisation of scFv production in an Sf9 expression system. *(a) Expression yields of scFvs produced in E. coli TOP10 cells or Sf9 insect cells per 1 L of cells. (b) Coomassie blue-stained SDS-PAGE gel showing the final purity of scFvs after purification from Sf9 cells by sequential IMAC and Protein A (image generated from different purification experiments). (c-d) Examples of DSF buffer screen results. The thermal unfolding of scFvs in different buffer conditions is measured by fluorescence signal emitted by SYPRO Orange dye. Fluorescence data was processed and fitted using a tool developed by Radek Nowak and ProteoPlex (Chari et al., 2015) (c) Results of the RUBIC buffer screen showing pH-dependent stability of scFv-3. (d) Results of scFv-3 screen investigating the negative impact of increasing amounts of sodium chloride versus buffer-only ionic strength provided by 100 mM Tris-HCl pH 8 solution.*

Simultaneously, a number of buffers and ionic strength conditions were screened by differential scanning fluorimetry (DSF) (**Methods 2.12**). The antibodies had generally good thermal stability (>55°C, 330 K) achieved in the majority of conditions above pH 5 when significantly diluted below 0.3 mg/mL (**Figure 4.5c**) (Chari et al., 2015). Interestingly, increasing salt concentrations decreased thermal stability by up to 4°C (**Figure 4.5d**). In practical terms, some of the best conditions decreased

precipitation in the case of scFv-2 and scFv-4, but most conditions had to be further confirmed experimentally and rarely allowed high concentrations to be achieved. One exception was scFv-3 which achieved concentration to 12 mg/mL when 100 mM Tricine pH 8 was used. Despite extensive optimisations, I only managed to exclude buffers deleterious to scFvs, but the inherent solubility of scFvs appeared low and appropriate stabilising conditions were difficult to identify. Since antigen-scFv interaction can change the biochemical properties of the resulting complex, improvement in the solubility could be expected after TREM2 addition (**5.2.1, 5.3.1**).

4.4.2 Analysis of oligomeric state by SEC and SEC-MALS

Despite an appropriately long VH-VL linker, which should predominantly facilitate monomer formation, the scFvs contained other oligomeric species. SEC analysis was finally achieved by keeping the protein solution below 2 mg/mL in 50 mM Tris-HCl pH 8 150 mM NaCl for scFv-2, 3 and 4 and 300 mM NaCl or at pH 9 in the case of scFv-2. Any protein concentration step led to the formation of soluble aggregates and therefore had to be avoided. It revealed two significant protein species in scFv-1, scFv-3 and scFv-4, which were most likely a monomer and dimer (**Figure 4.6a**). In normal circumstances, SEC analysis allows for the identification of oligomeric species based on their retention volumes, but similarly to TREM2, scFvs were delayed on Superdex 200 due to non-specific interactions with Superdex, a feature typical for some antibody fragments (Zimmermann et al., 2020). It was desirable to confirm whether the two main elution species for scFv-3 and scFv-4 are monomeric and dimeric since scFv can create potentially higher oligomeric structures (Kortt et al., 2001). The scFv samples were submitted to the Molecular Biophysics Suite (MBS) within the Department of Biochemistry for multi-angle light scattering (MALS) analysis.

A MALS detector connected in tandem to a SEC column allows for measurement of the molecular weights of separated proteins. As expected, the smaller proteins eluting at 26 mL were identified as monomers, whereas the higher molecular weight complexes were identified as a dimer of scFv-4 (approx. 50 kDa) and a mixture of monomers and dimers for scFv-3 (**Figure 4.6b**).

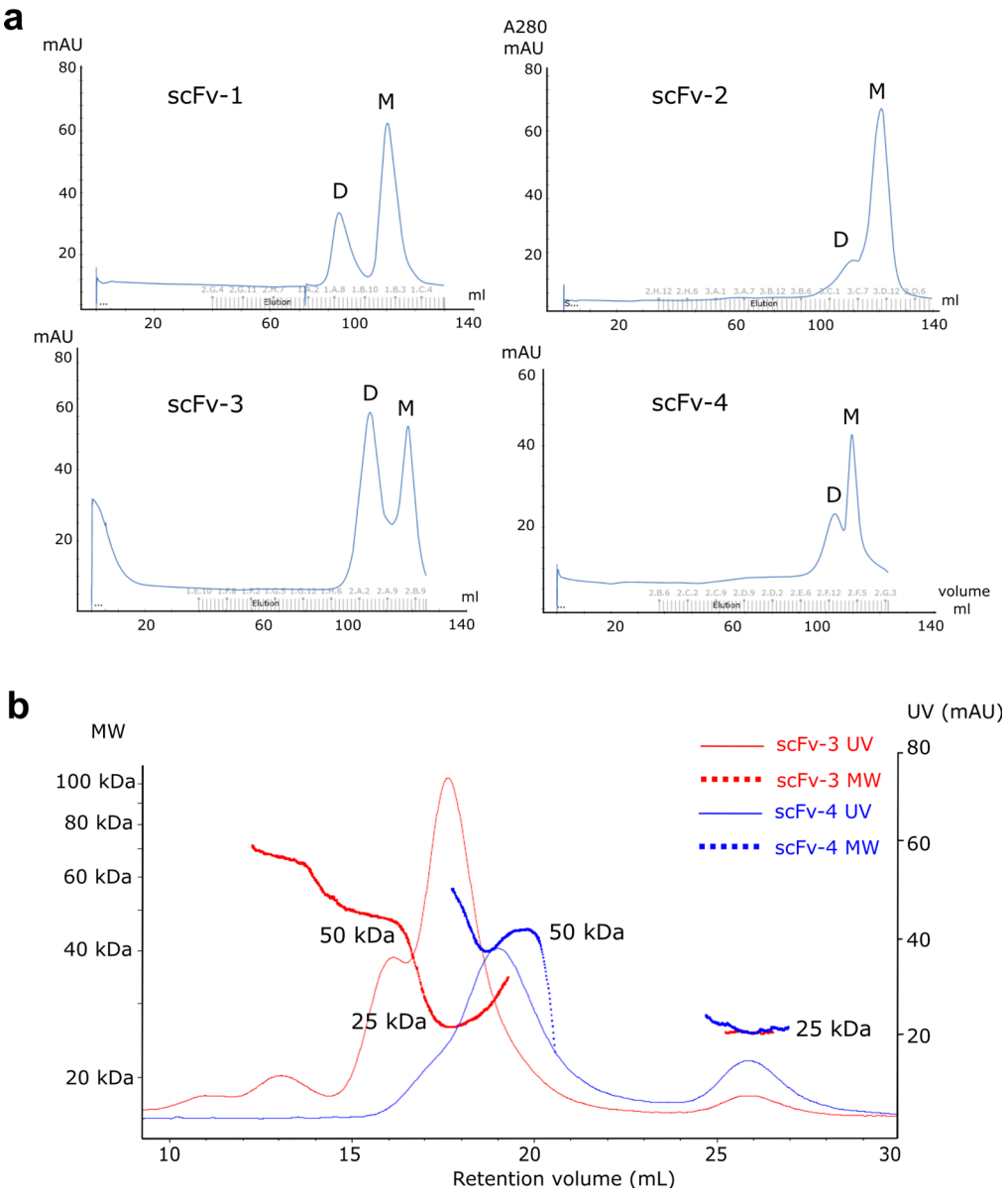


Figure 4.6. Validation of scFvs oligomeric state. *(a) SEC analysis was performed on a Superdex 200 16/60 column. Potential monomer (M) and dimer (D) are labelled. (b) Molecular weights (MW) were detected by a HELEOS-II 8-angle light scattering detector during SEC*

analysis for scFv-3 and scFv-4 samples (bold line). UV trace measured at 280 nm is shown in the fine line. Approximate MW identified for each component are labelled.

The SEC-MALS analysis of scFv-3 and scFv-4 confirmed the presence of monomers and dimers in antibody preparations, which was subsequently found to be essential for the functional activity described Chapter 6.

4.4.3 ScFvs monomer-dimer equilibrium

Due to the non-covalent nature of scFv dimers, some change in monomer-dimer equilibrium was expected, and care was taken in protein handling and avoiding freeze-thaw cycles. Initially, during the purification of monomers and dimers for cell biology experiments, I achieved relatively lasting separation, which allowed me to generate the majority of data presented Chapter 6 (**Figure 4.7a**). However, with time, it became evident that composition is changing towards monomer-dimer equilibrium as early as a week after storage at -80°C and that this process can be accelerated by the freeze/thaw cycle (**Figure 4.7c-d**). The oligomers were prepared freshly, often in small batches, which required a gentle concentration step after oligomer separation. However, the change in composition occurred despite identical protocol and even before freezing (**Figure 4.7b**). A number of conditions, such as ionic strength and concentration by HLPC-Dionex were screened, but none appeared to impact the oligomeric state. No further attempts were taken to screen for appropriate conditions since molecular biology methods of creating stable scFv dimers have been described in the literature (Cai et al., 2016; Kim et al., 2016).

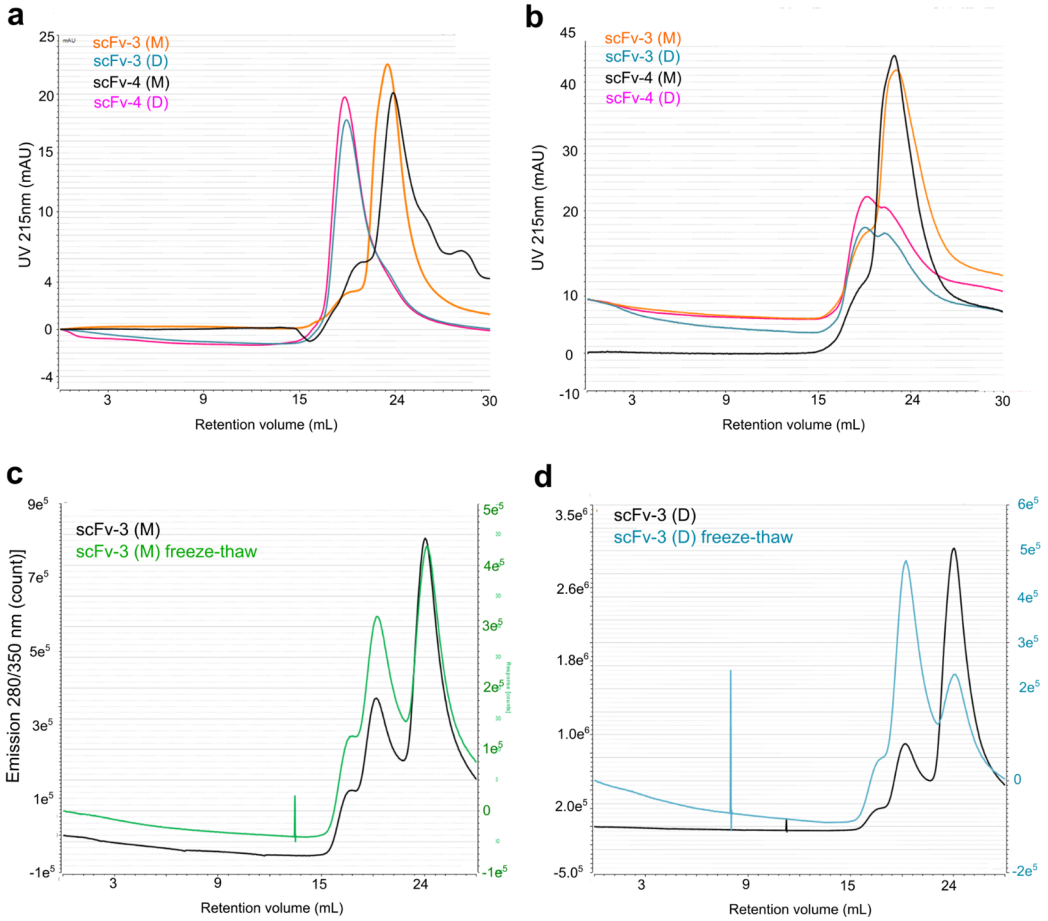


Figure 4.7. Stability of scFv dimer and monomers. *(a) Initial purifications performed by sequential SEC on Superdex 200 were analysed two weeks after freezing on the analytical Dionex- Sepax SRT SEC-300 column. (b) Another set of purifications is shown, the same protocol was employed. This time, however, samples were concentrated immediately after purification to 1mg/mL and were analysed on Dionex before freezing to assess equilibrium changes. (c-d) Analysis of the stability of scFv-3 preparations upon multiple freeze and thaw cycles. Protein signal was measured by tryptophan fluorescence (280 excitation and 350 nm emission). The same sample of scFv monomer or scFv dimer is freeze-thawed only once (black line) or twice (green or blue, denoted as freeze-thaw).*

4.4.4 Confirmation of binding to TREM2

Simultaneously during validation of the oligomeric states, the affinity of the new scFvs produced in *Sf9* cells to glycosylated TREM2 (a.a.19-174) from mammalian expression had to be validated. The latter was necessary to confirming the binding of

the new *Sf9*-produced scFv preparations to human TREM2 to support their future use in experiments on macrophages. As previously, I used BLI to measure scFv-TREM2 affinity, but an optimised protocol with longer association times was used to facilitate equilibration. Additionally, a single sensor was used per each concentration of the scFv to exclude any analyte carry-over. Surprisingly, the resulting K_D values calculated by the steady-state analysis were higher than previously calculated and were characterised by a poor fit to 1:1 model (data not shown). However, it confirmed poor binding of scFv-1 from previous experiments (**Figure 4.2b, Figure 4.3c**), and as a result, this protein was excluded from further investigations.

To confirm that the observed affinity decrease was caused by technical differences between BLI and SPR rather than loss of affinity to TREM2, additional SPR experiments were performed by Jingjing Yang (Eisai). Better quality data was obtained, which was similar to previously reported $^{App}K_D$ values for *E. coli*-produced scFvs and *Sf9*-produced TREM2. Since the discovery of the dimeric scFvs, the association (k_{on}) and dissociation (k_{off}) may also contain an avidity component, especially in the case of scFv-3 and scFv-4. Consequently, Apparent K_D ($^{App}K_D$) is used to describe the results of scFvs binding. The resulting $^{App}K_D$ values were calculated by fitting the kinetic data to a 1:1 model and were scFv-2 $^{App}K_D$ = 1.6 nM, scFv-4 $^{App}K_D$ = 0.6 nM (**Figure 4.8a,c**). Consistently with previous results, scFv-3 dissociated rapidly from the TREM2, so $^{App}K_D$ was calculated by steady-state analysis and was estimated at 54 nM (**Figure 4.8b**).

The avidity component and some non-specific interactions hindered accurate analysis of scFv binding. Only scFv-2 behaved according to a good fit to 1:1 model interaction during SPR according to its predominantly monomeric state (**Figure 4.8a**). As a result, the more accurate measurements of scFv-3 and scFv-4 affinities would require more homogenous sample preparation without a bivalent component.

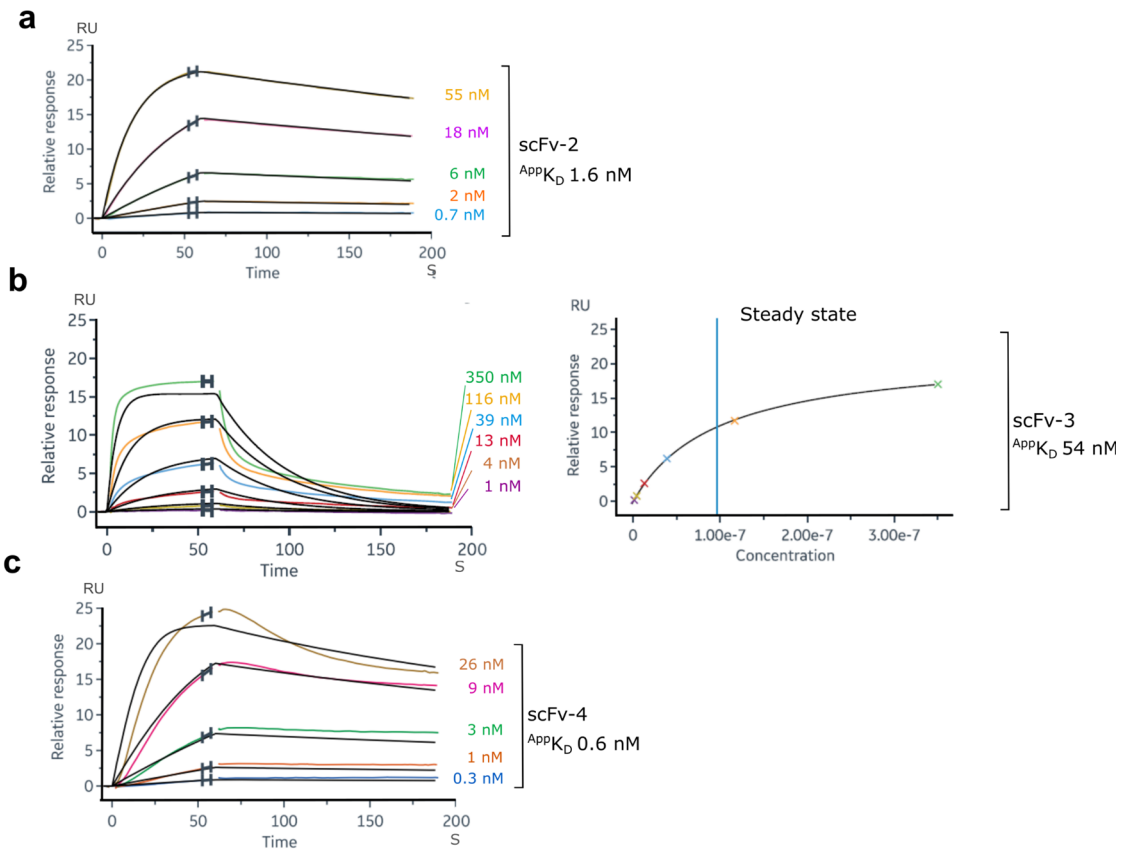


Figure 4.8. B BLI and SPR analysis of binding of Sf9 produced scFvs to the glycosylated TREM2 (a.a.19-174) from Expi293F™ expression. *(a-c) Surface plasmon resonance (SPR) was performed by collaborators on a Biacore 8K instrument, and apparent $^{App}K_D$ values were calculated based on kinetic data (except for scFv-3). Serial dilution of analytes were allowed to bind to SPR chip for 50 s followed by dissociation for 150 s at flow rate of 5 µL/. Due to potential precipitation, lower concentrations were analysed during SPR for scFv-2 and scFv-4. (c) Data from scFv-3 did not fit well into 1:1 model so $^{pp}K_D$ was calculated from the steady-state analysis. (Permission to publish figure was obtained from Eisai).*

4.5 Development and validation of antibody IgG1 and Fab conversions

In order to improve protein solubility, measure accurate binding affinity and stabilise multivalence states, IgG1 and Fab antibody conversions were generated based on CDR sequences produced as a result of phage display. ScFv-2 and scFv-4 were

selected for conversion since they had superior characteristics of binding to TREM2 than scFv-3 measured by BLI and SPR. Cloning and purification of conversions of scFv-2 (mAb-2/Fab-2) and scFv-4 (mAb-4/Fab-4) were performed by colleagues at Eisai (Weihua Li). Since the Fab fragments are monovalent, another SPR experiment was performed to validate the previous results more accurately (Jingjing Yang, Eisai). The binding of Fab-2 revealed K_D of 1.2 nM, similar to the one obtained for scFv-2 while Fab-4 affinity was lower than scFv-4 and estimated at K_D of 8.7 nM (**Figure4.9a,c**). Since animal models are frequently used to study TREM2 impact on AD, Fab fragments were also tested for binding to mouse TREM2 sequence and revealed a 55 and 31 fold decrease in the affinity for Fab-2 and Fab-4, respectively (**Figure4.9a,b, Table 4.1**). To validate similar affinity of bivalent IgG1 conversions, binding of IgG1 to human and mouse TREM2 was analysed using a bivalent analyte binding model. The binding of scFv-2 based antibodies to TREM2 was characterised by slow dissociation rates from TREM2, leading to superior affinity (**Figure4.9a,c, Table 4.1**).

While the affinity of mAb-2 to human TREM2 reflected values calculated for Fab fragments, the affinity of mAb-4 to human TREM2 decreased compared to Fab-4 (**Figure 4.9ab,d, Table 4.1**). This was unexpected since functional activity often increases upon bivalent antibody conversion. On the other hand, the affinity of mAb-4 to mouse TREM2 increased compared to Fab-4, suggesting additional factors in the functional affinity of this antibody. However, further repeats are necessary to validate these findings fully.

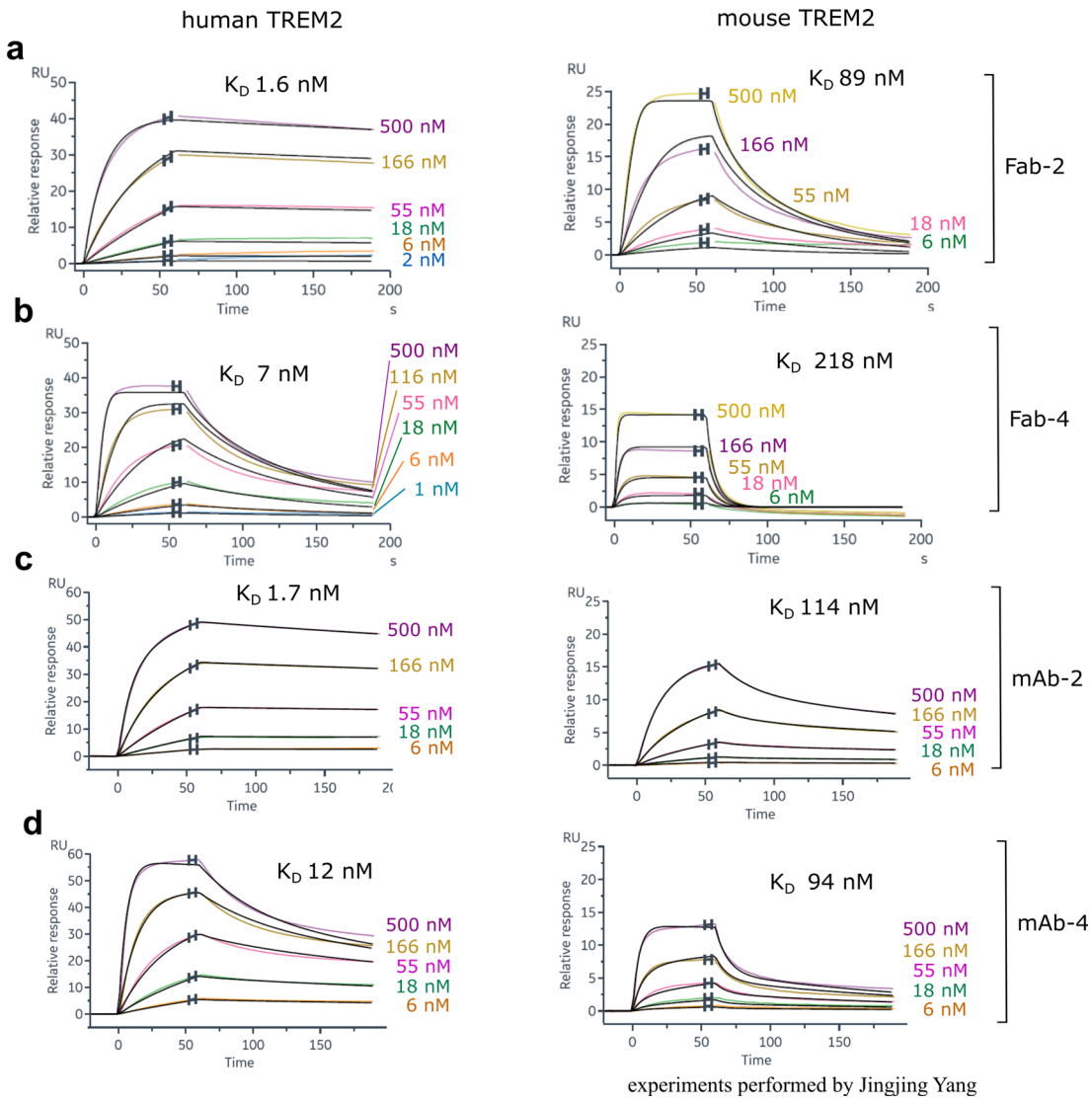


Figure 4.9. Binding kinetics of Fab and IgG1 antibodies based on scFvs sequences to human and mouse TREM2. *(a) Binding of Fab-2 to human and mouse TREM2 (a.a.19-174) measured by SPR. (b) Binding of Fab-4 to human and mouse TREM2. Reaction rate constants for a-b were calculated using the Biacore 8K evaluation software 3.1 using the 1:1 Langmuir binding model fitted to kinetics data. (c) Binding of mAb-2 to human and mouse TREM2. (d) Binding of mAb-4 to human and mouse TREM2. For c-d, reaction rate constants were calculated using the Biacore 8K evaluation software 3.1 using the bivalent analyte binding model fitted to kinetics data (Permission to publish figure was obtained from Eisai).*

	scFv-2	Fab-2	mAb-2	scFv-3	scFv-4	Fab-4	mAb-4
hTREM2	1.6	1.6	1.7	54	0.6	7	12
mTREM2		89	114			218	94
fold change		56	67			31	8

Table 4.1 Comparison of antibody fragments and full-length antibody affinities toward human and mouse TREM2 measured by SPR. *Affinity values are coloured with the lowest affinity in red and highest in green. hTREM2-human TREM2 immobilised, mTREM2-mouse TREM2 immobilised, fold change- change (decrease) in affinity when mTREM2 is used.*

4.6 Discussion

This chapter described the selection, validation, and optimisation of scFvs produced against the human TREM2 Ig-domain. Charlotte Preger and Edvard Wigren at Karolinska Institute generated and validated the four antibody binders by phage display, and I have optimised their expression and optimisation. Furthermore, colleagues at Eisai successfully generated and characterised the binding of antibody conversions to TREM2.

The number of unique binders obtained was lower than expected, which can be caused by a low number of antigenic sites on TREM2. Furthermore, TREM2 is a relatively small compact domain that results in a limited number of sites with particular biochemistry suitable to phage display library enriched in tyrosine, serine and glycine residues in the CDR sequences. The presence of glycans is indispensable to assure binding to human TREM2 in cells. However, the phage accessibility could have been compromised by longer than expected mannose chains in *Sf9*-produced glycans, and

phage display could benefit from the use of Endo H treated mammalian protein, which was developed later.

Despite the possibility of producing scFvs in *E. coli*, producing significant amounts of scFvs was challenging. The yields obtained by my collaborators and me using various *E. coli* methods were not satisfactory. Instead, the *Sf9* baculovirus system was chosen for further optimisations since and it proved to work previously for TREM2 production, which also contained two disulphides in the structure. After initial optimisations, yields dramatically improved for all antibodies. These results confirmed that despite the cheap costs of *E. coli* production, an eukaryotic expression system might be necessary to rescue the production of large amounts of complex proteins for X-ray crystallography.

Despite improvements in expression, the solubility of the scFvs produced from the SciLifeLab library was significantly reduced at high concentrations. The poor solubility of the artificially linked VH and VL domains due to the lack of stabilising interactions present in full-length antibodies has been reported previously in the literature (Ewert et al., 2003; Holliger and Hudson, 2005). Therefore, a considerable amount of effort was spent screening for stabilising buffer, pH and salt conditions by TSA screens with significant success in increasing scFv-1 and scFv-3 solubility. This is interesting, since scFv-3 differs from scFv-4 mostly in the CDR-H3 sequence with identical scaffold sequence and indicates stark differences in protein stability caused by change in single loop. It has been noted that increased affinity often leads to decreased antibody stability due to a lack of compensatory mutations occurring during natural antibody maturation (Julian et al., 2015, 2017). This finding is consistent with the high affinity of scFv-2 and scFv-4 but their poor solubility. As a result, the antibodies could

be used for cell biology experiments in DPBS (Dulbecco's PBS) at low concentrations below 2mg/mL, but crystallisation studies presented a more significant challenge.

SEC and SEC-MALS revealed that the scFvs formed a mix of monomer and dimer species. The use of a longer (15 amino acid) linker between the VH and VL domain was expected to help the production of monomers, but surprisingly, SEC revealed a large proportion of oligomer in preparations of scFv-1, scFv-3 and scFv-4 (Kortt et al., 2001). ScFv-2 preparations showed only a small amount of dimer, which was stable upon freezing, indicating a preference for monomeric structure in the equilibrium. Due to non-specific interactions with SEC column, additional MALS analysis was performed to exclude the presence of trimers or tetramers. MALS experiments confirmed that scFv-4 contained monomer and dimer species in the expected fractions. However, the scFv-3 result indicates a mixture of monomer and dimer in a larger oligomer fraction. The reason for this is not clear, but it can be caused by the poor separation of proteins due to a substantial proportion of aggregation or the particular instability of dimer conformations upon elution. The latter was detected later with monomer-dimer equilibrium changes occurring during protein handling.

Stable antibody conversions improved the results of affinity measurements and protein stability. ScFv-2 and scFv-4 were shown to bind human TREM2 with high affinity and were selected for conversions to Fab and IgG1 antibodies. The Fab facilitated more reliable SPR affinity measurements to human TREM2 and murine TREM2 with superior affinity identified for scFv-2 conversions. The scFv-4 epitope seemed to be less sensitive to change from human to mouse protein than that of scFv-2. A more detailed analysis of the epitope by methods such as X-ray crystallography is necessary to validate the residues responsible for the decrease in affinity. Still, overall

the experiments showed that both antibodies can bind TREM2 and can be used to target both human and murine receptors in a variety of uses.

The major limitation is the lack of specificity data on selected antibodies. The Luminex experiments were able to test only non-specific interactions with a limited number of proteins in the selection panel, excluding only the general non-specificity of selected scFvs. More studies combining immunoprecipitation with MS or cell biology experiments are necessary to estimate the possible binding to other surface receptors and off-target effects.

While scFvs can have many advantages for the identification of CDRs and for crystallisation, these advantages are counter-balanced by reduced stability of conformations and reduced solubility. The development of stable conversions led to improved properties and should be considered when reagents are not to be produced for co-crystallisation. While the potential success of the latter decreased with the identification of high conformational instability, the success rate of co-crystallisation experiments described in **Chapter 5** confirms that the scFv format may be beneficial for that purpose.

Chapter 5

Structure and epitope determination of TREM2-scFv complexes

Parts of this chapter are based on the publication: *Selection and structural characterization of anti-TREM2 scFvs that reduce levels of shed ectodomain*, Structure, 2021, https://doi.org/10.1016/j.str.2021.06.010. Permission to publish relevant figures was obtained under conditions described in the Creative Commons CC-BY licence.

5.1 Introduction

We hypothesised that scFv antibody fragments binding at different sites on TREM2 might differentially affect receptor signalling, internalisation or cleavage and, therefore, that an appreciation of their binding sites is important. Additionally, a known epitope is an important part of the verification of antibodies as tools. Hence, we decided to determine the crystal structures of TREM2 bound to scFv-2, scFv-3 and scFv-4 antibodies whose binding kinetics suggested strong interactions with TREM2. The

outcomes of crystallisation trials could also establish whether scFvs can be used as TREM2 crystallisation chaperones in future studies of TREM2-ligand complexes.

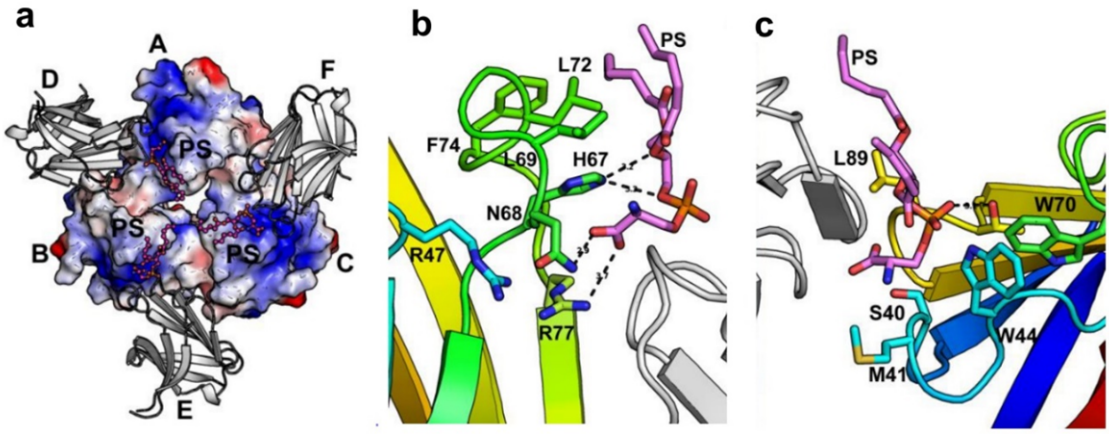


Figure 5.1 Phosphatidylserine (PS) soaked into TREM2 crystal between two TREM2 subunits. *(a) View on TREM2 hexamer from the top. Three molecules of PS are positioned between three TREM2 subunits (PBD:68BO). (b) PS packing with CDR-2 of TREM2 chain D. (c) Packing of PS with surface of TREM2 chain A. (Figure adapted from Sudom et al., 2018, Permission to publish figure was obtained under conditions described in Creative Commons CC-BY licence).*

Prior to this work, there were no structures of TREM2 bound to natural ligands or any antibody binders. The only exception is phosphatidylserine lipid (Avanti) soaked into the crystal of TREM2 post-crystallisation (PDB:6B8O Sudom et al., 2018)(**Figure 5.1**). However, the weak electron density and position between the crystal packing interfaces of TREM2 means that further experiments to validate these interactions are required (Byrne et al., 2021). Recently, several TREM2 monoclonal antibodies (mAbs) with functional properties were published; however, structural data are not available for any of them (Cheng et al., 2018; Ellwanger et al., 2021; Fassler et al., 2021; Ibach et al., 2021; Schlepckow et al., 2020; Wang et al., 2020). In fact, only two of these antibodies had an epitope mapped to the linear stalk of TREM2, which crucially allowed elaboration on the mechanism of action and should inform future studies (Ibach et al., 2021; Schlepckow et al., 2020). Contrary to scFvs, monoclonal antibodies are large (150 kDa) and glycosylated with considerable conformational flexibility.

As a consequence, structures of mAbs are less likely to be found in the Protein Data Bank (PDB) than Fab or scFvs fragments. Consequently, I have chosen to develop smaller antibody fragments against TREM2 suitable both for structure determination and functional studies.

I selected X-ray crystallography to generate the structural data and identify the TREM2 epitopes because it is the most definitive method compared to other means of epitope mapping, allowing for the detection of specific side chain interactions in the complex. Other epitope mapping protocols employ elaborate mass spectroscopy methods, computational predictions or peptide arrays, which are often restricted to linear epitopes (Bourquard et al., 2018). The latter is most common and easy to implement, but peptide array mapping of the three-dimensional epitope would result in only a fragmented picture of interactions at best. Contrary to mAbs, scFvs are smaller and more compact, increasing chances to form crystals in the presence of antigen and can therefore serve as crystallisation chaperones for otherwise crystallisation-resistant proteins (Griffin and Lawson, 2011; Tsai et al., 2020). The latter has the advantage to allow for more reliable crystallisation of TREM2. As noted by Byrne et al., TREM2 crystallisation can be unreliable and involves crystal contact formation between CDR regions, which can lead to difficulties in obtaining ligand co-crystals (Byrne et al., 2021). Of note, the only crystal structure of TREM2 with a ligand published in the PDB, utilises that crystal contact surface and, therefore, could be a result of non-specific interactions (Sudom et al., 2018) (**Figure 5.1**).

This chapter describes experimental attempts to obtain TREM2-scFv complexes, including optimisation of complex formation and crystallisation conditions for the resulting crystal structures. Crystallisation screens were first established using WT *Sf*9-produced TREM2 (a.a.19-161), one of the first folded TREM2 proteins obtained during this project (**3.4**). After these attempts, crystallisation trials used TREM2 ectodomain (a.a.19-131), supplied by Eisai through a subcontract with Viva Biotechnology (Kober

et al., 2016; Sudom et al., 2018). Later, the use of Avi-tagged TREM2 Ig domain only (a.a.19-131) and ectodomain containing stalk (a.a.19-174) led to improved biophysical behaviour of the complexes and collection of the highest resolution diffraction dataset.

5.2 Structure of TREM2 (a.a.19-131) and scFv-2

5.2.1 Optimisation of complex formation and initial screening

Before protocols for TREM2 purification from human Expi293F^{TM} cells were established, crystal trials were attempted for WT and mutant TREM2 (a.a.19-161) produced in Sf9 cells. Each scFv sample purified on Protein A and desalted to appropriate buffer was mixed with TREM2 purified on SEC column (**3.5.1**, **3.5.5**). Even when initial components were kept at low concentrations, WT TREM2 complex formation with scFv-2 was accompanied by precipitation. Nevertheless, despite the sample loss, the complex was successfully concentrated to 9 mg/mL for crystal screens using vapour diffusion and sitting drops. In most experiments, protein complexes were tested against 900 different precipitant conditions at two different temperatures (4°C and 20°C) and three different ratios of precipitant solution to protein solution (2:1, 1:1 and 1:2), resulting in the screening of 5700 conditions in total. Crystal drop images were recorded at 0, 1, 4, 7, 14, 30 and 60 days (**2.13.2**). For this specific scFv-2 complex, crystal growth at 4°C was monitored for two months without success.

Next, I tried to stabilise the complex formation by co-expression of scFv-2 with TREM2 in *Sf9* cells. Co-expression of a single glycosylation mutant TREM2 N79A (a.a.19-161) and scFv-2 resulted in a substoichiometric fraction of the latter, so the crystal trials were not attempted (data now shown). Since crystallisation failures could

be caused by glycosylation, de-glycosylated TREM2 expressed in Expi293F^{TM} cells was used in the future experiments.

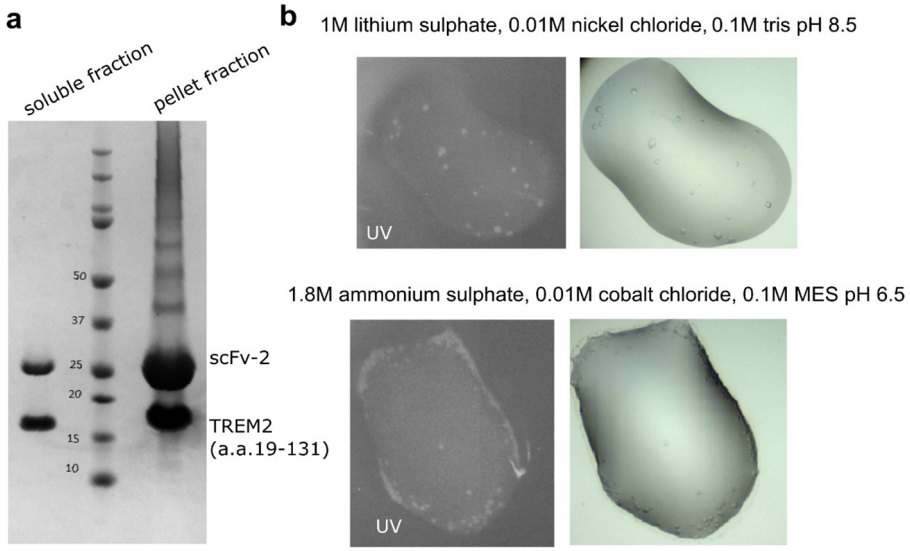


Figure 5.2 Preparation and crystallisation of pTT5:TREM2 (a.a.19-131) and scFv-2. *(a) Content of soluble and precipitated fractions during complex preparation after soluble and pelleted precipitant were separated by centrifugation and analysed by SDS-PAGE. (b) Two of the initial crystallisation hits showed in UV (left) and visible light (right). Both conditions contained similar reagents and were picked for further optimisation.*

A complex of scFvs and TREM2 produced in Expi293F^{TM} produced the first positive crystallisation outcomes. Ig-only TREM2 from the expression construct pTT5:TREM2 (a.a.19-131) was very sensitive to any additives and changes in temperature. As a result, the addition of scFv-2 was consistently associated with significant precipitation and 70% sample loss during concentration, and the complex could not be analysed efficiently by SEC. Several additives were explored, including L-arginine and L-glutamic acid mixtures and NDSB-201 detergent, which reduced loss of TREM2 (Vuillard et al., 1995) (data not shown). Concentration above 10 mg/mL was reached in the presence of 200 mM L-arginine and 200 mM L-glutamic acid. SDS-PAGE analysis of pelleted precipitant and soluble fraction confirmed that none of the components preferentially precipitated out of the solution (**Figure 5.2a**). Four different

crystallisation conditions that yielded initial crystals were identified after 4-7 days at 20℃. Since components of the precipitant solution can also create salt crystals, thus protein composition was confirmed by ultraviolet (UV) light imaging, which generates aromatic amino acid fluorescence (**Figure 5.2b**). All UV-positive conditions were selected for growth optimisation.

5.2.2 Optimisation of crystallisation of TREM2-scFv-2 complex

The further optimisations of pTT5:TREM2 (a.a.19-131) - scFv-2 complex crystal growth were performed and led to significantly improved resolution from 6 Å to 3.4 Å. Interestingly, the majority of crystal growth was observed at 20℃, and the same conditions at 4℃ did not produce crystals even after two months. The optimisation of conditions containing lithium and ammonium for salt concentrations and pH range resulted in significantly increased crystal size (**Figure 5.3a-b)**. Optimisation of the crystallisation process is time-consuming, so the presence of both proteins in the complex was established first. Each component was conjugated to different Alexa fluor dye, and crystals were checked for co-localisation of fluorescence signal using appropriate imaging wavelength (**2.13.1**). All crystals were Alexa fluor-488 and Alexa fluor-555 positive, which indicated TREM2-scFv-2 complex formation (**Figure 5.3b**).

The crystal optimisation led to successful improvements in size and morphology, but the resolution of diffraction remained poor. Initially, morphologically robust crystals were obtained in conditions containing 1.2 M lithium sulphate and 20 mM cobalt chloride at pH 6.2 (**Figure 5.3b**). Unfortunately**,** a large number of screened crystals diffracted only to 6-8 Å resolution. Subsequently, the impact of cryo-preservant and vitrification on the quality of the mounted crystals was tested. Different concentrations of sucrose and glycerol negatively affected crystal integrity and attempt

to grow crystals in conditions containing a low concentration of these cryo-preservants inhibited crystal growth. Seeding of crystalline matter into new crystal screens was also attempted with no success. A silver bullet (Hampton research) screen containing a number of additives resulted in poor crystallisation and no improvement in the diffraction.

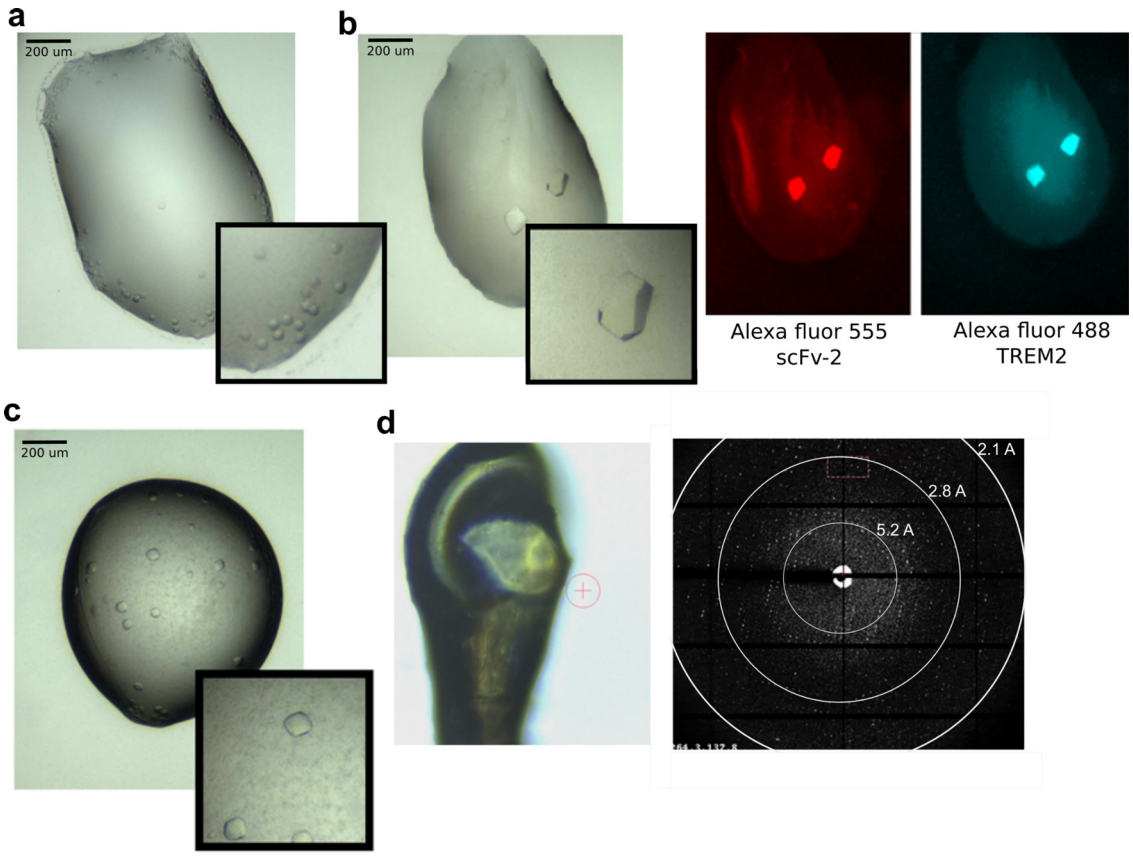


Figure 5.3 Optimisation of TREM2-scFv-2 crystal growth and diffraction. *(a) Crystals growing in 1 M lithium sulphate, 10 mM nickel chloride, 0.1 M Tris-HCl pH 8.5 at 20°C imaged on day 4. (b) The improved size was observed in conditions containing 1.2 M lithium sulphate, 20 mM cobalt chloride, 0.1 M MES pH 6.2 (on the left). Crystals contained both proteins as shown by signal for Alexa fluor 555 (red, conjugated with scFv-2) and Alexa fluor 488 (blue, conjugated with TREM2). (c) Crystals growing in 2.2 M ammonium acetate, 0.015 M nickel chloride, 0.1 M Tris-HCl pH 8.5. From this condition, a single crystal diffracted below 3.5 Å.*

(d) I24 microfocus image of mounted crystal shown in panel c in liquid nitrogen stream during data collection and diffraction pattern obtained on I03 beamline.

	6YYE (scFv-2)	6YMQ (scFv-4)	6Y6C (scFv-4)
Data collection			
Space group	I 2 2 2	P 21 21 2	P 41 2 2
Cell dimensions			
a, *b*, *c* (Å)	113.94 126.20 225.01	167.51 180.77 125.51	111.66 111.66 232.20
α, β, γ (°)	90 90 90	90 90 90	90 90 90
Resolution (Å)	110.07 - 3.36 (3.36-3.57)	75.99 - 3.07 (3.18 - 3.07)	100.63 - 2.26 (2.341 - 2.26)
R_{merge}	0.266 (1.55)	0.2811 (1.86)	0.2129 (2.041)
$I / \sigma I$	7.4 (1.7)	4.2 (1.0)	9.96 (1.25)
Completeness (%)	92 (68.9)	99.83 (99.90)	99.80 (99.34)
Redundancy	13.4 (12.7)	6.4 (6.6)	21.4 (14.3)
Wilson B-factor	68.7	69.70	39.44
Refinement			
Resolution (Å)	3.36	3.07	2.26
No. reflections	16272 (70)	71714 (7075)	69383 (6776)
R_{work} / R_{free}	0.298/0.328	0.2730/0.2871	0.191/0.216
No. atoms			
Protein	5038	15625	5368
Ligand/ion	14	92	28
Water	-	13	375
B-factors			
Protein	91.39	88.15	42.31
Ligand/ion	91.5	90.45	67.13
Water	-	58.05	47.65
R.m.s. deviations			
Bond lengths (Å)	0.003	0.001	0.002
Bond angles (°)	0.56	0.40	0.51
Solvent (%)	77.18	69%	73.85
Average B-factor (Å²)	91.0	88.14	42.0
Anisotropy	0.041	0.641	0.484
Ramachandran favoured (%)	93.73	92.59	97.21
Ramachandran allowed (%)	5.97	7.41	2.79
Ramachandran outliers (%)	0.3	0.0	0.0
Rotamer outliers (%)	2.35	0.92	0.35
Clashscore	6.01	4.76	2.56

Table 5.1. Data collection and refinement statistics (molecular replacement). Data for the highest resolution shell is shown in brackets.

Replacement of lithium sulphate with sodium malonate or ammonium acetate conditions produced crystals of reduced size with more rounded morphology (**Figure 5.3c**). Contrary to expectations, a single crystal out of six screened from the same well containing 2.2 M ammonium acetate diffracted to 3.4 Å resolution (**Figure 5.3d**). Furthermore, data collection benefited from I24 microfocus beamline, which operates a higher flux electron density beam than I03 or I04. As a result, the optimisation efforts led to improvement in crystal size and morphology but also demonstrated that morphology is not correlated with improved resolution.

Generally, crystals grew in space group I*222* with an unusually large unit cell of 114, 126, 225 Å dimensions (a,b,c) (**Table 5.1**) (**Figure 5.4a-b**). The high values of resolution-dependent Matthews correlation coefficient (MCC) of multimerisation states in a crystal indicate low protein content in the crystal, which can result in weak diffraction and reduced resolution (Kantardjieff and Rupp, 2003; Matthews, 1968). MCC probability distribution indicated that at least four TREM2-scFvs complexes should be present in the asymmetric unit of the crystal (ASU) at 3.4 Å resolution (**Figure 5.4b**). However, only two complexes were detected by Phenix molecular replacement with a high MCC of 5 $Å^3$ /Da and resulting solvent content of 77% (**Figure 5.4b**). These calculations indicated significant solvent content in the crystal. Since crystal dehydration can reduce solvent and cell dimensions and improve resolution, tests aimed to dehydrate crystals and shrink the unit cell by either exposure to air or the addition of higher salt concentration to the crystallisation drop were performed (Jennifer, 2005). Only minor variation in the unit cell size was observed, with no improvement in the resolution. Given these points, I concluded that the maximum resolution for the complex crystallised in this particular space group might have been reached.

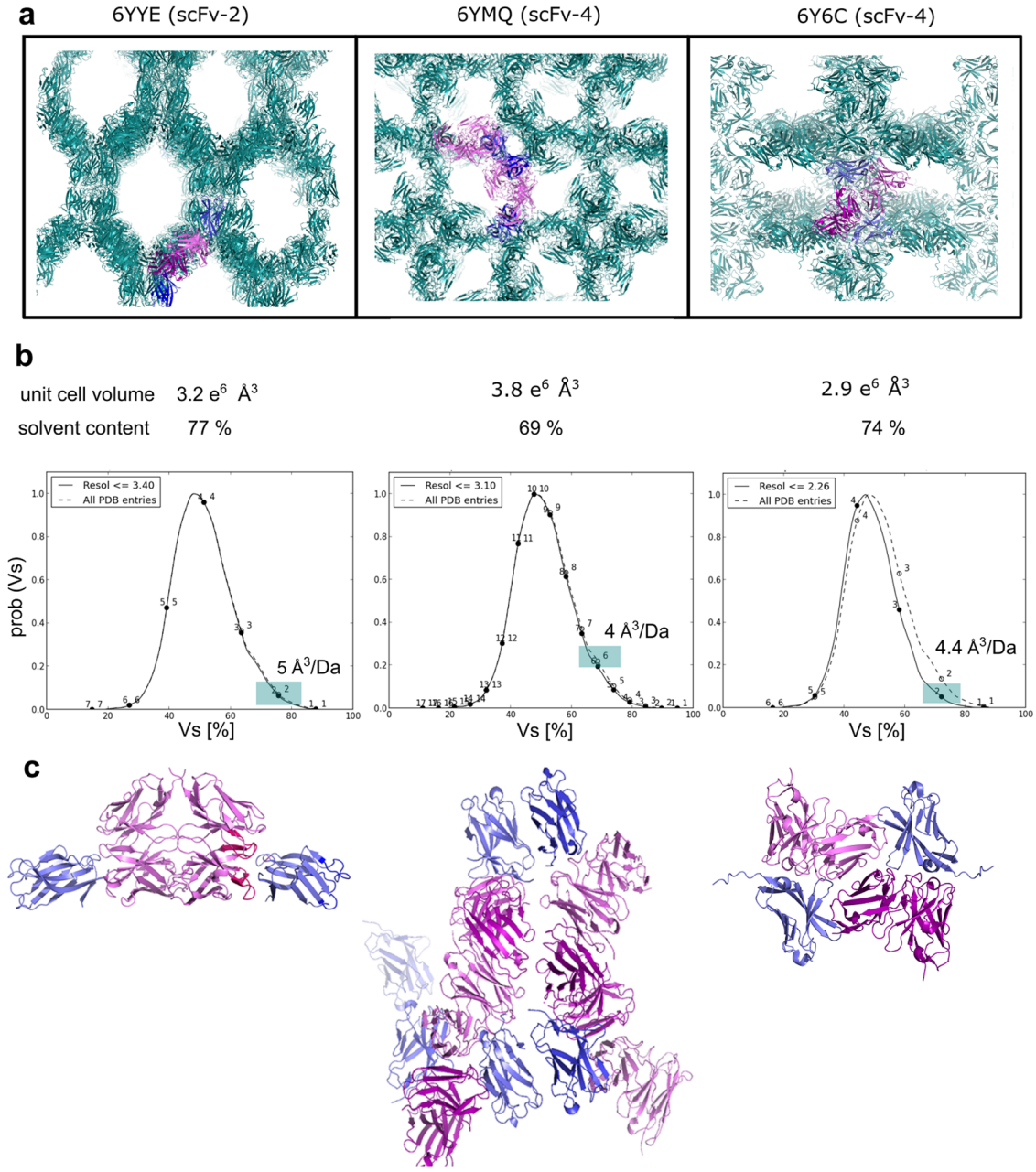


Figure 5.4. Comparison of lattices and ASU of TREM2 and scFvs structures. *(a) The pattern of the lattice for all determined structures shows the large solvent channels present in the crystals. TREM2 is shown in slate blue, and scFvs are shown in pink and magenta. (b) Matthews coefficient (Vm) and solvent content (Vs) is plotted against probability based on existing structures deposited in the PDB and calculated by the http://www.ruppweb.org/mattprob/ server. The distribution of multimerisation probabilities is shown with probabilities for all PBD entries and entries at achieved resolution shown by two lines. The actual number of scFv-TREM2 complexes in the ASU and resulting Vm are shown in the green box. The volume of the unit cell and solvent content are shown above. (c) Components of the asymmetric unit in each crystal. The ASU of the TREM2-scFv-2 crystals consisted of 2 subunits of the complex, while*

the ASUs of the different TREM2-scFv-4 crystals obtained consisted of 6 and 2 subunits of the complex, respectively.

5.2.3 Optimisation of the solubility of TREM2-scFv complexes

Simultaneously with the optimisation of the crystallisation methods, the optimisation of complex biophysical properties by use of different constructs or antibody fragments was attempted. More importantly, different amino acid sequences in the components can lead to the formation of different crystal contacts resulting in a change in space group and resolution. Firstly, I used TREM2-avi (a.a.19-138) and (a.a.19-174) constructs expressed from Expi293F^{TM} cells using the vector pHTBV1.1-SecNH-Bio instead of pTT5:TREM2 (a.a.19-131) (**Chapter 3.6.1**). Complex formation was associated with significantly less precipitation, and complexes at different concentrations were tested but unexpectedly did not produce crystals in any of the tested conditions.

Next, TREM2 crystallisation trials with previously described Fab-2 fragment, which has a higher solubility than scFv-2 were performed. The addition of Fab to TREM2-avi (a.a.19-174) during SEC resulted in the appearance of an additional peak, which was confirmed to contain both components by non-denaturing SDS-PAGE (**Figure 5.5a**). During crystallisation, some of the previously observed conditions were recapitulated, but complete novel conditions were prioritised in order to select a new crystal form. The phosphate-based condition produced morphologically beautiful crystals and was optimised to increase the crystal size (**Figure 5.5b**). Unfortunately, the resulting crystals did not diffract beyond 10 Å (**Figure 5.5c**). In conclusion, replacing either TREM2 or scFv-2 with more soluble components led to a surprising decrease in crystallisation success rates.

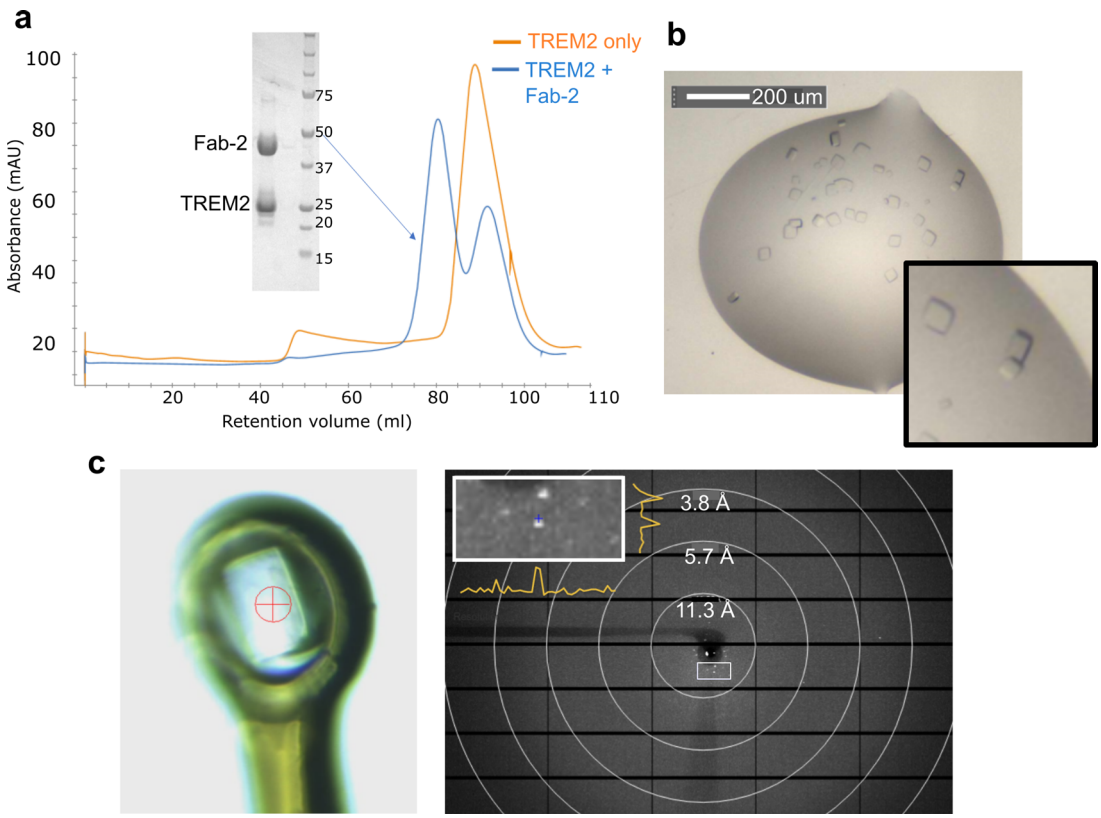


Figure 5.5. Crystallisation and resolution of TREM2-Fab-2 complexes. *(a) TREM2-avi (a.a.19-174) was analysed on Superdex 200 16/60 (orange line). Fab-2 was added to TREM2 and the same analysis was performed (blue line). Both elution peaks of the complex were analysed; the non-reducing SDS-PAGE image of the first one, which was later crystallised, is shown in the box. (b) Image of crystals growing in 1.46 M sodium phosphate monobasic, 0.24 M potassium phosphate dibasic at 20°C for 7 days. (c) Image of a mounted crystal in the liquid nitrogen stream during data collection on the I24 beamline and diffraction pattern obtained. Resolution rings are shown, and the highest diffraction signal is shown by the white box, which is enlarged in the top left corner.*

5.2.4 Structure of TREM2 with scFv-2

After screening over 200 crystals, the TREM2:pTT5 (a.a.19-131)-scFv-2 structure was finally solved to 3.35 Å from a single best-diffracting crystal growing in 2.2 M ammonium acetate (**Figure 5.3c-d**). The TREM2-scFv-2 dataset was phased with the previously solved TREM2 a.a 19-131 structure (5UD7) and another scFv structure (PDB:6G8R) generated from the same SciLifeLab library (Fairhead et al., 2019; Sudom

et al., 2018). The resulting R_{work} and R_{free} values for the refined model were 0.3 and 0.39, indicating appropriate fit of the model to experimental data and, according to PDB statistics, are satisfactory values at such a moderate resolution (**Table 5.1**). The moderately low number of amino acids in Ramachandran favoured conformations (<94%) reflects the conservative refinement, which was performed due to the low resolution of the dataset. Despite that, the model was sufficient to define the scFv-2/TREM2 interface. Nevertheless, some of the sidechains had to be removed to match electron density, and the model is characterised by high average temperature factors (B-factors) typical for low-resolution models. As a result, CDR interactions described below should be interpreted with caution, and any calculations aimed to compare the strength of TREM2 and scFv-2 interactions.

The globular ectodomain of TREM2 displayed a classic β-sandwich fold consisting of 9 β-strands, including strands, A-G common to all Ig-like domains and a C'-C" insertion typical for the V-set Ig domains (**Figure 5.6a**).

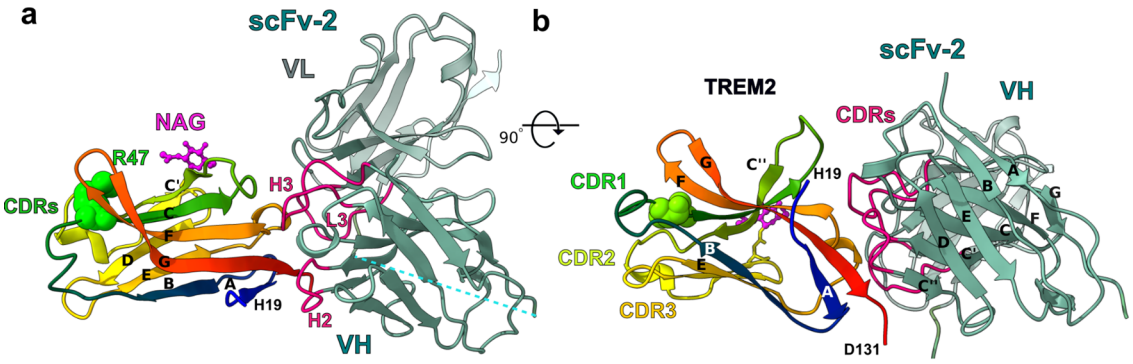


Figure 5.6. Overview of TREM2 structure with scFv-2. *(a) Cartoon representation of TREM2 bound to scFv-2. TREM2 β-sheets A-G are labelled and coloured in the rainbow. ScFv-2 is coloured in green with VH domain positioned on the same plane as VL in lighter green. CDR loops involved in TREM2 binding are labelled and coloured in magenta. R47 in CDR2 of TREM2 is coloured green in space fill, N-acetyl glucosamine remaining after de-glycosylation is coloured in pink and shown as ball and stick. (b) The same structure rotated by 90o resulting*

in rotation of VH domain to the front and VL domain behind. β-sheets of VH scFv-2 V-type domain are visible and labelled.

The overall structure does not differ significantly from the previously solved WT TREM2 (PDB 5UD7) with root mean square deviation (RMSD) of Cα atoms at 0.7 Å calculated by Chimera X (Kober et al., 2016; Sudom et al., 2018). However, the CDR-2 loop of TREM2 has been significantly disordered in one of the subunits in the ASU. The loop was modelled based on the other subunit.

ScFv-2 consisted of the same V-type fold and was found to bind to the TREM2 epitope located at the opposite end to the TREM2 complementarity-determining regions (CDRs1-3) (**Figure 5.6a,b**). The variable heavy (VH) and light domains (VL) of scFv-2 displayed canonical β-sandwich folds tethered by an engineered glycine-serine rich linker that was disordered and therefore absent in the refined structure (**Figure 5.6b**).

The binding of scFv-2 to TREM2 was mediated mostly by three CDR loops varied in the scFv phage display library, including the variable heavy domain CDRs-H2 and H3 and variable light domain CDR-L3 (**Figure 5.6a**). Limited contribution from CDR-L2 was observed in the crystal structure. As expected, these loops were enriched in tyrosine and serine residues which that contributed to a mix of hydrophobic and hydrogen bond interactions. Notably, TREM2 Glu127 (βG strand) was within hydrogen-bonding distance of three scFv-2 side chains, including Ser54, Ser56 and Ser59 from CDR-H2 (numbering corresponding to PDB entry sequences). CDR-H2 Ser59 was additionally within hydrogen-bonding distance of TREM2 Gln25 (βA) (**Figure 5.7a**).

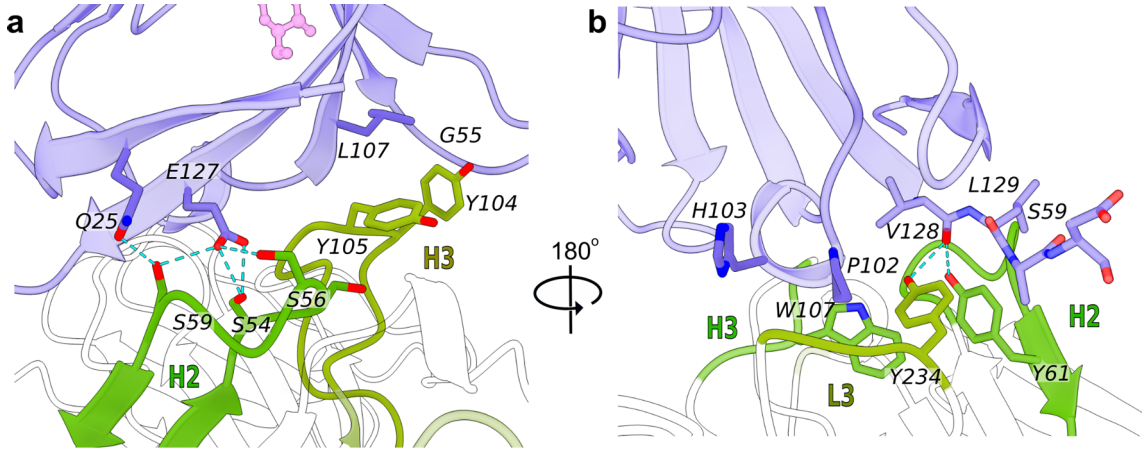


Figure 5.7. Interactions of scFv-2 with the TREM2 ectodomain. *(a) Residues involved in hydrogen bonding and hydrophobic packing are represented as sticks and shown in blue (TREM2) or green (scFv-2). The aliphatic side chains of tyrosines 104 and 105 in CDR-H3 pack against the backbone of the C-C' loop (Gly55) and Leu107 of TREM2. The serine-rich CDR-H2 mediates multiple hydrogen bonds with the side chains of TREM2 Glu127 and Gln25. Hydrogen bonds between are shown in blue dashed lines. Only hydrogen bonds that are 3.5 Å or shorter with an angle of 180°±10° are shown. (b) 180°C rotated view of the interface between TREM2 and scFv-2. Further hydrophobic packing is mediated by Trp107 (H3) and other side chains from CDR-H2 and CDR-L3. Hydrogen bonds are detected between the hydroxyl groups of Tyr234 (L3) and Tyr61 (H2) and the carbonyl of TREM2 Val128.*

Hydrophobic interactions were mediated predominantly by aliphatic portions of tyrosine side chains in scFv-2 and hydrophobic residues of TREM2: Leu107, His103, Pro102, but also the aliphatic side chain of Glu127 and backbone carbonyl groups were observed (**Figure 5.7a, b**).

5.3 Structure of TREM2 (a.a.19-131) and (a.a.19-174) with scFv-4

5.3.1 Optimisation of complex formation and initial screening

Similarly to scFv-2 complexes, co-crystallisation of scFv-4 was first attempted with *Sf*9-produced TREM2 (a.a.19-161). Again, precipitation was observed, but on this

occasion, SEC analysis was possible. **Figure 5.8a** chromatogram shows the shift towards higher molecular weight after the addition of scFv-4 despite previously described delayed migration of scFv-4 oligomers at 110-130 mL (**Figure 4.6**). Thus, the presence of just a single rather than two peaks indicated complex formation with increased homogeneity. Due to the initial sample loss, crystal trials were set up only at 4°C with no positive outcome.

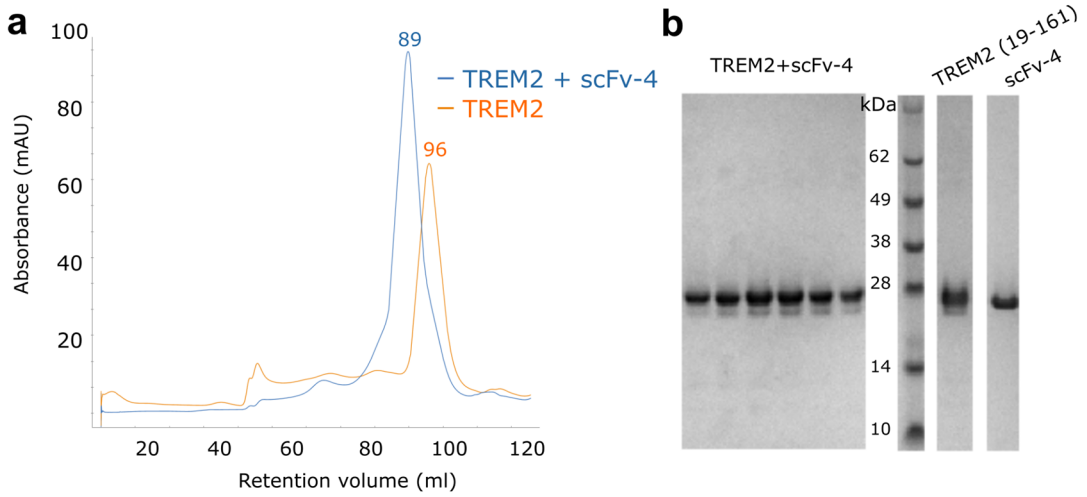


Figure 5.8. Complex formation between scFv-4 and TREM2 (a.a.19-166). *(a) SEC chromatogram of TREM2 (orange line) and TREM2 with scFv-4 (blue line) on Superdex 200 16/600. A shift from retention volume of 96 to 89 mL towards larger MW is observed. (b) SDS-PAGE of the SEC peak at 89 mL for the complex and individual components before complex formation.*

Next, crystallisation of scFv-4 with fully deglycosylated pTT5:TREM2 (a.a.19-131) produced in Expi293F™ was attempted. Once more, the complex formation was achieved by mixing both components and led to precipitation. Despite that, crystals appeared as early as on day one at 4°C and 20°C. Despite other, larger, and better-formed crystals, only crystals growing in 30% MPD at 4°C diffracted to 4 Å (**Figure**

5.9a). Although no improvement in crystal morphology was achieved, increasing MPD concentration to 39% resulted in a dataset that diffracted to 3.1 Å (**Figure 5.9b**).

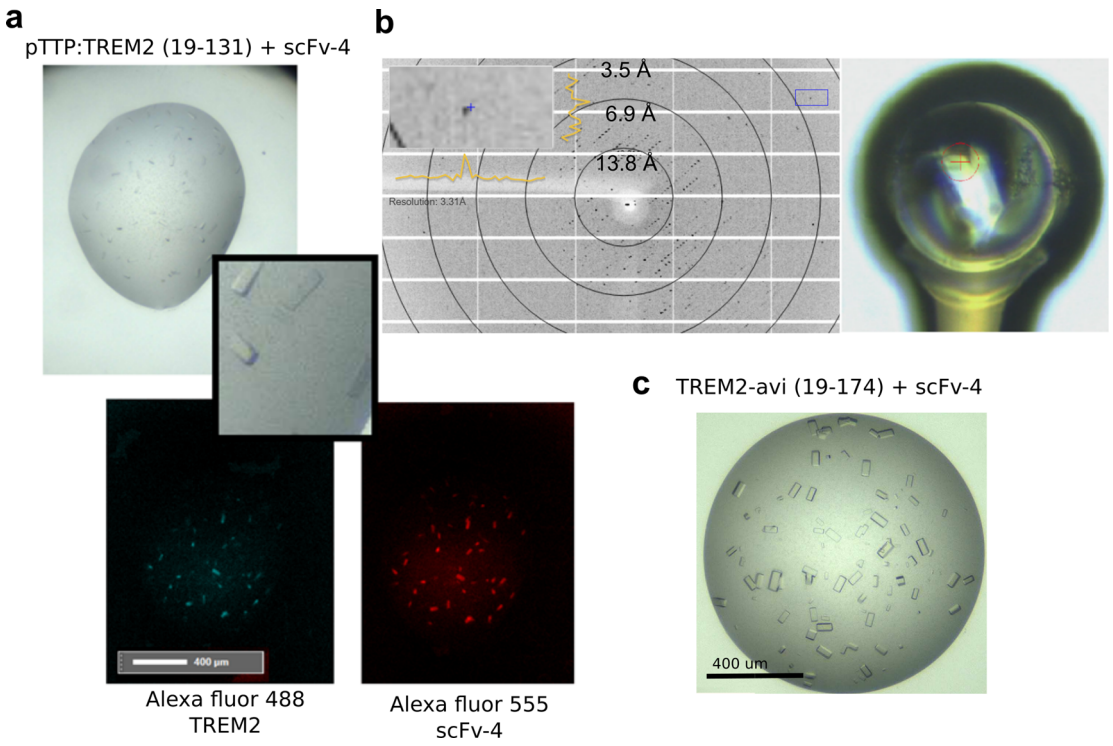


Figure 5.9. Optimisation of TREM2 crystallisation with scFv-4. *(a) Image of crystals of scFv-4 and TREM2:pTT5 (a.a.19-131) growing in 39% MPD, 0.2 M ammonium acetate, 0.1 M citrate pH 5.5 at 4°C at day 4. (b) I24 microfocus beamline diffraction of one of the crystals from improved condition (39% MPD, 0.2 M ammonium acetate, 0.1 M citrate pH 5) and data collection at Diamond light source. (c) Crystals of a different scFv-2 complex containing longer TREM2 (a.a.19-174) and scFv-4 grown in 35% pentaerythritol propoxylate 5/4, 0.2 M potassium chloride, 0.1 M HEPES pH 7.5 at 20°C for 7 days. These crystals did not require optimisation and diffracted to 2.2 Å.*

However, a significant improvement in the biochemical behaviour of the complex was achieved by using the longer construct TREM2-avi (a.a.19-174). During complex preparation, no precipitation was observed, and large crystals appeared in a new condition containing 35% pentaerythritol propoxylate 5/4 (**Figure 5.9c**). These crystals did not require optimisation as one of them resulted in a 2.2 Å resolution dataset collection. In conclusion, despite my previous failed attempts to improve resolution by

improving the solubility of the complex, the expected improvement was finally achieved for scFv-4 and TREM2 complexes.

5.3.2 Structure of TREM2 with scFv-4

The of pTT5:TREM2 (a.a.19-131) in complex with scFv-4 (PDB:6YMQ) was solved as a first and the resulting model was used for molecular replacement of pTT5:TREM2 (a.a.19-131) and scFv-2 structure (PDB:6YYE) and the another scFv-4 structure with scFv-4 in complex with TREM2 (a.a.19-174) (PDB:6Y6C). The 6YMQ structure consisted of six molecules of TREM2 and six molecules of scFv-4 in the asymmetric unit, requiring time-consuming refinement (**Figure 5.4b**). The complex crystallised in space group $P2_12_12$ and had a large unit cell (167, 180, 225 Å dimensions) with 69% solvent content. The model quality according to R_{work} and R_{free} was 0.27 and 0.29, respectively, indicating a good fit with nevertheless high B-factors caused by high crystal anisotropy and poor electron density for two of TREM2 subunits (**Table 5.1**). As a result, another better model of TREM2-scFv-4 interaction was used to describe interactions.

The scFv-4 structure with loner TREM2-avi (a.a.19-174) (PDB:6Y6C) was crystallised in a 112, 112, 232 Å unit cell in space group $P4_122$ and solvent content of 74% (**Table 5.1**). The structure was solved to 2.2 Å resolution with only two copies of the complex in the ASU and better model quality demonstrated by lowered R_{work} and R_{free} values of 0.19 and 0.21 (**Figure 5.4b**). In this model, temperature factors B were also lower, and a majority of the amino acids were refined in favoured Ramachandran conformations (>97%) due to increased order and higher resolution than previously solved structures (**Table 5.1**). Still, no significant differences were observed in scFv-4 binding to the TREM2 ectodomain in the equivalent structure using the shorter TREM2

construct pTT5:TREM2 (a.a.19-131) (**Figure 5.10b**). The majority of the electron density for the stalk sequence is absent, resulting in a lack of structural information past Asp137. Therefore, the higher resolution 6Y6C was used to analyse these interactions in detail.

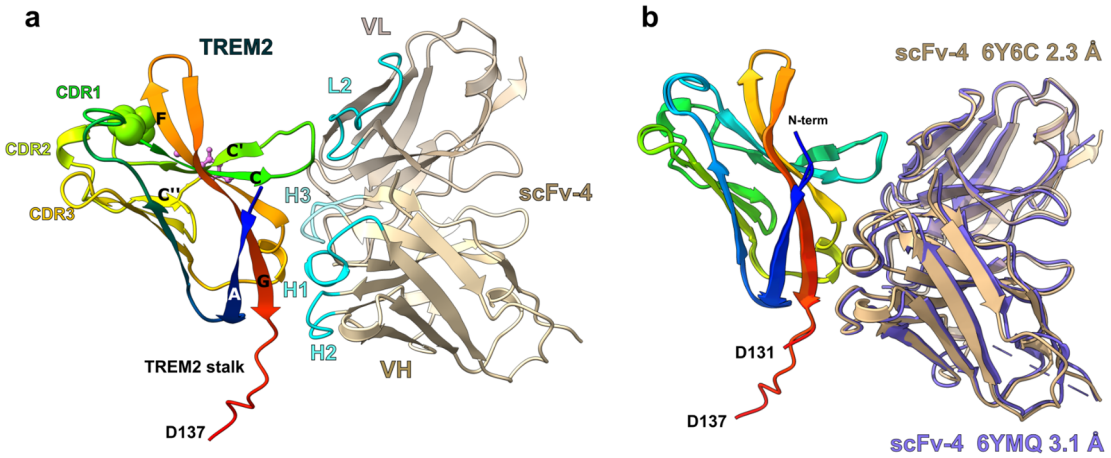


Figure 5.10. Overview of TREM2 and scFv-4 structures. *(a) Cartoon representation of TREM2 bound to scFv-4. TREM2 β-sheets are labelled and coloured in rainbow. ScFv-4 is coloured in tan with VH domain positioned on the same plane as VL in tan. CDR loops involved in TREM2 binding are coloured in cyan. R47 in CDR2 is coloured green in space fill, N-acetyl glucosamine remaining after de-glycosylation is coloured in pink and shown as ball and stick. (b) Superposition of the two TREM2-sc Fv-4 structures showed excellent agreement (Cα RMSD = 0.5 Å). ScFv-4 in complex with long TREM2 (a.a.19-174, PDB:6Y6C) is shown in tan, whereas scFv-4 in complex with short pTT5:TREM2 (19-131, 6YQM) is shown in purple.*

Similarly to scFv-2, the epitope of TREM2 consisted of strand βA (T17-A28) residues in βF (P102-L107) and βG (L125-D131) but also loop C-C' (R52-P59), which resulted in an extended interaction surface (**Figure 5.10**). TREM2 structure was similar to previously published TREM2 structures with RMSD values at 0.4 Å indicating lack of conformational change upon scFv-4 binding.

The binding of scFv-4 to TREM2 was centred on the CDR3 loop of the scFv-4 VH domain (herein CDR-H3), flanked by interactions from CDRs-H1 and -H2 and by

the VL domain CDR-L2 (**Figure 5.10a**). CDR sequence selections in scFv-4 were enriched in tyrosine residues (**4.2, Figure 5.11a-b**).

Strikingly, CDR-H3 contained six consecutive tyrosine residues, interrupted only by Gly104, which was likely selected to avoid the steric clashes that would result from any other amino acid at this position. Tyrosine residues 33, 59, 102, 103, 106, 107 and 187 in scFv-4 contributed to extensive hydrophobic packing interactions with the non-polar TREM2 residues Val23, Pro102, Leu107, Leu125, Val128 and Ala130 (**Figure 5.11a-b**). The latter amino acids contributed to similar interactions in the scFv-2 complex structure (**Figure 5.7a, b**).

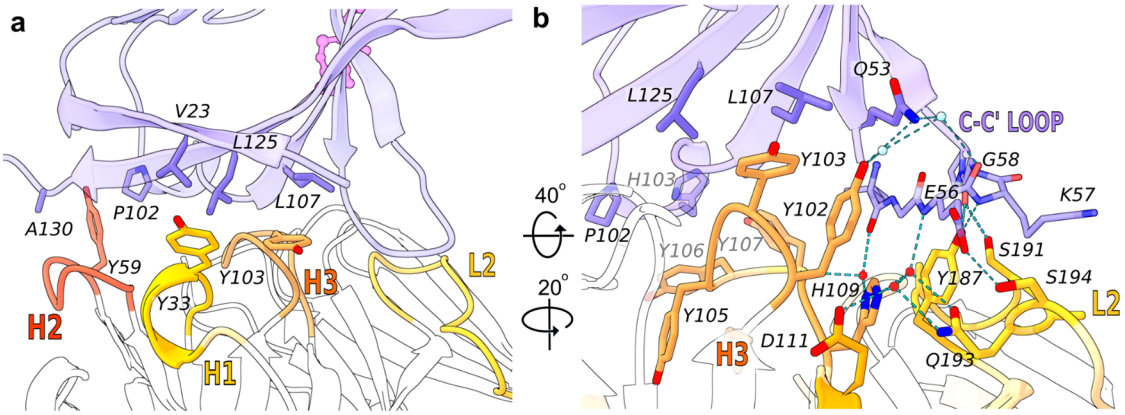


Figure 5.11. Interactions of scFv-4 with the TREM2 ectodomain. *(a) Tyrosine residues of CDR-H1, H2 and H3 intercalating between TREM2 β-sheets rich in hydrophobic residues are highlighted as sticks. Interface residues are presented as slate blue for TREM2 or orange, red and yellow for different CDR loops of scFv-4. (b) The same structure visualised by rotation as indicated. Residues involved in the hydrogen bond network between CDR-H3, CDR-L2 and TREM2 are presented as sticks. Only hydrogen bonds generated by scFv-4 side chains are shown together with water molecules mediating hydrogen bonding when applicable (red sphere). Calculated hydrogen bonds are 3.5 Å or shorter with an angle of 180°±10°.*

Additional side chain and water-mediated hydrogen bond interactions were provided by scFv-4 loops CDR-H3 and CDR-L2 (**Figure 5.11b**). The most extensive

hydrogen bond interactions occurred between the CDR-L2 with the C-C' loop of TREM2. Here, the scFv-4 residues Tyr187, Ser191 and Ser194 formed hydrogen bonds with TREM2 residues Lys47, Gly58 and Glu56, respectively **Figure 5.11b**).The side chain of Tyr102 from CDR-H3 also inserted between TREM2 β-strands C and F to form a further hydrogen bond with TREM2 Gln53 (**Figure 5.11b**).

5.4 Comparison of TREM2 structures and biological assembly prediction

The overall TREM2 structures in complexes with scFvs do not differ significantly from the previously solved WT TREM2 (5UD7) indicating lack of change in TREM2 structure upon scFv binding. Both antibodies bind TREM2 on the opposite side to the putative ligand-binding site of TREM2, consisting of CDRs 1-3 and located close to Arg47 (Kober et al., 2016; Sudom et al., 2018) (**Figure 5.12a**). Here, the β-sandwich of TREM2 splayed between β-strands C and F to provide an extended surface for the scFvs to bind that included parts of β-strands A, F, G and loop C-C' (**Figure 5.12a**). However, the overlay of the two TREM2-scFv complexes revealed that the binding epitopes on TREM2 were only partially similar. In particular, scFv-4 formed extensive interactions with the C-C' (R52-P59) loop in TREM2 that were largely absent in the scFv-2 complex, resulting in a different VL domain orientation towards TREM2 and change in overall structure (**Figure 5.12b-e**). As a result, the similar epitope on TREM2 led to surprisingly different global orientation of the complexes.

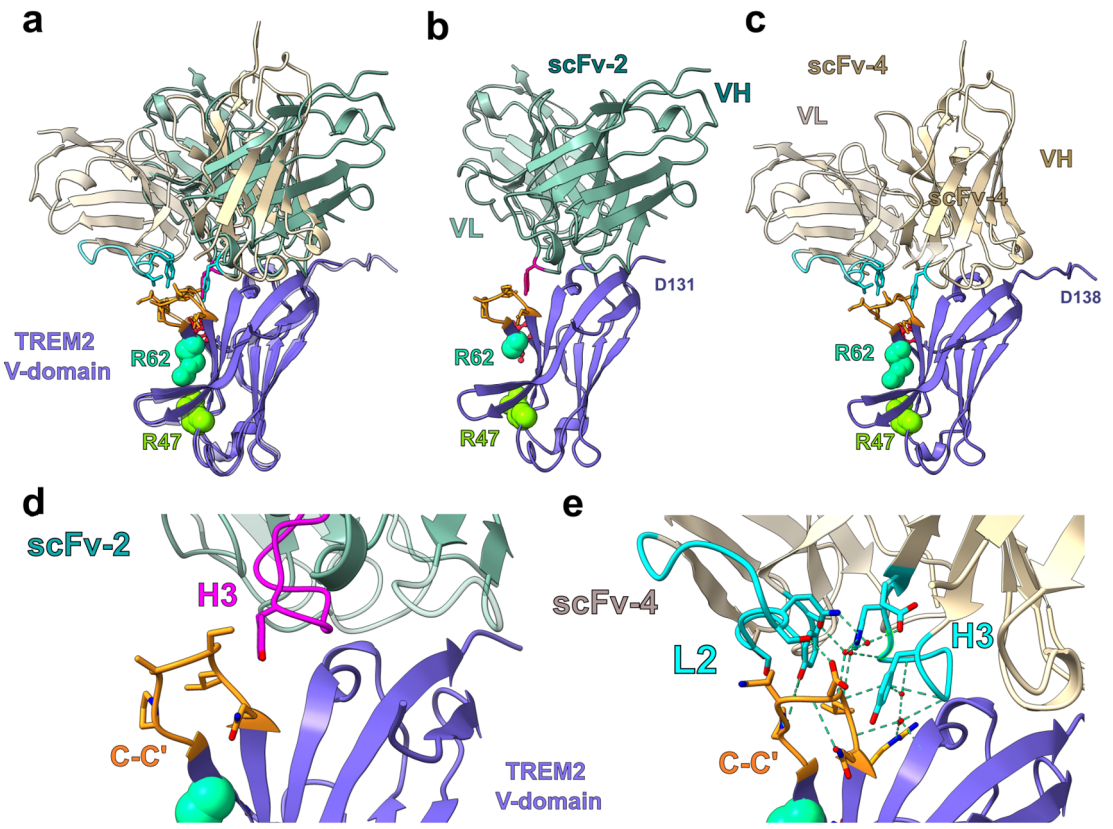


Figure 5.12. Superimposition of selected TREM2 and scFv-2 and scFv-4 co-structures. *(a) Superimposition of scFv-2 (6YYE, green) and scFv-4 (6YMQ, tan) structures. TREM2 is shown in slate blue with AD mutant sites at R62 and R47 shown in space fill and cyan and blue. C-C' loop is shown in orange with side-chains visible. (b) The overview of scFv-2 and TREM2 structure with sidechain of CDR-H3 taking part in C-C' loop interactions shown in magenta. (c) The overview of scFv-4 and TREM2 structure with sidechain of CDR-H3 and CDR-L2 taking part in C-C' loop interactions shown in cyan. (d) Interaction between C-C' loop of TREM2 and scFv-2, no hydrogen bonds were detected. (e)) Interaction between C-C' loop of TREM2 and scFv-4, hydrogen bonds are shown between C-C' loop (orange), water molecules (red) and CDR-L2 and CDR-H3 of scFv-4. For clarity, amino acids numbering is not shown – for detailed description refer to figure 5.11b.*

Biological assembly is described as oligomeric state of the complex present natively in solution rather than in a crystal. Both complexes have multiple subunits present in the asymmetric unit which can be caused by the native conformation or crystallisation artefact. Identification of the biological assembly in scFv-TREM2

structures is challenging due to instability of VH-VL interface which has been shown to be responsible for domain swapping between two monomers and scFv dimer formation (Arndt et al., 1998; Kim et al., 2016; Kortt et al., 2001; Wörn et al., 2001).

Crucially, electron density for linker connecting VH-VL domain which can identify domain swapping is absent from both TREM2-scFv structures. ScFv-2 is largely monomeric in the absence of antigen, as shown by SEC (**4.4.2**), but a significant dimer presence cannot be dismissed at high concentrations. The similar distance between VL and VH domains of each complex indicates that both domains could potentially be swapped between each of the monomers to form a dimer. However, the prediction of biological assembly performed with PISA software (https://www.ebi.ac.uk/pdbe/pisa/) during structure deposition indicated that heterodimer of monomeric scFv and single TREM2 are the most likely structure in solution (PDB:6YYE) (Krissinel and Henrick, 2007).

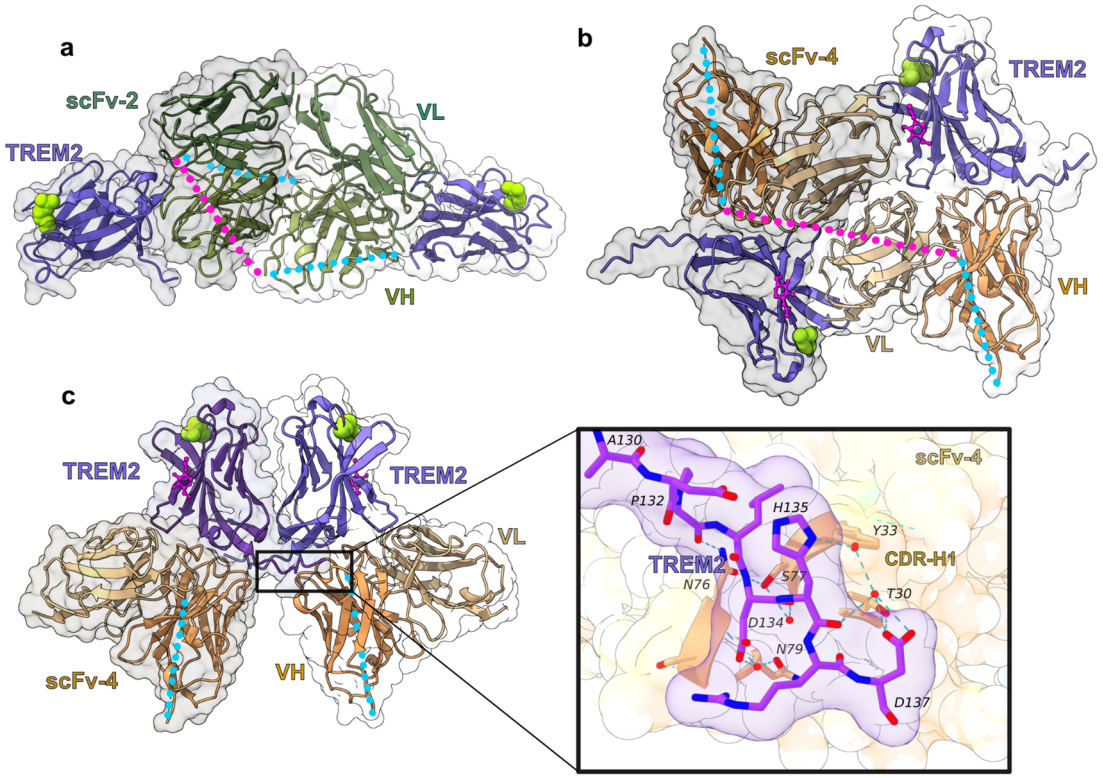


Figure 5.13 Different crystal packing of TREM2- scFv-2/scFv4 complexes and scFv-4-stalk interactions. *Crystal packing between scFv-2 subunits in the TREM2 complex (PDB:6YYE). The scFv-2 VH and VL domains are coloured in different shades of green; the length of the disordered linker between VH and VL domains is shown by a dotted cyan line. The alternative linker required for domain swapping and dimeric scFv-2 is shown in pink, TREM2 is coloured slate blue. A molecular surface representation of each TREM2-scFv-2 complex is shown in a different transparent shade of grey. (b) Crystal packing between scFv-4 subunits (tan) observed in the TREM2 (a.a.174) co-structure (PDB 6Y6C). Each scFv-4 subunit packs against two molecules of TREM2 by interaction with the primary TREM2 epitope as well as an additional surface consisting of the TREM2 C-C' and F-G loops. (c) Neighbouring crystal packing of TREM2 dimer with two scFv-4 observed in the same structure but containing stalk interaction shown in the box. Each TREM2 subunit interacts with two scFv-4 molecules through interactions from the TREM2 ectodomain and stalk region. Residues forming hydrogen bond interactions are presented as sticks and waters as red spheres.*

Despite the presence of monomer and dimer in solutions of scFv-4 (**4.4.2**), the monomers of scFv-4 do not appear to pack well against each other, indicating that domain swapping is unlikely (**Figure 5.b**). However, this time PISA prediction identified a large biological assembly created by four complexes which included interactions with the TREM2 stalk (PDB:6Y6C, **Figure 5.c**). This is in contrast to results of the SEC analysis of complex formed between scFv-4 and insect cell-produced TREM2 containing stalk sequence (a.a.19-166), which did not indicate the existence of such a large assembly in solution (**Figure 5.8**). On the contrary, only a single homogenous species was detected, indicating antigen-mediated change in confirmation and improvement in homogeneity (Arndt et al., 1998). Moreover, the PISA results for pTT5:TREM2 (a.a.19-131) predict a single complex in the biological assembly strengthening the case for monomer interactions (PDB:6YMQ).

While the primary scFv-4 interaction was mediated by the CDRs and ectodomain described before, crystal packing interactions with other TREM2 Ig surfaces as well as the stalk sequence were detected (**Figure 5.c**). The latter involved a neighbouring

subunit of scFv-4 and allowed the stalk to be traced in the electron density maps up to Asp137 in the C-terminus. Here, the TREM2 C-terminal stalk sequence Pro132-Asp137 packs against ScFv-4 CDR-H1 and Asn76-Asn79 residues forming a number of hydrogen bonds (**Figure 5.c**). The multiple packing surfaces contribute to the higher density of these scFv-4 crystals but may not be a part of the biological assembly.

Furthermore, more structures involve crystal packing interfaces between TREM2 CDR-1-3 regions which was previously described for other structures of TREM2 deposited in PDB (Byrne et al., 2021) (**Figure 5.13a,b**). In TREM2-scFv-4 structure, crystal packing between two TREM2 molecules is mediated prominently by components of the hydrophobic patch highlighted in gold colour (**Figure 5.13a,c**). Four residues of Phe74 from four subunits of TREM2 (A-D) together with surrounding Leu71 and Leu72 create a large hydrophobic interaction surface. Similar string hydrophobic interactions are observed for Trp70, Trp44 and Met4 between TREM2 chain C and B (**Figure 5.13c**). In scFv-2-TREM2 model, the same CDR are involved in packing, but the interaction surface is more shallow than in the other model, which can be partially attributed to some missing sidechain density (**Figure 5.13b,d**). In chain C, CDR-2 containing Phe4 is removed from the main packing interface and neighbours the same loop from chain D, which was partially disordered due to weak electron density in the area. Met41 (chain A) is the most exposed to mediate hydrophobic interactions with neighbouring Met41 (chain C), but there is also potential for interactions involving Trp44 sidechain, which had to be removed during the refinement (**Figure 5.13d**).

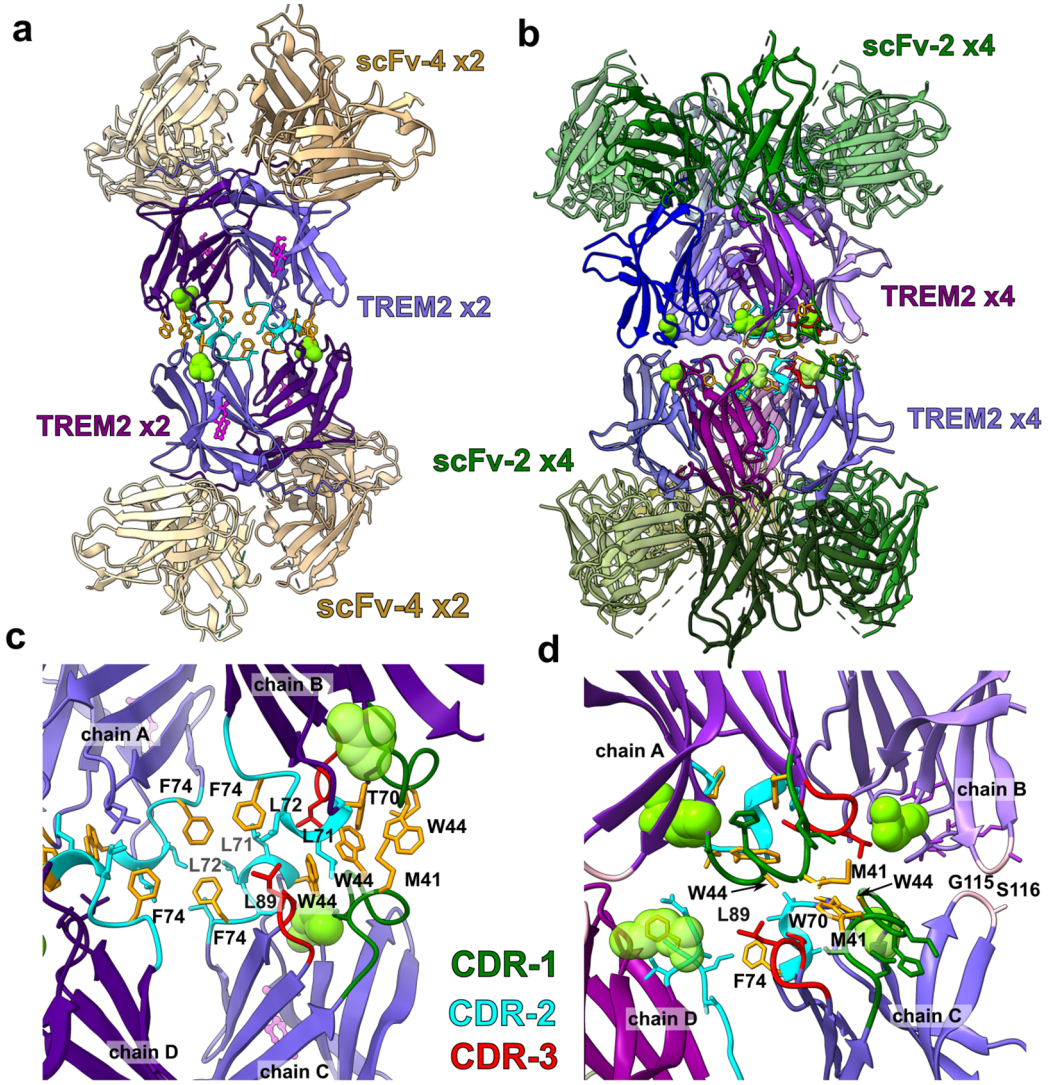


Figure 5.13. Crystal packing in TREM2 between CDR loops. *(a) Structure of scFv-4 with TREM2 (6Y6C) showing TREM2-TREM2 interaction in the crystal lattice. R47 is shown in space fill in green, and NAG is shown in fuchsia. (b) Structure of TREM2 with scFv-2 (6YYE) showing TREM2-TREM2 interactions. (c) Enlarged image showing TREM2 residues in TREM2-scFv-4 structure taking part in crystal packing interactions, CDR are shown in different colours, hydrophobic patch residues are shown in gold. (d) Enlarged image showing TREM2 residues in TREM2-scFv-2 structure taking part in crystal packing interactions. Residues are coloured as in C. Additionally, residues in Gly115-Ser116 loop which pack against the same loop in another TREM2 is shown in light pink.*

5.5 Mapping of scFv-3 and TREM2 epitope with use of mAb conversions

After successful crystallisation trials of scFv-2 and scFv-4, the overlapping location of the epitope on TREM2 was validated in order to establish whether the function of scFv-3 has the potential to vary significantly from scFv-2 and scFv-4. The attempts to crystallise scFv-3 were not successful so instead, I used an enzyme-linked immunosorbent assay (ELISA) approach and validated whether epitopes for scFv-2 (mAb-2) or scFv-4 (mAb-4) are overlapping with scFv-3. A commercial standard TREM2 peptide (a.a.19-174, SynoBiologicals) was mixed with scFv-3 or buffer only, and plates coated with mAb-2 or mAb-4 were evaluated for the ability to detect TREM2. Additionally, scFv-4 and scFv-2, respectively, were used as a positive control for epitope overlap. The addition of scFv-3 monomer reduced detection by mAb-2 or mAb-4 conversion, indicating similar epitope overlap to scFv-2 and scFv-4 CDRs (**Figure 5.14a,b**). Given these results, the TREM2 epitope for all three scFvs appears to be located on the surface distal from the ligand-binding pocket.

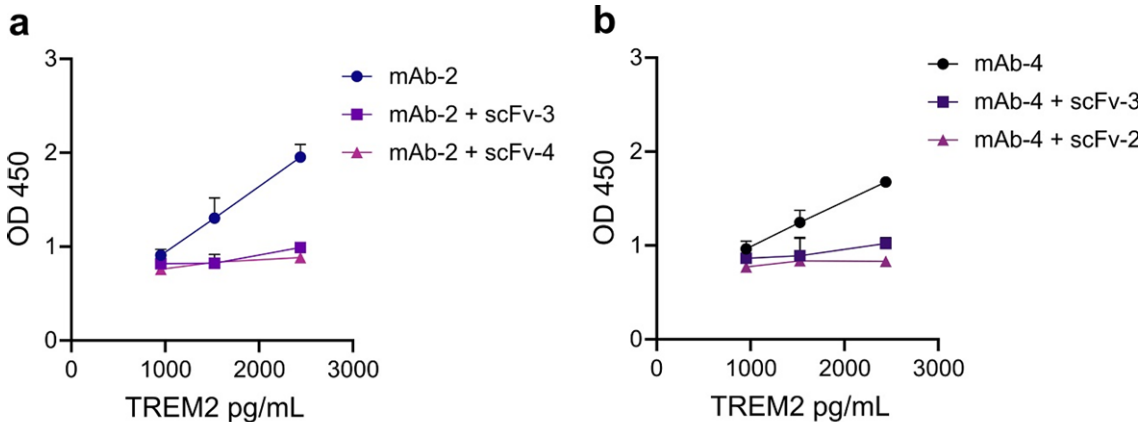


Figure 5.14. Identification of overlapping epitopes on TREM2 for scFvs by ELISA approach. *(a) mAb-2 was used to coat the ELISA plate overnight. Solutions with a standard peptide with or without the addition of scFv-3 and scFv-4 monomers were incubated and TREM2 was detected with antibody BAF1828 (R&D biosystems). The amount of standard peptide is plotted against absorbance measured at 450 nm. Data represent mean ± SD (n=1, two technical*

repeats). (b) mAb-4 was used to capture TREM2 standard peptide solutions with or without the addition of scFv-2 and scFv-3 monomers. Data represent mean ± SD (n=1, two technical repeats).

5.6 Discussion

The structure-function relationship can shed light on the mechanism of TREM2 activation but also facilitate the development of fully validated reagents for future mechanistic studies. This chapter presented the experimental approach to structurally characterise scFvs raised against human TREM2 by phage display. The structures of two scFvs bound to TREM2 have been solved, which provided the first crystallographic structures of unambiguous interactions with TREM2 extracellular Ig domain.

Diffracting crystals were first obtained for the complexes of the smaller TREM2 Ig-like domain with both scFv-2 and scFv-4, but not scFv-3, enabling their structure determination at 3.36 and 3.07 Å resolution, respectively. However, a higher resolution structure of the scFv-4 complex was obtained using the longer TREM2-avi (a.a.19-174) construct comprising both the Ig-like domain and part of the stalk and refined to 2.26 Å resolution. Despite high solvent content in all crystal lattices, TREM2-avi (a.a.19-174) in complex with scFv-4 diffracted to 2.2 Å, which can be attributed to additional packing between stalk (a.a.131-138) and CDR-H1 of scFv-4, the interactions which were lacking in lower resolution scFv-4 structure. This is surprising since the long stalk sequence of TREM2 would not be considered the first choice of a construct for crystallisation due to the increased flexibility of that region.

The stalk interaction is of interest due to the importance of the stalk region in TREM2 biology, but it cannot yet be established whether it is purely a crystallisation artefact. Initially, a peptide spanning the TREM2 region of interaction was designed for competition experiments. However, the peptide was shown to compete with an epitope

for the EPR20243 antibody (Abcam), and as such, this interaction could not be confirmed by competition ELISA (data now shown). The hope is that cell biology experiments could reveal whether this interaction exists and has biological potential.

The optimisation of TREM2-scFv crystallisation was very challenging, with difficulties in complex formation and reproducibility. Similar difficulties were observed by others in the literature in the crystallisation of TREM2 (Byrne et al., 2021). Byrne et al. noted that all TREM2 structures deposited in the PDB contain crystal-packing interactions between CDR-2 of two neighbouring TREM2 molecules with a potentially negative impact on TREM2 ligand studies. Unfortunately, a packing involving all CDR sequences occurs in crystal lattices obtained in our study and indicates a strong preference for the formation of crystal contacts likely caused by their hydrophobic nature described by Kober group (Kober et al.,2021). In fact, Trp44, Phe74 and Leu89, which are involved in packing interactions, were shown to be also involved in phosphatidyl serine interactions (Sudom et al., 2018). Interestingly, CDR-2 in TREM2-scFv-2 structure is buried within the crystal packing interface but not prominently involved in crystal packing interactions and therefore remains more disordered, similarly to the new MBP-TREM2 structure (PDB:6XDS)(Byrne et al., 2021).

Additional crystallisation difficulties can be attributed to the low solubility of each component and heterogeneity caused by shifting equilibrium between scFvs monomer and dimer. Consequently, the most surprising finding was the ease of TREM2 and scFv-4 complex crystallisation and resulting high-resolution dataset. ScFv-4 displayed high structural heterogeneity when analysed previously by SEC, which was only expected to increase further after the addition of TREM2. Since the complex produced highly diffracting crystals, it is possible that antigen binding improved homogeneity as indicated by early experiments with TREM2 protein produced in *Sf9*

cells. Further studies of the crystallised complex by SEC-MALS may reveal whether this was the case.

Both antibodies bind TREM2 epitope positioned on the other side of putative ligand-binding TREM2 CDR loops. **Figure 5.15** demonstrates the detailed mapping of residues in TREM2 epitope observed by generated X-ray structural models, which can explain the loss of affinity observed in the previous chapter when murine TREM2 is used. In the case of both epitopes, the mouse TREM2 sequence differs at two positions involved in CDR engagement shown in pink.



Figure 5.15. Detailed analysis of human and mouse TREM2 epitope. *(a) Comparison of human and mouse TREM2 amino acid sequences with residues comprising the epitope shown in purple and pink and residue number is shown. The residues absent in mouse TREM2 are shown in pink. Hydrophobic patch residues are shown in yellow while AD mutant locations are in green. The number of scFv-2 CDR involved in each interaction is shown in green. (b) The*

same analysis was performed for scFv-4 binding. The number of scFv-4 CDR involved in each interaction is shown in orange.

Despite their similar epitopes, the structures of scFv-2 and scFv-4 bound to TREM2 are surprisingly distinctive due to differences in binding of the TREM2 C-C' loop (**Figure 5.15**). Interestingly, the interaction of scFv-4 with C-C' is mediated by CDR-L2 loop, which was not used to create variability in SciLifeLab library. This C-C' loop is surrounded by Arg62 and Arg47 as well as residues comprising the hydrophobic patch shown to be involved in APOE binding (Kober et al., 2020) (**Figure 5.15**). There is no obvious conformational change in this region upon scFv-4 binding (RMSD=0.72 Å compared to 5UD7), but the inherent flexibility of these loops makes any prediction regarding the impact on TREM2 functions difficult. Cell biology experiments may be necessary to reveal any potential changes in ligand binding in the presence of scFv-4.

All the antibodies were confirmed to occupy a similar epitope on TREM2 structure. Such an overlap for three independent antibody fragments is a striking coincidence. A most likely explanation is a particular biochemical predisposition of that site to form interactions with tyrosine and serine residues enriched in paratopes in the phage library. Additionally, due to documented interaction of TREM2 with lipids and lipoproteins and the hydrophobic nature of TREM2 CDR1-3, the possibility that *Sf*9-produced TREM2 was bound to a ligand, blocking access to the other surfaces of TREM2, cannot be excluded. In support of this, I have previously found ApoA1 in TREM2 pull-down samples from insect cell-conditioned medium (**3.5.4**).

Since this project aimed to map the relationship between TREM2 epitopes and their function, it was a surprise to discover that all scFv fragments engaged the same epitope on the TREM2 surface. The modest number of selected scFvs impacted the

variability of the selected epitopes. Still, the resulting structures of scFv-2 and scFv-4 bound to a similar epitope are surprisingly different and, together with different affinity to TREM2 may lead to functional changes. In summary, we described the first well-defined TREM2 epitopes located outside of the stalk region in TREM2, qualifying them as reliable reagents independently of their possible functional properties which will be investigated in the next chapter.

Chapter 6

Functional impact of scFvs and mAb antibodies on cells expressing TREM2 and DAP12

Parts of this chapter are based on the publication: *Selection and structural characterization of anti-TREM2 scFvs that reduce levels of shed ectodomain*, Structure, 2021, https://doi.org/10.1016/j.str.2021.06.010. Permission to publish relevant figures was obtained under conditions described in the Creative Commons CC-BY licence.

6.1 Introduction

The importance of TREM2 in neurodegeneration was demonstrated by the impact of TREM2 on AD progression in early animal studies and the recent discovery that TREM2 expression is necessary in the transition of microglial cells into potentially neuroprotective disease-associated microglia (DAM) (Keren-Shaul et al., 2017) (Jay et al., 2015; Jonsson et al., 2013; Leyns et al., 2017; Wang et al., 2016). However, the need to investigate TREM2 function at various stages of the disease with pharmacological probes became imperative after inconclusive results of the animal

studies. Thus, after the successful development of scFvs and epitope identification in the previous chapters, we investigated whether generated molecules have an impact on TREM2 functions, such as receptor shedding and agonism. Additionally, due to the proven role of dimerisation and clustering in receptor internalisation and activation, our Eisai collaborators generated stable mAb and Fab conversions based on the CDR sequences towards the end of my project, so their initial functional properties were also evaluated.

Numerous TREM2 ligands, including apolipoproteins, lipids, bacterial cells, apoptotic cells exposing phosphatidylserine (PS) and Aβ oligomers, were shown to interact and in some cases activate TREM2 signalling. However, studies of TREM2 interaction with lipoproteins, including lipidated-APOE, often led to conflicting results (Atagi et al., 2015; Bailey et al., 2015; Kober et al., 2021; Yeh et al., 2016). Our laboratory's attempts to activate TREM2 signalling in iPSC-derived macrophages (iMacs) with liposomes containing phosphatidylserine (DOPS, 1,2-dioleoyl-sn-glycero-3-phospho-L-serine) and Aβ oligomers did not replicate some of the positive results reported in the literature and by our collaborators (Juliane Obst, Peter George-Hyslopp, proprietary data)(Cosker et al., 2021; Nugent et al., 2019; Sudom et al., 2018; Zhao et al., 2018). A significant amount of data on TREM2 agonists was generated using HEK293 cells heterogeneously expressing TREM2 and DAP12, often requiring extensive incubation times to elicit signalling. The interdependency between shedding, activation and receptor internalisation has not been fully analysed. Specifically, the interdependency of shedding with the initiation of positive TREM2 signalling was of particular interest following the discovery of H157Y variants, and the inhibition of shedding could result in a modulated signalling cascade. Previously, the research relied heavily on the use of human monocyte-derived macrophages. The development of human iPSC technology has been a crucial milestone enabling the study of tissue-

resident macrophage lineages, such as microglia, and the modelling of human diseases (Gosselin et al., 2017; Lee et al., 2018b). Thus, the aim was to investigate TREM2 activation in more physiological cellular systems when determining the mechanism of action of functional antibodies.

The availability of TREM2 antibodies has been limited, and they are poorly validated, the latter a common issue for commercially available mAbs (Baker, 2020). Apart from the unknown epitope, commercial antibodies are often non-specific or do not recognise folded protein during immunocytochemistry experiments despite commercial claims. The majority of TREM2 antibodies were not suitable for detecting three-dimensional epitopes and did not have reproducible functional activity, with the notable exception of AF1828 (R&D systems), which was later identified as a robust TREM2 agonist (Hall-Roberts et al., 2020). Unfortunately, its polyclonal nature hampers its use as a well-characterised tool in cell biology experiments. Additionally, heavy endotoxin contamination of the commercial prep was identified, a particular problem for *in vitro* work with macrophage-like cells.

I chose to develop TREM2 scFvs and antibodies with collaborators at Eisai, Karolinska Institute and SciLifeLab, because they are useful tools in structural and cell biology and have the potential to modulate TREM2 function in several ways. First and foremost, antibodies can be agonists or antagonists of the receptors and trigger downstream signalling cascades (**Figure 6.1**). The TREM2 signalling cascade can be monitored by phosphorylation of spleen tyrosine kinase (SYK) (**Figure 6.1**) (Saunders, 2019; Varnum et al., 2017). During TREM2 activation, SYK phosphorylation leads to calcium influx and changes in gene expression pattern, which in turn results in increased phagocytosis, migration or survival (Schlepckow et al., 2020; Wang et al., 2020). Each of these functions can be monitored as a measure of TREM2 activation or inhibition.

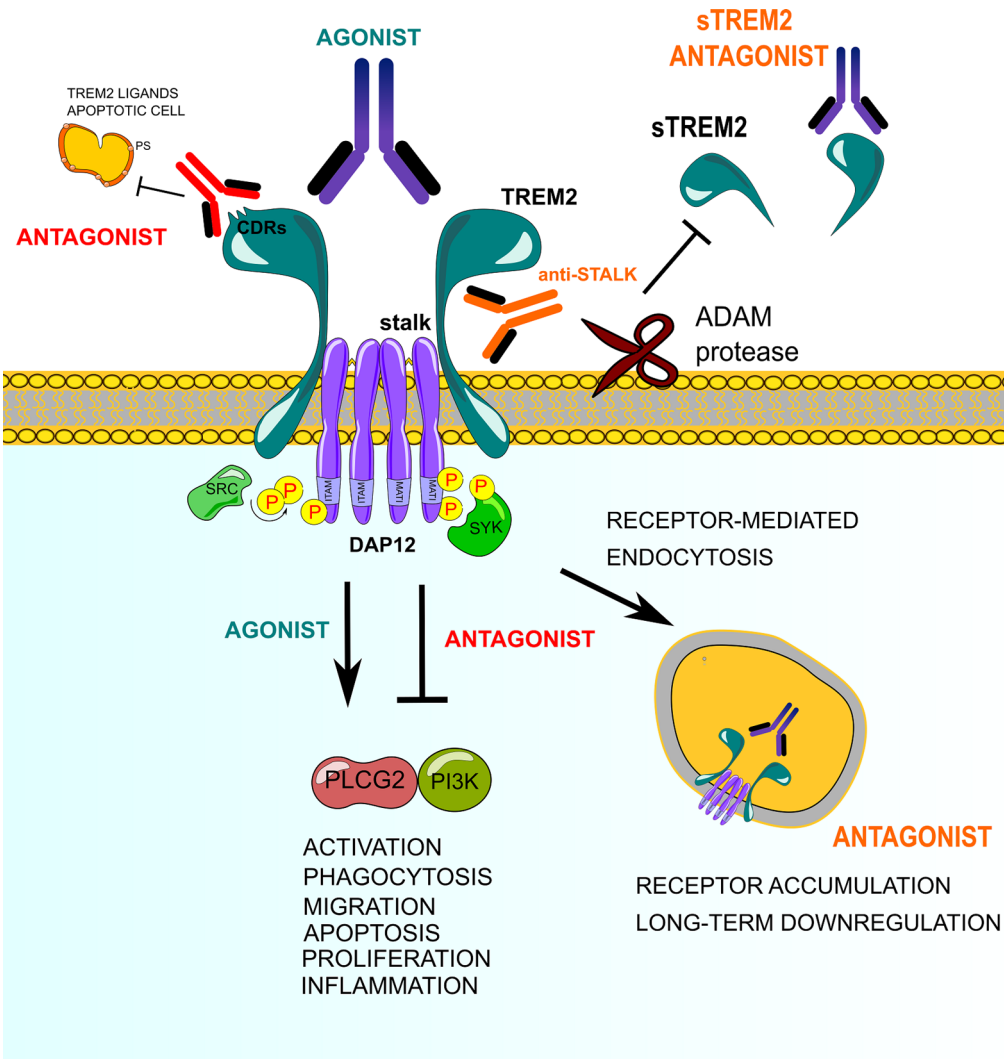


Figure 6.1. Possible outcomes of targeting TREM2 with antibodies and antibody fragments. *Monoclonal antibodies (mAb) or bivalent antibody fragments can lead to receptor dimerisation, and activation followed or simultaneous to receptor internalisation events. mAb interfering with ligand recognition or ADAM protease cleavage can result in antagonistic properties against full-length receptor or soluble TREM2.*

Since the H157Y TREM2 mutation was shown to shed TREM2 more rapidly and is associated with increased incidence of AD, targeting of the TREM2 stalk domain became an attractive target for therapeutic mAbs. Antibodies, or fragments of, may modulate the shedding of soluble TREM2 (sTREM2) from the plasma membrane by blocking ADAM protease-mediated cleavage due to masking of the cleavage point within the stalk domain of TREM2. An alternative way to modulate TREM2 shedding

is via the promotion of receptor internalisation, leading to the removal of the receptor substrate for cleavage by sheddases located in the plasma membrane. Receptor internalisation may lead to receptor degradation in lysosomes; alternatively, the receptor can be recycled back to the plasma membrane (Leyton, 2020). Both the inhibition of shedding or promotion of internalisation will lead to a decrease in the production of sTREM2, whilst having the potential for different effects on signalling. Furthermore, the alteration of sTREM2 production may have secondary effects due to the potential bioactivity of sTREM2 (Zhong et al., 2019).

This chapter describes the successful identification of scFv and mAb activity against TREM2 receptor in simple HEK293 and more physiologically relevant iMac cells. Bivalent TREM2 antibody molecules binding to Ig-domain led to a decrease in sTREM2 due to receptor internalisation in cells over-expressing TREM2 and robust P-SYK activation in iMac cells. Some of the results hinted at potentially significant changes in the way TREM2 is expressed and made available to mAb targeting on the surface of these different cell types.

6.2 Expression levels of TREM2 in THP-1, HEK-TREM2/DAP12 and iPSC-derived macrophages

I first confirmed levels of total and shed TREM2 in cell types that I planned to use for functional screening of antibody fragments and mAbs. A HEK293 cell line transfected with TREM2 and DAP12 constructs was a gift from Peter St George-Hyslop and was previously used to investigate TREM2 shedding by ADAM proteases (Thornton et al., 2017). On account of the simplicity of their maintenance, this was the first cell type with which was screened for an impact of antibodies on TREM2 shedding. Different cells likely express different levels of house-keeping genes, such as GAPDH.

Nonetheless, it was used to demonstrate a good quality transfer of protein samples to the nitrocellulose membrane. The cell line had high levels of total TREM2 and high levels of sTREM2 constitutively secreted into the medium (**Figure 6.2**, **lane 1 and 6**). In particular, glycosylated and mature forms of TREM2 are visible as smeared bands on SDS-PAGE and are considered to be properly folded receptor potentially present on the cell surface (**Figure 6.2, all lanes**). Surprisingly, immature TREM2 appears to be larger compared to other cell types (**Figure 6.2, lane 2**).

IPSC-like macrophages (iMac) express low levels of TREM2 (**Figure 6.2**, **lane 9 and 10**). iMac were obtained according to the protocol developed by Sally Cowley and were differentiated as described previously (Wilgenburg et al., 2013). iMac, just like microglia, have the signature of resident tissue macrophages, which undergo MYB-independent differentiation and therefore are more suitable for the study of microglial functions than monocyte-derived macrophages or monocytic lines such as THP-1 (Wilgenburg et al., 2013). The maintenance and differentiation of iMac cells is complex and tedious compared to a routine clonal cell line and were provided by Juliane Obst in Alzheimer's Research UK-Oxford Drug Discovery Institute (ODDI) during this project. The total cell extracts of iMac in **Figure 6.2, lanes 4, 5** show relatively low levels of TREM2 and its mature forms in fully differentiated cells. However, total TREM2 appears to be downregulated upon differentiation for 7 days. Differentiated iMac cells at day 1 and 8 also shed similar levels of TREM2 (**Figure 6.2, lanes 9, 10**). Not surprisingly, the levels are lower than the heterologous expression observed in transfected HEK293 cells and are also lower than those seen in THP-1 cells (**Figure 6.2, lanes 6, 7**). TREM2 KO iMac cell line was confirmed to not contain any TREM2 and was shown to be less viable than WT cells (**Figure 6.2, lanes 3, 8**, data not shown).

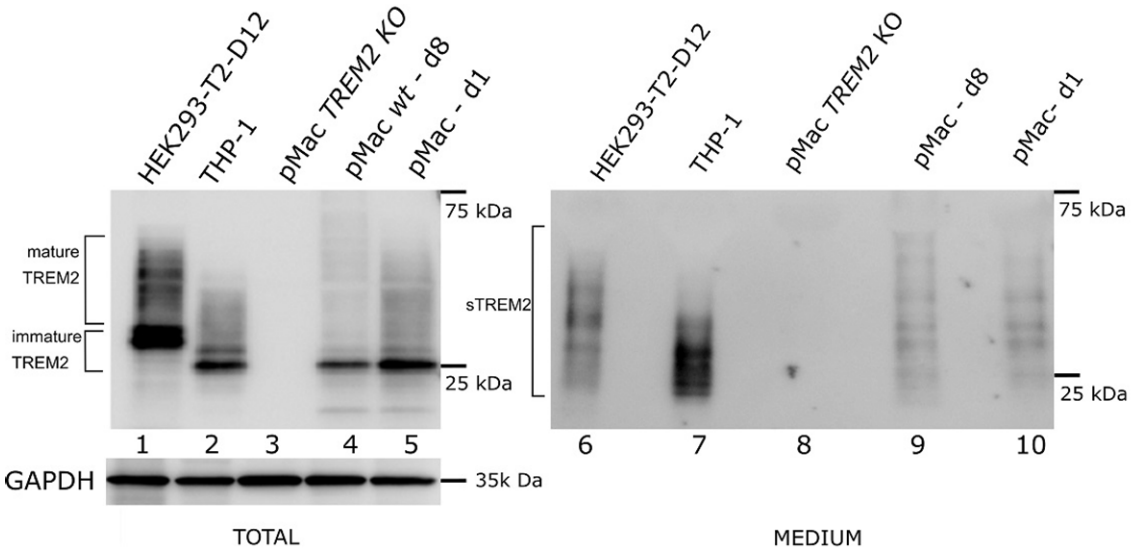


Figure 6.2. Expression levels of TREM2 in different expression systems. (*a) Western blot of total extracts of HEK293 transfected with TREM2 and DAP12 plasmid, THP-1 and iPSC cells incubated with anti-TREM2 antibody (Abcam; EPR20243). Cells were seeded at 1x10^6 cells per well. HEK293 were seeded at 0.5x10^6 day before the experiment; THP-1 cells were differentiated for 3 days in a medium containing 100 ng/mL PMA; iMac cells were differentiated for 1 or 8 days in MCSF-1 containing medium. Cells were washed with PBS, and 1 mL of medium was added for 17 hours. The next day, cells were lysed, and a medium containing sTREM2 was harvested. Loading was controlled after measuring total protein with Bradford assay. Membrane after stripping was incubated with GAPDH antibody. (b) Western blot of cell-conditioned media. The amount of media loaded was normalised to the total protein concentration measured by Bradford.*

The last cell line used during the project was THP-1, a monocyte cell line that can be differentiated to macrophages by treatment with 100 ng/mL PMA for 72 hours (Park et al., 2007). Differentiated THP-1 cells were selected to investigate shedding in another cell line than iMac expressing TREM2 natively. In these cells, total levels of TREM2 were between HEK293 and iMac levels (**Figure 6.2**, **lanes 2, 7**). Surprisingly, the amount of shed TREM2 appears to be very high in these cells with a considerably less heterogenous glycosylation pattern resulting in fewer and more intense bands. Furthermore, activation of ADAM17 by treatment with PMA during THP-1 differentiation may result in increased production of sTREM2 for some time after PMA

removal (**Figure 6.2, lane 7**) (Lorenzen et al., 2016). Deglycosylation by PNGase treatment was performed to facilitate a better comparison of sTREM2 levels but unfortunately, it did not result in full deglycosylation (data not shown).

6.3 Impact of scFvs on soluble TREM2 and internalisation

Despite other laboratories showing phosphorylation of SYK in response to stimuli in various HEK293 cell lines, we were not able to investigate agonism in these cells due to the lack of an appropriate SYK phosphorylation signal (Emma Mead, unpublished data) (Schlepckow et al., 2020; Wang et al., 2020). However, HEK293 were appropriate for investigating the impact of scFvs on sTREM2 production since ADAM protease activity generates sTREM2 in these cells (Feuerbach et al., 2017; Thornton et al., 2017). Subsequent accumulation of sTREM2 can be measured in the conditioned medium by sandwich ELISA (**Figure 6.3a**).

Poorly characterised epitopes of the commercial ELISA capture and detection antibodies required testing for epitope overlap between these antibodies and the newly developed scFvs. In the scenario where a sTREM2 epitope is masked by bound scFv, sTREM2 detection would be decreased regardless of the biological functions of scFvs (**Figure 6.3b**). Compatibility was assessed by the addition of scFvs to the conditioned medium from transfected HEK293 cells. None of the scFvs tested reduced detection of sTREM2 compared to vehicle only control (**Figure 6.3c**).

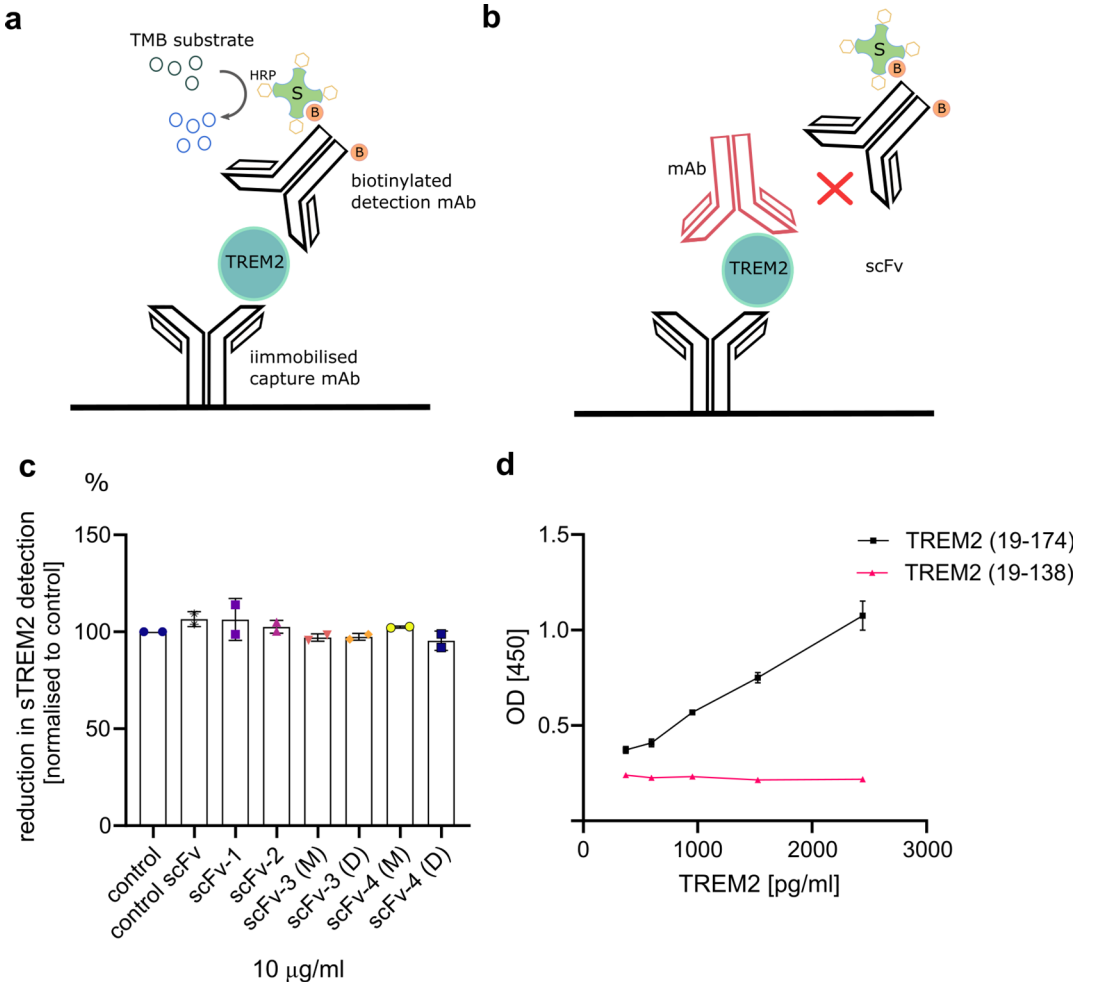


Figure 6.3. Schematic representation of sandwich ELISA and validation of approach for scFv studies. *(a) The TREM2 capture antibody (Abcam, EPR20243) is immobilised on a plate and after blocking, conditioned medium containing sTREM2 is incubated in the plate followed by washing and incubation with biotinylated detection antibody (bio-techne, BAF1282). Streptavidin (S) conjugated enzyme horseradish peroxidase (HRP) catalyses oxidation reaction of 3,3',5,5'-tetramethylbenzidine (TMB) into the blue coloured product which after quenching can be measured at 450 nm. (b) The hypothetical scenario of sandwich ELISA assay performed where antibodies (mAb) or scFvs remain bound to sTREM2 after the treatment and mask epitopes resulting in steric hindrance. (c) Conditioned medium was harvested after 5 hours and scFvs were added at 10 µg/mL before the ELISA assay to exclude epitope masking. Results were normalised to control/vehicle signal and shown as a percentage of control. Bars represent mean with SD (n=2), individual values are shown. (d) Two types of TREM2 proteins (purified in Sf9) of various lengths were used to assess potential to bind both meprin β (cleavage after Arg136) and ADAM10 (cleavage after Ser156) cleavage products. Detection of TREM2 was analysed by comparing signal measured by absorbance at 450 nm and comparing both curves*

obtained from a serial dilution of the analyte. Represented as mean values with SD (n=1, 3 technical repeats).

The characterisation of the captured sTREM2 revealed that the stalk sequence downstream of Ala138 is required for the sTREM2 detection by EPR20243. Recently, another metalloprotease, meprin β, with a cleavage site between Arg136 and Asp137 located upstream of the ADAM cleavage site (His157), has been implicated in TREM2 shedding (Berner et al., 2020). To characterise the exact type of product detected by the commercial ELISA antibodies, I tested two purified TREM2 proteins with varying deletions of stalk sequence. In contrast to the construct containing full stalk sequence TREM2 (a.a.19-174), ELISA antibodies did not capture the shorter protein, TREM2 (a.a.19-138) (**Figure 6.3d**). Later my colleagues confirmed that EPR20243 requires stalk sequence for TREM2 binding by BLI (Emma Murphy, unpublished data). In conclusion, sTREM2 captured in the assay was identified as the longer ADAM cleavage product.

6.3.1 Reduction of sTREM2 accumulation in HEK293 conditioned medium by scFv-3 and scFv-4

To test the impact on sTREM2 production, HEK-TREM2/DAP12 were treated with single doses of the unseparated, total, preparations of scFvs at 10 µg/mL for 5 hours. Batimastat, a broad specificity metalloprotease inhibitor, was used as a positive control. ScFv-3 and scFv-4 reduced sTREM2 accumulation in HEK293 conditioned medium. Previous optimisation experiments had shown that treatment for 5, 17 or 20 hours resulted in a similar quality of data with the exception of the 20-hour time-point, where variation increased due to signal saturation (**Figure 6.4a-c**). The 5-hour time point was used due to improved normalisation to the cell number by confocal

microscopy and sufficient concentrations of accumulated sTREM2 in the conditioned medium. The 10 µg/mL dose of scFvs exhibited less variation across different time points. In these conditions, scFv-3 and scFv-4 reduced sTREM2 accumulation by approximately 15 and 40%, while scFv-1 and scFv-2 did not show a significant impact (**Figure 6.4**).

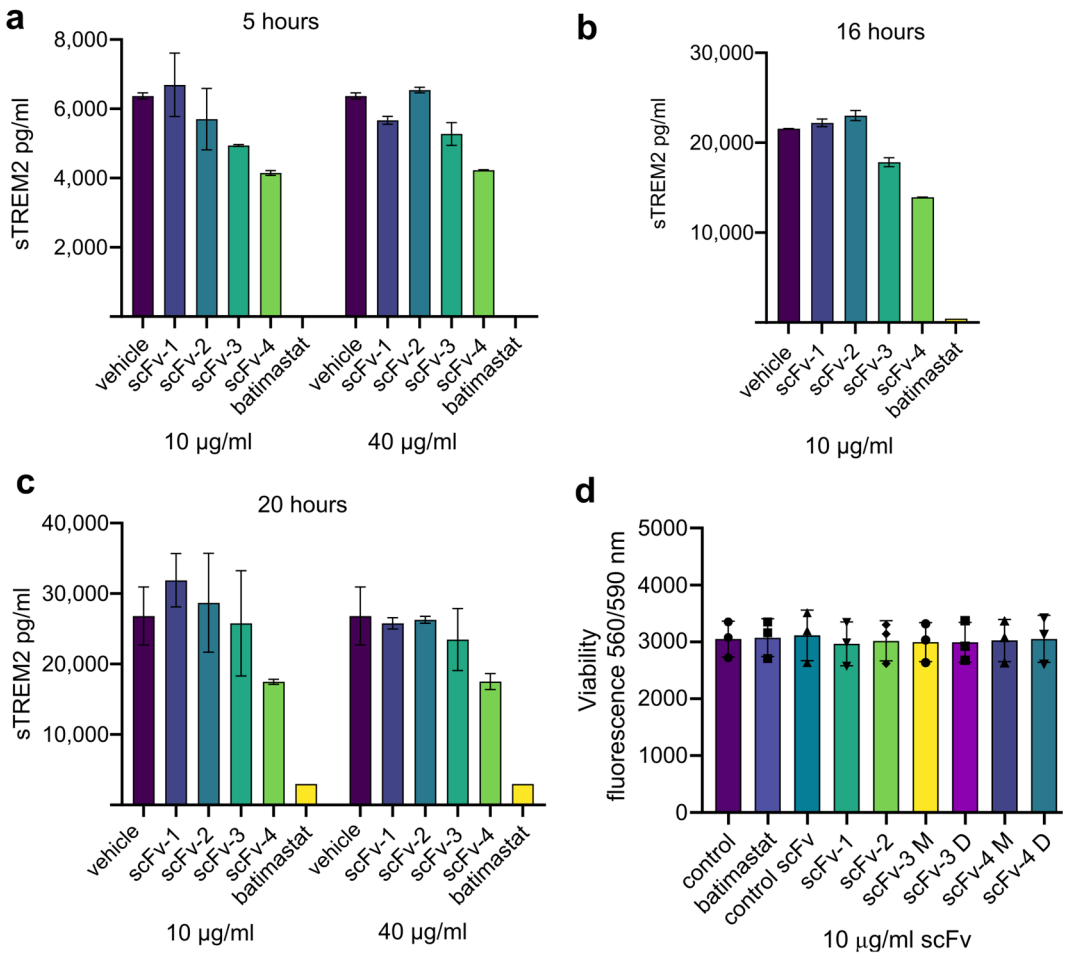


Figure 6.4. Optimisation of shedding assay for scFv treatment. *HEK cells were incubated in presence of 10 or 40 µg/mL of scFv for 5 (a), 16 (b) or 20 (c) hours. 10 µg/mL corresponds to approximately 380 nM scFvs concentration. Data represent mean of three technical repeats ± SD (n=1). (d) Impact of various scFv preparations on HEK293 cell viability. After 5 hour treatment with 10 µg/mL scFv, cell viability was measured after incubation for 1 hour with*

Presto Blue HS reagent and recording of fluorescence at 560/590 nm (excitation/emission). Data represent mean ± SD (n=3).

The initial screening in HEK293 was performed before SEC profiles and oligomerisation states were validated for scFvs. The SciLifeLab library produces scFvs separated by a 15-amino acid-long linker, which according to theoretical predictions, should produce monomers (Kortt et al., 2001). A monomeric scFv with TREM2 shedding-blocking properties was an exciting prospect as it would be predicted to have a low propensity to cause internalisation.

Change in sTREM2 levels, however, was found to be dependent on the bivalent nature of scFvs. Upon successful improvement of scFv purification and SEC-MALS validation, the presence of dimer fractions in preparations of scFv-3 and scFv-4 was detected (**4.4.2**). Impact on viability was recorded and used for data normalisation in each experiment (**Figure 6.4d**). ScFv-2, which binds TREM2 with high affinity but contains a low concentration of a dimer, showed no effect on sTREM2 accumulation (**Figure 6.5a**). On the other hand, the low affinity of scFv-1 could explain the lack of impact despite the considerable dimer presence (**Figure 6.5a**). Thus, I investigated whether dimeric fractions abundant in scFv-3 and scFv-4 were responsible for the observed effect. The separation of oligomers was challenging due to the non-covalent interaction within dimers. Strikingly, re-equilibrium occurred as early as one week after storage and thawing from -80 ℃ and occasionally even before freezing. A sequential double SEC was employed to separate the oligomers and remove any potential open conformations, slowing down the equilibration rate (Arndt et al., 1998).

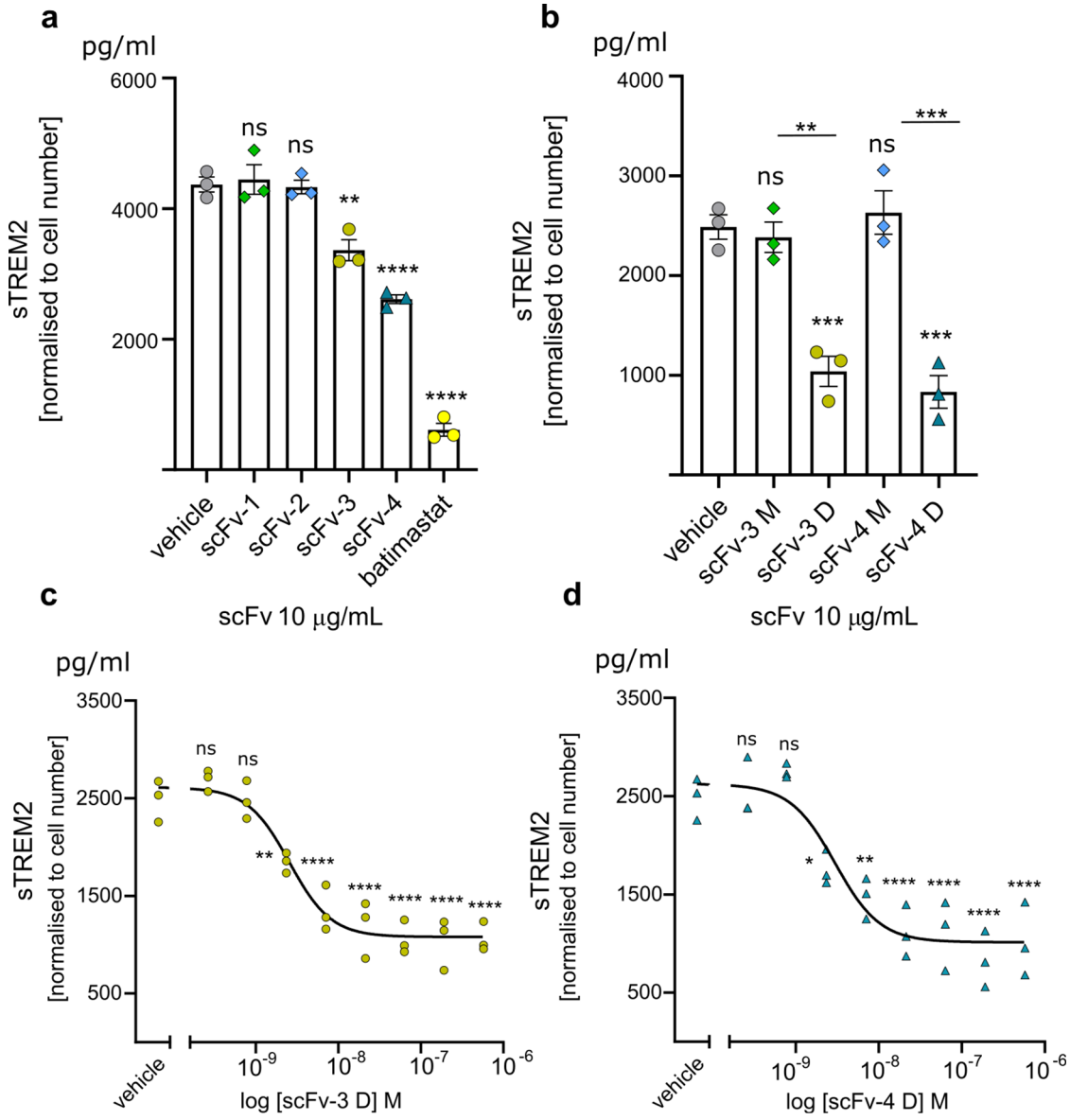


Figure 6.5. ScFv-3 and scFv-4 dimers reduce TREM2 shedding in HEK293 cells overexpressing TREM2 and DAP12. *HEK293-TREM2/DAP12 cells were treated with scFvs at 10 µg/mL (380 nM) for 5 hours or with 20 µM batimastat or vehicle samples as controls. Data represent the mean ± SEM. One-way ANOVA, Dunnett's post hoc test multiple comparisons to vehicle only was carried out with significant P values scFv-3 vs control=0.0011, scFv-4 vs control <0.0001, batimastat vs control < 0.0001. (b) Results of shedding assay described above for separated scFv monomers (M) or dimers (D). 10 µg/mL corresponds to approximately 384 nM of monomer and 192 nM dimer. Individual data points are shown as ± SEM. One-way ANOVA, Tukey's post hoc test comparison with significant P values scFv-3 (D) vs control = 0.0007, scFv-4 (D) vs control = 0.0002, scFv-3 M vs D = 0.0013, scFv-4 M vs D = 0.0004 sTREM2, batimastat levels were below detection threshold and are not shown. (c) ScFv-3 reduces sTREM2 accumulation conditioned medium in a concentration-*

dependent manner. Individual data points from 3 independent experiments are shown in colour with the fitted curve in black (EC50=2.5 nM). One-way ANOVA, Dunnett's post hoc comparison to buffer control, test P < 0.0001 (d) Dimer of scFv-3 reduces sTREM2 accumulation in a concentration-dependent manner. Individual data points are shown in colour with the fitted curve in black (EC50=3 nM). One-way ANOVA, Dunnett's post hoc comparison to buffer control, test P < 0.0001. Data from a-d was normalised to cell density or cell number and represent 3 biological repeats, including 3 technical repeats each.

When correctly separated, dimeric scFv-3 and scFv-4 were responsible for 58 and 66% reduction in sTREM2, respectively (**Figure 6.5b**). ScFvs decreased sTREM2 accumulation in a dose-dependent manner characterised by half-maximal effective concentration (EC50) of 2.5 nM and 3 nM (**Figure 6.5c-d**). The monomeric antibody fragments had no significant activity (**Figure 6.5b**). Furthermore, in some preparations where equilibration occurred, the increased presence of monomer correlated with a lower activity, indicating that bivalent scFvs are the active molecule in the assay (data now shown).

6.3.2 Dimers of scFv-3 and scFv-4 lead to TREM2 internalisation

Receptor dimerisation, or clustering, followed by internalisation is a well-established step in signalling through the G-protein-coupled receptors (GPCR) or tyrosine kinase receptors such as epidermal growth factor receptor (EGFR) (Gyun et al., 2007; Wang et al., 2015a). The mode of action of the antibodies, the difference between direct inhibition of sTREM2 shedding compared to receptor-mediated endocytosis, will profoundly impact the range of physiological effects mediated by the antibodies. Immediate lysosomal degradation can follow receptor agonism; however, a net antagonist rather than agonist effect may well be achieved upon chronic exposure to the antibody due to receptor down-regulation (Aldeghaither et al., 2019; Mazot et al.,

2012). Based on the previous data demonstrating a requirement for bivalency, I hypothesised that dimeric scFvs act similarly to some mAbs and lead to receptor-mediated endocytosis.

To demonstrate that scFv dimers lead to receptor internalisation, scFvs were conjugated to Alexa fluor 647 and (**Figure 6.6a**). Initially, the intracellular rather than surface signal location was confirmed by washing the cells with DMEM pH 2 to dissociate surface-bound antibodies or later by confocal reconstruction of the cell slices (**Figure 6.6a, middle panel, Figure 6.7a-b**). The acid wash did not affect signal strength, consistent with the detection of high concentrations of fluorescence signal in intracellular foci. The staining was dependent on TREM2 expression, as shown by the low signal in non-transfected HEK293 cells (**Figure 6.6a, bottom panel**).

The functional effect could only be observed with dimerised scFv because of an inability to prepare labelled monomer. Initially, monomers and dimers of scFv-3 and scFv-4 were stained separately, but a similar intracellular signal was observed for both species (data not shown). In order to characterise the biochemical composition of the sample after Alexa conjugation, size exclusion was performed before and after incubation with the dye (**Figure 6.6b**).

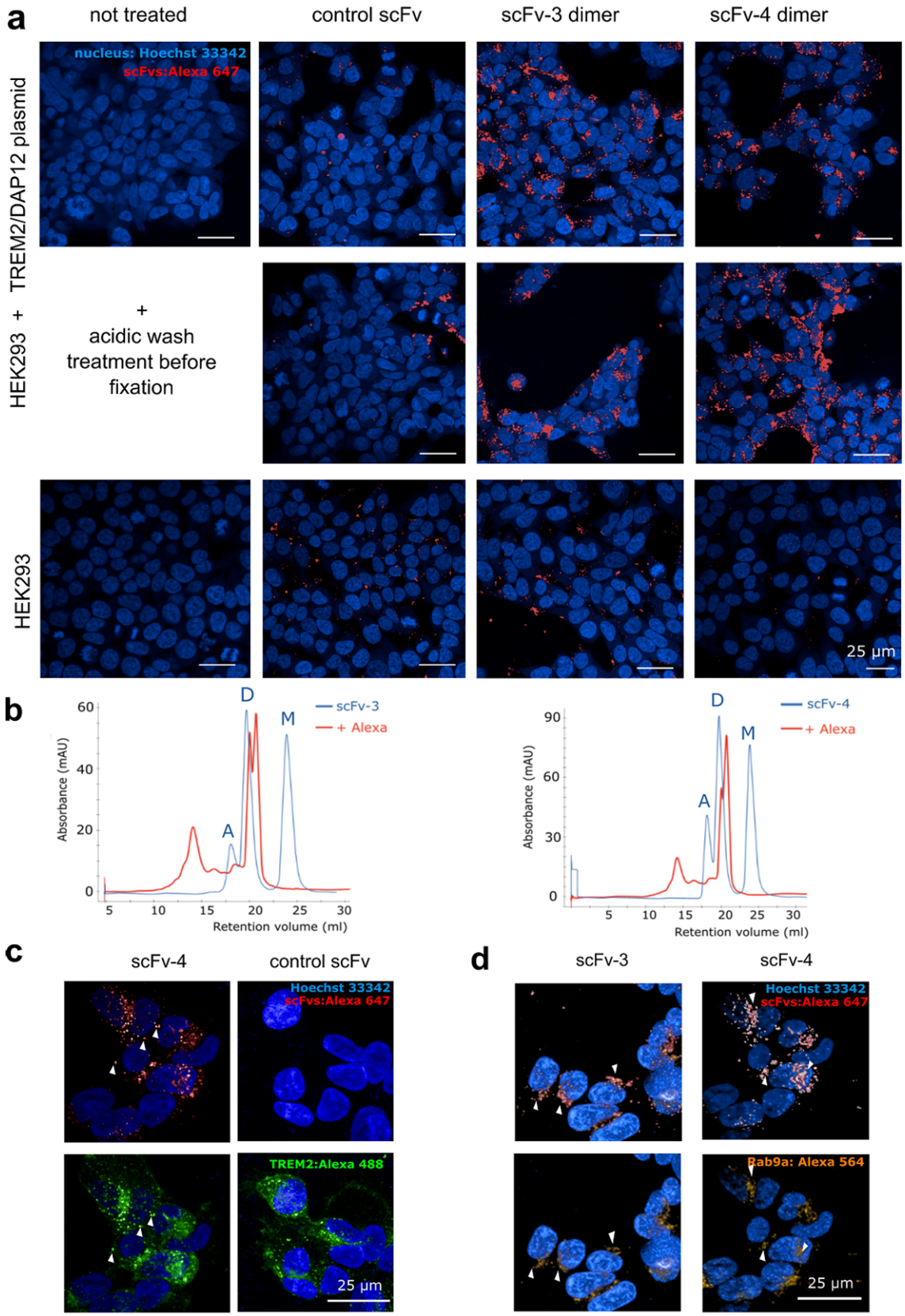


Figure 6.6. Alexa conjugated scFv-3 and scFv-4 antibody fragments lead to intracellular accumulation of TREM2-scFv complexes. *(a) Confocal images of HEK293-T2-D12 cells treated with scFv-3, scFv-4, control scFv conjugated to Alexa fluor 647 for 5 hours at 5 µg/mL.*

Middle panel corresponds to cells washed in DMEM pH 2. Naive HEK293 cells were treated to demonstrate specificity of binding of antibodies or fluorochrome. 40 x magnification, Opera Phenix. (b) A mixture of monomer and dimer of scFvs was incubated with Alexa fluor 647 o/n at 4°C. Control sample was separated on Superdex 200 10/30 without treatment (blue line). After conjugation, scFvs were separated by the same method (red line). (M) monomer, (D) dimer, (A) aggregates. (c) Cells were treated as previously with scFv conjugates and later were stained with TREM2 antibody (AF1828, green) and anti-goat secondary Alexa fluor 488 antibody (yellow). Images were obtained by maximum projection of 35 stacks (0.5 µm) and 64x magnification. (d) The same cells were stained for co-localisation with endosomal marker – rab9a. (c-d) New experiments, images were obtained as previously but maximum projection 3D reconstruction images are shown. Bar represents 25 µm.

Strikingly, the monomeric species could not be recovered after conjugation to Alexa dyes, as shown by gel filtration (**Figure 6.6b**). A retention volume shift was observed, which can reflect changes in the previously reported non-specific interactions of scFvs and superdex resin. Furthermore, a low staining efficiency was achieved for scFv-2, in contrast to scFv-3, scFv-4 and the control scFv. This result may indicate a shift of the equilibrium towards the dimeric form in the presence of Alexa fluor dye. As a result, the intended direct comparison with monovalent molecules could not be achieved.

To investigate whether scFv conjugates dissociated from TREM2 receptors in endocytic pathways, co-localisation of TREM2 and scFvs was tested. Staining with anti-TREM2 AF1828 showed good overlap with the Alexa-fluor 647 signal (**Figure 6.6c**). After confirming the presence of TREM2-scFv complexes, localisation in the endocytic/exocytic pathway was investigated. Co-staining with anti-Rab9a, a late endosome marker revealed partial co-localisation with scFvs with reduction in signal resolution (**Figure 6.6d**) (Wandinger-Ness and Zerial, 2014). This was consistent with TREM2 recycling in retromer-dependent fashion involving Rab9a (Yin et al., 2016).

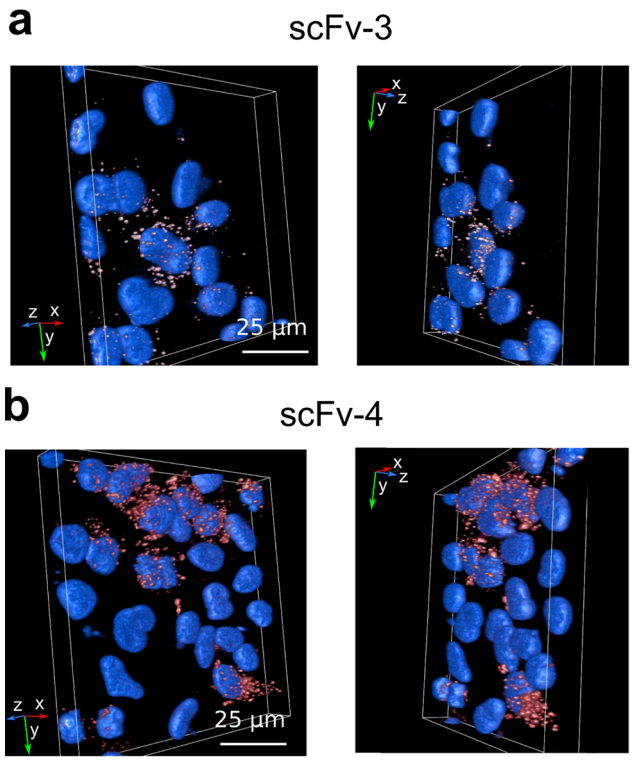


Figure 6.7. Intracellular localisation of scFv-3 and scFv-4. *Cells were treated for 5 hours with scFv-3 (a) and scFv-4 (b). ScFv-3 and scFv-4 is pseudo coloured in white and red depending on intensity. Confocal reconstruction of 3D images obtained from 35 stacks (0.5 µm) and 64x magnification. Second panel is obtained by rotating image by approx. 90º, xyz axis is shown to demonstrate the position.*

Inhibition of endocytosis results in a decrease in intracellular localisation. Accumulation of scFv-3 and scFv-4 conjugates was abolished when endocytosis was inhibited with a chemical dynamin inhibitor– dynasore providing further evidence that the internalisation evoked by scFv-3 and -4 is an endocytic process (**Figure 6.8a**). A time-course experiment showed a gradual accumulation of the fluorescent signal over time, implying that TREM2 can be retained in the endocytic pathway together with scFvs (**Figure 6.8b**). A lack of complete TREM2 recycling is consistent with the observed reduction in levels of sTREM2 through removal of the TREM2 in the plasma membrane.

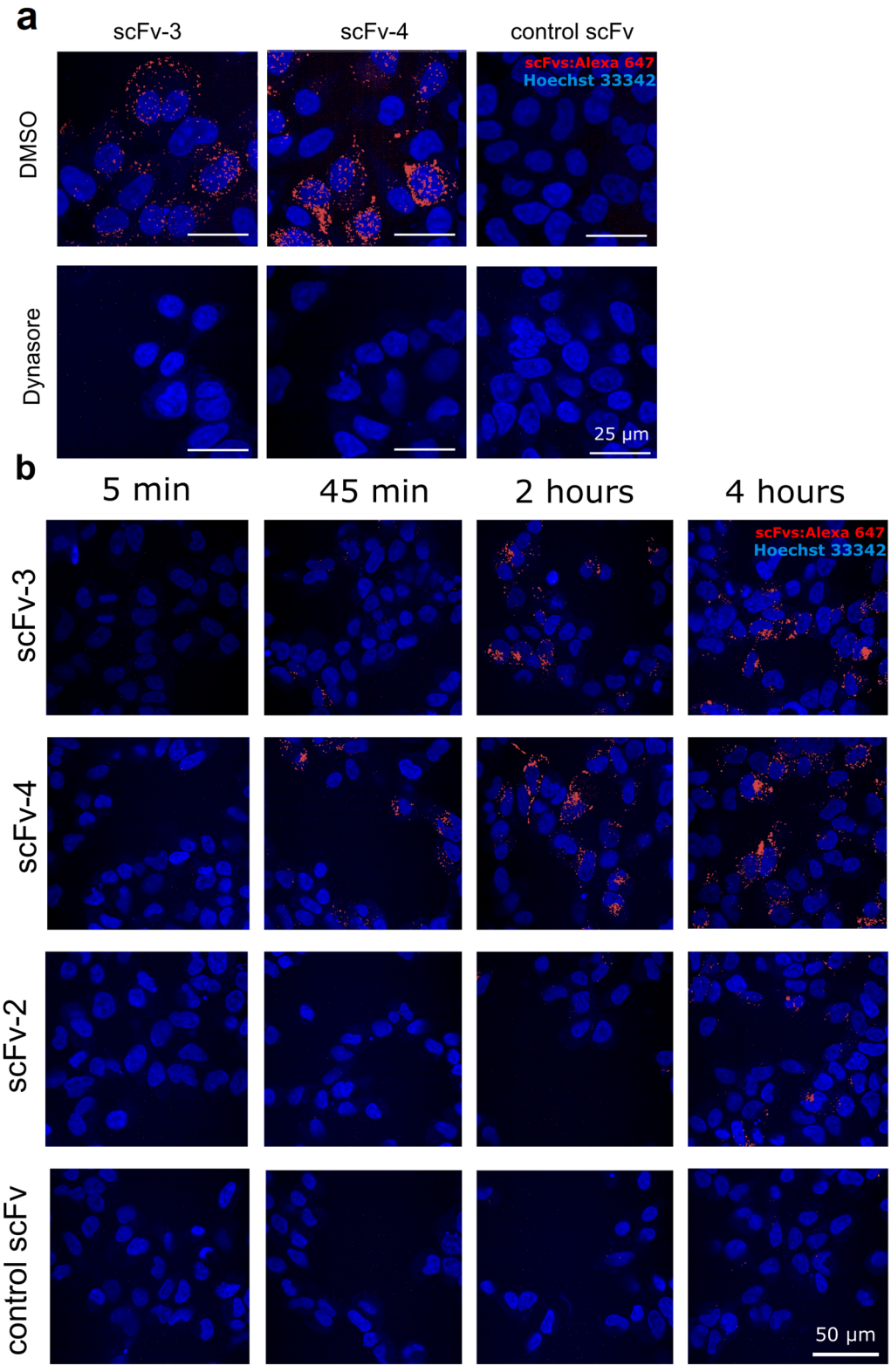


Figure 6.8 Dynasore treatment and Time-dependent accumulation of scFv-3 and scFv-4 dimers in HEK cells over-expressing TREM2 and DAP12. *(a) Cells were pre-treated with 80 µM dynasore or DMSO in minimal medium and then treated by scFv-Alexa conjugates in presence or absence of dynasore. Maximum projection of 30 different stacks, 64 x magnification. (b) Cells were treated with 5 µg/mL of conjugated antibodies for specified times*

and fixed with 4% PFA. Nucleus was stained with Hoechst 33342 and imaged were obtained by Opera Phenix, single plain confocal microscopy by 40x water objective. Bar represent 25 µm

To further test the hypothesis that scFvs cause TREM2 internalisation, cell surface TREM2 was measured. I have optimised an assay previously described for capturing surface receptor levels (Thompson and Kanamarlapudi, 2015). Non-permeabilised gently fixed cells are blocked and incubated with the detection antibody (R&D, BAF1828) followed by standard HRP-Strep and TMB ELISA detection and OD measurement. As expected for internalisation, after 4-hour treatment with scFvs, dimers were observed to decrease surface TREM2, while batimastat increased it (**Figure 6.9**). However, due to a low number of biological replicates, this preliminary data requires further experiments and provides only supporting evidence that dimeric binders cause internalisation of TREM2.

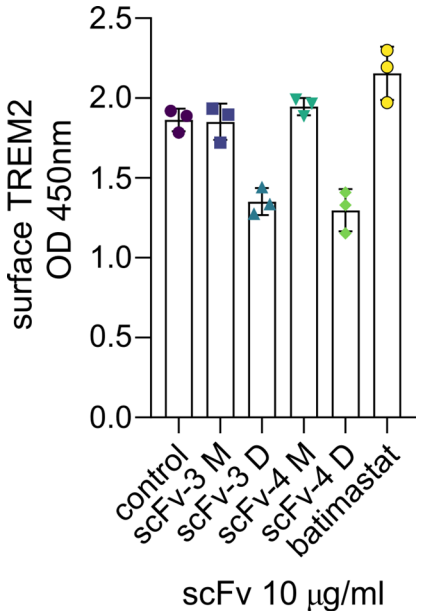


Figure 6.9. Treatment with scFvs dimers reduce surface TREM2 levels. *Fixed, non-permeabilised cells were blocked and incubated with AF1828 antibody conjugated to biotin. HRP-streptavidin was used to amplify the signal and measure absorbance at 450 nm after addition of TMB substrate and quenching. Data represent individual data point of 3 technical repeats ±SD (n=1).*

6.4 ScFv dimers are modest agonists of TREM2 in iPSC-macrophages

Since scFvs were shown to be functional against TREM2 in HEK293, a similar functional properties were investigated in more physiologically relevant cell systems such as iMac and differentiated THP-1 cells. TREM2 activation and signalling are commonly measured by monitoring phosphorylation of SYK at tyrosine 525/526 (referred here as P-SYK). A recently developed HTRF (Homogeneous Time-Resolved Fluorescence, Cis-Bio) assay allows for high-throughput detection of high and low P-SYK signals.

Dimers of scFv-3 and scFv-4 led to a modest increase in SYK phosphorylation in iMac cells (**Figure 6.10a**). Similarly to effects on sTREM2 accumulation, I detected activation only with dimeric scFv molecules but not the monomeric molecules including scFv-2 (**Figure 6.10b**). A decrease in P-Syk signal was observed when dimeric scFv preparations contained monomer (panel b) compared to mostly dimeric preparation (panel a) due to changes in dimer composition (**Figure 6.10a,b**). **Figure 4.7a-b** demonstrates difference in monomer and dimer composition analysed by SEC for treatment **6.10a** and **6.10b**. The changes in monomer-dimer equilibrium and iPSC technical aspects meant that statistical analysis could not be performed. The P-SYK levels induced by scFvs were shown to be TREM2 specific as the phosphorylation signal was absent in TREM2 knock-out iMac cells and reached a maximum at 5-10 minutes post-stimulation (n=1) (**Figure 6.10a,c**). The resulting activation was modest compared to that evoked by the commercial agonist polyclonal antibody (AF1828, R&D Systems) but had the advantage of lack of Fc-related background responses described in later section (**Figure 6.10c**).

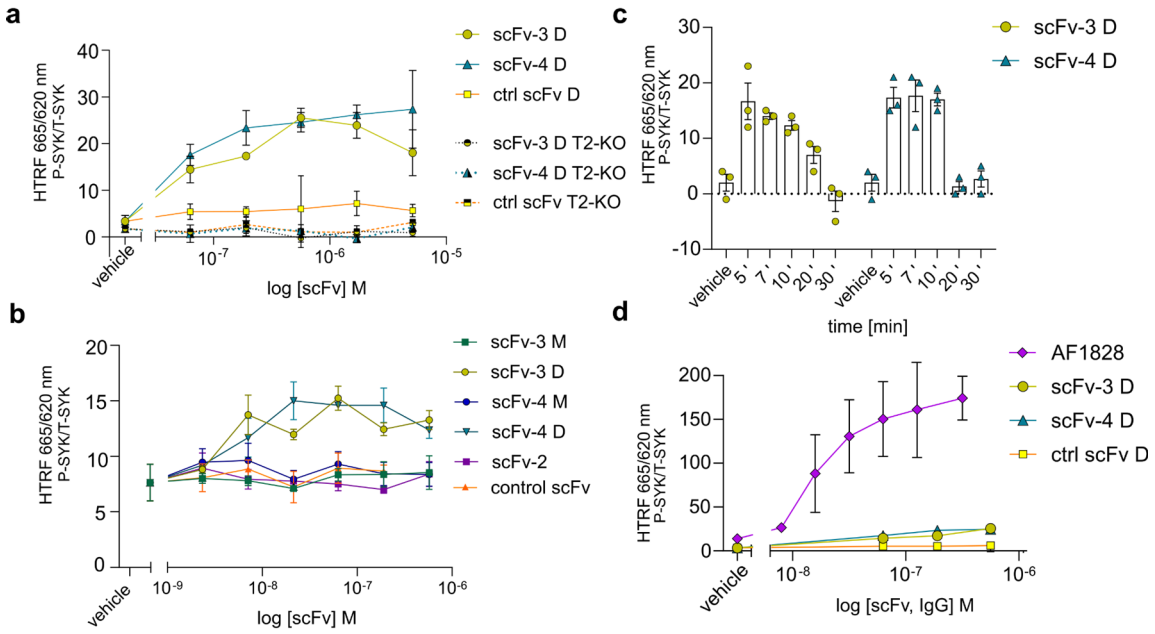


Figure 6.10. ScFv dimers are modest agonists of TREM2 in iPSC-macrophages. *(a) Parent and TREM2-KO iPSC-macrophages were stimulated with increasing concentrations of scFv dimers for 5 min. Phosphorylation of SYK was measured by P-SYK HTRF (CisBio) emission of 665 nm to 620 nm multiplied by 10^3. P-SYK HTRF was normalised to signal for total SYK (T-SYK) measured for all of the HTRF experiments. Data represent the mean of three technical repeats ± SD (n=1). (b) The same experiments as in panel a performed on different scFvs preparations. The oligomeric state was controlled at the time of the assay by SEC: scFvs monomers (M) were confirmed to contain monomer only, whereas dimers (D) contained a 1:1 mixture of both species. Data represent the mean of three technical repeats ± SD (n=1). (c) iMac cells were stimulated by scFv dimers for different time lengths. Data represent the mean of three technical repeats ± SD (n=1). (d) concentration-response experiment of commercial polyclonal antibody AF1828 used as a control in the majority of the experiments. Data represent the mean of three technical repeats ± SD (n=3) and is presented together with low doses from the experiment (a) for comparison due to MW difference and resulting molarity.*

6.4.1 ScFvs do not cause lasting TREM2 internalisation in iMac cells

To investigate whether agonism in iMac cells is related to internalisation, sTREM2 levels were measured by ELISA. The differences in expression levels of TREM2 and DAP12 between these cell lines can have potentially significant effects on receptor

recycling and antibody properties (**Figure 6.2**). Results of shedding assays in human iMac were characterised by increased variation in sTREM2 detected and higher background in iMac TREM2 KO cells (**Figure 6.11a**). The increased variability of iMac cells have previously been reported by others (Schapansky et al., 2021). Because iMac shed less sTREM2, extended scFv treatment times were tested first (**Figure 6.2**,

Figure 6.11a). The preliminary data (n=1) suggested a modest decrease in sTREM2 after treatment with unseparated scFv-3 and scFv-4 for 17 hours (**Figure 6.11a**).

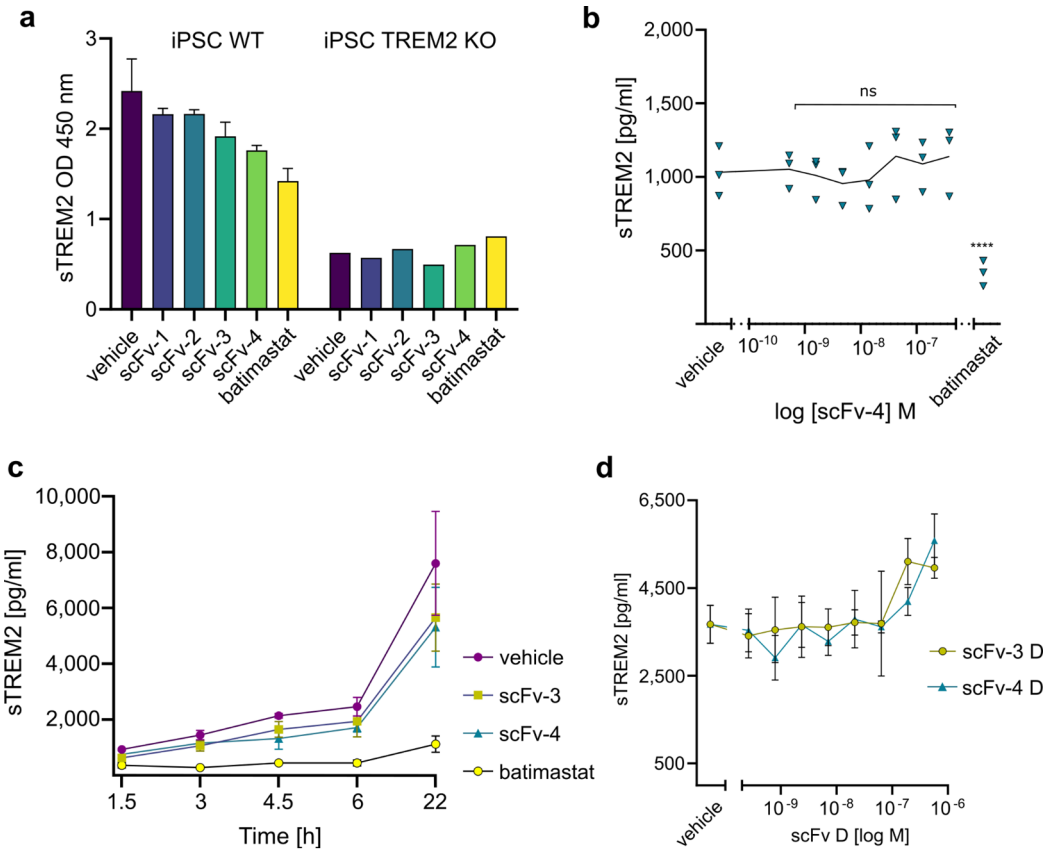


Figure 6.11. ScFvs have no impact on sTREM2 accumulation in iPSC-derived macrophages. *Preliminary results of sTREM2 ELISA in iMac and iMac TREM2 KO cells. iMac cells were treated with 10 µg/mL of unpurified scFvs for 17 hours and conditioned medium was assayed after dilution. Data represent mean ± SD for 3 technical repeats (n=1). (b) Dose response experiment of iMac cells treated for 5 hours with increasing doses of non-separated scFv-4. Individual data points are shown with a mean for 3 technical repeats (n=3). One-way ANOVA, Dunnett's post hoc comparison to buffer control was non-significant except for batimastat (P < 0.0001). (c) sTREM2 ELISA results of the time-response experiment for scFv-3 and scFv-4 (monomer and dimer mixture). Data represents mean ± SD for 3 technical replicates (n=1). (c)*

Results of sTREM2 ELISA dose-response experiment for scFv after LPS removal after 5-hour treatment. iMac macrophages were treated with increasing concentrations of dimers of scFv-3 and scFv-4. Data represent mean ± SD for 3 technical replicates (n=1). (d) Dose-response experiment of iMac cells treated for 16 hours with increasing doses of LPS-free scFv-3 and scFv-4 dimers. Data represent mean ± SD for 3 technical replicates (n=1).

However, the subsequent dose-response experiments for scFv-4 did not reveal any reduction in sTREM2 when cells were treated for 5 hours (n=3) (**Figure 6.11b**). A single time-course experiment was performed to validate whether the previously observed reduction could be detected only after long incubation times and revealed a similar reduction across all the time-points tested (**Figure 6.11c**). Since the reduction in scFv-3 and scFv-4 dimer activity in the presence of monomer was observed, new dimer preparations were made and assessed preliminarily (n=1). Because endotoxin contamination was shown to increase sTREM2 concentration in iMac cells, the scFvs were purified of endotoxin by EndoTrapHD column. Dimers prepared in this way did not reduce sTREM2 accumulation; in contrast, an increase was detected at doses above 10 µg/mL after 17 hours (**Figure 6.11d**). Due to a low number of biological replicates in the latter experiment and a lack of similar increase in previous treatments (Figure 6.11a-c), this data needs to be interpreted cautiously. In summary, the sTREM2 reduction in iMac cells could not be detected under these experimental conditions.

6.4.2 ScFvs potentially induce sTREM2 accumulation and SYK phosphorylation in differentiated THP-1 cells

A strong relationship between internalisation and activation of receptors is considered an integral part of signalling cascades (Gyun et al., 2007; Wang et al., 2015a). However, despite the activation of SYK cascade in iMac, scFvs did not cause changes in sTREM2 production or internalisation in these cells. Unlike in HEK293

cells, my data indicated that TREM2 did not accumulate intracellularly. I speculated that internalisation may be occurring in iMac cells but that low levels of cell surface levels of TREM2 or rapid receptor recycling rates led to minimal changes in rates of sTREM2 shedding, at the time points tested (Schapansky et al., 2021; Steinman et al., 1983).

The primary concern, however, is that the differences between HEK293 and iMac cells are related to strikingly different physiology and/or expression levels of TREM2-DAP12 and effects of scFvs will be abrogated. Since THP-1 cells express TREM2 natively, as demonstrated by Western blot, I investigated whether internalisation can be observed in these cells upon differentiation to macrophages (Lee et al., 2018b; Tedesco et al., 2018). Preliminary dose-response experiments with separated dimers showed strikingly similar effects to those observed previously in HEK-TREM2/DAP12 cells, with sTREM2 accumulation inhibited by a maximum of 56% for scFv-3 dimer (**Figure 6.12a**). The calculated EC50 was comparable to HEK293 cells and reached 2 nM for scFv-3, although more biological repeats are necessary to validate the significance of this analysis. Considerably higher amounts of sTREM2 and, therefore, potentially more surface-expressed TREM2 in THP-1 and HEK293 might explain the very similar functional impact of scFvs on these cells (**Figure 6.2**).

ScFv-3 and scFv-4 also stimulated the SYK activation cascade in THP-1 cells in a single preliminary experiment. Phosphorylation of SYK was higher in THP-1 than in iMac cells and also detected in scFv-3 and scFv-4 monomer containing samples due to increased storage and equilibration (**Figure 6.12b**). No activation was detected with scFv-2, which has a low propensity to form dimers or scFv-1 or control scFvs (**Figure 6.12b**). These results allowed me to support previous results, which suggested that scFv

molecules are active against natively expressed TREM2 and perform further experiments in iMac cells.

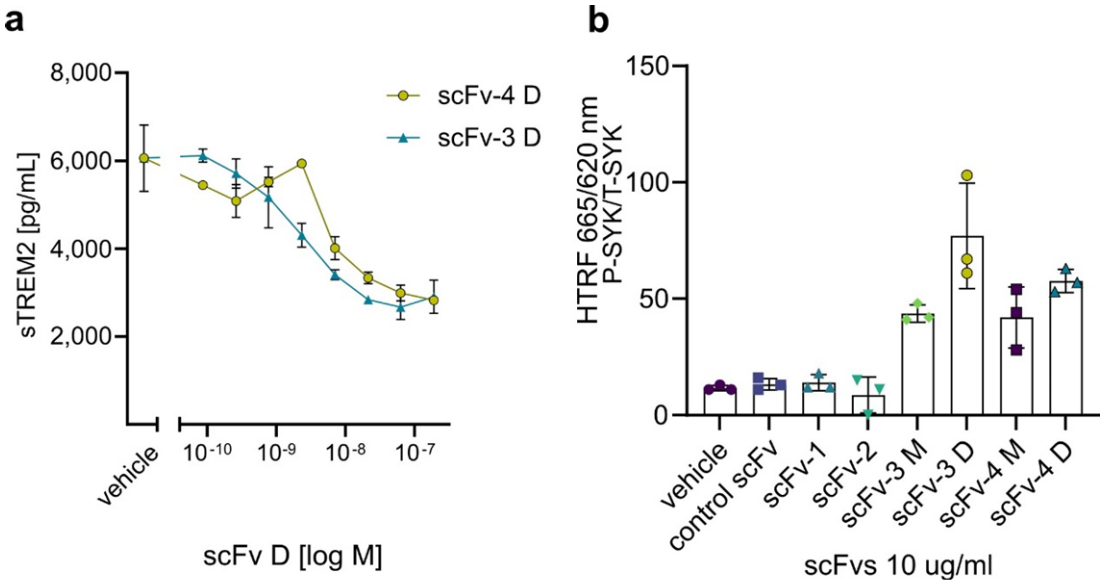


Figure 6.12. Dimeric scFv-3 and scFv-4 antibodies lead to phosphorylation of Syk in THP-1 cells. *(a) THP-1 cells differentiated to macrophages with 100 ng/uL PMA for 72 hours were treated with scFvs for 5 hours and sTREM2 from conditioned medium was measured by sTREM2 ELISA. Data represents mean ± SD for 3 technical replicates (n=1). (b) Activation measured by P-SYK/T-SYK HTRF in differentiated THP-1 cells treated with scFvs at 10 µg/mL (~380 nM for scFv monomeric molecule). Data represents mean ± SD for 3 technical replicates (n=1).*

6.5 Activity of monoclonal antibody conversions in iMac cells

Next, we asked whether higher agonism in iMac can be increased by stable bivalent IgG1 conversions. Furthermore, stable conversions were necessary to obtain better quality biological replicates necessary to estimate significance of our findings. For this purpose, I used previously introduced Fab and IgG1 conversions, LPS-free and conformationally stable monovalent and bivalent versions of scFvs. Unfortunately, the IgG1 antibodies interfered with the detection of sTREM2 using the previously optimised ELISA, presumably due to their larger size and antigen crosslinking, leading

to increased epitope masking, so the effects on levels of sTREM2 production could not be tested reliably (**Figure 6.13a**).

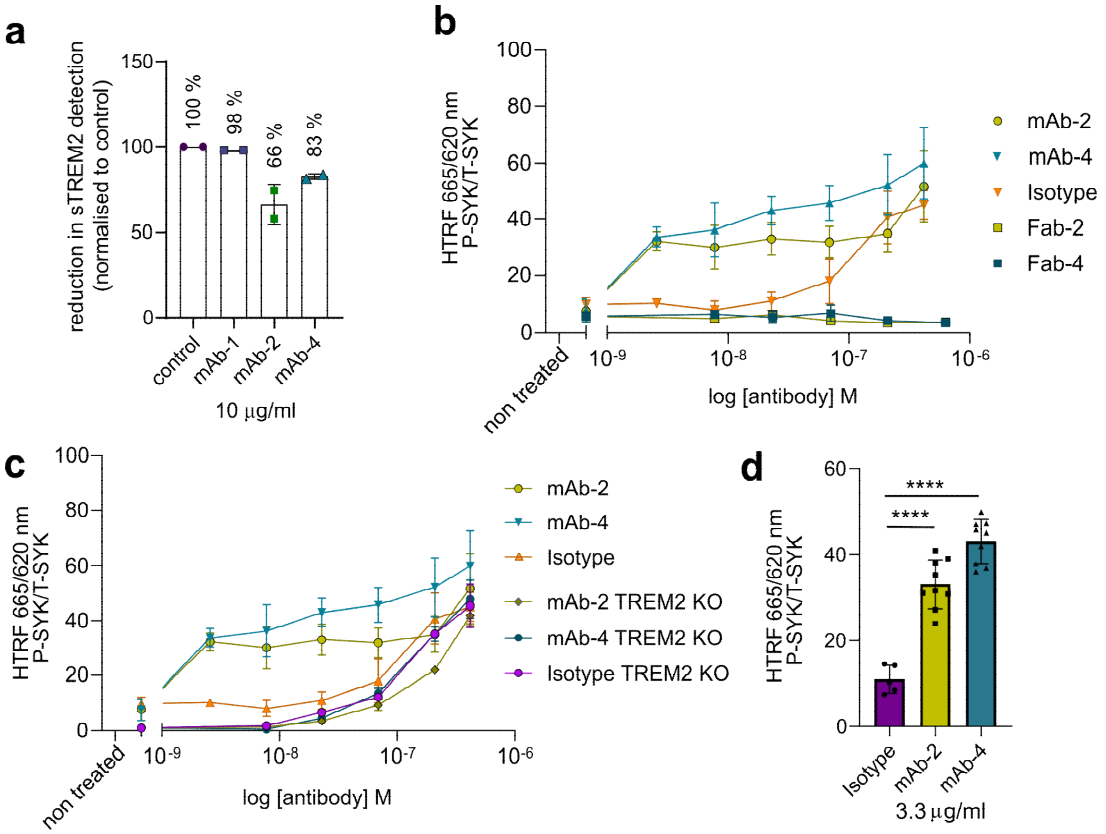


Figure 6.13 Activity of mAb conversions. *(a) sTREM2 ELISA compatibility with mAb conversions. Medium conditioned in transfected HEK293 cells for 5 hours was harvested and incubated with mAb-1, 2 and 4. Results are represented as percentage of vehicle control with mean ± SEM. (b) iMac cells were treated with increasing concentrations of monovalent Fab-2 and Fab-4 and bivalent mAb-2 and mAb-4. The background Fc response has been using an IgG1 isotype antibody. Cells were stimulated for 5min, and HTRF P-SYK signal was normalised to the total SYK HTRF signal performed simultaneously on the same lysates. Data represent mean +/- SD from 3 technical repeats (mAb2 and 4 n=3, isotype n=2, Fab n=1 biological replicates). (c) TREM2 KO and WT iMac cells were treated with increasing concentrations of mAbs to estimate non-specific responses. Data represent mean +/- SD from 3 technical repeats (TREM2 KO n=1). (d) Comparison of mAb-1 and mAb-2 activity to commercial isotype at dose 3.3 µg/mL Results are represented as individual values +/- SD (n=3). One-way ANOVA, Dunnett's post hoc comparison to isotype **** P < 0.0001.*

Both mAb-2 and mAb-4, but not their corresponding Fab fragments elicited SYK activation in iMac cells (**Figure 6.13b**). Because phosphorylation of SYK is a step in both TREM2 and Fc-γ activation pathways, the Fc portion of IgG1 conversions elicited basal P-SYK activation in a TREM2-independent manner (**Figure 6.13c**). The TREM2-dependent response could be detected at the lowest doses, whereas the non-specific Fc response contributed to the overall signal at concentrations above 6.6 µg/mL concentrations (**Figure 6.13c**). The mAb-4 efficacy was higher than mAb-2 and reached 5.5-fold over isotype response while 4.2-fold over background was detected for mAb-2 at 3.3 µg/mL, which is comparable to scFv-3 and scFv-4 (**Figure 6.13b,d**). Unfortunately, dose-response experiments at low concentrations need to be performed to estimate the full potency of the mAbs.

6.6 Validation of a physiological iMac ligand for further studies of the functional properties of derivative mAbs

To provide alternative evidence for an effect of the mAbs on receptor internalisation, for which the sTREM2 ELISA was not suitable, I started developing an assay for co-simulation with a physiological ligand. This was based on the hypothesis that a short pre-treatment with scFv or mAb might induce TREM2 internalisation, resulting in a decrease in surface TREM2 and lowered response to a subsequent agonist stimulus. Alternatively, TREM2 agonism could be blocked by inhibition of native-ligand mediated oligomerisation. However, this required development of a ligand for co-stimulation studies. The most reliable TREM2 activation can be achieved by AF1828 antibody, but the polyclonal character increases the complexity of the experimental outcomes (**Figure 6.14a, green bars).** Therefore, the goal was to develop more physiological ligands that would work effectively to stimulate both THP-1 and

iMacs. The comparison of both cell types could establish whether various TREM2 expression and shedding levels may result in different internalisation and activation outcomes.

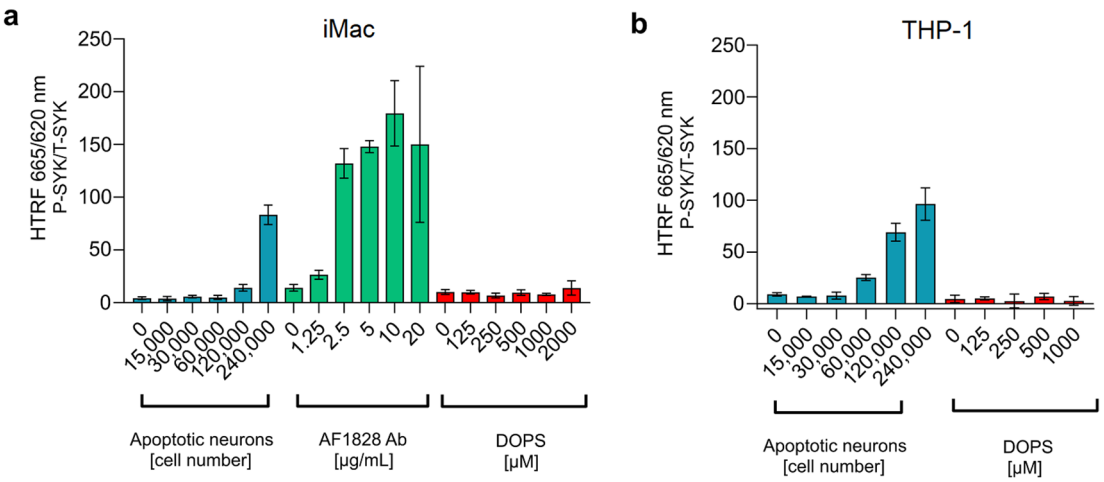


Figure 6.14. Stimulation of P-SYK in iMac cells and sTREM2 reduction upon SYK inhibition. *(a) Dose response agonist panel for iMac cells. Cells were treated with commercial agonist AF1828 or DOPS for 5 min or apoptotic SH-SY5Y neurons for 30 min. Cells were lysed and HTRF for P-SYK and T-SYK was performed. Results are represented as average with mean ± SD (n=1, 3 technical repeats). (b) Dose response of apoptotic SH-SY5Y and DOPS treatment of THP-1 cells. THP-1 cells were washed before treatment and treated according to the same protocol as iMac. Results are represented as average with mean ± SD (n=1, 3 technical repeats).*

SYK phosphorylation was triggered by stimulation with apoptotic SH-SY5Y neuroblastoma cells but not DOPS liposomes containing phosphatidylserine in iMac and THP-1 cells. Since others have reported TREM2-dependent P-SYK activation in response to phosphatidylserine (PS) exposed on the surface of either apoptotic neurons or liposomes, we tested both reagents for activation of SYK in differentiated iMac and THP-1 cells (Hall-Roberts et al., 2020; Nugent et al., 2019; Shirotani et al., 2019). The PS containing DOPS liposomes were prepared by Thomas Smith, and both cell types were treated with increasing concentrations without any positive outcome (**Figure**

6.14). More importantly, I tested a potentially more physiological ligand: apoptotic neuroblastoma SH-SY5Y cells, which had been treated with 2% PFA to induce apoptosis and PS exposure. Activation of SYK was achieved in a dose-dependent manner in a single preliminary experiment for both THP-1 and iMac cells. In agreement with previous results, THP-1 cells were more responsive to the stimulus (**Figure 6.14**). Since many phagocytic receptors can exist on macrophages, the next step was to validate TREM2-dependence of this activation using TREM2 KO iMac cells. Unfortunately, these experiments could not be completed due to time constraints and technical difficulties with Covid-19 restrictions and iPSC factory supply. However, similar results on TREM2-dependent P-SYK response in iPSC-microglia upon apoptotic neuron stimulation were described more recently in the literature (Hall-Roberts et al., 2020).

6.7 Discussion

We have demonstrated that novel antibody fragments directed towards new epitopes on the Ig domain of the TREM2 ectodomain have functional activity. This activity is intrinsic to bivalent species and can be observed in cellular responses, including: (i) an alteration in the amounts of sTREM2 shed into the conditioned medium, (ii) stimulation of receptor endocytosis and (iii) induction of SYK phosphorylation in a time and dose-dependent manner. Interestingly, the ability to observe these different functional effects depended on the cell model used.

A key finding was that all effects observed, whether using a scFv preparation or IgG1 conversions, were dependent on a bivalent reagent. When separated, dimeric species led to a robust reduction in the amount of sTREM2 present in HEK293 and THP-1 conditioned medium; however, the latter requires further experiments to be

performed. Potential reduction in sTREM2 might impact the availability of full-length receptor or could have biological implications for signalling cascades dependent on sTREM2, so I investigated the underlying mechanism of action.

Internalisation rather than shedding inhibition has been identified to be responsible for the decrease in sTREM2. Dimer-containing ScFv-3 and scFv-4 conjugated to fluorochrome co-localised with TREM2 in intracellular foci in a time-dependent manner, suggesting that antibodies remain bound to TREM2 and do not recycle back to the plasma membrane. The latter is likely responsible for the lowered substrate concentration for ADAM cleavage in the plasma membrane. Interestingly, similar sTREM2 ELISA dependency on bivalency were recently confirmed for other TREM2 mAb but shedding inhibition was identified as a mechanism of action due to different epitope location (Schlepckow et al., 2020). Unfortunately, the proof that monovalent molecules have no effect had to be provided by another ELISA assay performed only once thus far. Alternatively, stable fluorochrome conjugation can be achieved with Fab and IgG1 conversions for improved imaging experiments. Because receptor-mediated internalisation is common for surface receptors and is exploited in the design of antibody-drug conjugates (ADC), I aimed to confirm the same properties in resident tissue macrophage model-iMac cells (Gyun et al., 2007; Mary et al., 2012; Mayes et al., 2018; Moody et al., 2015; Wang et al., 2015a).

A key difference between the human iPSC derived macrophages and the HEK293, and THP-1 cell models was that a decrease in the shed TREM2 could not be detected in iMac cells. Surprisingly, transfected HEK293 and THP-1 had a similar response to treatment with dimeric antibodies in our preliminary experiments, indicating similar mechanisms governing TREM2 trafficking and internalisation. The possible limitation is the unknown sensitivity of iMac to LPS contamination which is

much higher than HEK293 or THP-1 cells (Babolmorad et al., 2021; MacRedmond et al., 2005). Therefore LPS response could potentially cause an increase in sTREM2 despite the scFv contamination levels measured below 0.05-0.1 EU/ml, which are within values tolerated by dendritic cells (Schwarz et al., 2014). However, both HEK293 and THP-1 express and shed considerably higher amounts of TREM2 than iMac cells indicating higer surface expression. The latter, in turn, was shown to impact the fate and internalisation rates of some surface receptors (Ram et al., 2014). Consequently, the low surface expression of TREM2 in iMac cells has recently been confirmed by others (Hall-Roberts et al., 2020; Schapansky et al., 2021). However, the lack of detectable sTREM2 difference can also be caused by faster recycling rates of naked TREM2 receptors or plasma membrane in the macrophages, which cannot be detected by ELISA (Hao and Maxfield, 2000). Alternatively, TREM2 can dissociate from scFvs in endocytic pathways and recycle back to the surface. It remains to be investigated whether the lack of the effect is caused by these biologically relevant processes or more technical limitations.

In order to study TREM2 agonism in the most physiological system available, the agonist studies were conducted only on iMac cells. In theory, THP-1 or transfected cells could be used, but large TREM2 expression changes were shown recently to negatively impact the potency of developed molecules (Ibach et al., 2021, Schapansky et al., 2021). In agreement with bivalency-dependent activity, the P-SYK signal was detected upon conversion of otherwise functionally dormant scFv-2 to bivalent mAb-2 in iMac cells. Unfortunately, due to Fc-receptor activation in isotype only controls, the EC50 could not be calculated, and new treatment protocols employing lower concentrations need to be generated. Nonetheless, since only one study investigated the ability of TREM2 mAb to elicit P-SYK in iMac, the efficacies demonstrated by our study are the highest reported thus far in the literature (Ibach et al., 2021). Others

investigated TREM2 agonism in monocyte-derived macrophages, which, similarly to the THP-1 may express more TREM2 and cannot be effectively compared with our data (Ellwanger et al., 2021; Fassler et al., 2021; Schlepckow et al., 2020; Wang et al., 2020).

We demonstrate for the first time that multivalent antibody molecules binding to this particular Ig epitope have agonist potential. Nevertheless, the impact of mAb-2 and mAb-4 stimulation on TREM2-dependent functions such as survival, migration or phagocytosis need to be established. Thus, optimisations of stimulation with DOPS and apoptotic neuroblastoma cells attempted to estimate net agonist or antagonist effects at P-SYK level were attempted. This work remains largely unfinished despite the initial success of apoptotic SH-SY5Y in TREM2 activation. However, recent work in the field supports the existence of the TREM2 dependent P-SYK pathway (Cosker et al., 2021; Hall-Roberts et al., 2020; Shirotani et al., 2019). Further experimental work is necessary to estimate the true relevance of these reagents to human microglia biology.

Taken together, the literature and above data highlight the importance of multivalence for the functional activities of anti-TREM2 antibodies. I have shown that epitopes on TREM2 Ig-domain surface in combination with the crosslinking ability of bivalent antibodies lead to agonist and receptor internalisation functional effects. The work needs further experiments to evaluate potency and impact on downstream microglial cellular functions, and ultimately, it would be interesting to explore the effects of these antibodies *in vivo*.

6.7.1 Comparison of scFvs with published mAb molecules

Since TREM2 is a potential therapeutic target for AD, the pharmaceutical industry has initiated several projects aimed at developing TREM2 antibody therapeutics, with at least two candidates having commenced clinical trials. Data have

been reported for AL002, hT2AB, 4D9 and 4B2A3, which allows for an interesting comparison with antibodies developed during this project (Ellwanger et al., 2021; Ibach et al., 2021; Schlepckow et al., 2020; Wang et al., 2020) (**Table 6.1**). Other functionally active antibodies have either not been widely published (WO2016023019A2) or the epitope has not been mapped and, therefore, are not included in the discussion below (Cheng et al., 2018; Fassler et al., 2021).

Authors	Name	TREM2 antigen	Fc type	target	Kd	Syk phosphorylation
Fassler et al.,2021	AbT1	"extracellular" TREM2	IgG4	human, mouse	5.7 nM	mouse bone marrow-derived macro-phages (BMDM)
Elwwanger et al., 2021	hT2AB	TREM2-DAP12 cDNA	IgG1	human only	50 nM	human monocyte-derived macrophages (MDM) EC50 122pM (45min incubation times) bivalency-dependent
Ibach et al., 2021	4B2A3	stalk 131-149 a.a.	IgG1	human only	N/A	HEK293 and iMac (10x fold decrease in activity) iMac: **1.5 fold** over background bivalency-dependent
Schlepkow et al., 2020	1D9	stalk 137-145 a.a.	IgG1	mouse only	68 pM	HEK293 reporter cell line
Wang et al., 2020	Al002	112-157	IgG1	Al002 - human Al002c-mice	N/A N/A	2B4 cells (NFAT reporter) Human monocyte macrophages (hMDM)
This work	mAb-2	epitope verified	IgG1	primarily human, mice	1.7 nM (human)	iMac: 4.2 over background bivalency-dependent
This work	mAb-4	epitope verified	IgG1	primarily human, mice	12 nM (human)	iMac: 5.5 over background bivalency-dependent

Table 6.1. Comparison of published TREM2 mAb with mAb-2 and mAb-4. *Basic antibody characteristics such as antigen used to generate the antibodies, IgG/Fc type, target species antigen, affinity values (K_D) and type of cell used to generate activation data are shown. For studies using iMac cells, the efficacy is described by a signal over background (fold).*

X-ray crystallographic data which accurately define the antibody/TREM2 interfaces is not publicly available for any of these reagents. AL002 is an agonist antibody with a poorly defined epitope, between residues TREM2 112-174, while 4D9 and 4B2A3 have epitopes defined by peptide mapping to residues Asp137-Gly145 and Asp131-149, respectively (Ibach et al., 2021; Schlepckow et al., 2020; Wang et al.,

2020) (**Table 6.1**). As such, they target TREM2 epitopes N-terminal of the α-secretase cleavage site at H157, whereas our X-ray crystallography data shows that scFv-2/scFv-4 bind the immunoglobulin domain of TREM2. In January this year, Ellwanger and his team published data on an agonist hT2AB with an unknown epitope on human TREM2 (Ellwanger et al., 2021). hT2AB can target both human and murine TREM2 similarly to 4B2A3, whereas the other two mAbs show some cross-species variation, 4D9 is specific for mouse TREM2, and AL002 has a high affinity for human TREM2. The scFv we developed were shown to bind murine TREM2, albeit in a diminished manner (**4.5**).

All of these antibody tools were shown to have agonist properties *in vitro* (**Table 6.1**). AL002 elicits TREM2 mediated secondary intracellular signalling, demonstrated using an NFAT reporter cell line and phosphorylation of a protein of equal molecular weight to DAP12 in bone-derived macrophages (Wang *et al.* 2020). Similarly, 4D9 shows agonism, but only when a bivalent antibody was used to challenge cells; SYK phosphorylation did not occur following exposure of cells to 4D9 Fab fragment, similarly to my results. The requirement for a bivalent antibody for the function of AL002 has not been reported, but these observations with 4D9 led the authors to hypothesise that the functional effects of 4D9 are dependent upon a bivalent antibody and crosslinking of TREM2 molecules (Schlepckow *et al.* 2020). Similar dependence on bivalency has been described for hT2AB, which can increase phosphorylation of SYK in human monocyte-derived macrophages (MDM). Some of these antibodies were shown to increase mouse BMM and human MDM viability *in vitro* but the work described in this thesis is the first to show robust mAb mediated phosphorylation of SYK in human iPSC-macrophages. Surprisingly, SYK activation caused by hT2AB required extensive 1 hour-long mAb treatments, contrary to the response elicited by the scFvs, which peak and return to basal levels after 20 minutes (Ellwanger et al., 2021).

This suggests that hT2AB may act via a different signal transduction pathway, which may support prolonged TREM2 stimulation.

AL002, 4D9 and hT2AB were all shown to reduce the shedding of TREM2 in monocyte or bone marrow-derived macrophages or transfected HEK293. Since AL002 and 4D9 are likely to be stalk binding antibodies, they might affect cleavage of TREM2 by virtue of sterically hindering access by ADAMs. hT2AB was also shown to reduce TREM2 shedding, but its epitope has not been defined. Additionally, reduction in sTREM2 has been confirmed for the first time in humans with AL002 (Wang *et al*. 2020). In the case of 4D9 this function is dependent upon the use of a bivalent antibody, as the Fab failed to inhibit the shedding of sTREM2 by cells despite the fact that the epitope is located only 11 amino acids upstream of ADAM cleavage site at His157.

In light of the above, Schlepckow et al. has investigated the mechanism of 4D9 function and concluded that it exerts some of its effects by stabilising TREM2 at the plasma membrane, explaining the potentiation of signalling in response to liposomes in HEK cells (Schlepckow et al. 2020). The proposed mechanism of action is particularly exciting and draws parallels with studies of SYK activation triggered by B cell antigen receptor (BCR) agonists, where some portion of the receptor is destined for internalisation (and perhaps recycling), but another remains on the surface and supports agonism (Hong et al., 2002; Hou et al., 2006). Inhibition of cleavage could be achieved in both receptor pools, especially if ADAM cleavage of TREM2 can occur in the endosomal pathway, as was shown in the case for Notch signalling (Chastagner et al., 2017).

At present, the mechanism of action for the lowering of sTREM2 by AL002 and hT2AB antibody reagents is unclear. It is likely that all bivalent anti-TREM2 antibodies cross-link and cause the internalisation of TREM2 receptors, similarly to scFv-mediated

internalisation in HEK293. I speculate, however, that some such as 4D9 and 4B2A3 exert more or less effect by additional mechanisms such as direct inhibition of shedding or different recycling kinetics.

In vivo, 4D9 was shown to reduce plaque burden in APP mice models of AD, whereas AL002 did not show a similar effect on 5XFAD mice. The latter was reported to increase microglial activation and phagocytosis with a simultaneous reduction in dystrophic neurites and Spp1, a marker for inflammation. The mice also exhibited a modest but significant change in anxiety-like traits (Wang et al., 2020). More recently, another human and mouse TREM2 antibody, Ab-T1, was shown to promote Aβ uptake and attenuate cognitive decline in 5xFAD mice (Fassler et al., 2021). Surprisingly, Ellwanger et al. demonstrated that TREM2 activation can increase microglia proliferation but only in TREM2 R47H/5XFAD mice and remained sceptical about the potential for therapeutic antibodies for the general population without the R47H mutation (Ellwanger et al., 2021). However, murine models have been poor predictors of successful outcomes in clinical trials, so the results of the upcoming trial of AL002 are of great interest and will provide useful validation data for the therapeutic value of TREM2 agonists in AD therapy.

Chapter 7

Discussion and future plans

TREM2 research is a rapidly evolving field with the potential to offer novel insights and exciting new strategies for the treatment of Alzheimer's disease. At the time of initiation of this project, only a few tools were available to study TREM2, with little structural data to help investigate the structure-function relationship of this receptor. Thus, we hypothesised that novel TREM2 scFv binders could be produced by phage display against human TREM2 Ig-domain. The use of scFv antibody fragments which are relatively small and rigid should facilitate characterisation of TREM2 epitope and potential conformational change by X-ray crystallography. Furthermore, the surface expression of TREM2 should assure the functionality of developed antibodies which can be assessed by cell biology experiments in several cell types, including iPSC-derived macrophages.

After phage display and extensive optimisation of TREM2 and scFv purification strategies, four novel scFv antibody fragments were successfully produced, and three novel crystal structures of TREM2 in complex with scFv-2 and scFv-4 were solved. The value of scFv as TREM2 reagents was validated by mapping their TREM2 epitopes to the opposite side of the TREM2 Ig domain to the putative native-ligand binding site. Since native TREM2 ligands are heterogeneous and range from lipids to dead cells, this particular quality of binding an epitope removed from the recognised ligand binding

site may be useful for detecting TREM2 in applications that include stimulation with ligands. Finally, we confirmed the activity of three out of four generated antibody CDR combinations against TREM2 expressed in HEK293 and iMac cells, validating the phage display antibody platform as a useful methodology in developing active antibodies against human surface receptors. It was exciting to have developed antibodies to a previously unrecognised epitope with a range of different affinities to human TREM2 and generated the first X-ray structures of a well-defined agonist with TREM2.

Very few clonal antibodies are recognised as binding TREM2 Ig domain. The two best-characterised TREM2 epitopes for 4D9 and 4B2A3 are positioned in the stalk sequence (Ibach et al., 2021; Schlepckow et al., 2020). Surprisingly, the scFvs all recognised similar overlapping epitopes on TREM2 through CDRs enriched in tyrosine residues. The narrow variation in the scFvs selected might have been due to the bias in the representation of the phage library or generally poor antigenicity of TREM2 Ig-domain. However, the novel epitope on TREM2 globular domain, which we validated, raises the possibility that the antibodies we generated might have unique properties compared to other reagents.

The monovalent nature of scFv offered some interesting possibilities in functional studies. However, the results of my studies demonstrated the necessity of bivalency for the function of both scFvs and antibody conversions. The reduction in sTREM2 shedding from HEK293-TREM2/DAP12 cells and the agonism in iMac cells required a bivalent antibody fragment in agreement with recently published work (Schlepckow et al., 2020) (**Figure 7.1a,c**). Further investigation of the inhibitory effect on sTREM2 accumulation in the conditioned medium of transfected HEK293 cells revealed that the underlying mechanism of action is via receptor-mediated endocytosis,

which removes receptor substrate for ADAM protease from the cell surface and decreases the accumulation of sTREM2 (**Figure 7.1b,c**).

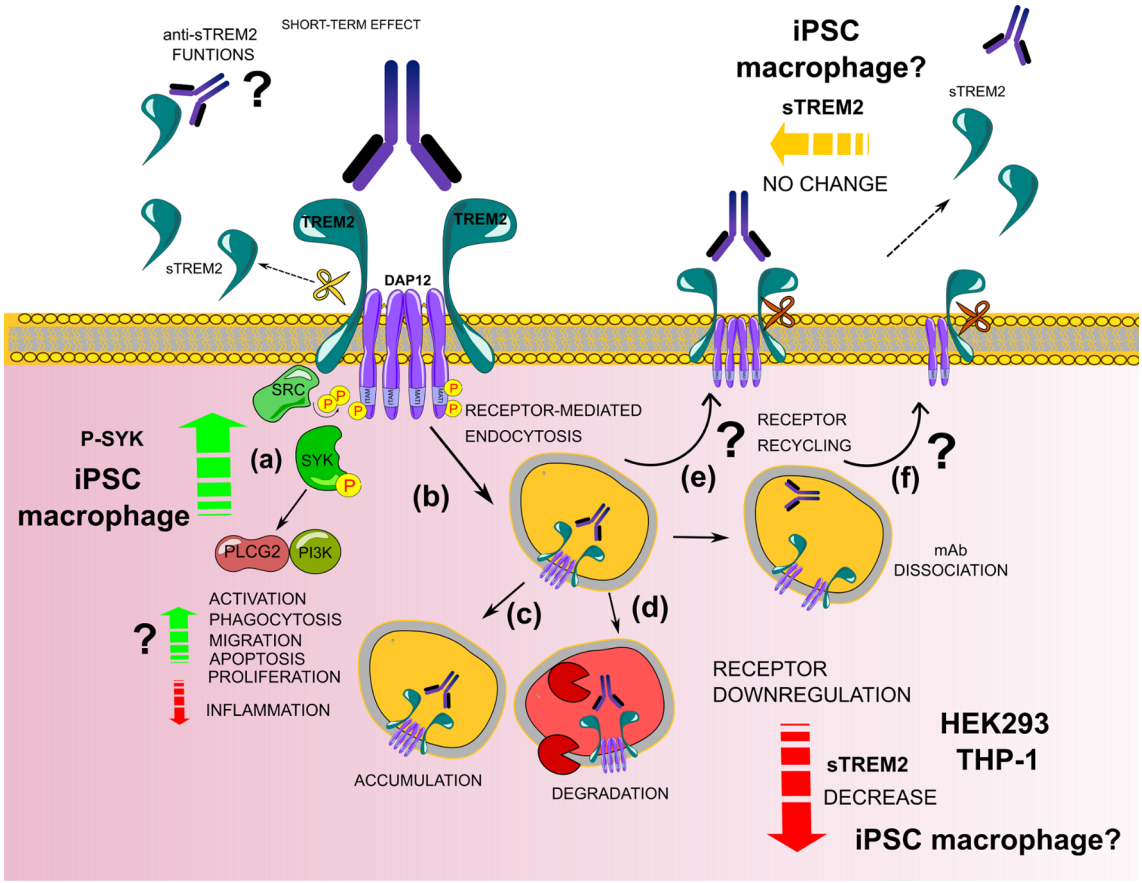


Figure 7.1. Potential effects of bivalent antibody action on full length TREM2 and sTREM2 in iMac and HEK293 cells*. Activation (a) and TREM2 internalisation (b-f) following bivalent antibody treatment with a resulting impact on sTREM2 levels and microglia cell functions are shown. The case when TREM2 is internalised independently of the mAb is not shown. ADAM10/17 protease is shown as pair of scissors. The bold font signifies the cell system in which the particular effects were observed or marked by a question mark where the mechanism remains to be confirmed.*

It remains to be investigated to what extent the mAbs developed during this project can lead to the internalisation of TREM2 in human microglia. Receptor-mediated internalisation, such as the one I demonstrated for dimeric scFvs in HEK293, could lead to overall receptor down-regulation and contribute antagonistic effect upon prolonged treatment with mAbs (Aldeghaither et al., 2019) (**Figure 7.1c,d**). Since some

of the recently published mAbs were developed as shedding inhibitors, the extent to which sTREM2 reduction is caused by internalisation or inhibition of ADAM cleavage is unclear. Data showing stabilisation of surface TREM2 in mouse bone marrow-derived macrophages (BMDMs) is available only for 4D9 and contrasts with my preliminary data showing a loss of surface TREM2 expression in HEK293 (Schlepckow et al., 2020). Stalk binding antibodies like 4D9 may stabilise receptors at the cell surface by preventing shedding and result in a positive modulatory signalling effect, as has been shown for batimastat (a sheddase inhibitor) and 4D9 in mouse BMDMs and HEK293 (Schlepckow et al., 2020). Antibodies, where this mode of action is significant, will be expected to differentiate from antibodies that internalise the TREM2 receptor. Nevertheless, internalisation and agonism are tightly regulated by SRC kinases and the presence of phosphorylated SYK in immune cells, thus the mAb-mediated internalisation in human tissue-resident macrophages may be regulated differently than in HEK293 cells or BMDMs and remains to be investigated in iMac cells (Hong et al., 2002; Hou et al., 2006).

All tested bivalent antibodies and antibody fragments produced agonist effects as detected by phosphorylation of SYK in iMac cells (**Figure 7.1a**). The novel monoclonal antibodies generated in this study were shown to have the strongest affinity to human TREM2 and reached the highest P-SYK activation levels in iMac cells published thus far (Ellwanger et al., 2021; Fassler et al., 2021; Ibach et al., 2021; Schlepckow et al., 2020; Wang et al., 2020). It is tempting to speculate whether the increased efficacy of the novel antibodies is a consequence of their epitope on the TREM2 Ig domain or high affinity. The majority of the recently generated TREM2 mAbs have not been studied in tissue-resident macrophages, and thus the direct comparison with these molecules is not feasible (Ellwanger et al., 2021; Fassler et al., 2021; Schlepckow et al., 2020; Wang et al., 2020). For example, the Ibach group noted a ten-fold decrease in T1b activity in

iMac compared to their HEK293 reporter cells (Ibach et al., 2021). Such decreased efficacy can result from the lowered surface expression of TREM2 and can potentially apply to all of these newly developed reagents (Schapansky et al., 2021). These issues highlight why the use of iMac cells can be valuable and necessary in the development of molecules targeting human microglia.

Crystallographic structure models are not free from experimental artefacts. TREM2 stalk interactions with scFv-4 or TREM2-TREM2 CDR packing interface are good examples of interactions challenging to assess for their biological potential. Interactions between CDR-regions of TREM2 within crystal structures are also present in previously published structures (Byrne et al., 2021, Kober et al., 2016, Sudom et al., 2018). Moreover, the phosphatidylserine soaked into TREM2 crystals interacted with two neighbouring TREM2 subunits (Sudom et al., 2018). Such evidence would imply the possibility of the biological dimer existence in normal circumstances, especially that dimerisation has been confirmed for the TREM2 homologue- TREM1 (Carrasco et al., 2019). However, TREM2-TREM2 interactions between CDR regions are often different despite the involvement of the same hydrophobic residues, as evidenced in our data and others, implying a non-specific nature of these interactions, at least in the case of TREM2 self-oligomerisation. This observation perhaps sheds light on why TREM2-ligand in vitro studies often led to different conclusions when sticky hydrophobic molecules such as lipids or lipoproteins were used or why TREM2 can bind so many different ligands. Unfortunately, due to these CDR interactions in scFv-TREM2 crystals and poor scFv solubility and changes in monomer-dimer equilibrium, the scFvs utilisation as crystallisation chaperons may be reduced.

Despite the high efficacy of generated mAbs, it has been noted that the phosphorylated SYK levels are lower than the widely used AF1828 polyclonal

antibody. Clustering caused by cross-linking of different epitopes caused by the polyclonal nature of AF1828 may be the mechanism behind the exceptional efficacy in iMac cells despite their low TREM2 surface expression. Due to overlapping epitope on TREM2 for the antibodies generated in my study, it was not possible to pair multiple antibodies to investigate the impact of polyclonality on TREM2 agonism. Interestingly, agonist antibodies which stimulate clustering are more efficacious when they dissociate faster from the target protein allowing for cross-linking more than two ectodomains (Chodorge et al., 2012; Mayes et al., 2018). Among the antibodies generated, scFv-3, which was shown to dissociate from TREM2 rapidly, has the potential to increase TREM2 clustering after conversion to IgG1 antibody and could be investigated to confirm this possibility.

Unfortunately, the low number of scFvs limited my ability to investigate multiple epitopes on TREM2 and compare their functional relevance to TREM2 biology. However, since the antibodies are characterised by variable affinity and avidity towards TREM2, which often can determine functional outcomes such as receptor recycling or degradation, the scFv, Fab, and IgG1 molecules generated might still exhibit different properties (de Andrés et al., 2012; Bien-Ly et al., 2014). An unexplored characteristic of antibodies we have generated that is necessary to accomplish full validation status is antibody specificity. Our data confirmed TREM2-specific SYK response, but it was only limited to macrophage cells and SYK cascades. Further work is necessary to establish whether these antibodies can lead to activation of other surface receptors in different cell types leading to adverse effects.

The issue of internalisation in iMac cells remains to be investigated further to explain the modes of antibody actions and predict their functional effects. Due to its low expression of TREM2 in iMac cells, more sensitive methods than sTREM2 ELISA,

which we used in our study, will be necessary to investigate TREM2 internalisation events. On the other hand, our work may also indicate that TREM2 may be recycled back to the plasma membrane in iMac cells without accumulation effects observed in HEK293 cells (**Figure 7.1b,e,f**). Alternatively, TREM2 can also be internalised in a receptor-independent manner as part of high plasma membrane turnover in macrophage cells. Furthermore, since LPS tolerance levels for human iMac cells are unknown, the LPS contamination thresholds were allowed at levels shown to be tolerated by dendritic cells, THP-1 and HEK293 cells (Babolmorad et al., 2021; MacRedmond et al., 2005; Schwarz et al., 2014). However, low levels of LPS contaminating scFv preparations could potentially increase sTREM2 accumulation and mask internalisation effects. As a result, more work is required to validate antibody-mediated endocytosis, which can be one of the means to predict the overall functional effect and propose the mechanism of mAb action.

How mAb stimulation translates into effects upon microglial physiology is not immediately apparent, especially in the light of receptor down-regulation (**Figure 7.1c,d**). In particular, the antagonistic potential of monovalent and bivalent antibodies has not been explored due to incomplete data on iMac stimulation with apoptotic neurons. It would be interesting to study the co-application of the antibodies and native ligands for evidence of pharmacological interaction, as has been proposed in a study of an hT2AB antibody (Ellwanger et al., 2021). Of particular interest would be determining if the antibodies generated in this project have different functional effects on microglia survival, migration, cytokine production, Aβ accumulation and phagocytosis; and comparing where possible with data published for the other mAbs that are progressing into the clinic (Ellwanger et al., 2021; Fassler et al., 2021; Schlepckow et al., 2020; Wang et al., 2020). So far, the overwhelming evidence from novel mAbs published in 2020/21 indicates that stimulation of the TREM2 pathway

remains a valid therapeutic approach in neurodegenerative diseases (Fassler et al., 2021; Price et al., 2020).

Administration of mAb or antibody fragments that bind the ectodomain of TREM2 may have a neutralising effect on soluble TREM2, which was demonstrated to have pro-inflammatory and pro-survival functions independently of full-length TREM2 (Zhong et al., 2017, 2019). An interesting possibility that requires further investigation is that because the novel antibodies bind the Ig domain, as compared to the stalk-binding of other antibodies, they might have different effects on the biological function of soluble TREM2 (Ibach et al., 2021; Schlepckow et al., 2020). Furthermore, due to increased sTREM2 relevance as a biomarker which is increased in CSF of AD patients, the mAb-2 antibody, which has a superior affinity to TREM2, could be trialled for TREM2 detection as a more cost-effective or alternative to commercial antibodies (Ewers et al., 2019). This is a field requiring further development as the receptors mediating sTREM2 effects have still not been identified.

Despite the proven bivalency requirement, it is unclear whether ligand-induced dimerisation of TREM2 is part of the physiological signalling cascade. Many of the antibody-mediated immune signalling cascades seem to be responsive to cross-linkers such as mAbs based on the amplified response of ITAM-containing receptors to ligands with increased avidity (Billadeau and Leibson, 2002; Ben Mkaddem et al., 2019). To bypass crystallisation artefacts and the heterogeneous nature of TREM2 ligands, cryogenic electron microscopy (cryo-EM) could be a better method of choice than crystallography in order to investigate TREM2 complexes in the presence and absence of ligands such as phosphatidylserine, sphingomyelin or lipidated APOE (Kober et al., 2021; Nugent et al., 2019). At the start of this project, I conducted some work to investigate how co-expression with DAP12 could improve the expression of TREM2,

which has laid some encouraging groundwork for future work to determine the structures of TREM2 receptor complexed with the accessory proteins that transduce its signals. Furthermore, the Fab fragments generated in this study could also be used as tools to increase the complex size or facilitate labelling of TREM2 subunits (Wu et al., 2012).

Structures of TREM2-DAP12 complex could also guide the development of molecules targeting TREM2 and DAP12 interactions. Using antibodies for the treatment of CNS diseases is not without difficulties because of the impermeability of the blood-brain barrier (BBB). Obtaining adequate exposure is possible, as shown for the anti-β amyloid antibodies and transferrin receptor (Bien-Ly et al., 2014). However, these issues require researchers to consider developing small molecule inhibitors or agonists for the TREM2 receptor. In addition to molecules targeting TREM2 ligand-binding regions, small-molecule probes which disrupt or stabilise protein-protein interactions have been described in the literature and can be used to modulate TREM2 to DAP12 interactions (Jamart-gre et al., 2009; Lee et al., 2011; Ottmann et al., 2018). However, at the moment, it is not known whether TREM2 and DAP12 share extensive interaction surfaces outside of the membrane or even if this interaction follows ligand recognition events. Therefore, it would be interesting to investigate full-length TREM2-DAP12 structures and solve questions on ligand-mediated oligomerisation or complex composition using reagents developed during this project.

As a result of this project, the first crystal structures of well-defined ligands in complex with TREM2 were generated and provided the first detailed descriptions of the binding epitopes of two novel functional antibody fragments. I also determined that these novel antibodies bind different regions of TREM2 to previously published antibodies, identified the dependency upon bivalency for activity and described the

functional effects upon sTREM2 shedding and receptor agonism in a range of heterologous and native TREM2 cellular models. These antibodies can be used as fully validated molecules for technical research applications, improving experimental design and reducing costs of research. They may also be used to validate the targeting of the TREM2 pathway as a therapeutic strategy and, if their Ig domain binding differentiates them from the present antibodies in clinical development, could provide a basis for a new class of therapeutic antibodies.

Appendix

Start (a.a.)	End (a.a.)	Vector Name	Forward Primer
Initial expression campaign for TREM2			
H19	D131	pBASF	tacttccaatccatgcacaacaccacagtgttcc
H19	A138	pBASF	tacttccaatccatgcacaacaccacagtgttcc
H19	G145	pBASF	tacttccaatccatgcacaacaccacagtgttcc
H19	R161	pBASF	tacttccaatccatgcacaacaccacagtgttcc
H19	G166	pBASF	tacttccaatccatgcacaacaccacagtgttcc
H19	S174	pBASF	tacttccaatccatgcacaacaccacagtgttcc
H19	D131	pBASA	tacttccaatccatgcacaacaccacagtgttcc
H19	G145	pBASA	tacttccaatccatgcacaacaccacagtgttcc
H19	G166	pBASA	tacttccaatccatgcacaacaccacagtgttcc
H19	A197	pBASA	tacttccaatccatgcacaacaccacagtgttcc
H19	E210	pBASA	tacttccaatccatgcacaacaccacagtgttcc
H19	T230	pBASA	tacttccaatccatgcacaacaccacagtgttcc
H19	D131	pFB-Sec-NH	tacttccaatccatgcacaacaccacagtgttcc
H19	A138	pFB-Sec-NH	tacttccaatccatgcacaacaccacagtgttcc
H19	G145	pFB-Sec-NH	tacttccaatccatgcacaacaccacagtgttcc
H19	R161	pFB-Sec-NH	tacttccaatccatgcacaacaccacagtgttcc
H19	G166	pFB-Sec-NH	tacttccaatccatgcacaacaccacagtgttcc
H19	S174	pFB-Sec-NH	tacttccaatccatgcacaacaccacagtgttcc
M1	A130	pFB-CT10HF-LIC	ttaagaaggagatatactatggagcctctccggctgctc
M1	A138	pFB-CT10HF-LIC	ttaagaaggagatatactatggagcctctccggctgctc
M1	G145	pFB-CT10HF-LIC	ttaagaaggagatatactatggagcctctccggctgctc
M1	R161	pFB-CT10HF-LIC	ttaagaaggagatatactatggagcctctccggctgctc
M1	G166	pFB-CT10HF-LIC	ttaagaaggagatatactatggagcctctccggctgctc
M1	S174	pFB-CT10HF-LIC	ttaagaaggagatatactatggagcctctccggctgctc
H19	A130	pFB-CT10HF-LIC	ttaagaaggagatatactatgcacaacaccacagtgttccagg
H19	A138	pFB-CT10HF-LIC	ttaagaaggagatatactatgcacaacaccacagtgttccagg
H19	G145	pFB-CT10HF-LIC	ttaagaaggagatatactatgcacaacaccacagtgttccagg
H19	R161	pFB-CT10HF-LIC	ttaagaaggagatatactatgcacaacaccacagtgttccagg
H19	G166	pFB-CT10HF-LIC	ttaagaaggagatatactatgcacaacaccacagtgttccagg
H19	S174	pFB-CT10HF-LIC	ttaagaaggagatatactatgcacaacaccacagtgttccagg
H19	D131	pFB-LIC-Bse	tacttccaatccatgcacaacaccacagtgttcc
H19	A138	pFB-LIC-Bse	tacttccaatccatgcacaacaccacagtgttcc
H19	G145	pFB-LIC-Bse	tacttccaatccatgcacaacaccacagtgttcc
H19	R161	pFB-LIC-Bse	tacttccaatccatgcacaacaccacagtgttcc

H19	G166	pFB-LIC-Bse	tacttccaatccatgcacaacaccacagtgttcc
H19	S174	pFB-LIC-Bse	tacttccaatccatgcacaacaccacagtgttcc
M1	A130	pHTBV1.1-CT10H-SIII-LIC	ttaagaaggagatatactatggagcctctccggctgc
M1	A138	pHTBV1.1-CT10H-SIII-LIC	ttaagaaggagatatactatggagcctctccggctgc
M1	G145	pHTBV1.1-CT10H-SIII-LIC	ttaagaaggagatatactatggagcctctccggctgc
M1	R161	pHTBV1.1-CT10H-SIII-LIC	ttaagaaggagatatactatggagcctctccggctgc
M1	G166	pHTBV1.1-CT10H-SIII-LIC	ttaagaaggagatatactatggagcctctccggctgc
M1	S174	pHTBV1.1-CT10H-SIII-LIC	ttaagaaggagatatactatggagcctctccggctgc
TREM2 biotinylated constructs for antigen production			
H19	D131	pFB-Sec-Bio5	tacttccaatccatgcacaacaccacagtgttcc
H19	A138	pFB-Sec-Bio5	tacttccaatccatgcacaacaccacagtgttcc
H19	S174	pFB-Sec-Bio5	tacttccaatccatgcacaacaccacagtgttcc
TREM2 N79A glycosylation mutants			
H19	D137	pFB-Sec-NH	tacttccaatccatgcacaacaccacagtgttcc
H19	R161	pFB-Sec-NH	tacttccaatccatgcacaacaccacagtgttcc
H19	G166	pFB-Sec-NH	tacttccaatccatgcacaacaccacagtgttcc
T21	D137	pFB-Sec-NH	tacttccaatccatgaccacagtgttccagggcgtg
T21	R161	pFB-Sec-NH	tacttccaatccatgaccacagtgttccagggcgtg
T21	G166	pFB-Sec-NH	tacttccaatccatgaccacagtgttccagggcgtg
TREM2-avi for crystallography			
H19	A138	pHTBV1.1-SecNH-Bio	tacttccaatccatgcacaacaccacagtgttcc
H19	S174	pHTBV1.1-SecNH-Bio	tacttccaatccatgcacaacaccacagtgttcc
TREM2 produced by Eisai			
H19	D131	pTT5	Ctcgagtgatcattagtgatggtgatggtggtgcttggt accgtctgccagcacctccaccaggac
H19	S174	pTT5-avi	Gattggaagtagaggttctctgccccgg ggaaccagagatc
scFv-1-4: *E. coli* expression			
E1	K243	pNIC-MBP2-LIC	tatccacctttactgtcatttgatctccagcttggt
scFv-1-4+avi-tag: E. *coli* expression			
E1	K243	pNIC-MBP2-LIC	tatccacctttactgcttttgatctccagcttggt
scFv-1-4: *Sf9* expression			
E1	K243	pFB-Sec-NH	tacttccaatccatggaggtgcaattgttggagagc
control scFv: *Sf9* expression (SPRTNC)			
E1	K243	pFB-Sec-NH	tacttccaatccatggaggtgcaattgttg

Appendix Table 1. List of constructs and forward primers used to generate inserts.

Start	End(a.a.)	Vector Name	Reverse primer
Initial expression campaign for TREM2			
H19	D131	pBASF	tatccacctttactgtcagtctgccagcacctccac
H19	A138	pBASF	tatccacctttactgtcaagcatcccggtgatccag
H19	G145	pBASF	tatccacctttactgtcacccggggaaccagagatc
H19	R161	pBASF	tatccacctttactgtcacctggagatgctgtgctc
H19	G166	pBASF	tatccacctttactgtcatccttccaagaggctcct
H19	S174	pBASF	tatccacctttactgtcaggaagtgggtgggaaggg
H19	D131	pBASA	tatccacctttactgtcagtctgccagcacctccac
H19	G145	pBASA	tatccacctttactgtcacccggggaaccagagatc
H19	G166	pBASA	tatccacctttactgtcatccttccaagaggctcct
H19	A197	pBASA	tatccacctttactgtcaggctgcagcccagagggc
H19	E210	pBASA	tatccacctttactgtcattcactgggtggatgtgt
H19	T230	pBASA	tatccacctttactgtcacgtgtctctcagccctgg
H19	D131	pFB-Sec-NH	tatccacctttactgtcagtctgccagcacctccac
H19	A138	pFB-Sec-NH	tatccacctttactgtcaagcatcccggtgatccag
H19	G145	pFB-Sec-NH	tatccacctttactgtcacccggggaaccagagatc
H19	R161	pFB-Sec-NH	tatccacctttactgtcacctggagatgctgtgctc
H19	G166	pFB-Sec-NH	tatccacctttactgtcatccttccaagaggctcct
H19	S174	pFB-Sec-NH	tatccacctttactgtcaggaagtgggtgggaaggg
M1	A130	pFB-CT10HF-LIC	gattggaagtagaggttctctgcgtctgccagcacctccac
M1	A138	pFB-CT10HF-LIC	gattggaagtagaggttctctgcagcatcccggtgatccag
M1	G145	pFB-CT10HF-LIC	gattggaagtagaggttctctgccccggggaaccagagatc
M1	R161	pFB-CT10HF-LIC	gattggaagtagaggttctctgccctggagatgctgtgctc
M1	G166	pFB-CT10HF-LIC	gattggaagtagaggttctctgctccttccaagaggctcct
M1	S174	pFB-CT10HF-LIC	gattggaagtagaggttctctgcggaagtgggtgggaaggg
H19	A130	pFB-CT10HF-LIC	gattggaagtagaggttctctgcgtctgccagcacctccac
H19	A138	pFB-CT10HF-LIC	gattggaagtagaggttctctgcagcatcccggtgatccag
H19	G145	pFB-CT10HF-LIC	gattggaagtagaggttctctgccccggggaaccagagatc
H19	R161	pFB-CT10HF-LIC	gattggaagtagaggttctctgccctggagatgctgtgctc
H19	G166	pFB-CT10HF-LIC	gattggaagtagaggttctctgctccttccaagaggctcct
H19	S174	pFB-CT10HF-LIC	gattggaagtagaggttctctgcggaagtgggtgggaaggg
H19	D131	pFB-LIC-Bse	tatccacctttactgtcagtctgccagcacctccac
H19	A138	pFB-LIC-Bse	tatccacctttactgtcaagcatcccggtgatccag
H19	G145	pFB-LIC-Bse	tatccacctttactgtcacccggggaaccagagatc
H19	R161	pFB-LIC-Bse	tatccacctttactgtcacctggagatgctgtgctc
H19	G166	pFB-LIC-Bse	tatccacctttactgtcatccttccaagaggctcct
H19	S174	pFB-LIC-Bse	tatccacctttactgtcaggaagtgggtgggaaggg
M1	A130	pHTBV1.1-CT10H-SIII-LIC	gattggaagtagaggttctctgcgtctgccagcacctccac
M1	A138	pHTBV1.1-CT10H-SIII-LIC	gattggaagtagaggttctctgcagcatcccggtgatccag
M1	G145	pHTBV1.1-CT10H-SIII-LIC	gattggaagtagaggttctctgccccggggaaccagagatc
M1	R161	pHTBV1.1-CT10H-SIII-LIC	gattggaagtagaggttctctgccctggagatgctgtgctc
M1	G166	pHTBV1.1-CT10H-SIII-LIC	gattggaagtagaggttctctgctccttccaagaggctcct
M1	S174	pHTBV1.1-CT10H-SIII-LIC	gattggaagtagaggttctctgcggaagtgggtgggaaggg

TREM2 biotinylated constructs for antigen production			
H19	D131	pFB-Sec-Bio5	tatccacctttactgctgtctgccagcacctccac
H19	A138	pFB-Sec-Bio5	tatccacctttactgctagcatcccggtgatccag
H19	S174	pFB-Sec-Bio5	tatccacctttactgctggaagtgggtgggaaggg
TREM2 N79A glycosylation mutants			
H19	D137	pFB-Sec-NH	tatccacctttactgatcccggtgatccaggggtc
H19	R161	pFB-Sec-NH	tatccacctttactgtcacctggagatgctgtgctc
H19	G166	pFB-Sec-NH	tatccacctttactgtcatccttccaagaggctcct
T21	D137	pFB-Sec-NH	tatccacctttactgatcccggtgatccaggggtc
T21	R161	pFB-Sec-NH	tatccacctttactgtcacctggagatgctgtgctc
T21	G166	pFB-Sec-NH	tatccacctttactgtcatccttccaagaggctcct
H19	D131	pHTBV1.1-SecNH-Bio	tatccacctttactgctagcatcccggtgatccag
H19	S174	pHTBV1.1-SecNH-Bio	tatccacctttactgctggaagtgggtgggaaggg
TREM2 produced by Eisai for Expi293F			
H19	D131	pTT5	gatgggttgcgtagctgaaaccggtcacaacacca ccgtgttccagggcgt
H19	S174	pTT5-avi	Acggatctctagcgaattcaccatggagcctctgcg cctgctgatc
scFv-1-4: *E. coli* expression			
E1	K243	pNIC-MBP2-LIC	tacttccaatccatggaggtgcaattgttggagagc
scFv-1-4+avi-tag: *E. coli* expression			
E1	K243	pNIC-MBP2-LIC	tacttccaatccatggaggtgcaattgttggagagc
scFv-1-4: *Sf9* expression			
E1	K243	pFB-Sec-NH	tatccacctttactgtcatttgatctccagcttggt
control scFv: *Sf9* expression (SPRTNC)			
E1	K243	pFB-Sec-NH	tatccacctttactgtttgatctccagcttggt

Appendix Table 2. List of constructs and reverse primers used to generate insert.

Bibliography

Ajami, B., Bennett, J.L., Krieger, C., Tetzlaff, W., and Rossi, F.M. V (2007). Local self-renewal can sustain CNS microglia maintenance and function throughout adult life. Nat. Neurosci. *10*, 1538–1543.

Aldeghaither, D.S., Zahavi, D.J., Murray, J.C., Fertig, E.J., Graham, G.T., Zhang, Y.-W., O'Connell, A., Ma, J., Jablonski, S.A., and Weiner, L.M. (2019). A Mechanism of Resistance to Antibody-Targeted Immune Attack. Cancer Immunol. Res. *7*, 230–243.

Alsema, A.M., Jiang, Q., Kracht, L., Gerrits, E., Dubbelaar, M.L., Miedema, A., Brouwer, N., Hol, E.M., Middeldorp, J., van Dijk, R., et al. (2020). Profiling Microglia From Alzheimer's Disease Donors and Non-demented Elderly in Acute Human Postmortem Cortical Tissue. Front. Mol. Neurosci. *13*, 1–14.

Alzheimer, A. (1906). Über einen eigenartigen schweren Erkrankungsprozeβ der Hirnrincle. Neurol Cent. *25*, 1134.

Alzheimer, A., Stelzmann, R.A., Schnitzlein, H.N., and Murtagh, F.R. (1995). An English translation of Alzheimer's 1907 paper, "Uber eine eigenartige Erkankung der Hirnrinde". Clin. Anat. *8*, 429–431.

Andreone, B.J., Przybyla, L., Llapashtica, C., Rana, A., Davis, S.S., Lengerich, B. Van, Lin, K., Shi, J., Mei, Y., Astarita, G., et al. (2020). Alzheimer's-associated PLCγ2 is a signaling node required for both TREM2 function and the inflammatory response in human microglia. Nat. Neurosci. *23*, 927–938.

de Andrés, C., Teijeiro, R., Alonso, B., Sánchez-Madrid, F., Martínez, M.L., de Villoria, J.G., Fernández-Cruz, E., and Sánchez-Ramón, S. (2012). Long-Term Decrease in VLA-4 Expression and Functional Impairment of Dendritic Cells during Natalizumab Therapy in Patients with Multiple Sclerosis. PLoS One *7*, e34103.

Arboleda-Velasquez, J.F., Lopera, F., O'Hare, M., Delgado-Tirado, S., Marino, C., Chmielewska, N., Saez-Torres, K.L., Amarnani, D., Schultz, A.P., Sperling, R.A., et al. (2019). Resistance to autosomal dominant Alzheimer's disease in an APOE3 Christchurch homozygote: a case report. Nat. Med. *25*, 1680–1683.

Arndt, K.M., Müller, K.M., and Plückthun, A. (1998). Factors influencing the dimer to monomer transition of an antibody single-chain Fv fragment. Biochemistry *37*, 12918–12926.

Atagi, Y., Liu, C.-C., Painter, M.M., Chen, X.-F., Verbeeck, C., Zheng, H., Li, X., Rademakers, R., Kang, S.S., Xu, H., et al. (2015). Apolipoprotein E Is a Ligand for Triggering Receptor Expressed on Myeloid Cells 2 (TREM2). J. Biol. Chem. *290*, 26043–26050.

Babolmorad, G., Latif, A., Domingo, I.K., Pollock, N.M., Delyea, C., Rieger, A.M., Allison, W.T., and Bhavsar, A.P. (2021). Toll-like receptor 4 is activated by platinum and contributes to cisplatin-induced ototoxicity. EMBO Rep. *22*, 1–14.

Bailey, C.C., DeVaux, L.B., and Farzan, M. (2015). The Triggering Receptor Expressed on Myeloid Cells 2 Binds Apolipoprotein E. J. Biol. Chem. *290*, 26033–26042.

Baker, M. (2020). When antibodies mislead: the quest for validation. Nature *585*, 313–314.

Bause, E. (1983). Structural requirements of N-glycosylation of proteins. Studies with proline peptides as conformational probes. Biochem. J. *209*, 331–336.

Bemiller, S.M., McCray, T.J., Allan, K., Formica, S. V., Xu, G., Wilson, G., Kokiko-Cochran, O.N., Crish, S.D., Lasagna-Reeves, C.A., Ransohoff, R.M., et al. (2017). TREM2 deficiency exacerbates tau pathology through dysregulated kinase signaling in a mouse model of tauopathy. Mol. Neurodegener. *12*, 74.

Berner, D.K., Wessolowski, L., Armbrust, F., Schneppenheim, J., Schlepckow, K., Koudelka, T., Scharfenberg, F., Lucius, R., Tholey, A., Kleinberger, G., et al. (2020). Meprin β cleaves TREM2 and controls its phagocytic activity on macrophages. FASEB J. *34*, 6675–6687.

Bien-Ly, N., Yu, Y.J., Bumbaca, D., Elstrott, J., Boswell, C.A., Zhang, Y., Luk, W., Lu, Y., Dennis, M.S., Weimer, R.M., et al. (2014). Transferrin receptor (TfR) trafficking determines brain uptake of TfR antibody affinity variants. J. Exp. Med. *211*, 233–244.

Billadeau, D.D., and Leibson, P.J. (2002). ITAMs versus ITIMs: striking a balance during cell regulation. J. Clin. Invest. *109*, 161–168.

Bourquard, T., Musnier, A., Puard, V., Tahir, S., Ayoub, M.A., Jullian, Y., Boulo, T., Gallay, N., Watier, H., Bruneau, G., et al. (2018). MAbTope: A Method for Improved Epitope Mapping. J. Immunol. *201*, 3096–3105.

Boza-Serrano, A., Ruiz, R., Sanchez-Varo, R., García-Revilla, J., Yang, Y., Jimenez-Ferrer, I., Paulus, A., Wennström, M., Vilalta, A., Allendorf, D., et al. (2019). Galectin-3, a novel endogenous TREM2 ligand, detrimentally regulates inflammatory response in Alzheimer's disease. Acta Neuropathol. *138*, 251–273.

Braak, H., and Braak, E. (1991). Neuropathological stageing of Alzheimer-related changes. Acta Neuropathol. *82*, 239–259.

Bricogne, G., Blanc, E., Brandl, M., Flensburg, C., Keller, P., Paciorek, W., Roversi, P., Sharff, A., Smart, O.S., Vonrhein, C., et al. (2016). BUSTER version

X.Y.Z. Cambridge, United Kingdom Glob. Phasing Ltd.

Bruce, D., Cardew, E., Freitag-Pohl, S., and Pohl, E. (2019). How to Stabilize Protein: Stability Screens for Thermal Shift Assays and Nano Differential Scanning Fluorimetry in the Virus-X Project. J. Vis. Exp.

Bruttger, J., Karram, K., Wörtge, S., Regen, T., Marini, F., Hoppmann, N., Klein, M., Blank, T., Yona, S., Wolf, Y., et al. (2015). Genetic Cell Ablation Reveals Clusters of Local Self-Renewing Microglia in the Mammalian Central Nervous System. Immunity *43*, 92–106.

Buchan, D.W.A., and Jones, D.T. (2019). The PSIPRED Protein Analysis Workbench: 20 years on. Nucleic Acids Res. *47*, W402–W407.

Buée, L., Bussière, T., Buée-Scherrer, V., Delacourte, A., and Hof, P.R. (2000). Tau protein isoforms, phosphorylation and role in neurodegenerative disorders11These authors contributed equally to this work. Brain Res. Rev. *33*, 95–130.

Byrne, N.J., Lee, A.C., Kostas, J., Reid, J.C., Partridge, A.T., So, S.S., Cowan, J.E., Abeywickrema, P., Huang, H., Zebisch, M., et al. (2021). Development of a robust crystallization platform for immune receptor TREM2 using a crystallization chaperone strategy. Protein Expr. Purif. *179*, 105796.

Cacace, R., Sleegers, K., and Van Broeckhoven, C. (2016). Molecular genetics of early-onset Alzheimer's disease revisited. Alzheimer's Dement. *12*, 733–748.

Cai, Y., Zhang, J., Lao, X., Jiang, H., Yu, Y., Deng, Y., Zhong, J., Liang, Y., Xiong, L., and Deng, N. (2016). Construction of a disulfide-stabilized diabody against fibroblast growth factor-2 and the inhibition activity in targeting breast cancer. Cancer Sci. *107*, 1141–1150.

Call, M.E. (2010). The structural basis for intramembrane assembly of an

activating immunoreceptor complex. Nat. Immunlogy *11*, 1023–1031.

Campion, D., Dumanchin, C., Hannequin, D., Dubois, B., Belliard, S., Puel, M., Thomas-Anterion, C., Michon, A., Martin, C., Charbonnier, F., et al. (1999). Early-onset autosomal dominant Alzheimer disease: Prevalence, genetic heterogeneity, and mutation spectrum. Am. J. Hum. Genet. *65*, 664–670.

Carrasco, K., Boufenzer, A., Jolly, L., Le Cordier, H., Wang, G., Heck, A.J., Cerwenka, A., Vinolo, E., Nazabal, A., Kriznik, A., et al. (2019). TREM-1 multimerization is essential for its activation on monocytes and neutrophils. Cell. Mol. Immunol. *16*, 460–472.

Castellano, J.M., Kim, J., Stewart, F.R., Jiang, H., DeMattos, R.B., Patterson, B.W., Fagan, A.M., Morris, J.C., Mawuenyega, K.G., Cruchaga, C., et al. (2011). Human apoE isoforms differentially regulate brain amyloid-β peptide clearance. Sci Transl Med *3*, 89ra57.

Chang, V.T., Crispin, M., Aricescu, A.R., Harvey, D.J., Nettleship, J.E., Fennelly, J.A., Yu, C., Boles, K.S., Evans, E.J., Stuart, D.I., et al. (2007). Glycoprotein Structural Genomics: Solving the Glycosylation Problem. Structure *15*, 267–273.

Chari, A., Haselbach, D., Kirves, J.M., Ohmer, J., Paknia, E., Fischer, N., Ganichkin, O., Möller, V., J Frye, J., Petzold, G., et al. (2015). ProteoPlex: Stability optimization of macromolecular complexes by sparse-matrix screening of chemical space. Nat. Methods *12*, 859–865.

Chastagner, P., Rubinstein, E., and Brou, C. (2017). Ligand-activated Notch undergoes DTX4-mediated ubiquitylation and bilateral endocytosis before ADAM10 processing. Sci. Signal. *10*, eaag2989.

Cheng, Q., Danao, J., Talreja, S., Wen, P., Yin, J., Sun, N., Li, C.M., Chui, D., Tran, D., Koirala, S., et al. (2018). TREM2-activating antibodies abrogate the negative

pleiotropic effects of the Alzheimer's disease variant Trem2R47Hon murine myeloid cell function. J. Biol. Chem. *293*, 12620–12633.

Chodorge, M., Züger, S., Stirnimann, C., Briand, C., Jermutus, L., Grütter, M.G., and Minter, R.R. (2012). A series of Fas receptor agonist antibodies that demonstrate an inverse correlation between affinity and potency. Cell Death Differ. *19*, 1187–1195.

Cignarella, F., Filipello, F., Bollman, B., Cantoni, C., Locca, A., Mikesell, R., Manis, M., Ibrahim, A., Deng, L., Benitez, B.A., et al. (2020). TREM2 activation on microglia promotes myelin debris clearance and remyelination in a model of multiple sclerosis. Acta Neuropathol. *140*, 513–534.

Ciryam, P., Kundra, R., Freer, R., Morimoto, R.I., Dobson, C.M., and Vendruscolo, M. (2016). A transcriptional signature of Alzheimer's disease is associated with a metastable subproteome at risk for aggregation. Proc. Natl. Acad. Sci. U. S. A. *113*, 4753–4758.

Citron, M., Westaway, D., Xia, W., Carlson, G., Diehl, T., Levesque, G., Johnson-wood, K., Lee, M., Seubert, P., Davis, A., et al. (1997). Mutant presenilins of Alzheimer's disease increase production of 42-residue amyloid β-protein in both transfected cells and transgenic mice. Nat. Med. *3*, 67–72.

Condello, C., Yuan, P., Schain, A., and Grutzendler, J. (2015). Microglia constitute a barrier that prevents neurotoxic protofibrillar Aβ42 hotspots around plaques. Nat. Commun. *6*, 6176.

Corder, E., Saunders, A., Strittmatter, W., Schmechel, D., Gaskell, P., Small, G., Roses, A., Haines, J., and Pericak-Vance, M. (1993). Gene dose of apolipoprotein E type 4 allele and the risk of Alzheimer's disease in late onset families. Science (80-.). *261*, 921–923.

Cosker, K., Mallach, A., Limaye, J., Piers, T.M., Staddon, J., Neame, S.J., Hardy,

J., and Pocock, J.M. (2021). Microglial signalling pathway deficits associated with the patient derived R47H TREM2 variants linked to AD indicate inability to activate inflammasome. Sci. Rep. *11*, 13316.

Cunningham, C.L., Mart\'\inez-Cerdeño, V., and Noctor, S.C. (2013). Microglia Regulate the Number of Neural Precursor Cells in the Developing Cerebral Cortex. J. Neurosci. *33*, 4216–4233.

Dagert, M., and Ehrlich, S.D. (1979). Prolonged incubation in calcium chloride improves the competence of Escherichia coli cells. Gene *6*, 23–28.

Dash, P.K., and Moore, A.N. (1995). Enhanced processing of APP induced by IL-1 beta can be reduced by indomethacin and nordihydroguaiaretic acid. Biochem. Biophys. Res. Commun. *208*, 542–548.

Davalos, D., Grutzendler, J., Yang, G., Kim, J. V., Zuo, Y., Jung, S., Littman, D.R., Dustin, M.L., and Gan, W.-B. (2005). ATP mediates rapid microglial response to local brain injury in vivo. Nat. Neurosci. *8*, 752–758.

Davis, S.J., and Crispin, M. (2010). Solutions to the Glycosylation Problem for Low- and High-Throughput Structural Glycoproteomics. In Functional and Structural Proteomics of Glycoproteins, (Dordrecht: Springer Netherlands), pp. 127–158.

Daws, M.R., Sullam, P.M., Niemi, E.C., Chen, T.T., Tchao, N.K., and Seaman, W.E. (2003). Pattern Recognition by TREM-2: Binding of Anionic Ligands. J. Immunol. *171*, 594–599.

De, S., Wirthensohn, D.C., Flagmeier, P., Hughes, C., Aprile, F.A., Ruggeri, F.S., Whiten, D.R., Emin, D., Xia, Z., Varela, J.A., et al. (2019). Different soluble aggregates of Aβ42 can give rise to cellular toxicity through different mechanisms. Nat. Commun. *10*, 1541.

Dean, H.B., Roberson, E.D., and Song, Y. (2019). Neurodegenerative Disease–Associated Variants in TREM2 Destabilize the Apical Ligand-Binding Region of the Immunoglobulin Domain. Front. Neurol. *10*, 1–15.

Deczkowska, A., Keren-Shaul, H., Weiner, A., Colonna, M., Schwartz, M., and Amit, I. (2018). Disease-Associated Microglia: A Universal Immune Sensor of Neurodegeneration. Cell *173*, 1073–1081.

Donnelly, R.J., Friedhoff, A.J., Beer, B., Blume, A.J., and Vitek, M.P. (1990). Interleukin-1 stimulates the beta-amyloid precursor protein promoter. Cell. Mol. Neurobiol. *10*, 485–495.

Duan, Y., Sahley, C.L., and Muller, K.J. (2009). ATP and NO dually control migration of microglia to nerve lesions. Dev. Neurobiol. *69*, 60–72.

Efthymiou, A.G., and Goate, A.M. (2017). Late onset Alzheimer's disease genetics implicates microglial pathways in disease risk. Mol. Neurodegener. *12*, 1–12.

Ellgaard, L. (1999). Setting the Standards: Quality Control in the Secretory Pathway. Science (80-.). *286*, 1882–1888.

Ellwanger, D.C., Wang, S., Brioschi, S., Shao, Z., Green, L., Case, R., Yoo, D., Weishuhn, D., Rathanaswami, P., Bradley, J., et al. (2021). Prior activation state shapes the microglia response to antihuman TREM2 in a mouse model of Alzheimer's disease. Proc. Natl. Acad. Sci. *118*, e2017742118.

Emsley, P., Lohkamp, B., Scott, W.G., and Cowtan, K. (2010). Features and development of Coot. Acta Crystallogr. Sect. D Biol. Crystallogr. *75*, 861–877.

Escott-Price, V., Sims, R., Bannister, C., Harold, D., Vronskaya, M., Majounie, E., Badarinarayan, N., Morgan, K., Passmore, P., Holmes, C., et al. (2015). Common polygenic variation enhances risk prediction for Alzheimer's disease. Brain *138*, 3673–

3684.

Evans, P. (2006). Scaling and assessment of data quality. Acta Crystallogr. D. Biol. Crystallogr. *62*, 72–82.

Ewers, M., Franzmeier, N., Suárez-Calvet, M., Morenas-Rodriguez, E., Caballero, M.A.A., Kleinberger, G., Piccio, L., Cruchaga, C., Deming, Y., Dichgans, M., et al. (2019). Increased soluble TREM2 in cerebrospinal fluid is associated with reduced cognitive and clinical decline in Alzheimer's disease. Sci. Transl. Med. *11*, eaav6221.

Ewert, S., Huber, T., Honegger, A., and Plückthun, A. (2003). Biophysical Properties of Human Antibody Variable Domains. J. Mol. Biol. *325*, 531–553.

Fairhead, M., Preger, C., Wigren, E., Strain-Damerell, C., Ossipova, E., Ye, M., Makola, M., Burgess-Brown, N.A., Persson, H., von Delft, F., et al. (2019). Strategies to improve scFvs as crystallization chaperones suggested by analysis of a complex with the human PHD-bromodomain SP140. BioRxiv.

Fassler, M., Rappaport, M.S., Cuño, C.B., and George, J. (2021). Engagement of TREM2 by a novel monoclonal antibody induces activation of microglia and improves cognitive function in Alzheimer's disease models. J. Neuroinflammation *18*, 1–18.

Feng, J., Garrity, D., Call, M.E., Moffett, H., and Wucherpfennig, K.W. (2005). Convergence on a Distinctive Assembly Mechanism by Unrelated Families of Activating Immune Receptors. Immunity *22*, 427–438.

Feuerbach, D., Schindler, P., Barske, C., Joller, S., Beng-Louka, E., Worringer, K.A., Kommineni, S., Kaykas, A., Ho, D.J., Ye, C., et al. (2017). ADAM17 is the main sheddase for the generation of human triggering receptor expressed in myeloid cells (hTREM2) ectodomain and cleaves TREM2 after Histidine 157. Neurosci. Lett. *660*, 109–114.

Fitz, N.F., Nam, K.N., Wolfe, C.M., Letronne, F., Playso, B.E., Iordanova, B.E., Kozai, T.D.Y., Biedrzycki, R.J., Kagan, V.E., Tyurina, Y.Y., et al. (2021). Phospholipids of APOE lipoproteins activate microglia in an isoform-specific manner in preclinical models of Alzheimer's disease. Nat. Commun. *12*, 1–18.

Garcia, K.C., Degano, M., Stanfield, R.L., Brunmark, A., Jackson, M.R., Peterson, P.A., Teyton, L., and Wilson, I.A. (1996). An alphabeta T cell receptor structure at 2.5 A and its orientation in the TCR-MHC complex. Science *274*, 209–219.

Gatz, M., Reynolds, C.A., Fratiglioni, L., Johansson, B., Mortimer, J.A., Berg, S., Fiske, A., and Pedersen, N.L. (2006). Role of Genes and Environments for Explaining Alzheimer Disease. Arch. Gen. Psychiatry *63*, 168–174.

Gehrmann, J., Mies, G., Bonnekoh, P., Banati, R., Iijima, T., Kreutzberg, G.W., and Hossmann, K. (1993). Microglial Reaction in the Rat Cerebral Cortex Induced by Cortical Spreading Depression. Brain Pathol. *3*, 11–17.

Ginhoux, F., Greter, M., Leboeuf, M., Nandi, S., See, P., Gokhan, S., Mehler, M.F., Conway, S.J., Ng, L.G., Stanley, E.R., et al. (2010). Fate mapping analysis reveals that adult microglia derive from primitive macrophages. Science *330*, 841–845.

Goddard, T.D., Huang, C.C., Meng, E.C., Pettersen, E.F., Couch, G.S., Morris, J.H., and Ferrin, T.E. (2018). UCSF ChimeraX: Meeting modern challenges in visualization and analysis. Protein Sci. *27*, 14–25.

Gómez-Isla, T., Hollister, R., West, H., Mui, S., Growdon, J.H., Petersen, R.C., Parisi, J.E., and Hyman, B.T. (1997). Neuronal loss correlates with but exceeds neurofibrillary tangles in Alzheimer's disease. Ann. Neurol. *41*, 17–24.

Gomez-Nicola, D., and Perry, V.H. (2015). Microglial dynamics and role in the healthy and diseased brain: A paradigm of functional plasticity. Neuroscientist *21*, 169–184.

Gomez-Nicola, D., Fransen, N.L., Suzzi, S., and Perry, V.H. (2013). Regulation of Microglial Proliferation during Chronic Neurodegeneration. J. Neurosci. *33*, 2481–2493.

Gosselin, D., Skola, D., Coufal, N.G., Holtman, I.R., Schlachetzki, J.C.M., Sajti, E., Jaeger, B.N., O'Connor, C., Fitzpatrick, C., Pasillas, M.P., et al. (2017). An environment-dependent transcriptional network specifies human microglia identity. Science (80-.). *356*, eaal3222.

Gouna, G., Klose, C., Bosch-Queralt, M., Liu, L., Gokce, O., Schifferer, M., Cantuti-Castelvetri, L., and Simons, M. (2021). TREM2-dependent lipid droplet biogenesis in phagocytes is required for remyelination. J. Exp. Med. *218*.

Graeber, M.B., Tetzlaff, W., Streit, W.J., and Kreutzberg, G.W. (1988). Microglial cells but not astrocytes undergo mitosis following rat facial nerve axotomy. Neurosci. Lett. *85*, 317–321.

Graille, M., Stura, E.A., Corper, A.L., Sutton, B.J., Taussig, M.J., Charbonnier, J.-B., and Silverman, G.J. (2000). Crystal structure of a Staphylococcus aureus protein A domain complexed with the Fab fragment of a human IgM antibody: Structural basis for recognition of B-cell receptors and superantigen activity. Proc. Natl. Acad. Sci. *97*, 5399–5404.

Griffin, L., and Lawson, A. (2011). Antibody fragments as tools in crystallography. Clin. Exp. Immunol. *165*, 285–291.

Griffin, W.S.T., Stanley, L.C., Ling, C., White, L., MacLeod, V., Perrot, L.J., White, C.L., and Araoz, C. (1989). Brain interleukin 1 and S-100 immunoreactivity are elevated in Down syndrome and Alzheimer disease. Proc. Natl. Acad. Sci. *86*, 7611–7615.

Guerreiro, R., Wojtas, A., Bras, J., Carrasquillo, M., Rogaeva, E., Majounie, E.,

Cruchaga, C., Sassi, C., Kauwe, J.S.K., Younkin, S., et al. (2013). *TREM2* Variants in Alzheimer's Disease. N. Engl. J. Med. *368*, 117–127.

Guo, Y., Wang, Q., Chen, S., and Xu, C. (2021). Functions of amyloid precursor protein in metabolic diseases. Metabolism. *115*, 154454.

Gyun, J.S., Jones, B.W., and Hinkle, P.M. (2007). Dimerization of the thyrotropin-releasing hormone receptor potentiates hormone-dependent receptor phosphorylation. Proc. Natl. Acad. Sci. U. S. A. *104*, 18303–18308.

Haass, C., and Selkoe, D.J. (2007). Soluble protein oligomers in neurodegeneration: Lessons from the Alzheimer's amyloid β-peptide. Nat. Rev. Mol. Cell Biol. *8*, 101–112.

Hakola, H.P. (1972). Neuropsychiatric and genetic aspects of a new hereditary disease characterized by progressive dementia and lipomembranous polycystic osteodysplasia. Acta Psychiatr. Scand. Suppl. *232*, 1–173.

Halaby, D.M., and Mornon, J.P.E. (1998). The immunoglobulin superfamily: An insight on its tissular, species, and functional diversity. J. Mol. Evol. *46*, 389–400.

Hall-Roberts, H., Agarwal, D., Obst, J., Smith, T.B., Monzón-Sandoval, J., Di Daniel, E., Webber, C., James, W.S., Mead, E., Davis, J.B., et al. (2020). TREM2 Alzheimer's variant R47H causes similar transcriptional dysregulation to knockout, yet only subtle functional phenotypes in human iPSC-derived macrophages. Alzheimer's Res. Ther. *12*, 1–27.

Hamerman, J.A., Jarjoura, J.R., Beth, M., Nakamura, M.C., Seaman, W.E., Lanier, L.L., and Trem, M.C. (2006). Cutting Edge: Inhibition of TLR and FcR Responses in Macrophages by Triggering Receptor Expressed on Myeloid Cells (TREM)-2 and DAP12. J Immunol *177*, 2051–2055.

Hao, M., and Maxfield, F.R. (2000). Characterization of Rapid Membrane Internalization and Recycling. J. Biol. Chem. *275*, 15279–15286.

Hardy, J. (2019). Failures in Protein Clearance Partly Underlie Late Onset Neurodegenerative Diseases and Link Pathology to Genetic Risk. Front. Neurosci. *13*, 1–4.

Hebert, L.E., Weuve, J., Scherr, P.A., and Evans, D.A. (2013). Alzheimer disease in the United States (2010-2050) estimated using the 2010 census. Neurology *80*, 1778–1783.

Hegde, R.S., and Bernstein, H.D. (2006). The surprising complexity of signal sequences. Trends Biochem. Sci. *31*, 563–571.

Held, D. (2018). Tips & Tricks GPC/ SEC: What Are the Differences Between GPC, SEC, and GFC, and How Do You Get Started with the Technique? The Column *14*, 2–8.

Hentrich, C., Ylera, F., Frisch, C., Ten Haaf, A., and Knappik, A. (2018). Chapter 3 - Monoclonal Antibody Generation by Phage Display: History, State-of-the-Art, and Future. S.K. Vashist, and J.H.T.B.T.-H. of I.T. Luong, eds. (Academic Press), pp. 47–80.

Holliger, P., and Hudson, P.J. (2005). Engineered antibody fragments and the rise of single domains. Nat. Biotechnol. *23*, 1126–1136.

Holmes, C., and Butchart, J. (2011). Systemic inflammation and Alzheimer's disease. Biochem. Soc. Trans. *39*, 898–901.

Hong, J.J., Yankee, T.M., Harrison, M.L., and Geahlen, R.L. (2002). Regulation of Signaling in B Cells through the Phosphorylation of Syk on Linker Region Tyrosines. J. Biol. Chem. *27t*, 31703–31714.

Hoozemans, J.J.M., Veerhuis, R., Rozemuller, J.M., and Eikelenboom, P. (2011). Soothing the inflamed brain: effect of non-steroidal anti-inflammatory drugs on Alzheimer's disease pathology. CNS Neurol. Disord. Drug Targets *10*, 57–67.

Hou, P., Araujo, E., Zhao, T., Zhang, M., Massenburg, D., Veselits, M., Doyle, C., Dinner, A.R., and Clark, M.R. (2006). B cell antigen receptor signaling and internalization are mutually exclusive events. PLoS Biol. *4*, 1147–1158.

Hsieh, C.L., Koike, M., Spusta, S.C., Niemi, E.C., Yenari, M., Nakamura, M.C., and Seaman, W.E. (2009). A role for TREM2 ligands in the phagocytosis of apoptotic neuronal cells by microglia. J. Neurochem. *109*, 1144–1156.

Huang, L.K., Chao, S.P., and Hu, C.J. (2020). Clinical trials of new drugs for Alzheimer disease. J. Biomed. Sci. *27*, 1–13.

Huang, Y., Happonen, K.E., Burrola, P.G., O'Connor, C., Hah, N., Huang, L., Nimmerjahn, A., and Lemke, G. (2021). Microglia use TAM receptors to detect and engulf amyloid β plaques. Nat. Immunol. *22*, 586–594.

Huynh, T.-P. V, Liao, F., Francis, C.M., Robinson, G.O., Serrano, J.R., Jiang, H., Roh, J., Finn, M.B., Sullivan, P.M., Esparza, T.J., et al. (2017). Age-Dependent Effects of apoE Reduction Using Antisense Oligonucleotides in a Model of β-amyloidosis. Neuron *96*, 1013-1023.e4.

Ibach, M., Mathews, M., Linnartz-Gerlach, B., Theil, S., Kumar, S., Feederle, R., Brüstle, O., Neumann, H., and Walter, J. (2021). A reporter cell system for the triggering receptor expressed on myeloid cells 2 reveals differential effects of disease-associated variants on receptor signaling and activation by antibodies against the stalk region. Glia *69*, 1126–1139.

Jack, C.R.J., Knopman, D.S., Jagust, W.J., Petersen, R.C., Weiner, M.W., Aisen, P.S., Shaw, L.M., Vemuri, P., Wiste, H.J., Weigand, S.D., et al. (2013). Tracking

pathophysiological processes in Alzheimer's disease: an updated hypothetical model of dynamic biomarkers. Lancet. Neurol. *12*, 207–216.

Jamart-gre, B., Pannecouque, C., and Clercq, E. De (2009). Dimer Disruption and Monomer Sequestration by Alkyl Tripeptides Are Successful Strategies for Inhibiting Wild-Type and Multidrug-Resistant Mutated HIV-1. 379–387.

Jansen, I.E., Savage, J.E., Watanabe, K., Bryois, J., Williams, D.M., Steinberg, S., Sealock, J., Karlsson, I.K., Hägg, S., Athanasiu, L., et al. (2019). Genome-wide meta-analysis identifies new loci and functional pathways influencing Alzheimer's disease risk. Nat. Genet. *51*, 404–413.

Jay, T.R., Miller, C.M., Cheng, P.J., Graham, L.C., Bemiller, S., Broihier, M.L., Xu, G., Margevicius, D., Karlo, J.C., Sousa, G.L., et al. (2015). TREM2 deficiency eliminates TREM2+ inflammatory macrophages and ameliorates pathology in Alzheimer's disease mouse models. J. Exp. Med. *212*, 287–295.

Jay, T.R., von Saucken, V.E., and Landreth, G.E. (2017a). TREM2 in Neurodegenerative Diseases. Mol. Neurodegener. *12*, 56.

Jay, T.R., Hirsch, A.M., Broihier, M.L., Miller, C.M., Neilson, L.E., Ransohoff, R.M., Lamb, B.T., and Landreth, G.E. (2017b). Disease Progression-Dependent Effects of TREM2 Deficiency in a Mouse Model of Alzheimer's Disease. J. Neurosci. *37*, 637–647.

Jendresen, C., Årskog, V., Daws, M.R., and Nilsson, L.N.G. (2017). The Alzheimer's disease risk factors apolipoprotein E and TREM2 are linked in a receptor signaling pathway. J. Neuroinflammation *14*, 59.

Jennifer, L. (2005). Post-crystallization treatments for improving diffraction quality of protein crystals. 1173–1180.

Ji, K.Y., Kim, S.M., Yee, S.M., Kim, M.J., Ban, Y.J., Kim, E.M., Lee, E.H., Choi, H.R., Yun, H., Lee, C.W., et al. (2021). Cyclophilin A is an endogenous ligand for the triggering receptor expressed on myeloid cells-2 (TREM2). FASEB J. *35*, 1–12.

Ji, Z.S., Fazio, S., and Mahley, R.W. (1994). Variable heparan sulfate proteoglycan binding of apolipoprotein E variants may modulate the expression of type III hyperlipoproteinemia. J Biol Chem *269*, 13421–13428.

Jiang, T., Tan, L., Chen, Q., Tan, M.S., Zhou, J.S., Zhu, X.C., Lu, H., Wang, H.F., Zhang, Y.D., and Yu, J.T. (2016). A rare coding variant in TREM2 increases risk for Alzheimer's disease in Han Chinese. Neurobiol. Aging *42*, 217.e1-217.e3.

Jin, M., Shepardson, N., Yang, T., Chen, G., Walsh, D., and Selkoe, D.J. (2011). Soluble amyloid β-protein dimers isolated from Alzheimer cortex directly induce Tau hyperphosphorylation and neuritic degeneration. Proc. Natl. Acad. Sci. U. S. A. *108*, 5819–5824.

Jin, S.C., Benitez, B.A., Karch, C.M., Cooper, B., Skorupa, T., Carrell, D., Norton, J.B., Hsu, S., Harari, O., Cai, Y., et al. (2014). Coding variants in TREM2 increase risk for Alzheimer's disease. Hum. Mol. Genet. *23*, 5838–5846.

Jones, D.T. (1999). Protein secondary structure prediction based on position-specific scoring matrices. J. Mol. Biol. *292*, 195–202.

Jones, L., Holmans, P.A., Hamshere, M.L., Harold, D., Moskvina, V., Ivanov, D., Pocklington, A., Abraham, R., Hollingworth, P., Sims, R., et al. (2010). Genetic evidence implicates the immune system and cholesterol metabolism in the aetiology of Alzheimer's disease. PLoS One *5*.

Jonsson, T., Atwal, J.K., Steinberg, S., Snaedal, J., Jonsson, P. V., Bjornsson, S., Stefansson, H., Sulem, P., Gudbjartsson, D., Maloney, J., et al. (2012). A mutation in APP protects against Alzheimer's disease and age-related cognitive decline. Nature

488, 96–99.

Jonsson, T., Stefansson, H., Steinberg, S., Jonsdottir, I., Jonsson, P. V, Snaedal, J., Bjornsson, S., Huttenlocher, J., Levey, A.I., Lah, J.J., et al. (2013). Variant of TREM2 associated with the risk of Alzheimer's disease. N Engl J Med *368*, 107–116.

Julian, M.C., Lee, C.C., Tiller, K.E., Rabia, L.A., Day, E.K., Schick, A.J., and Tessier, P.M. (2015). Co-evolution of affinity and stability of grafted amyloid-motif domain antibodies. Protein Eng. Des. Sel. *28*, 339–350.

Julian, M.C., Li, L., Garde, S., Wilen, R., and Tessier, P.M. (2017). Efficient affinity maturation of antibody variable domains requires co-selection of compensatory mutations to maintain thermodynamic stability. Sci. Rep. *7*, 45259.

Jun, G., Ibrahim-Verbaas, C.A., Vronskaya, M., Lambert, J.-C., Chung, J., Naj, A.C., Kunkle, B.W., Wang, L.-S., Bis, J.C., Bellenguez, C., et al. (2016). A novel Alzheimer disease locus located near the gene encoding tau protein. Mol. Psychiatry *21*, 108–117.

Kabsch, W., T., B.A., K., D., A., K.P., K., D., S., M., G., R.R.B., P., E., S., F., K., W., et al. (2010). *XDS*. Acta Crystallogr. Sect. D Biol. Crystallogr.

Kang, J., Lemaire, H.G., Unterbeck, A., Salbaum, J.M., Masters, C.L., Grzeschik, K.H., Multhaup, G., Beyreuther, K., and Müller-Hill, B. (1987). The precursor of Alzheimer's disease amyloid A4 protein resembles a cell-surface receptor. Nature *325*, 733–736.

van der Kant, R., Langness, V.F., Herrera, C.M., Williams, D.A., Fong, L.K., Leestemaker, Y., Steenvoorden, E., Rynearson, K.D., Brouwers, J.F., Helms, J.B., et al. (2019). Cholesterol Metabolism Is a Druggable Axis that Independently Regulates Tau and Amyloid-β in iPSC-Derived Alzheimer's Disease Neurons. Cell Stem Cell *24*, 363-375.e9.

Kantardjieff, K.A., and Rupp, B. (2003). Matthews coefficient probabilities: Improved estimates for unit cell contents of proteins, DNA, and protein-nucleic acid complex crystals. Protein Sci. *12*, 1865–1871.

Karch, C.M., and Goate, A.M. (2015). Alzheimer's Disease Risk Genes and Mechanisms of Disease Pathogenesis. Biol. Psychiatry *77*, 43–51.

Kelker, M.S., Foss, T.R., Peti, W., Teyton, L., Kelly, J.W., Wüthrich, K., and Wilson, I.A. (2004). Crystal structure of human triggering receptor expressed on myeloid cells 1 (TREM-1) at 1.47 A. J. Mol. Biol. *342*, 1237–1248.

Keren-Shaul, H., Spinrad, A., Weiner, A., Matcovitch-Natan, O., Dvir-Szternfeld, R., Ulland, T.K., David, E., Baruch, K., Lara-Astaiso, D., Toth, B., et al. (2017). A Unique Microglia Type Associated with Restricting Development of Alzheimer's Disease. Cell *169*, 1276-1290.e17.

Kim, H.-J., Cho, M.-H., Shim, W.H., Kim, J.K., Jeon, E.-Y., Kim, D.-H., and Yoon, S.-Y. (2017). Deficient autophagy in microglia impairs synaptic pruning and causes social behavioral defects. Mol. Psychiatry *22*, 1576–1584.

Kim, J., Onstead, L., Randle, S., Price, R., Smithson, L., Zwizinski, C., Dickson, D.W., Golde, T., and McGowan, E. (2007). Abeta40 inhibits amyloid deposition in vivo. J. Neurosci. *27*, 627–633.

Kim, J.H., Song, D.H., Youn, S.J., Kim, J.W., Cho, G., Kim, S.C., Lee, H., Jin, M.S., and Lee, J.O. (2016). Crystal structures of mono- and bi-specific diabodies and reduction of their structural flexibility by introduction of disulfide bridges at the Fv interface. Sci. Rep. *6*, 1–12.

Kim, T., Vidal, G.S., Djurisic, M., William, C.M., Birnbaum, M.E., Garcia, K.C., Hyman, B.T., and Shatz, C.J. (2013). Human LilrB2 Is a -Amyloid Receptor and Its Murine Homolog PirB Regulates Synaptic Plasticity in an Alzheimer's Model. Science

(80-.). *341*, 1399–1404.

Kleinberger, G., Yamanishi, Y., Suarez-Calvet, M., Czirr, E., Lohmann, E., Cuyvers, E., Struyfs, H., Pettkus, N., Wenninger-Weinzierl, A., Mazaheri, F., et al. (2014). TREM2 mutations implicated in neurodegeneration impair cell surface transport and phagocytosis. Sci. Transl. Med. *6*, 243ra86-243ra86.

Kleinberger, G., Brendel, M., Mracsko, E., Wefers, B., Groeneweg, L., Xiang, X., Focke, C., Deussing, M., Suarez-Calvet, M., Mazaheri, F., et al. (2017). The FTD-like syndrome causing TREM2 T66M mutation impairs microglia function, brain perfusion, and glucose metabolism. EMBO J. *36*, 1837–1853.

Knobich, K. (2015). transmembrane complexes of DAP12 crystallised in lipid membranes provide insights into control of oligomerization in immunoreceptor assembly. Cell Rep. 1184–1192.

Kober, D.L., and Brett, T.J. (2017). TREM2-Ligand Interactions in Health and Disease. J Mol Biol *429*, 1607–1629.

Kober, D.L., Wanhainen, K.M., Johnson, B.M., Randolph, D.T., Holtzman, M.J., and Brett, T.J. (2014). Preparation, crystallization, and preliminary crystallographic analysis of wild-type and mutant human TREM-2 ectodomains linked to neurodegenerative and inflammatory diseases. Protein Expr. Purif. *96*, 32–38.

Kober, D.L., Alexander-Brett, J.M., Karch, C.M., Cruchaga, C., Colonna, M., Holtzman, M.J., and Brett, T.J. (2016). Neurodegenerative disease mutations in TREM2 reveal a functional surface and distinct loss-of-function mechanisms. Elife *5*, e20391.

Kober, D.L., Stuchell-Brereton, M.D., Kluender, C.E., Dean, H.B., Strickland, M.R., Steinberg, D.F., Nelson, S.S., Baban, B., Holtzman, D.M., Frieden, C., et al. (2020). Functional insights from biophysical study of TREM2 interactions with apoE and Aβ(1-42). Alzheimers. Dement.

Kober, D.L., Stuchell-Brereton, M.D., Kluender, C.E., Dean, H.B., Strickland, M.R., Steinberg, D.F., Nelson, S.S., Baban, B., Holtzman, D.M., Frieden, C., et al. (2021). Functional insights from biophysical study of TREM2 interactions with apoE and Aβ 1-42. Alzheimer's Dement. *17*, 475–488.

Köhler, G., and Milstein, C. (1975). Continuous cultures of fused cells secreting antibody of predefined specificity. Nature *256*, 495–497.

Korbie, D.J., and Mattick, J.S. (2008). Touchdown PCR for increased specificity and sensitivity in PCR amplification. Nat. Protoc. *3*, 1452–1456.

Kortt, A.A., Dolezal, O., Power, B.E., and Hudson, P.J. (2001). Dimeric and trimeric antibodies: High avidity scFvs for cancer targeting. Biomol. Eng. *18*, 95–108.

Kotzsch, A., Vernet, E., Hammarström, M., Berthelsen, J., Weigelt, J., Gräslund, S., and Sundström, M. (2011). A secretory system for bacterial production of high-profile protein targets. Protein Sci. *20*, 597–609.

Krasemann, S., Madore, C., Cialic, R., Baufeld, C., Calcagno, N., El Fatimy, R., Beckers, L., O'Loughlin, E., Xu, Y., Fanek, Z., et al. (2017). The TREM2-APOE Pathway Drives the Transcriptional Phenotype of Dysfunctional Microglia in Neurodegenerative Diseases. Immunity *47*, 566-581.e9.

Krissinel, E., and Henrick, K. (2007). Inference of Macromolecular Assemblies from Crystalline State. J. Mol. Biol. *372*, 774–797.

Kunkle, B.W., Grenier-Boley, B., Sims, R., Bis, J.C., Damotte, V., Naj, A.C., Boland, A., Vronskaya, M., van der Lee, S.J., Amlie-Wolf, A., et al. (2019). Genetic meta-analysis of diagnosed Alzheimer's disease identifies new risk loci and implicates Aβ, tau, immunity and lipid processing. Nat. Genet. *51*, 414–430.

Lambert, J.C., Ibrahim-Verbaas, C.A., Harold, D., Naj, A.C., Sims, R.,

Bellenguez, C., Jun, G., DeStefano, A.L., Bis, J.C., Beecham, G.W., et al. (2013). Meta-analysis of 74,046 individuals identifies 11 new susceptibility loci for Alzheimer's disease. Nat. Genet. *45*, 1452–1458.

Lanier, L.L., Corliss, B.C., Wu, J., Leong, C., and Phillips, J.H. (1998). Immunoreceptor DAP12 bearing a tyrosine-based activation motif is involved in activating NK cells. Nature *391*, 703–707.

Lee, C.Y.D., Daggett, A., Gu, X., Jiang, L.L., Langfelder, P., Li, X., Wang, N., Zhao, Y., Park, C.S., Cooper, Y., et al. (2018a). Elevated TREM2 Gene Dosage Reprograms Microglia Responsivity and Ameliorates Pathological Phenotypes in Alzheimer's Disease Models. Neuron *97*, 1032-1048.e5.

Lee, C.Z.W., Kozaki, T., and Ginhoux, F. (2018b). Studying tissue macrophages in vitro: are iPSC-derived cells the answer? Nat. Rev. Immunol. *18*, 716–725.

Lee, G.M., Shahian, T., Baharuddin, A., Gable, J.E., and Craik, C.S. (2011). Enzyme Inhibition by Allosteric Capture of an Inactive Conformation. J. Mol. Biol. *411*, 999–1016.

Lee, J.-W., Lee, I.-H., Iimura, T., and Kong, S.W. (2021a). Two macrophages, osteoclasts and microglia: from development to pleiotropy. Bone Res. *9*, 11.

Lee, S.H., Meilandt, W.J., Xie, L., Gandham, V.D., Ngu, H., Barck, K.H., Rezzonico, M.G., Imperio, J., Lalehzadeh, G., Huntley, M.A., et al. (2021b). Trem2 restrains the enhancement of tau accumulation and neurodegeneration by β-amyloid pathology. Neuron *109*, 1283-1301.e6.

Lefranc, M.-P., Pommié, C., Ruiz, M., Giudicelli, V., Foulquier, E., Truong, L., Thouvenin-Contet, V., and Lefranc, G. (2003). IMGT unique numbering for immunoglobulin and T cell receptor variable domains and Ig superfamily V-like domains. Dev. Comp. Immunol. *27*, 55–77.

Lessard, C.B., Malnik, S.L., Zhou, Y., Ladd, T.B., Cruz, P.E., Ran, Y., Mahan, T.E., Chakrabaty, P., Holtzman, D.M., Ulrich, J.D., et al. (2018). High-affinity interactions and signal transduction between Aβ oligomers and <scp>TREM</scp> 2. EMBO Mol. Med. *10*, 1–13.

Lewcock, J.W., Schlepckow, K., Di Paolo, G., Tahirovic, S., Monroe, K.M., and Haass, C. (2020). Emerging Microglia Biology Defines Novel Therapeutic Approaches for Alzheimer's Disease. Neuron *108*, 801–821.

Lewis, F., Schaffer, S.K., Sussex, J., O'Neill, P., and Cockcroft, L. (2014). The trajectory of dementia in the UK – making a difference. Rep. Alzheimer's Res. UK by OHE Consult.

Leyns, C.E.G., Ulrich, J.D., Finn, M.B., Stewart, F.R., Koscal, L.J., Remolina Serrano, J., Robinson, G.O., Anderson, E., Colonna, M., and Holtzman, D.M. (2017). TREM2 deficiency attenuates neuroinflammation and protects against neurodegeneration in a mouse model of tauopathy. Proc. Natl. Acad. Sci. 201710311.

Leyton, J. V. (2020). Improving Receptor-Mediated Intracellular Access and Accumulation of Antibody Therapeutics—The Tale of HER2. Antibodies *9*, 32.

Libeu, C.P., Lund-Katz, S., Phillips, M.C., Wehrli, S., Hernáiz, M.J., Capila, I., Linhardt, R.J., Raffaï, R.L., Newhouse, Y.M., Zhou, F., et al. (2001). New insights into the heparan sulfate proteoglycan-binding activity of apolipoprotein E. J Biol Chem *276*.

Liebschner, D., Afonine, P. V., Baker, M.L., Bunkoczi, G., Chen, V.B., Croll, T.I., Hintze, B., Hung, L.W., Jain, S., McCoy, A.J., et al. (2019). Macromolecular structure determination using X-rays, neutrons and electrons: Recent developments in Phenix. Acta Crystallogr. Sect. D Struct. Biol.

Liu, C.-C., Zhao, N., Fu, Y., Wang, N., Linares, C., Tsai, C.-W., and Bu, G. (2017). ApoE4 Accelerates Early Seeding of Amyloid Pathology. Neuron *96*, 1024-

1032.e3.

Liu, W., Taso, O., Wang, R., Bayram, S., Graham, A.C., Garcia-Reitboeck, P., Mallach, A., Andrews, W.D., Piers, T.M., Botia, J.A., et al. (2020). Trem2 promotes anti-inflammatory responses in microglia and is suppressed under pro-inflammatory conditions. Hum. Mol. Genet. *29*, 3224–3248.

Livingston, G., Huntley, J., Sommerlad, A., Ames, D., Ballard, C., Banerjee, S., Brayne, C., Burns, A., Cohen-Mansfield, J., Cooper, C., et al. (2020). Dementia prevention, intervention, and care: 2020 report of the Lancet Commission. Lancet *396*, 413–446.

Lorenzen, I., Lokau, J., Korpys, Y., Oldefest, M., Flynn, C.M., Künzel, U., Garbers, C., Freeman, M., Grötzinger, J., and Düsterhöft, S. (2016). Control of ADAM17 activity by regulation of its cellular localisation. Sci. Rep. *6*.

Lowell, C.A. (2011). Src-family and Syk Kinases in Activating and Inhibitory Pathways in Innate Immune Cells: Signaling Cross Talk. Cold Spring Harb. Perspect. Biol. *3*, a002352–a002352.

MacRedmond, R., Greene, C., Taggart, C.C., McElvaney, N., and O'Neill, S. (2005). Respiratory epithelial cells require Toll-like receptor 4 for induction of Human β-defensin 2 by Lipopolysaccharide. Respir. Res. *6*, 116.

Mahajan, P., Strain-Damerell, C., Mukhopadhyay, S., Fernandez-Cid, A., Gileadi, O., and Burgess-Brown, N.A. (2021). Screening and Production of Recombinant Human Proteins: Protein Production in Insect Cells BT - Structural Genomics: General Applications. Y.W. Chen, and C.-P.B. Yiu, eds. (New York, NY: Springer US), pp. 67–94.

Mahley, R.W., Huang, Y., and Rall, S.C. (1999). Pathogenesis of type III hyperlipoproteinemia (dysbetalipoproteinemia): questions, quandaries, and paradoxes.

J. Lipid Res. *40*, 1933–1949.

Makin, S. (2018). The amyloid hypothesis on trial. Nature *559*, S4–S7.

Mancuso, R., Fryatt, G., Cleal, M., Obst, J., Pipi, E., Monzón-Sandoval, J., Ribe, E., Winchester, L., Webber, C., Nevado, A., et al. (2019). CSF1R inhibitor JNJ-40346527 attenuates microglial proliferation and neurodegeneration in P301S mice. Brain *142*, 3243–3264.

Martoglio, B., and Dobberstein, B. (1998). Signal sequences: More than just greasy peptides. Trends Cell Biol. *8*, 410–415.

Mary, C., Coulon, F., Poirier, N., Dilek, N., Martinet, B., Blancho, G., and Vanhove, B. (2012). Antagonist properties of monoclonal antibodies to human CD28: role of valency and heavy-chain constant domain. J. Transl. Med. *10*, P17.

Matthews, B.W. (1968). Solvent content of protein crystals. J. Mol. Biol. *33*, 491–497.

Mawuenyega, K.G., Sigurdson, W., Ovod, V., Munsell, L., Kasten, T., Morris, J.C., Yarasheski, K.E., and Bateman, R.J. (2010). Decreased Clearance of CNS β-Amyloid in Alzheimer's Disease. Science (80-.). *330*, 1774.

Mayes, P.A., Hance, K.W., and Hoos, A. (2018). The promise and challenges of immune agonist antibody development in cancer. Nat. Rev. Drug Discov. *17*, 509–527.

Mazot, P., Cazes, A., Dingli, F., Degoutin, J., Irinopoulou, T., Boutterin, M.C., Lombard, B., Loew, D., Hallberg, B., Palmer, R.H., et al. (2012). Internalization and down-regulation of the ALK receptor in neuroblastoma cell lines upon monoclonal antibodies treatment. PLoS One *7*, 1–10.

Meilandt, W.J., Ngu, H., Gogineni, A., Lalehzadeh, G., Lee, S.H., Srinivasan, K., Imperio, J., Wu, T., Weber, M., Kruse, A.J., et al. (2020). TREM2 deletion reduces late-

stage amyloid plaque accumulation, elevates the Aβ42:Aβ40 ratio, and exacerbates axonal dystrophy and dendritic spine loss in the PS2ApP Alzheimer's mouse model. J. Neurosci. *40*, 1956–1974.

Mesters, J.R., and Hilgenfeld, R. (2007). Protein glycosylation, sweet to crystal growth? Cryst. Growth Des. *7*, 2251–2253.

Miguel-Álvarez, M., Santos-Lozano, A., Sanchis-Gomar, F., Fiuza-Luces, C., Pareja-Galeano, H., Garatachea, N., and Lucia, A. (2015). Non-steroidal anti-inflammatory drugs as a treatment for Alzheimer's disease: a systematic review and meta-analysis of treatment effect. Drugs Aging *32*, 139–147.

Mitra, N., Sinha, S., Ramya, T.N.C., and Surolia, A. (2006). N-linked oligosaccharides as outfitters for glycoprotein folding, form and function. Trends Biochem. Sci. *31*, 156–163.

Ben Mkaddem, S., Benhamou, M., and Monteiro, R.C. (2019). Understanding Fc Receptor Involvement in Inflammatory Diseases: From Mechanisms to New Therapeutic Tools. Front. Immunol. *10*.

Moody, P.R., Sayers, E.J., Magnusson, J.P., Alexander, C., Borri, P., Watson, P., and Jones, A.T. (2015). Receptor Crosslinking: A General Method to Trigger Internalization and Lysosomal Targeting of Therapeutic Receptor:Ligand Complexes. Mol. Ther. *23*, 1888–1898.

Mullard, A. (2021a). Landmark Alzheimer's drug approval confounds research community. Nature *594*, 309–310.

Mullard, A. (2021b). Failure of first anti-tau antibody in Alzheimer disease highlights risks of history repeating. Nat. Rev. Drug Discov. *20*, 3–5.

Nagata, S., Suzuki, J., Segawa, K., and Fujii, T. (2016). Exposure of

phosphatidylserine on the cell surface. Cell Death Differ. *23*, 952–961.

Nettleship, J.E., Aplin, R., Radu Aricescu, A., Evans, E.J., Davis, S.J., Crispin, M., and Owens, R.J. (2007). Analysis of variable N-glycosylation site occupancy in glycoproteins by liquid chromatography electrospray ionization mass spectrometry. Anal. Biochem. *361*, 149–151.

Nettleslip, J. (2012). Structural Biology of Glycoproteins. In Glycosylation, S. Petrescu, ed. (InTech), p.

Nimmerjahn, A., Kirchhoff, F., and Helmchen, F. (2005). Resting microglial cells are highly dynamic surveillants of brain parenchyma in vivo. Science *308*, 1314–1318.

Nugent, A.A., Lin, K., Van Lengerich, B., Lianoglou, S., Przybyla, L., Davis, S.S., Llapashtica, C., Wang, J., Kim, D.J., Xia, D., et al. (2019). TREM2 Regulates Microglial Cholesterol Metabolism upon Chronic Phagocytic Challenge. Neuron *105*, 837-854.e9.

Obst, J., Simon, E., Martin-Estebane, M., Pipi, E., Barkwill, L.M., Gonzalez-Rivera, I., Buchanan, F., Prescott, A.R., Faust, D., Fox, S., et al. (2020a). Inhibition of IL-34 Unveils Tissue-Selectivity and Is Sufficient to Reduce Microglial Proliferation in a Model of Chronic Neurodegeneration. Front. Immunol. *11*, 1–14.

Obst, J., Bradshaw, W., Roberts, H.H., Priestley, R., Jimenez-Antunez, C., Cowley, S.A., Gileadi, O., Mead, E., Daniel, E. Di, and Davis, J.B. (2020b). Targeting SHIP1 for therapeutic intervention in Alzheimer's disease. Alzheimer's Dement. *16*, 1–2.

Office for National Statistics (2018). Deaths registered in England and Wales. Off. Natl. Stat. 1–8.

Olah, M., Menon, V., Habib, N., Taga, M.F., Ma, Y., Yung, C.J., Cimpean, M.,

Khairallah, A., Coronas-Samano, G., Sankowski, R., et al. (2020). Single cell RNA sequencing of human microglia uncovers a subset associated with Alzheimer's disease. Nat. Commun. *11*.

Orlandi, R., Güssow, D.H., Jones, P.T., and Winter, G. (1989). Cloning immunoglobulin variable domains for expression by the polymerase chain reaction. Proc. Natl. Acad. Sci. U. S. A. *86*, 3833–3837.

Otero, K., Turnbull, I.R., Poliani, P.L., Vermi, W., Cerutti, E., Aoshi, T., Tassi, I., Takai, T., Stanley, S.L., Miller, M., et al. (2009). Macrophage colony-stimulating factor induces the proliferation and survival of macrophages via a pathway involving DAP12 and β-catenin. Nat. Immunol. *10*, 734–743.

Otero, K., Shinohara, M., Zhao, H., Cella, M., Gilfillan, S., Colucci, A., Faccio, R., Ross, F.P., Teitelbaum, S.L., Takayanagi, H., et al. (2012). TREM2 and β-catenin regulate bone homeostasis by controlling the rate of osteoclastogenesis. J. Immunol. *188*, 2612–2621.

Ottmann, C., Thiel, P., Kaiser, M., and Ottmann, C. (2018). Small-Molecule Stabilization of Protein – Protein Interactions : An Underestimated Concept in Drug Discovery ?**. 2012–2018.

Paloneva, J., Manninen, T., Christman, G., Hovanes, K., Mandelin, J., Adolfsson, R., Bianchin, M., Bird, T., Miranda, R., Salmaggi, A., et al. (2002). Mutations in Two Genes Encoding Different Subunits of a Receptor Signaling Complex Result in an Identical Disease Phenotype. Am. J. Hum. Genet. *71*, 656–662.

Paloneva, J., Mandelin, J., Kiialainen, A., Böhling, T., Prudlo, J., Hakola, P., Haltia, M., Konttinen, Y.T., and Peltonen, L. (2003). DAP12/TREM2 Deficiency Results in Impaired Osteoclast Differentiation and Osteoporotic Features. J. Exp. Med. *198*, 669–675.

Panza, F., Lozupone, M., Logroscino, G., and Imbimbo, B.P. (2019). A critical appraisal of amyloid-β-targeting therapies for Alzheimer disease. Nat. Rev. Neurol. *15*, 73–88.

Paolicelli, R.C., Bolasco, G., Pagani, F., Maggi, L., Scianni, M., Panzanelli, P., Giustetto, M., Ferreira, T.A., Guiducci, E., Dumas, L., et al. (2011). Synaptic Pruning by Microglia Is Necessary for Normal Brain Development. Science (80-.). *333*, 1456–1458.

Park, E.K., Jung, H.S., Yang, H.I., Yoo, M.C., Kim, C., and Kim, K.S. (2007). Optimized THP-1 differentiation is required for the detection of responses to weak stimuli. Inflamm. Res. *56*, 45–50.

Park, P.W., Reizes, O., and Bernfield, M. (2000). Cell Surface Heparan Sulfate Proteoglycans: Selective Regulators of Ligand-Receptor Encounters. J. Biol. Chem. *275*, 29923–29926.

Parodi, A.J. (2000). Protein glucosylation and its role in protein folding. Annu. Rev. Biochem. *69*, 69–93.

Patterson C (2018). World Alzheimer report 2018. Alzheimer's Dis. Int. (ADI, London).

Peng, Q., Malhotra, S., Torchia, J.A., Kerr, W.G., Coggeshall, K.M., and Humphrey, M.B. (2010). TREM2- and DAP12-Dependent Activation of PI3K Requires DAP10 and Is Inhibited by SHIP1. Sci. Signal. *3*, ra38–ra38.

Perkins, D.N., Pappin, D.J., Creasy, D.M., and Cottrell, J.S. (1999). Probability-based protein identification by searching sequence databases using mass spectrometry data. Electrophoresis *20*, 3551–3567.

Petrescu, A.-J., Milac, A.-L., Petrescu, S.M., Dwek, R.A., and Wormald, M.R.

(2004). Statistical analysis of the protein environment of N-glycosylation sites: implications for occupancy, structure, and folding. Glycobiology *14*, 103–114.

Piccio, L., Buonsanti, C., Cella, M., Tassi, I., Schmidt, R.E., Fenoglio, C., Rinker, J., Naismith, R.T., Panina-Bordignon, P., Passini, N., et al. (2008). Identification of soluble TREM-2 in the cerebrospinal fluid and its association with multiple sclerosis and CNS inflammation. Brain *131*, 3081–3091.

Pitas, R.E., Boyles, J.K., Lee, S.H., Hui, D., and Weisgraber, K.H. (1987). Lipoproteins and their receptors in the central nervous system. Characterization of the lipoproteins in cerebrospinal fluid and identification of apolipoprotein B,E(LDL) receptors in the brain. J. Biol. Chem. *262*, 14352–14360.

Poliani, P.L., Wang, Y., Fontana, E., Robinette, M.L., Yamanishi, Y., Gilfillan, S., and Colonna, M. (2015). TREM2 sustains microglial expansion during aging and response to demyelination. J. Clin. Invest. *125*, 2161–2170.

Prada, I., Ongania, G.N., Buonsanti, C., Panina-Bordignon, P., and Meldolesi, J. (2006). Triggering receptor expressed in myeloid cells 2 (TREM2) trafficking in microglial cells: Continuous shuttling to and from the plasma membrane regulated by cell stimulation. Neuroscience *140*, 1139–1148.

Prado, C.E., Watt, S., Treeby, M.S., and Crowe, S.F. (2019). Performance on neuropsychological assessment and progression to Dementia: A meta-analysis. Psychol. Aging *34*, 954–977.

Preger, C., Wigren, E., Ossipova, E., Marks, C., Lengqvist, J., Hofström, C., Andersson, O., Jakobsson, P.-J., Gräslund, S., and Persson, H. (2020). Generation and validation of recombinant antibodies to study human aminoacyl-tRNA synthetases. J. Biol. Chem. *295*, 13981–13993.

Price, B.R., Sudduth, T.L., Weekman, E.M., Johnson, S., Hawthorne, D.,

Woolums, A., and Wilcock, D.M. (2020). Therapeutic Trem2 activation ameliorates amyloid-beta deposition and improves cognition in the 5XFAD model of amyloid deposition. J. Neuroinflammation *17*, 1–13.

Raber, J., Huang, Y., and Ashford, J.W. (2004). ApoE genotype accounts for the vast majority of AD risk and AD pathology. Neurobiol. Aging *25*, 641–650.

Radaev, S., Kattah, M., Rostro, B., Colonna, M., and Sun, P.D. (2003). Crystal structure of the human myeloid cell activating receptor TREM-1. Structure *11*, 1527–1535.

Ram, S., Kim, D., Ober, R.J., and Ward, E.S. (2014). The level of HER2 expression is a predictor of antibody-HER2 trafficking behavior in cancer cells. MAbs *6*, 1211–1219.

Ransohoff, R.M. (2016). A polarizing question: do M1 and M2 microglia exist? Nat. Neurosci. *19*, 987–991.

Raran-Kurussi, S., and Waugh, D.S. (2012). The Ability to Enhance the Solubility of Its Fusion Partners Is an Intrinsic Property of Maltose-Binding Protein but Their Folding Is Either Spontaneous or Chaperone-Mediated. PLoS One *7*, e49589.

Reeves, P.J., Callewaert, N., Contreras, R., and Khorana, H.G. (2002). Structure and function in rhodopsin: high-level expression of rhodopsin with restricted and homogeneous N-glycosylation by a tetracycline-inducible N-acetylglucosaminyltransferase I-negative HEK293S stable mammalian cell line. Proc. Natl. Acad. Sci. U. S. A. *99*, 13419–13424.

Roberson, E.D., Halabisky, B., Yoo, J.W., Yao, J., Chin, J., Yan, F., Wu, T., Hamto, P., Devidze, N., Yu, G.-Q., et al. (2011). Amyloid-β/Fyn-induced synaptic, network, and cognitive impairments depend on tau levels in multiple mouse models of Alzheimer's disease. J. Neurosci. *31*, 700–711.

Robinson, M., Lee, B.Y., and Hane, F.T. (2017). Recent Progress in Alzheimer's Disease Research, Part 2: Genetics and Epidemiology. J. Alzheimer's Dis. *57*, 317–330.

de Rojas, I., Moreno-Grau, S., Tesi, N., Grenier-Boley, B., Andrade, V., Jansen, I.E., Pedersen, N.L., Stringa, N., Zettergren, A., Hernández, I., et al. (2021). Common variants in Alzheimer's disease and risk stratification by polygenic risk scores. Nat. Commun. *12*, 3417.

Roy, S., Zhang, B., Lee, V.M.-Y., and Trojanowski, J.Q. (2005). Axonal transport defects: a common theme in neurodegenerative diseases. Acta Neuropathol. *109*, 5–13.

Säll, A., Walle, M., Wingren, C., Müller, S., Nyman, T., Vala, A., Ohlin, M., Borrebaeck, C.A.K., and Persson, H. (2016). Generation and analyses of human synthetic antibody libraries and their application for protein microarrays. Protein Eng. Des. Sel. *29*, 427–437.

Saunders, K.O. (2019). Conceptual approaches to modulating antibody effector functions and circulation half-life. Front. Immunol. *10*, 1–20.

Savitsky, P., Bray, J., Cooper, C.D.O., Marsden, B.D., Mahajan, P., Burgess-Brown, N.A., and Gileadi, O. (2010). High-throughput production of human proteins for crystallization: the SGC experience. J. Struct. Biol. *172*, 3–13.

Schafer, D.P., Lehrman, E.K., Kautzman, A.G., Koyama, R., Mardinly, A.R., Yamasaki, R., Ransohoff, R.M., Greenberg, M.E., Barres, B.A., and Stevens, B. (2012). Microglia Sculpt Postnatal Neural Circuits in an Activity and Complement-Dependent Manner. Neuron *74*, 691–705.

Schapansky, J., Grinberg, Y.Y., Osiecki, D.M., Freeman, E.A., Walker, S.G., Karran, E., Gopalakrishnan, S.M., and Talanian, R. V. (2021). MEK1/2 activity modulates TREM2 cell surface recruitment. J. Biol. Chem. *296*, 100218.

Scheuner, D., Eckman, C., Jensen, M., Song, X., Citron, M., Suzuki, N., Bird, T.D., Hardy, J., Hutton, M., Kukull, W., et al. (1996). Secreted amyloid β–protein similar to that in the senile plaques of Alzheimer's disease is increased in vivo by the presenilin 1 and 2 and APP mutations linked to familial Alzheimer's disease. Nat. Med. *2*, 864–870.

Schlepckow, K., Kleinberger, G., Fukumori, A., Feederle, R., Lichtenthaler, S.F., Steiner, H., and Haass, C. (2017). An Alzheimer-associated TREM2 variant occurs at the ADAM cleavage site and affects shedding and phagocytic function. EMBO Mol. Med. *9*, 1356–1365.

Schlepckow, K., Monroe, K.M., Kleinberger, G., Cantuti-Castelvetri, L., Parhizkar, S., Xia, D., Willem, M., Werner, G., Pettkus, N., Brunner, B., et al. (2020). Enhancing protective microglial activities with a dual function TREM2 antibody to the stalk region. EMBO Mol. Med. e11227.

Schmechel, D.E., Saunders, A.M., Strittmatter, W.J., Crain, B.J., Hulette, C.M., Joo, S.H., Pericak-Vance, M.A., Goldgaber, D., and Roses, A.D. (1993). Increased amyloid beta-peptide deposition in cerebral cortex as a consequence of apolipoprotein E genotype in late-onset Alzheimer disease. Proc. Natl. Acad. Sci. *90*, 9649–9653.

Schoch, K.M., Ezerskiy, L.A., Morhaus, M.M., Bannon, R.N., Sauerbeck, A.D., Shabsovich, M., Jafar-Nejad, P., Rigo, F., and Miller, T.M. (2021). Acute Trem2 reduction triggers increased microglial phagocytosis, slowing amyloid deposition in mice. Proc. Natl. Acad. Sci. U. S. A. *118*, 1–10.

Schwarz, H., Schmittner, M., Duschl, A., and Horejs-Hoeck, J. (2014). Residual endotoxin contaminations in recombinant proteins are sufficient to activate human CD1c+ dendritic cells. PLoS One *9*.

Scott-Hewitt, N., Perrucci, F., Morini, R., Erreni, M., Mahoney, M., Witkowska,

A., Carey, A., Faggiani, E., Schuetz, L.T., Mason, S., et al. (2020). Local externalization of phosphatidylserine mediates developmental synaptic pruning by microglia. EMBO J. *39*, 1–20.

Selkoe, D.J. (2008). Soluble oligomers of the amyloid beta-protein impair synaptic plasticity and behavior. Behav. Brain Res. *192*, 106–113.

Selkoe, D.J., and Hardy, J. (2016). The amyloid hypothesis of Alzheimer's disease at 25 years. EMBO Mol. Med. *8*, 595–608.

Sellgren, C.M., Gracias, J., Watmuff, B., Biag, J.D., Thanos, J.M., Whittredge, P.B., Fu, T., Worringer, K., Brown, H.E., Wang, J., et al. (2019). Increased synapse elimination by microglia in schizophrenia patient-derived models of synaptic pruning. Nat. Neurosci. *22*, 374–385.

Sevier, C.S., and Kaiser, C.A. (2002). Formation and transfer of disulphide bonds in living cells. Nat. Rev. Mol. Cell Biol. *3*, 836–847.

Sharoar, M.G., Hu, X., Ma, X.-M., Zhu, X., and Yan, R. (2019). Sequential formation of different layers of dystrophic neurites in Alzheimer's brains. Mol. Psychiatry *24*, 1369–1382.

Shental-Bechor, D., and Levy, Y. (2008). Effect of glycosylation on protein folding: A close look at thermodynamic stabilization. Proc. Natl. Acad. Sci. *105*, 8256–8261.

Shi, Y., Yamada, K., Liddelow, S.A., Smith, S.T., Zhao, L., Luo, W., Tsai, R.M., Spina, S., Grinberg, L.T., Rojas, J.C., et al. (2017). ApoE4 markedly exacerbates tau-mediated neurodegeneration in a mouse model of tauopathy. Nature *549*, 523–527.

Shirotani, K., Hori, Y., Yoshizaki, R., Higuchi, E., Colonna, M., Saito, T., Hashimoto, S., Saito, T., Saido, T.C., and Iwata, N. (2019). Aminophospholipids are

signal-transducing TREM2 ligands on apoptotic cells. Sci. Rep. *9*, 1–9.

Shitaka, Y., Tran, H.T., Bennett, R.E., Sanchez, L., Levy, M.A., Dikranian, K., and Brody, D.L. (2011). Repetitive closed-skull traumatic brain injury in mice causes persistent multifocal axonal injury and microglial reactivity. J. Neuropathol. Exp. Neurol. *70*, 551–567.

Sims, R., van der Lee, S.J., Naj, A.C., Bellenguez, C.C., Badarinarayan, N., Jakobsdottir, J., Kunkle, B.W., Boland, A., Raybould, R., Bis, J.C., et al. (2017). Rare coding variants in PLCG2, ABI3, and TREM2 implicate microglial-mediated innate immunity in Alzheimer's disease. Nat. Genet. *49*, 1373–1384.

Smith, D.H., Chen, X.H., Pierce, J.E., Wolf, J.A., Trojanowski, J.Q., Graham, D.I., and McIntosh, T.K. (1997). Progressive atrophy and neuron death for one year following brain trauma in the rat. J. Neurotrauma *14*, 715–727.

Song, W., Hooli, B., Mullin, K., Jin, S.C., Cella, M., Ulland, T.K., Wang, Y., Tanzi, R.E., and Colonna, M. (2017). Alzheimer's disease-associated TREM2 variants exhibit either decreased or increased ligand-dependent activation. Alzheimer's Dement. *13*, 381–387.

Spillantini, M.G., Bird, T.D., and Ghetti, B. (1998). Frontotemporal dementia and Parkinsonism linked to chromosome 17: a new group of tauopathies. Brain Pathol. *8*, 387–402.

Stefano, L. (2009). The surface-exposed chaperone, HSp60, is an agonist of the microglial TREM2 receptor. J. Neurochem. *110*, 284–294.

Steiner, A., Schlepckow, K., Brunner, B., Steiner, H., Haass, C., and Hagn, F. (2020). γ-Secretase cleavage of the Alzheimer risk factor TREM 2 is determined by its intrinsic structural dynamics . EMBO J. *39*, 1–17.

Steinman, R.M., Mellman, I.S., Muller, W.A., and Cohn, Z.A. (1983). Endocytosis and the recycling of plasma membrane. J. Cell Biol. *96*, 1–27.

Strain-Damerell, C., Mahajan, P., Gileadi, O., and Burgess-Brown, N.A. (2014). Medium-Throughput Production of Recombinant Human Proteins: Ligation-Independent Cloning. In Structural Genomics: General Applications, Y.W. Chen, ed. (Totowa, NJ: Humana Press), pp. 55–72.

Suárez-Calvet, M., Kleinberger, G., Araque Caballero, M.Á., Brendel, M., Rominger, A., Alcolea, D., Fortea, J., Lleó, A., Blesa, R., Gispert, J.D., et al. (2016). sTREM 2 cerebrospinal fluid levels are a potential biomarker for microglia activity in early-stage Alzheimer's disease and associate with neuronal injury markers . EMBO Mol. Med. *8*, 466–476.

Sudom, A., Talreja, S., Danao, J., Bragg, E., Kegel, R., Min, X., Marcora, E., Thibault, S., Bradley, J., Wood, S., et al. (2018). Molecular basis for the loss-of-function effects of the Alzheimer's disease–associated R47H variant of the immune receptor TREM2. *293*, 12634–12646.

Takalo, M., Wittrahm, R., Wefers, B., Parhizkar, S., Jokivarsi, K., Kuulasmaa, T., Mäkinen, P., Martiskainen, H., Wurst, W., Xiang, X., et al. (2020). The Alzheimer's disease-associated protective Plcγ2-P522R variant promotes immune functions. Mol. Neurodegener. *15*, 1–14.

Taylor, C.J., Ireland, D.R., Ballagh, I., Bourne, K., Marechal, N.M., Turner, P.R., Bilkey, D.K., Tate, W.P., and Abraham, W.C. (2008). Endogenous secreted amyloid precursor protein-α regulates hippocampal NMDA receptor function, long-term potentiation and spatial memory. Neurobiol. Dis. *31*, 250–260.

Tedesco, S., De Majo, F., Kim, J., Trenti, A., Trevisi, L., Fadini, G.P., Bolego, C., Zandstra, P.W., Cignarella, A., and Vitiello, L. (2018). Convenience versus

biological significance: Are PMA-differentiated THP-1 cells a reliable substitute for blood-derived macrophages when studying in vitro polarization? Front. Pharmacol. *9*, 1–13.

Thompson, A., and Kanamarlapudi, V. (2015). Agonist-induced internalisation of the glucagon-like peptide-1 receptor is mediated by the Gαq pathway. Biochem. Pharmacol. *93*, 72–84.

Thornton, P., Sevalle, J., Deery, M.J., Fraser, G., Zhou, Y., Ståhl, S., Franssen, E.H., Dodd, R.B., Qamar, S., Gomez Perez-Nievas, B., et al. (2017). TREM2 shedding by cleavage at the H157-S158 bond is accelerated for the Alzheimer's disease-associated H157Y variant. EMBO Mol. Med. *9*, e201707673.

Tsai, Y.-C.I., Johansson, H., Dixon, D., Martin, S., Chung, C., Clarkson, J., House, D., and Rittinger, K. (2020). Single-Domain Antibodies as Crystallization Chaperones to Enable Structure-Based Inhibitor Development for RBR E3 Ubiquitin Ligases. Cell Chem. Biol. *27*, 83-93.e9.

Ulland, T.K., Song, W.M., Huang, S.C.-C.C., Ulrich, J.D., Sergushichev, A., Beatty, W.L., Loboda, A.A., Zhou, Y., Cairns, N.J., Kambal, A., et al. (2017). TREM2 Maintains Microglial Metabolic Fitness in Alzheimer's Disease. Cell *170*, 649-663.e13.

Ulrich, J.D., and Holtzman, D.M. (2016). TREM2 Function in Alzheimer's Disease and Neurodegeneration. ACS Chem. Neurosci. *7*, 420–427.

Varnum, M.M., Clayton, K.A., Yoshii-Kitahara, A., Yonemoto, G., Koro, L., Ikezu, S., and Ikezu, T. (2017). A split-luciferase complementation, real-time reporting assay enables monitoring of the disease-associated transmembrane protein TREM2 in live cells. J. Biol. Chem. *292*, 10651–10663.

Varshney, P., Yadav, V., and Saini, N. (2016). Lipid rafts in immune signalling: current progress and future perspective. Immunology *149*, 13–24.

Verghese, P.B., Castellano, J.M., Garai, K., Wang, Y., Jiang, H., Shah, A., Bu, G., Frieden, C., and Holtzman, D.M. (2013). ApoE influences amyloid-β (Aβ) clearance despite minimal apoE/Aβ association in physiological conditions. Proc. Natl. Acad. Sci. *110*, E1807--E1816.

Vonrhein, C., Flensburg, C., Keller, P., Sharff, A., Smart, O., Paciorek, W., Womack, T., and Bricogne, G. (2011). Data processing and analysis with the autoPROC toolbox. Acta Crystallogr. D. Biol. Crystallogr. *67*, 293–302.

Vonrhein, C., Tickle, I.J., Flensburg, C., Keller, P., Paciorek, W., Sharff, A., and Bricogne, G. (2018). Advances in automated data analysis and processing within autoPROC, combined with improved characterisation, mitigation and visualisation of the anisotropy of diffraction limits using STARANISO. Acta Crystallogr. Sect. A *74*, a360.

Vuillard, L., Braun-Breton, C., and Rabilloud, T. (1995). Non-detergent sulphobetaines: A new class of mild solubilization agents for protein purification. Biochem. J. *305*, 337–343.

Wandinger-Ness, A., and Zerial, M. (2014). Rab proteins and the compartmentalization of the endosomal system. Cold Spring Harb. Perspect. Biol. *6*, a022616.

Wang, Q., Chen, X., and Wang, Z. (2015a). Dimerization drives EGFR endocytosis through two sets of compatible endocytic codes. J. Cell Sci. *128*, 935–950.

Wang, S., Mustafa, M., Yuede, C.M., Salazar, S.V., Kong, P., Long, H., Ward, M., Siddiqui, O., Paul, R., Gilfillan, S., et al. (2020). Anti-human TREM2 induces microglia proliferation and reduces pathology in an Alzheimer's disease model. J. Exp. Med. *217*, e20200785.

Wang, Y., Cella, M., Mallinson, K., Ulrich, J.D., Young, K.L., Robinette, M.L.,

Gilfillan, S., Krishnan, G.M., Sudhakar, S., Zinselmeyer, B.H., et al. (2015b). TREM2 Lipid Sensing Sustains the Microglial Response in an Alzheimer's Disease Model. Cell *160*, 1061–1071.

Wang, Y., Mao, Y., Xu, X., Tao, S., and Chen, H. (2015c). Codon Usage in Signal Sequences Affects Protein Expression and Secretion Using Baculovirus/Insect Cell Expression System. PLoS One *10*.

Wang, Y., Ulland, T.K., Ulrich, J.D., Song, W., Tzaferis, J.A., Hole, J.T., Yuan, P., Mahan, T.E., Shi, Y., Gilfillan, S., et al. (2016). TREM2-mediated early microglial response limits diffusion and toxicity of amyloid plaques. J. Exp. Med. *213*, 667–675.

Wang, Z., Jackson, R.J., Hong, W., Taylor, W.M., Corbett, G.T., Moreno, A., Liu, W., Li, S., Frosch, M.P., Slutsky, I., et al. (2017). Human Brain-Derived Aβ Oligomers Bind to Synapses and Disrupt Synaptic Activity in a Manner That Requires APP. J. Neurosci. *37*, 11947–11966.

Wilgenburg, B. van, Browne, C., Vowles, J., and Cowley, S.A. (2013). Efficient, Long Term Production of Monocyte-Derived Macrophages from Human Pluripotent Stem Cells under Partly-Defined and Fully-Defined Conditions. PLoS One *8*, e71098.

Wingo, T.S., Lah, J.J., Levey, A.I., and Cutler, D.J. (2012). Autosomal recessive causes likely in early-onset Alzheimer disease. Arch. Neurol. *69*, 59–64.

Winter, G. (2010). Xia2: An expert system for macromolecular crystallography data reduction. J. Appl. Crystallogr. *43*, 186–190.

Winter, G., Waterman, D.G., Parkhurst, J.M., Brewster, A.S., Gildea, R.J., Gerstel, M., Fuentes-Montero, L., Vollmar, M., Michels-Clark, T., Young, I.D., et al. (2018). DIALS: Implementation and evaluation of a new integration package. Acta Crystallogr. Sect. D Struct. Biol. *74*, 85–97.

Wörn, A., and Plückthun, A. (2001). Stability engineering of antibody single-chain Fv fragments. J. Mol. Biol. *305*, 989–1010.

Wu, S., Avila-Sakar, A., Kim, J., Booth, D.S., Greenberg, C.H., Rossi, A., Liao, M., Li, X., Alian, A., Griner, S.L., et al. (2012). Fabs Enable Single Particle cryoEM Studies of Small Proteins. Structure *20*, 582–592.

Wunderlich, P., Glebov, K., Kemmerling, N., Tien, N.T., Neumann, H., and Walter, J. (2013). Sequential Proteolytic Processing of the Triggering Receptor Expressed on Myeloid Cells-2 (TREM2) Protein by Ectodomain Shedding and γ-Secretase-dependent Intramembranous Cleavage. J. Biol. Chem. *288*, 33027–33036.

Yamazaki, Y., Painter, M.M., Bu, G., and Kanekiyo, T. (2016). Apolipoprotein E as a Therapeutic Target in Alzheimer's Disease: A Review of Basic Research and Clinical Evidence. CNS Drugs *30*, 773–789.

Yamazaki, Y., Zhao, N., Caulfield, T.R., Liu, C.-C., and Bu, G. (2019). Apolipoprotein E and Alzheimer disease: pathobiology and targeting strategies. Nat. Rev. Neurol. *15*, 501–518.

Yao, H., Coppola, K., Schweig, J.E., Crawford, F., Mullan, M., and Paris, D. (2019). Distinct Signaling Pathways Regulate TREM2 Phagocytic and NFκB Antagonistic Activities. Front. Cell. Neurosci. *13*, 1–18.

Yeh, F.L., Wang, Y., Tom, I., Gonzalez, L.C., and Sheng, M. (2016). TREM2 binds to apolipoproteins, including APOE and CLU/APOJ, and thereby facilitates uptake of amyloid-beta by microglia. Neuron *91*, 328–340.

Yin, J., Liu, X., He, Q., Zhou, L., Yuan, Z., and Zhao, S. (2016). Vps35-dependent recycling of Trem2 regulates microglial function. Traffic *17*, 1286–1296.

Yuan, P., Condello, C., Keene, C.D., Wang, Y., Bird, T.D., Paul, S.M., Luo, W.,

Colonna, M., Baddeley, D., and Grutzendler, J. (2016). TREM2 Haplodeficiency in Mice and Humans Impairs the Microglia Barrier Function Leading to Decreased Amyloid Compaction and Severe Axonal Dystrophy. Neuron *92*, 252–264.

Zhang, G., Brokx, S., and Weiner, J.H. (2006). Extracellular accumulation of recombinant proteins fused to the carrier protein YebF in Escherichia coli. Nat. Biotechnol. *24*, 100–104.

Zhang, Q., Sidorenko, J., Couvy-Duchesne, B., Marioni, R.E., Wright, M.J., Goate, A.M., Marcora, E., Huang, K. lin, Porter, T., Laws, S.M., et al. (2020). Risk prediction of late-onset Alzheimer's disease implies an oligogenic architecture. Nat. Commun. *11*, 1–11.

Zhao, Y., Wu, X., Li, X., Jiang, L.L., Gui, X., Liu, Y., Sun, Y., Zhu, B., Piña-Crespo, J.C., Zhang, M., et al. (2018). TREM2 Is a Receptor for β-Amyloid that Mediates Microglial Function. Neuron *97*, 1023-1031.e7.

Zheng, H., Jia, L., Liu, C.-C., Rong, Z., Zhong, L., Yang, L., Chen, X.-F., Fryer, J.D., Wang, X., Zhang, Y., et al. (2017). TREM2 Promotes Microglial Survival by Activating Wnt/B-Catenin Pathway. J. Neurosci. *37*, 1772–1784.

Zheng, X., Baker, H., Hancock, W.S., Fawaz, F., McCaman, M., and Pungor, E. (2006). Proteomic analysis for the assessment of different lots of fetal bovine serum as a raw material for cell culture. Part IV. Application of proteomics to the manufacture of biological drugs. Biotechnol. Prog. *22*, 1294–1300.

Zhong, L., Chen, X.-F., Wang, T., Wang, Z., Liao, C., Wang, Z., Huang, R., Wang, D., Li, X., Wu, L., et al. (2017). Soluble TREM2 induces inflammatory responses and enhances microglial survival. J. Exp. Med. *214*, 597–607.

Zhong, L., Xu, Y., Zhuo, R., Wang, T., Wang, K., Huang, R., Wang, D., Gao, Y., Zhu, Y., Sheng, X., et al. (2019). Soluble TREM2 ameliorates pathological phenotypes

by modulating microglial functions in an Alzheimer's disease model. Nat. Commun. *10*, 1–16.

Zimmermann, I., Egloff, P., Hutter, C.A.J., Kuhn, B.T., Bräuer, P., Newstead, S., Dawson, R.J.P., Geertsma, E.R., and Seeger, M.A. (2020). Generation of synthetic nanobodies against delicate proteins. Nat. Protoc. *15*, 1707–1741.

Zou, W., Reeve, J.L., Liu, Y., Teitelbaum, S.L., and Ross, F.P. (2008). DAP12 Couples c-Fms Activation to the Osteoclast Cytoskeleton by Recruitment of Syk. Mol. Cell *31*, 422–431.